

Evaporation of the miombo woodland of southern Africa

A phenophase-based comparison of field observations to satellite-based evaporation estimates

Zimba, H.M.

DOI

[10.4233/uuid:55b7c07d-9b1b-4e0f-b935-cbfa434e3f9a](https://doi.org/10.4233/uuid:55b7c07d-9b1b-4e0f-b935-cbfa434e3f9a)

Publication date

2023

Document Version

Final published version

Citation (APA)

Zimba, H. M. (2023). *Evaporation of the miombo woodland of southern Africa: A phenophase-based comparison of field observations to satellite-based evaporation estimates*. [Dissertation (TU Delft), Delft University of Technology]. <https://doi.org/10.4233/uuid:55b7c07d-9b1b-4e0f-b935-cbfa434e3f9a>

Important note

To cite this publication, please use the final published version (if applicable).
Please check the document version above.

Copyright

Other than for strictly personal use, it is not permitted to download, forward or distribute the text or part of it, without the consent of the author(s) and/or copyright holder(s), unless the work is under an open content license such as Creative Commons.

Takedown policy

Please contact us and provide details if you believe this document breaches copyrights.
We will remove access to the work immediately and investigate your claim.



Evaporation of the miombo woodland of southern Africa

A phenophase-based comparison of field observations to satellite-based
evaporation estimates

Henry MUSONDA ZIMBA

“Thousands have lived without love.
Not one without water”

(Hugh Auden)

Evaporation of the miombo woodland of southern Africa

A phenophase-based comparison of field observations to satellite-based evaporation estimates

Dissertation

for the purpose of obtaining the degree of doctor

at Delft University of Technology

by the authority of the Rector Magnificus Prof. dr. ir. T.H.J.J. van der Hagen,

chair of the Board for Doctorates

to be defended publicly on

Tuesday 9 May 2023 at 15:00 o'clock

by

Henry MUSONDA ZIMBA

Master of Science in Integrated Water Resources Management, The University of Zambia,

Zambia

born in Zambia

This dissertation has been approved by the promotor.

Composition of the doctoral committee:

Rector Magnificus

Prof.dr.ir. H.H.G. Savenije

Dr.ir. A.M.J. Coenders

Chairperson

Delft University of Technology, promotor

Delft University of Technology, copromotor

Independent members:

Prof. dr. ir. Nick C. van de Giesen

Prof. dr. Graham P. W. Jewitt

Prof. dr. Anke Hildebrandt

Dr. Markus Hrachowitz

Delft University of Technology

IHE-Delft

Friedrich Schiller University, Jena, Germany

Delft University of Technology

Other members:

Dr. Kawawa E. Banda

University of Zambia, Zambia



This research has been funded by the Netherlands Organisation for Scientific Research, grant W 07.303.102.

© 2023 Henry M. Zimba, Water Resources Section, Faculty of Civil Engineering and Geosciences, Delft University of Technology

Title: Evaporation of the miombo woodland of southern Africa

A phenophase-based comparison of field observations to satellite-based evaporation estimates

Published by: Ipskamp Printing

Key words: Evaporation, Energy partitioning, Latent heat flux, miombo woodland, Phenophase, Sensible heat flux, Water balance

Front and back cover design: Henry M. Zimba

Copyright © 2023 by H.M. Zimba

PREFACE

Growing up in the village I had no idea that the environment I was growing up in would in future become a subject of my PhD study. Learning and reading about the importance of the miombo ecosystem in the food, water and energy (FWE) nexus of southern Africa brings the fondest memories of my childhood. It is now that I am able to put the pieces together and actually see the FWE nexus as a lived experience.

Back in the days our family harvested edible caterpillars (Ifishimu) from the miombo woodland. My grandmother knew all the sites which had the miombo species that caterpillars preferred. It was tens of kilometers from our village. We left very early in the morning and came back late in the evening with buckets full of caterpillars. Sometimes we would camp in the village that was near to these forests for days harvesting the caterpillars. It is the same environment where we harvested fresh mushrooms though these sometimes grew in the miombo bushes very close to home. Our crop fields were mainly based on the chitemene system, a shifting cultivation approach involving the cutting down, heaping and burning of miombo trees. By the age 10 I already had my own axe and hoe and a small crop field. When coming back from the crop fields we would pass through the bush collecting dry miombo logs to use for fire wood. Each one of us carried a bunch of logs as their age permitted. To tie the logs we used fresh fibre from suitable miombo species. I remember the axe was always wet with what I now know was water – back then I had no idea why the axe would be wet when cutting a fresh tree. We got timber to roof our house from the miombo woodland. Iron nails were a luxury and so fibre from miombo trees was used to fasten the roof. My grandfather taught us the various uses of several miombo species. At primary school we were given assignments to make an axe or hoe holders. Sometimes we were asked to make different types of stool using miombo trees. I knew which miombo species to go to for each assignment. Grandfather used to make planks from miombo trees. Whenever there was a funeral in the village I remember he would donate planks for making a casket. Back in the days we didn't have tap water. Unfortunately the situation hasn't changed. We used to draw water from a “shallow” spring well on an ant hill near the Nkanda River. What was fascinating is that the well is on the upland and drains into the river which is a few meters downwards. What I remember is that there was a miombo woodland surrounding the well.

Looking back I now see how our entire livelihood was basically sustained by the miombo ecosystem. I am now interested in learning more about the miombo woodland and how we can preserve the ecosystem so that it continues to provide the ecosystem services for many years to come.

What is also fascinating is that major rivers in the Zambezi Basin have origin in and pass through the miombo woodland providing several livelihood streams along the way. I am now interested in understanding the evaporative processes of the miombo woodland and to what extent the evaporation affects the availability of water resources at both local and regional level. I am glad I took up this opportunity to do a PhD focusing on the evaporation in the miombo woodland. This has laid a strong foundation for this desire to be fulfilled. Through this study I had the opportunity to learn more about the miombo ecosystem. I also learned how to estimate actual evaporation of a natural forest using state of the art technology

such as the distributed temperature system (DTS). I have also been able to establish highly beneficial relationships with colleagues from various universities around the world but most importantly those I had the privilege to interact with at TU Delft. The knowledge I gained through my interactions with Petra Hulsman and Bart Schilperoort is invaluable. This work wouldn't have been accomplished without feeding off such interactions. If my experience is anything to go by then I doubt if anyone can successfully finish a PhD study without establishing beneficial relationships at various levels.

This thesis involved setting up a flux observation tower. This was my first time to come into contact with the DTS system. I had no idea how the flux tower was to be set up and completely had no clue on how to process the data in Python. It was an extremely intimidating experience in the initial stages. However, I am glad that I was part of a project team that was ready to help me learn the ropes. From selecting the appropriate site for setting up the flux tower, through the various times when the optical fibre cable was damaged by moles and warthogs and had to be spliced, to learning the python code for processing the data, they had my back covered. The timer in the DTS malfunctioned to such an extent that six months of data was mingled up with no way of sorting it up. This timer problem could only be fixed at the Silixa LTD offices in the United Kingdom. The flux observation tower was initially constructed with local forest materials. Heavy rains caused havoc and damaged the tower and had to reconstruct a new one with iron bars. At this point I lost the hope that I would get good quality DTS data for estimating actual evaporation. It is not field work until you have both success and failure stories to tell. I want to document my experiences with BR-DTS approach in an African setup and I hope one day it will be used to spare an African researcher a few headaches and finances.

The study involved the use of both satellite-based data and field observations. The assumption was that all satellite-based data were wrong until proven right by field observations. Well, after the field observations all satellite-based evaporation data used in this study, except for one, were proven wrong, though this “wrongness” needs to be put into context which this thesis has provided. I wanted the satellite-based data to be proved correct especially that there is a scarcity of field observations in the miombo region in which satellite-based data appears to be a solution. This simply goes to show the irreplaceability of field observations in the application of satellite-based data in data scarce environments. This is why despite the many challenges I faced and the long distance I used to cover to collect field data I am glad that in the end it worked out. Because of this effort we now have the first known field-based actual evaporation estimates of the miombo woodland. There a lot of questions about the evaporation dynamics of the miombo woodland that need answers. This study, in my view, is a foundation on which many conversations on the evaporation of the miombo woodland can be initiated. For instance, the conversation has been started in the wet miombo woodland but there are many other miombo woodland strata that need to be assessed in order for us to have a relatively clearer understanding of the evaporation dynamics of the ecosystem. Will we have other researchers take up this call? Will we have the resources to do more on this aspect?

Henry Musondaimba
Delft, May 2023

SUMMARY

Through precipitation retention and evaporation (by both interception and transpiration), woodlands play a significant role in the global moisture cycle. Evaporation is the largest, but at the same time, the most difficult flux to observe in a woodland. Accounting for woodland evaporation is important for hydrological modelling for the efficient development and management of water resources. Assessing evaporation is a challenging undertaking that involves the use of a wide range of equipment and requires skilled personnel. Much work has been conducted on assessing evaporation in agricultural crops. Even satellite data-based models are largely structured to assess evaporation in agricultural crops to the exclusion of understanding evaporation dynamics in natural woodlands, especially in African ecosystems. However, evaporation in woodland surfaces accounts for a significant portion of the water cycle over the terrestrial land mass. Understanding the characteristics of woodland ecosystem evaporation like interception and transpiration, is key to monitoring climate impact on woodland ecosystems, which is important for hydrological modelling and the management of water resources at various scales. One of the key aspects to enable this understanding is the knowledge of woodland phenological interaction with climate variables and the seasonal environmental regimes. “Vegetation phenology” refers to the periodic biological life cycle events of plants, such as leaf flushing and senescence, and corresponding temporal changes in vegetation canopy cover. Solar radiation, temperature and water availability (i.e., rainfall and soil moisture) are some of the key environmental variables that influence plant phenology. The attributes of woodland phenology, solar radiation, temperature and water availability differ across the diverse ecosystems globally, therefore, requires better understanding at a more local or regional level. Yet, evaporation of natural woodlands, especially in African ecosystems, with respect to phenological phases, are poorly characterised. This is largely because phenological studies have mainly focused on northern mid-latitude regions to the exclusion of other regions like the miombo of southern Africa. For increasing the predictive power of hydrological models, it is important to account for the interaction of woodland phenology with climate variables over the seasons and to characterise evaporation.

This thesis aims at understanding the miombo woodland evaporation as a consequence of the vegetation phenological interaction with environmental and hydrological variables across seasons. Based on information in public domain, this study is the first independent field observation data-based characterisation of actual evaporation of the miombo woodland. The miombo is a heterogeneous woodland of the genus *Brachystegia* with the dominant species in the study location being *Bauhinia petersenia*, *Brachystegia longifolia*, *Brachystegia boehmii*, *Brachystegia speciformis*, *Jubenerdia panincolata*, *Pericopsis angolensis*, *Uapaca kirkiana* and *Uapaca sansibarica*. Unique phenological attributes are the simultaneous leaf fall, leaf flush and leaf colour changes that normally occur in the dry season between May and October. Most miombo woodland species are broad leaved and have developed dry season coping mechanisms such as deep rooting (capacity to access deep soil moisture and ground water) and vegetation water storage. The canopy closure is varied across the miombo woodland strata and is influenced by several factors

including rainfall, soil type, soil moisture and nutrients, species diversity and temperature. These phenological attributes are species dependent, with varied response to phenological stimuli. This study sought to answer the question on the role of the phenology of the miombo woodland in the evaporation dynamics. The thesis also endeavoured to show how phenology, potentially, affects satellite-based evaporation estimates of the miombo woodland. The Luangwa Basin in southern Africa, a largely miombo woodland covered basin, was used as the study area. This basin was chosen because it is located in both the dry miombo woodland and wet miombo woodland in the Zambezian miombo woodland which is the largest strata of the miombo woodland. Furthermore, the Luangwa Basin is located in Zambia which is described as the country possibly with the highest diversity of trees and is said to be the centre of endemism for *Brachystegia*, with 17 species.

To answer the questions on the importance of the phenology of the miombo woodland on the evaporation dynamics, the study used a coupled approach by applying both satellite data and field observations. Phenological changes of the miombo woodland across seasons were assessed using satellite-based data, the normalised difference vegetation index (NDVI) and leaf area index (LAI). Satellite-based data, land surface temperature (LST) and normalised difference infrared index (NDII), were used as proxies for climate variables canopy temperature and canopy vegetation water content. Point scale field estimates of evaporation across three different phenophases of the miombo woodland were obtained using the Bowen ratio distributed temperature sensing (BR-DTS) system. By measuring profiles of air temperature and wet bulb temperature, the evaporation could be estimated via the Bowen ratio method (BR-DTS). Six satellite-based evaporation estimates were compared across different phenophases of the miombo woodland. This was meant to observe the phenophases in which significant differences in the trend and magnitude of satellite-based evaporation estimates occurred. The general water balance approach was used to assess annual actual evaporation at basin scale. Consequently, satellite-based evaporation estimates were compared to the BR-DTS-based evaporation estimates at point scale and the water balance-based evaporation at basin scale.

Results, based on satellite data, show that the phenology of the miombo woodland, i.e., changes in woodland canopy cover and photosynthetic activities, have a season-dependent correlation with climate variables. Woodland canopy cover, across phenophases and seasons, appear to be more influenced rather by water than temperature. This may explain the particular species-dependent buffering mechanisms during water limited conditions i.e., leaf shedding, deep rooting systems with access to ground water, and the vegetation water storage mechanisms. In agreement with available literature in public domain it appears there is little variation in canopy cover/closure (i.e., proxied by LAI) in wet miombo woodland in the dry season.

At the wet miombo woodland site in Mpika, Zambia, the BR-DTS observations showed that, across the different phenophases, the actual evaporation trend and magnitude appeared to be more associated with the available energy than the changes in the woodland canopy cover. Further analysis showed that the net radiation has a greater influence on actual evaporation as it accounted for more variations in the actual evaporation compared to the changes in the woodland canopy cover (i.e., NDVI). The energy partitioning showed that

available energy expenditure varied with phenological season. In the green down phenophase during the cool dry season the available energy was largely partitioned as sensible heat flux. As the temperature and net radiation began to increase in the early dormant phenophase during the late cool dry season (July August) the available energy appeared to be equally partitioned between sensible and latent heat flux. In the late dormant phenophase during the early warm pre-rainy season (i.e., September) available energy was largely partitioned as latent heat flux. In the green-up phenophase during the late pre-warm rainy season (i.e., October) and early rainy season (i.e., November to December) the available energy was largely partitioned as latent heat flux. During the rain days the available energy appeared to be equally partitioned between latent and sensible heat flux. It appears that as the net radiation and canopy cover increased the available energy was largely partitioned as latent heat flux during the dry season. A remarkable observation was the continued rising trend of actual evaporation even during the lowest woodland canopy cover period in August and September. The rising trend in actual evaporation during the dry season may be due to the developed dry season water stress buffering mechanism such as deep rooting with access to moisture in deep soils and possibly access to ground water. The trend of the BR-DTS-based actual evaporation of the miombo woodland in the dry season points to the interaction between hydro-climate variables (i.e., precipitation linked soil moisture and net radiation) and the plant phenology.

When compared to field observations, at point scale, all satellite-based evaporation estimates underestimated actual evaporation of a wet miombo woodland in the dry season and part of the early rainy season. Substantial underestimations were in the dormant and the green-up phenophases. Additionally, except for the WaPOR, the trends of all other satellite-based evaporation estimates differed from that of field observations. Plausible explanations for the behaviour (trend and magnitude) of satellite-based evaporation estimates in the dry season include the non-integration of soil moisture directly into the modelling of transpiration and the optimisation of the rooting depth. For instance, the use of proxies such as the NDVI and LST for soil moisture in surface energy balance models, such as SSEBop, results in uncertainties as the proxies are unable to take into account other factors that influence the sensible heat flux. In MOD16 the use of relative humidity and vapour pressure difference as proxies for soil moisture may be a source of uncertainty in estimating transpiration. On the other hand it has been observed that direct integration of soil moisture in the MOD16 algorithm appeared to improve the accuracy of actual evaporation estimates. This may explain why the WaPOR which integrate soil moisture stress in the algorithm appeared to have a similar trend to field observations and also had higher estimates of actual evaporation compared to the other satellite-based evaporation estimates. It has also been shown that optimising the rooting depth improves the accuracy of transpiration estimates in vegetation with a dry season. Most miombo woodland species are deep rooting with access to deep soil moisture and potentially groundwater. Therefore, direct integration of soil moisture into the algorithms for the satellite-based evaporation estimates and optimising the rooting depth is likely to improve the accuracy of actual evaporation estimates for the miombo woodland.

The phenophase-based comparison at pixel scale in dry miombo woodland and wet miombo woodland and at the Luangwa Basin miombo woodland scale showed similar

results. In all three scenarios substantially high coefficients of variation in actual evaporation estimates among satellite-based evaporation estimates were observed in the water limited, high temperature and low woodland canopy cover conditions in the dormant phenophase. The coefficients of variation in actual evaporation estimates were also substantially high in the green-up phenophase at the boundary between the dry season and the rainy season. The lowest coefficients of variation in actual evaporation estimates were observed in water abundant, high temperature, high leaf chlorophyll content and high woodland canopy cover during the maturity/peak phenophase. The high coefficients of variation in actual evaporation estimates, among satellite-based evaporation estimates, in the dormant and green-up phenophases, points to the challenge of estimating the actual evaporation of the miombo woodland in the dry season and early rainy season. The same scenario emerged as was observed at point scale, with reference to field observations, in which satellite-based evaporation estimates which directly integrate soil moisture in their algorithm appeared to have higher estimates of actual evaporation in the dormant phenophase in the dry season. For instance, the FLEX-Topo and WaPOR integrate soil moisture in their algorithms. Compared to each other the FLEX-Topo and WaPOR appeared to have no statistically significant ($p\text{-value} > 0.5$) differences in their trends and mean estimates of actual evaporation in the dormant phenophase in the dry season. Compared to the FLEX-Topo and WaPOR the other four satellite-based evaporation estimates, GLEAM, MOD16, SSEBop and TerraClimate showed statistically significant ($p\text{-value} < 0.05$) differences in the trend and mean estimates of actual evaporation in the dormant phenophase in the dry season. Considering the canopy phenology and the associated physiological adaptation of the miombo woodland plants in the dry season, it appears that the direct integration of the soil moisture in the algorithms and optimising the rooting depth is likely to improve the accuracy of the satellite-based evaporation estimates. In the maturity/peak phenophase(s) during the mid-rainy season, compared to other satellite-based evaporation estimates, the MOD16 appeared to have significantly ($p\text{-value} < 0.05$) higher estimates of actual evaporation. The plausible explanation for this observation could be that the interception module of MOD16 is more responsive to the miombo woodland phenology. The wet miombo woodland intercepts between 17-20 percent of rainfall annually.

Compared to the general annual water balance-based actual evaporation all six satellite-based evaporation estimates underestimated actual evaporation of the Luangwa Basin. The implication of this observation is that satellite-based evaporation estimates likely underestimate evaporation even in non-miombo woodland such as the mopane woodland that are also part of the larger Luangwa Basin vegetation landscape. However, for a comprehensive overview of the performance of the satellite-based evaporation estimates there is need for vegetation type and land-cover type based assessments of actual evaporation for the Luangwa Basin.

At both point and basin scale-based assessments, there was a negative linear relationship between the spatial resolution of satellite-based evaporation estimates and the estimated actual evaporation. Satellite-based evaporation estimates with fine spatial resolutions showed lower underestimates compared to those with coarser resolutions. The implication is that the finer the spatial resolution the lower the underestimation. However, at

both assessment scales, the linear relationships between the spatial resolutions and the evaporation estimates were statistically insignificant (i.e., $p\text{-value} > 0.05$). The reason for this outcome is exhibited in that some satellite-based evaporation estimates with relatively coarser spatial resolutions, i.e., SSEBop at both point and basin scale and TerraClimate at basin scale, underestimated less compared to MOD16 which had a finer spatial resolution. Furthermore, at basin scale a coarser spatial resolution estimate FLEX-Topo and a finer spatial resolution estimate WaPOR showed similar magnitude of actual evaporation in the dormant phenophase in the dry season. The implication of this observation is that other factors (i.e., heterogeneity in the landscape, model structure, processes and inputs) influence more the estimated actual evaporation rather than the spatial resolutions of the satellite-based evaporation estimates. Consequently, it appears that satellite-based estimates at finer spatial resolution with the structure, processes and inputs that couple canopy transpiration with the root zone storage, taking into account the vertical upward (beyond 2.5 m) and horizontal moisture flux as well as the canopy phenological changes, are likely to provide actual evaporation estimates that reflect actual conditions of the miombo woodland. This is demonstrated by the WaPOR estimates which appears to include these aspects in simulating actual evaporation.

The field-based actual evaporation assessments were conducted in the wet miombo woodland. It is possible that the phenological response to changes in hydrological and climate regimes in the drier miombo woodland are different from the observations at the Mpika site. Therefore, there is need for similar observations to be performed in the drier miombo woodland and to compare the results. However, this thesis has demonstrated the importance of understanding and incorporating the canopy phenology and dry season physiological adaptation (i.e., deep rooting) of the miombo woodland in modelling actual evaporation. Additionally, for basins with heterogenous woodland types like the Luangwa, it is important to conduct actual evaporation assessments in the different vegetation types. This is likely to give a more representative understanding of basin scale evaporation dynamics. Nevertheless, this study has provided a foundation on which other studies can build towards a more comprehensive understanding of the actual evaporation dynamics in this unique woodland.

LIST OF SYMBOLS

e_a	Actual vapour pressure ($M L^{-1} T^{-2}$)
e_s	Saturated vapour pressure ($M L^{-1} T^{-2}$)
C_V	Coefficient of variation [-]
$\bar{E}_{a(DTS)}$	Mean of observed BR-DTS actual evaporation [$L T^{-1}$]
E_a	Actual evaporation ($L T^{-1}$)
$E_{a(DTS)}$	Actual evaporation ($L T^{-1}$) based on the BR-DTS approach
E_β	Actual evaporation ($L T^{-1}$) based on the Bowen ratio energy balance method
E_o	Reference evaporation ($L T^{-1}$)
$E_{c(PM)}$	Potential evaporation ($L T^{-1}$) based on the Penman-Monteith model
E_s	Satellite-based evaporation estimate [$L T^{-1}$]
$E_{a_{wb}}$	Water balance-based actual evaporation ($L T^{-1}$)
$E_{a_{Min}}$	Actual evaporation minimum ($L T^{-1}$)
$E_{a_{Max}}$	Actual evaporation maximum ($L T^{-1}$)
$E_{a_{Mean}}$	Actual evaporation mean ($L T^{-1}$)
F	Test statistic [-]
G_s	Soil heat flux [$M T^{-3}$]
G_{hr}	Hourly ground heat flux [$M T^{-3}$]
H	Sensible heat flux [$M T^{-3}$]
i	intercept [-]
K_c	Crop coefficient [-]
K	Kendall correlation coefficient [-]
LE	Latent heat flux [$M T^{-3}$]
M	Change in energy storage in the system canopy storage [$M T^{-3}$]
n	Number of observations [-]

P_a	Atmospheric pressure [$M L^{-1} T^{-2}$]
P	Precipitation [$L T^{-1}$]
Q	Runoff [$L T^{-1}$]
R_N	Net radiation [$M T^{-3}$]
r	Pearson correlation coefficient [-]
R^2	Coefficient of determination [-]
T_a	Dry bulb temperature [K]
T_w	Wet bulb temperature [K]
β_L	Unstandardized coefficient estimates with LST [-]
β_N	Unstandardized coefficient of estimates with NDII [-]
β	Bowen ratio [-]
τ	Kendall tau [-]
λ	Latent heat of vapourisation [$L^2 T^{-2}$]
γ	Pyschrometric constant [$M L^{-1} T^{-2} K^{-1}$]
Γ	Adiabatic lapse rate [$K L^{-1}$]
ΔT_a	Difference in air temperature [K]
Δz	Change in height [L]
α	Alpha [-]
σ	Standard deviation [-]
μ	Mean of the observations [-]
u	Wind speed [$L T^{-1}$]

LIST OF ACRONYMS

ANOVA	Analysis of Variance
BR	Bowen ratio
BR-DTS	Bowen ratio distributed temperature sensing
CCR	Correlated Component Regression
CCR.LM	Correlated Component Regression Linear Model
CFSR	Climate Forecasting System Reanalysis
CHIRPS	Climate Hazards Group Infra-Red Precipitation with Station data
DEM	Digital Elevation Model
DF	Degree of Freedom
DTS	Distributed temperature sensing
ECMWF	European Centre for Medium-Range Weather Forecasts
ERA5	The 5 th major atmospheric reanalysis produced by ECMWF
EVI	Enhanced Vegetation Index
EWT	Equivalent Water Thickness
FPAR	Fraction of Photosynthetically Active Radiation
GFSC _v	Goodness of Fit Statistics Cross-validated
GLEAM	Global Land Evaporation Amsterdam Model
GRDC	Global Runoff Data Centre
ITCZ	Inter-Tropical Convergence Zone
LAI_{Max}	Maximum leaf area index
LAI_{Mean}	Mean leaf area index
LAI_{Min}	Minimum leaf area index
LST_{Max}	Maximum land surface temperature
LST_{Mean}	Mean land surface temperature
LST_{Min}	Minimum land surface temperature

LAI	Leaf Area Index
LUT	Look Up Table
LST	Land Surface Temperature
MBE	Mean Bias Error
MODIS	MODerate resolution Imaging Spectroradiometer
$NDII_{Max}$	Maximum normalised difference infrared index
$NDII_{Mean}$	Mean normalised difference infrared index
$NDII_{Min}$	Minimum normalised difference infrared index
$NDVI_{Max}$	Maximum normalised difference vegetation index
$NDVI_{Mean}$	Mean normalised difference vegetation index
$NDVI_{Min}$	Minimum normalised difference vegetation index
NBAR-EVI2	Nadir Bidirectional reflectance distribution function Adjusted surface Reflectance Enhanced Vegetation Index 2
NDII	Normalised Difference Infra-Red Index
NDVI	Normalised Difference Vegetation Index
NIR	Near Infra-Red
NMSE	Normalised Mean Square Error
NOAA	National Ocean and Atmospheric Administration
RMSE	Root Mean Square Error
RM-ANOVA	Repeated Measure Analysis of Variance
SWIR	Short Wave Infra-Red
SSEBop	Operational Simplified Surface Energy Balance
UNFCCC	United nations framework convention on climate change
VOD	Vegetation Optical Depth
WaPOR	Water Productivity through Open access Remotely sensed derived data

CONTENTS

PREFACE	v
SUMMARY	vii
LIST OF SYMBOLS	xii
LIST OF ACRONYMS	xv
LIST OF TABLES	xxi
LIST OF FIGURES	xxii
CHAPTER 1	1
1 Introduction	
1.1 Woodlands and evaporation	2
1.2 Plant phenology, energy and water interactions	2
1.3 Remote Sensing, phenology and evaporation modelling	3
1.4 Field measurements of woodland evaporation	6
1.5 Why the miombo woodland	7
1.6 Problem statement	9
1.7 Research objectives	10
1.8 Thesis structure	10
CHAPTER 2	14
2 Canopy phenology of the miombo woodland and climate	14
2.1 Introduction	16
2.2 Materials and methods	19
2.2.1 Study site	19
2.2.2 Description of data sets	20
2.2.3 Study approach	22
2.2.4 Statistical approaches used to analyse the data	23
2.2.4.1 The Dixon test	23
2.2.4.2 Pearson r approach	23
2.2.4.3 RM-ANOVA test	24
2.2.4.4 Correlated component regression linear model (CCR.LM)	24
2.2.4.5 Homogeneity with Pettit test	25
2.2.4.6 Mann-Kendall trends test and Sens' method	25

2.3	Results	26
2.3.1	Assessment of outliers with the Dixon test and Z-score approach	26
2.3.2	Pattern observed in phenology, canopy cover, water content and temperature	26
2.3.3	Analysis of the observed patterns with the RM-ANOVA test	31
2.3.4	Pearson r correlation analysis of the relationship of variables	31
2.3.5	Regression of canopy cover relationship with canopy water content and canopy temperature using the CCR.LM	33
2.3.6	Assessment of abrupt change in variables with the Pettit test	37
2.3.7	Assessment of trends in values of variables with Mann–Kendall trends test	38
2.4	Discussion	40
2.4.1	Variations in canopy cover, canopy water content and canopy temperature	40
2.4.2	Canopy cover relationship with canopy water content and canopy temperature	41
2.4.3	Observed abrupt change point(s) and the trends in variables during the 2009 – 2018 period	42
2.5	Limitations of the study	43
2.6	Conclusions	43
	CHAPTER 3	45
3	Phenophase-based comparison of satellite-based evaporation estimates to field observations of a natural woodland: miombo woodland southern Africa	45
3.1	Introduction	47
3.2	Materials and methods	47
3.2.1	Study site	49
3.2.2	Study approach	50
3.2.3	Estimating potential evaporation	52
3.2.4	Conventional Bowen ratio energy balance method	52
3.2.5	BR-DTS energy balance approach	53
3.2.6	DTS data quality control	54
3.2.7	Actual evaporation estimation	55
3.2.8	Comparison of field estimates to satellite-based estimates	55
3.2.9	Statistical analysis	55
3.2.10	Flux observation tower set-up	57

3.3	Results and discussion	60
3.3.1	Evaporation flux foot print/fetch analysis	60
3.3.2	DTS data quality control	60
3.3.3	Comparison of DTS-based estimates with the ATMOS-41	
3.3.4	Meteorological conditions	61
3.3.5	Canopy phenophase-based Bowen ratio and evaporation trend	62
3.3.6	Comparison of daily potential evaporation and actual evaporation	64
3.3.7	Comparison of satellite-based evaporation estimates to field observations	67
3.3.8	Potential causes of the discrepancies between E_a (DTS) and satellite products	71
3.3.8.1	Global Land Evaporation Amsterdam Model (GLEAM)	71
3.3.8.2	MODerate resolution Imaging Spectroradiometer (MOD16)	72
3.3.8.3	Operational Simplified Surface Energy Balance (SSEBop)	73
3.3.8.4	Water Productivity through Open access Remotely sensed derived data (WaPOR)	74
3.3.9	Possible causes of the E_a (DTS) overestimation	74
3.4	Conclusions and recommendations	76
CHAPTER 4		78
4	On the importance of phenology in the Miombo Woodland evaporation	78
4.1	Introduction	80
4.2	Materials and methods	82
4.2.1	Study approach	82
4.2.2	Study site	82
4.2.3	Classification of phenophases and assessment of phenological conditions of the miombo woodland	84
4.2.4	Delineation of the miombo woodland components used in this study	85
4.2.5	Satellite-based evaporation estimates used in the study	86
4.2.6	Basin water balance-based actual evaporation	86
4.2.7	Satellite-based precipitation products used in this study	87
4.2.8	Runoff data	87
4.2.9	Field observations of woodland canopy phenology	88
4.2.10	Statistical analyses	89

4.3	Results and discussion	91
4.3.1	Basin scale miombo woodland climate and phenological conditions	91
4.3.2	Observed phenological conditions of the miombo woodland	92
4.3.3	Phenophase-based differences in satellite-based evaporation estimates	96
4.3.4	All pairwise multiple comparison of satellite-based evaporation estimates at Luangwa Basin scale	98
4.3.5	Variations within each climate, LAI, NDVI and satellite-based evaporation estimates	99
4.3.6	Differences in spatial distribution of satellite-based evaporation estimates and potential contributing factors	100
4.3.7	Comparison of satellite-based evaporation estimates with the water balance-based actual evaporation	103
4.4	Conclusions and recommendations	105
CHAPTER 5		108
5	Synthesis	108
5.1	Introduction	110
5.2	Limitations of using satellite products for phenology analysis	110
5.3	Relationship of LAI and NDVI with LST and NDII	110
5.4	Miombo canopy phenology, energy partitioning and observed actual evaporation trend	111
5.5	On the comparison of satellite evaporation products in the Miombo ecosystem	113
5.6	Opportunities and challenges with using the DTS approach in the African landscape	114
CHAPTER 6		116
6	Conclusions and recommendations	116
6.1	Introduction	118
6.2	Canopy cover of the miombo woodland and its relationship with vegetation water content and canopy temperature	118
6.3	Phenophase-based evaporation of the miombo woodland	118
6.4	Why do satellite-based estimates behave the way they do?	119
6.5	Outlook	121
References		122
Acknowledgements		145
Curriculum vitae		147
List of publications		148

LIST OF TABLES

	Page
Table 2.1 Characteristics of the MODerate resolution Imaging Spectroradiometer (MODIS) Terra/Aqua surface reflectance data	21
Table 2.2 Repeated measure-analysis of variance (RM-ANOVA) test results for variables	31
Table 2.3 Pearson (r) correlation statistics of the minimum, maximum, and mean values of LAI, LST, NDII, and NDVI at an annual scale	32
Table 2.4 CCR.LM coefficients of estimates and goodness of fit statistics at annual with NDII and LST as predictors	35
Table 2.5 CCR.LM coefficients of estimates and goodness of fit statistics during dry season with NDII and LST as predictors	35
Table 2.6 Petit test results for LAI, LST, NDII and NDVI for the period 2009 – 2018 for the study area	37
Table 2.7 Mann-Kendal trends test results for variables with abrupt change points	39
Table 3.1 Characteristics of the satellite products used in the study	57
Table 3.2 Comparison of the 2021 monthly cumulative evaporation at a miombo woodland in Mpika, Zambia	68
Table 4.1 Characteristics of the satellite products used in the study	87
Table 4.2 Dormant phenophase CV correlation	94

LIST OF FIGURES

	Page	
Figure 1.1	Location and extent of the miombo woodland in Africa	8
Figure 2.1	Extent of the miombo woodland in sub-Saharan Africa and the Luangwa sub-basin of the Zambezi River Basin showing the miombo woodland study location in Zambia.	20
Figure 2.2	Phenology calendar at the miombo woodland site in Mpika, Zambia based on the data for the period 2009 to 2017	27
Figure 2.3	Illustration of (a) seasonal pattern in 8-day mean values of canopy cover (i.e., LAI and NDVI), canopy water content (i.e., NDII) and canopy temperature (i.e., LST) and (b) seasonal pattern in 8-day mean values of actual evaporation (E_a). Shaded area for variables is the 5th and 95th percentiles	28
Figure 2.4	2009–2018 January to December minimum (a) and maximum (b) values of E_a , LAI, NDII, and NDVI	30
Figure 2.5	Correlation of mean values for the 8-day $NDVI_{Mean}$ and LAI_{Mean} with $NDII_{Mean}$ (a, b), as well as with LST_{Mean} (c, d) at the annual scale	32
Figure 2.6	Plots of the CCR.LM results at annual scale (January–December) (a, b) and dry season (May–October) (c, d): LAI regression graphs at annual scale (a) with NDII as only predictor variable and (b) with LST and NDII used simultaneously as predictors	34
Figure 2.7	Plots of the Pettit test for the 8-day LST_{Min} (a), LST_{Max} (b), LST_{Mean} (c), $NDII_{Max}$ (d), $NDVI_{Max}$ (e), and mean annual rainfall (f) for the period of 2009 to 2018 in the miombo woodland in the Luangwa Basin	38
Figure 2.8	Mann–Kendall trends test and the Sens' slope estimates for mean annual rainfall (a), mean annual LAI_{Mean} (b), mean annual $NDII_{Mean}$ (c), mean annual $NDVI_{Mean}$ (d), and mean annual LST_{Mean} (e) for the period of 2009 to 2018	39
Figure 3.1	Location and extent of the miombo woodland in Africa (a), spatial distribution of elevation for the Luangwa Basin (b), and the land cover characterization of the Luangwa Basin and at the study site in Mpika	50
Figure 3.2	Characterisation of canopy phenology at the study site in Mpika, Zambia	51
Figure 3.3	Schematic drawing (not to scale) of the field set-up of the observation tower at the study site in Mpika, Zambia	58
Figure 3.4	Installing the wet (left) and dry (right) fibre optic cable on the observation tower at Mpika site, Zambia	59

Figure 3.5	Comparison of DTS temperature (T_{DTS}) and actual vapour (VP_{DTS}) measurements with the ATMOS-41 ($T_{(ATMOS-41)}$ and $VP_{(ATMOS-41)}$) measurements at 10.5 m and 16.5 m above the woodland canopy	61
Figure 3.6	Daily meteorological conditions at the Mpika study site in the Luangwa Basin for the period May 2021 – December 2021	62
Figure 3.7	Canopy phenophase based hourly averages of wind direction (WD), wind speed (u), Energy flux (EF) (net radiation (R_N), ground heat flux (G_o), latent heat flux (LE) and sensible heat flux (H)), Bowen ratio (BR-DTS) and evaporation (E_a (DTS))	63
Figure 3.8	(a) May – December 2021 daily (6AM - 6PM) estimates of evaporation E_a (DTS) using the BR-DTS and E_c (PM) using the PM. (b) Comparison of dekadal evaporation estimates between E_a (DTS) estimates and E_c (PM) ($E_c = K_C \cdot E_o$)	64
Figure 3.9	Selected aerial view of the upwind direction (east direction) above the woodland canopy from the flux tower (left) at the study site across different phenophases for the year 2021.	65
Figure 3.10	Kendall correlation of $E_{a(DTS)}$ with R_N and NDVI in the Green-down, Dormant and Green-up phenophases of the miombo woodland at Mpika site, Zambia	66
Figure 3.11	Bar graphs with standard deviation error bars comparing dekadal averages of E_a (DTS) and E_c (PM) with satellite products at dekadal scale	68
Figure 3.12	Box plots showing variations in satellite-based evaporation estimates at dekadal scale across phenophases	69
Figure 3.13	Statistics of the comparison of E_a (DTS) to satellite-data evaporation estimates at dekadal scale across phenophases	70
Figure 3.14	Point scale-based correlation of satellite products' spatial resolution with estimates of actual evaporation	75
Figure 4.1	Spatial extent of the miombo woodland in Africa, spatial distribution of elevation and the land cover characterisation for the Luangwa Basin in Zambia	83
Figure 4.2	Characterisation of canopy phenophases of the miombo woodland in relation to seasonality for the Luangwa Basin used in the study	84
Figure 4.3	Delineation of the miombo woodland components used in this study	85

Figure 4.4	Procedure for extending near field observations run-off data for the period 2009 – 2020 using TerraClimate run-off data as the predictor	89
Figure 4.5	Luangwa Basin miombo woodland aggregated 2009-2020 climate and phenological conditions (net radiation (R_N), air temperature (T_a), specific humidity (SH), soil moisture (SM) and precipitation (P))	91
Figure 4.6	Dry season and rainy season tree layer, understory and field components of the miombo woodland site in Mpika, Zambia	92
Figure 4.7	Temporal trend of MODIS LAI, NDVI and the miombo woodland canopy display trend for the year 2021 at the study site in Mpika, Zambia	93
Figure 4.8	Coefficients of variation in the LAI and NDVI values at the dry miombo woodland and wet miombo woodland sites in the Luangwa Basin, Zambia	94
Figure 4.9	Heterogeneity in leaf fall and leaf flush activities among miombo woodland species observed from under canopy and above canopy	96
Figure 4.10	Comparison of aggregated (2009-2020) mean estimates of evaporation by satellite products across hydrological year (September – August) in the Luangwa Basin	97
Figure 4.11	Pixel-based comparison of satellite-based evaporation estimates across phenophases based on hydrological year for the dry and wet miombo Luangwa Basin	97
Figure 4.12	Number of times each satellite-based evaporation estimate was significantly different with one or more other satellite-based evaporation estimates	99
Figure 4.13	Standard deviations and coefficients of variation in estimates of satellite-based evaporation estimates, climate and phenological variables	100
Figure 4.14	Spatial distribution of satellite-based evaporation estimates across phenophases of the miombo woodland in the Luangwa Basin	101
Figure 4.15	Comparison of satellite-based evaporation estimates to the water balance-based estimates of evaporation for Luangwa Basin (a) and the results of the bias assessment (b)	103
Figure 4.16	Basin scale-based correlation of satellite products' spatial resolution with estimates of actual evaporation	104

Chapter 1

Introduction



Photograph showing clouds from under the canopy at the miombo woodland site at Mpika, Zambia
Image: H. Zimba

This chapter is based on:

- Zimba, H., Coenders-Gerrits, M., Banda, K., Hulsman, P., van de Giesen, N., Nyambe, I., and Savenije, H. H. G., 2023. On the importance of phenology in the evaporative process of the miombo woodland: Could it be why satellite-based evaporation estimates differ? *Hydrol. Earth Syst. Sci. Discuss.* [preprint], <https://doi.org/10.5194/hess-2023-39>, in review.
- Zimba, H. M., Coenders-gerrits, M. A. J., Banda, K. E., Schilperoort, B., Nyambe, I., van de Giesen, N., & Savenije, H. H. G., 2022. Measuring evaporation across canopy phenophases of a natural forest : Miombo forest , Southern Africa. *Hydrol. Earth Syst. Sci. Discuss.*, October, 1–23. doi: <https://doi.org/10.5194/hess-2022-303>, in review.
- Zimba, H., Coenders-Gerrits, M., Kawawa, B., Savenije, H., Nyambe, I., & Winsemius, H., 2020. Variations in canopy cover and its relationship with canopy water and temperature in the miombo woodland based on satellite data. *Hydrology*, 7(3). doi: 10.3390/hydrology7030058

Chapter 1

“I know there is pain when saw mills close and people lose jobs, but we have to make a choice. We need water and we need these forests”

(Wangari Maathai)

1.1 Woodlands and evaporation

Global woodland cover accounts for about 31 percent of the total terrestrial land cover (FAO, 2020). Through the processes of precipitation retention, infiltration, interception and transpiration woodlands play a significant role in the global moisture cycle (Arsyad *et al.*, 2019; Bonnesoeur *et al.*, 2019; Sheil, 2018; Van Der Ent *et al.*, 2014; Gerrits, 2010; Van Der Ent *et al.*, 2010; Gajic *et al.*, 2008; Gerrits *et al.*, 2007). Evaporation from woodland surfaces accounts for a significant portion of the water cycle over the terrestrial land mass (Sheil, 2018; Van Der Ent *et al.*, 2014; Gerrits, 2010; Van Der Ent *et al.*, 2010). Understanding the characteristics of various woodland ecosystems evaporation like interception and transpiration, is key for monitoring of climate impact on woodland ecosystems, important for hydrological modelling and the management of water resources at various scales (Kleine *et al.*, 2021; Bonnesoeur *et al.*, 2019; Roberts, (undated)). One of the key aspects to enable this understanding is the knowledge on the woodland phenological interaction with climate variables and seasonal environmental regimes (i.e., Zhao *et al.*, 2013). Solar radiation, temperature and water availability are some of the key environmental variables that influence plant phenology (Forrest *et al.*, 2010; Forrest & Miller-Rushing, 2010; Kramer *et al.*, 2000). The attributes of solar radiation, temperature and water availability differ across the diverse ecosystems globally, therefore, requiring better understanding at a more local or regional level with minimal variations. Yet, evaporation of natural woodlands, especially in African ecosystems, with respect to phenological phases are poorly characterised. This is largely because the development of measuring instruments and models has largely focused on understanding the phenological response of agricultural crops to climate variables and seasons. Furthermore, phenological studies have mainly focused on mid-latitude regions to the exclusion of other regions like Africa (Snyder *et al.*, 2013; Schwartz, 2013). It is important to account for woodland phenology interaction with climate variables and seasons when characterising evaporation in woodlands. This is because, for instance, accounting for phenological phases in evaporation models, increases predictive power (i.e., Forster *et al.*, 2022).

1.2 Plant phenology, energy and water interactions

“Vegetation phenology” refers to the periodic biological life cycle events of plants, such as leaf flushing and senescence, and corresponding temporal changes in vegetation canopy cover (Stöckli *et al.*, 2011; Cleland *et al.*, 2007). Plant phenology and climate are highly correlated (Pereira *et al.*, 2022; Niu *et al.*, 2013; Cleland *et al.*, 2007). Woodland plant phenological response to trigger elements like temperature, hydrological and day light regimes include but not limited to leaf fall and leaf flush, budburst, flowering and variation in photosynthetic activity due to changes in chlorophyll levels (Pereira *et al.*, 2022; Niu *et al.*, 2013; Cleland *et al.*, 2007). The phenological responses are species-dependent and are controlled by adapted physiological properties (i.e., Lu *et al.*, 2006). Plant phenology controls

access to critical soil resources (Nord and Lynch, 2009). The phenological response influences plant canopy cover and affects plant-water interactions. For instance, the phenophases associated variations in canopy leaf display, i.e., due to leaf fall and leaf flush, influences how much radiation is intercepted by plants (Shahidan, Salleh and Mustafa, 2007). Intercepted radiation influences canopy conductance (Jones and Rotenberg, 2001). In water limited conditions, at both individual species and woodland scales, leaf fall reduces canopy radiation interception while leaf flush and the consequent increase in canopy cover increases canopy radiation interception, leading to increased transpiration (Snyder and Spano, 2013) controlled by available moisture storage, both vegetative and root zone. Canopy cover and its interactions with atmosphere carbon dioxide, through the photosynthetic and autotrophic respiration processes, influences transpiration. Ultimately, plant phenological response to changes in the trigger elements influences woodland transpiration and actual evaporation (i.e., Marchesini *et al.*, 2015).

1.3 Remote Sensing, phenology and evaporation modelling

Remote sensing is anchored on the premise that all natural phenomena reflect, absorb and emit energy, albeit at characteristic different wavelengths, both within and outside the visible range of the electromagnetic spectrum (Lillesand *et al.*, 2015; Shefali, 2013). This is applicable to individual plant species, woodlands as ecosystems and many other natural and man-made features. Through changes in the feature dependent spectral reflectance characteristics (i.e., Lillesand *et al.*, 2015), that arise from the energy interactions with specific terrestrial features, in this case plants or vegetation, remote sensing is able to track the changes in plant characteristics that emanate from phenological transitions across seasons such as woodland canopy or leaf cover, leaf fall and leaf flush, changes in leaf colour as well as levels of chlorophyll (Lillesand *et al.*, 2015; Shefali, 2013). For instance, remote sensing is applied to monitor phenology linked vegetation attributes such as vegetation water content (i.e., Zhang *et al.*, 2019), plant stress (i.e., Ramoelo *et al.*, 2015), vegetation classification (i.e., Guerschman *et al.*, 2015), woodland canopy characterisation (i.e., Weishampel *et al.*, 1996; Peterson *et al.*, 1988) and vegetation condition (i.e., Lawley *et al.*, 2016). Neinavaz *et al.* (2021) and Quemada *et al.* (2021) provide comprehensive reviews of remote sensing-based approaches for vegetation monitoring across an array of spectral reflectance regimes related to plant phenophases.

Ascertaining evaporation using field observations is a tedious, complex and expensive undertaking, requiring specific devices and accurate measurements of various physical variables at different intervals and scale (i.e., Jiménez-Rodríguez *et al.*, 2020; Schilperoort *et al.*, 2018; Foken, Aubinet and Leuning, 2012; Gerrits *et al.*, 2009; Gerrits *et al.*, 2007; Dyck 1972). Furthermore, field observations, which are usually point based, are limited in application due to the heterogeneity in the land surface. To bridge these gaps, there has been accelerated development and application of satellite-based approaches to estimate evaporation at local, regional and global scales. Thus, evaporation estimates based on satellite data, to a large extent, are bridging the gaps associated with field data collection, i.e., spatial

and temporal constraints, though the approach comes with its own limitations (McCabe *et al.* 2019; Zhang *et al.*, 2016; Kalma *et al.*, 2008; McCabe and Wood, 2006). For instance, the model structure, inputs and processes of satellite-based evaporation models' result in varied performance (Stisen *et al.*, 2008; McCabe and Wood, 2006; Lakshmi, 2004). For example, McCabe and Wood (2006) showed that remote sensing data input from different sensors (i.e., ASTER, LANDSAT and MODIS) produced different estimates of evaporation and varied in scale behaviour. Additionally, one important limitation of satellite-based evaporation products is the discontinuity in temporal coverage by satellites, which entails having gaps in space and time on evaporation estimates. This creates difficulties for model inter-comparison and requires use of temporal upscaling techniques i.e., Tang *et al.*, (2013) and Ryu *et al.*, (2012) to overcome, though upscaling techniques have their own shortcomings.

A comprehensive review of the satellite-based approaches for computing evaporation was performed by Zang *et al.* (2016). Based on this review, there are at least six approaches on which computation of satellite-based evaporation estimates are anchored, of which four are the most common. Firstly, the Surface energy balance methods (i.e., SEBS (Su, 2002)) that combines the surface energy balance expression and land surface flux equations with remotely sensed temperature. In this approach evaporation is estimated as a residue of the surface energy budget based on the SEBS equation. Secondly, the Penman-Monteith (PM) based methods (Penman 1948; Monteith, 1965) generally compute the ratio of evaporation and latent heat flux directly and/or estimate sensible heat flux in conjunction with the energy balance equation. The success of PM using remote sensing data lies in the accurate estimation of surface/canopy resistance to water vapor or its inverse-surface/canopy conductance. Thirdly, the Priestley–Taylor (PT) (Priestley and Taylor, 1972) model is a simplification of the Penman – Monteith equation and was originally used to estimate evaporation under water unstressed conditions without computing aerodynamic and surface conductance. Lastly, the Water Balance Method in which evaporation is estimated as a residue of the water balance equation. In this approach, change in water storage is obtained by the balance of rainfall, evaporation, and discharge/catchment runoff, often involving conceptual modelling to account for storage variation (e.g., Savenije, 1997). The water balance method is the most used approach in large sparsely gauged basins. This is because despite the challenges with data runoff information in most basins, change in water storage and precipitation can be estimated from satellite data-based products (Stisen *et al.*, 2008; Wang *et al.*, 2015). Some commonly used satellite data based surface energy balance evaporation models, that map actual evaporation with satellite data based on the above approaches include, but not limited to, the Surface Energy Balance Algorithm for Land (SEBAL) (Bastiaanssen *et al.*, 1998), Surface Energy Balance System (SEBS) (Su, 2002), the Operational Simplified Surface Energy Balance (SSEBop) (Senay *et al.*, 2013), the Atmosphere-Land Exchange Inverse (ALEXI) model (Anderson *et al.*, 1997), Moderate-resolution Imaging Spectrometer (MODIS) MOD16 (Mu *et al.*, 2011; Mu *et al.*, 2007), Mapping Evapotranspiration at High Resolution with Internalized Calibration (METRIC) (Allen *et al.*, 2007) and the Global Land Evaporation Amsterdam Model (GLEAM) (Martens *et al.*, 2017; Miralles *et al.*, 2011). Despite the availability of numerous satellite-based evaporation estimates, the challenge now exists in that these products have varying performance outcomes depending on the land

surface. The differences in the outcomes are mainly associated with uncertainties in input data, model structure, model parameters, high number of parameters associated with too limited data, changing hydrological conditions and changes in land cover and use (Miralles *et al.* 2016; Zhang *et al.*, 2016). The overarching consequence of these challenges is that each model's evaluation of evaporation of a same surface (i.e., woodland) differ from each other both in time and space. Furthermore, each model's evaporation assessments are validated using different field approaches such as the Eddy covariance based on different sites of interest. However, the heterogeneity in the earth's landscape implies that model validation results from one point on the earth's surface cannot be used for "all other characteristically similar" locations on the earth surface. This is as a result of the influence of landscape heterogeneity on scaling behaviour of surface fluxes as observed by satellite sensors with different spatial resolutions (Zhang *et al.*, 2016). Furthermore, Bastiaanssen *et al.* (1998) showed that differences in approaches such as integration times (i.e., half hourly or hourly) for measured sensible and latent heat could result in errors. This is because sensible heat flux changes with solar elevation. Furthermore, the importance of evaporation products and calculation procedures have largely been crafted around and often limited to crop productivity. The overall consequence of this is inaccurate estimates of evaporation for other land surfaces and particularly for woodland ecosystems (Coenders-Gerrits *et al.*, 2020). There is, therefore, taking into account the landscape heterogeneity, need for localised modelling and validation of satellite data-based assessments such as the land surface heat fluxes (i.e., sensible and latent heat fluxes) and actual evaporation. What this situation presents is that, in the absence of comparison with field measurements, it becomes extremely difficult, if not impossible, to determine which of the satellite data-based evaporation estimates gives a close representation of the actual field conditions, both in time and space, of a given land surface. In the application of satellite-based evaporation estimates (i.e., at basin level) a lack of validation of these products causes difficulties in accounting for under- or overestimation of the evaporation flux which has significant consequence(s) on the allocation of water for food and energy production, as well as allocation for environmental flows, among many demands for water. Therefore, in order to enhance outcomes in the utilization of satellite-based evaporation estimates, especially with the noted (i.e., Agrawal *et al.*, 2008) climate change impacts in southern Africa, there is need for localized or regionalized land surface specific validation of satellite-based evaporation estimates (McCabe and Wood, 2006; Zhang *et al.*, 2016).

There is increased usage of satellite-based evaporation estimates in the management of water resources globally and in Africa (García *et al.*, 2016; Zhang *et al.*, 2016; Makapela, 2015). However, in Africa, and specifically the miombo woodland region, there is paucity of field observations due to extremely scarce or non-existent flux observation towers. It is, therefore, extremely difficult to select satellite-based evaporation estimates that are close to actual field conditions of the miombo woodland. Some satellite-based evaporation estimates were validated at global scale (i.e., Miralles *et al.* 2016) and across some African basins using two different approaches: flux observations (i.e., Ramoelo *et al.*, 2014), and the water balance (i.e., Blatchford *et al.*, 2020; Dile *et al.*, 2020; Weerasinghe *et al.*, 2020). Results showed that satellite-based evaporation estimates have a mixed performance across ecosystems or land

surfaces, they tend to either overestimate or underestimate actual evaporation. This mixed behaviour of underestimation and overestimation is mainly attributed to the uncertainties associated with model structure, forcing data, model processes and scaling (Pagán *et al.*, 2019). Ramoelo *et al.* (2004) showed significant inconsistencies between EC-actual evaporation observations and MOD16 satellite-based evaporation estimates. Ramoelo *et al.* (2004) attributed these inconsistencies to various factors that included errors in flux tower instruments, flux tower foot print, and the parameterization of the MOD16. While some satellite-based evaporation estimates have been validated in a number of African ecosystems (i.e., Blatchford *et al.*, 2020; Dile *et al.*, 2020; Weerasinghe *et al.*, 2020; Ramoelo *et al.*, 2004), none of the undertakings was performed in the miombo woodland as a characteristic land surface. However, in the miombo woodland, and the Luangwa Basin in particular, satellite-based evaporation estimates appear to perform differently from each other in this unique ecosystem. For instance, satellite products significantly differ in spatial and temporal estimates of actual evaporation across miombo phenophases (i.e., Zimba *et al.*, 2023, under review).

1.4 Field measurements of woodland evaporation

Limitations can be found in all available conventional approaches, such as the eddy covariance (EC) system (Foken *et al.*, 2012; Jarman *et al.*, 2009; Savage *et al.*, 1997), lysimeters (Sutanto, Wenninger, and Uhlenbrook, 2012; Teuling, 2018), scintillometry (Dzikiti *et al.*, 2014; Jarman *et al.*, 2009) and the conventional Bowen ratio (Everson, 2001; Savage *et al.*, 1997; Bowen, 1926). For instance, inability to account for energy fluxes near the observation tower causes energy closure problems in the EC-systems. Additionally, site heterogeneities introduces horizontal and vertical advective terms that are impossible to resolve by single point flux tower measurements (Foken *et al.*, 2012; Liu *et al.*, 2006). Furthermore, if the optical path is obscured, such as occurs in wet conditions, the EC's optical open-path sensors do not work properly and if the open-path analyzer is wet the evaporation which occurs shortly after a rainfall event is not observed (Coenders-Gerrits *et al.*, 2020; Hirschi *et al.*, 2017). In the case of the two vertical sensor-based Bowen ratio, each sensor has its own errors which are propagated to the Bowen ratio. Additionally, it is difficult to ensure that the two sensors are correctly aligned with each other which results in incorrect Bowen ratio estimates (Angus and Watts, 1984; Spittlehouse and Black, 1980). Jarman *et al.* (2009) assessed and reported on various conventional methods for estimating evaporation in different land surfaces in south Africa.

However, recent advances in the distributed temperature sensing system has expanded possibilities for improved accuracy in energy partitioning and the application of the Bowen ratio for evaporation flux assessment in forests (Euser *et al.*, 2014; Schilperoort *et al.*, 2020; Schilperoort *et al.*, 2018). In contrast to the conventional Bowen ratio approach, the Distributed Temperature Sensing Bowen ratio technique (BR-DTS) makes use of several vertical high resolution temperature measurements made with a single fibre optic cable. This eliminates the need for the conventional configuration with two individual sensors at different

locations and the associated errors with this type of set up. One section of the fibre optic cable measures the air temperature profile, while a second section, covered in a constantly wetted cloth, measures the wet-bulb temperature profile. The vapour pressure profile can be derived through the psychrometer principle. The DTS technique enables that wet and dry bulb temperature measurements can cover the entire vertical profile through a woodland stand: above the woodland canopy, within the canopy, and under the canopy. This is conducted simultaneously along a single fibre optic cable, thereby facilitating a deepened understanding of the energy partitioning in a woodland (Schilperoort *et al.*, 2020; Schilperoort *et al.*, 2018; Euser *et al.*, 2014). Coenders-Gerrits *et al.* (2020) have suggested that the DTS technique offers opportunities to assess woodland energy storage components that are not normally captured when using conventional approaches. The BR-DTS approach provides an avenue for enhanced understanding and increased accuracy in the estimation of woodland evaporation. This is notwithstanding the challenges associated with the BR-DTS approach such as the requirement for sufficient ventilation and constant wetting of the fibre optic cable. Furthermore, compared to the EC method the BR-DTS approach tends to minimally overestimate diurnal latent heat flux (LE) by a mean difference of 18.7 Wm^{-2} (Schilperoort *et al.*, 2018). Additionally, despite the highlighted advantages of the BR-DTS approach its major limitation is that it is a point measurement.

For the miombo Woodland, the need for field-based actual evaporation estimates is highlighted by the discrepancies in satellite-based evaporation estimates (Zimba *et al.*, 2023 under review). Due to a lack of field-based observations of actual evaporation of the miombo woodland the satellite-based evaporation estimate(s) that are close to field conditions are unknown. Therefore, an independent energy partitioning and estimates of miombo woodland actual evaporation that can be used to validate satellite-based evaporation estimates is of great importance in the management of water resources in this ecosystem.

1.5 Why the miombo woodland

The miombo is the largest tropical seasonal woodland in sub-Saharan Africa with a spatial extent of between 2.7 and 3.6 million square kilometres (Fig 1.1; White, 1983). The woodland forms the transition zone between the tropical rainforest and the African savanna woodland. The average annual rainfall and temperature in the miombo woodland is in the range 710–1365 mm/year and 18.0–23.1 °C, respectively (Chidumayo *et al.*, 2010; Chidumayo, 2001; Frost, 1996; White, 1983).

The miombo woodland plays a crucial role in the water, energy and food nexus of the countries it covers. For instance, the woodland provides food (wild foods and agriculture) and energy (i.e., firewood and charcoal) to millions of people across the countries it services (Gumbo *et al.*, 2018; Frost, 1996).

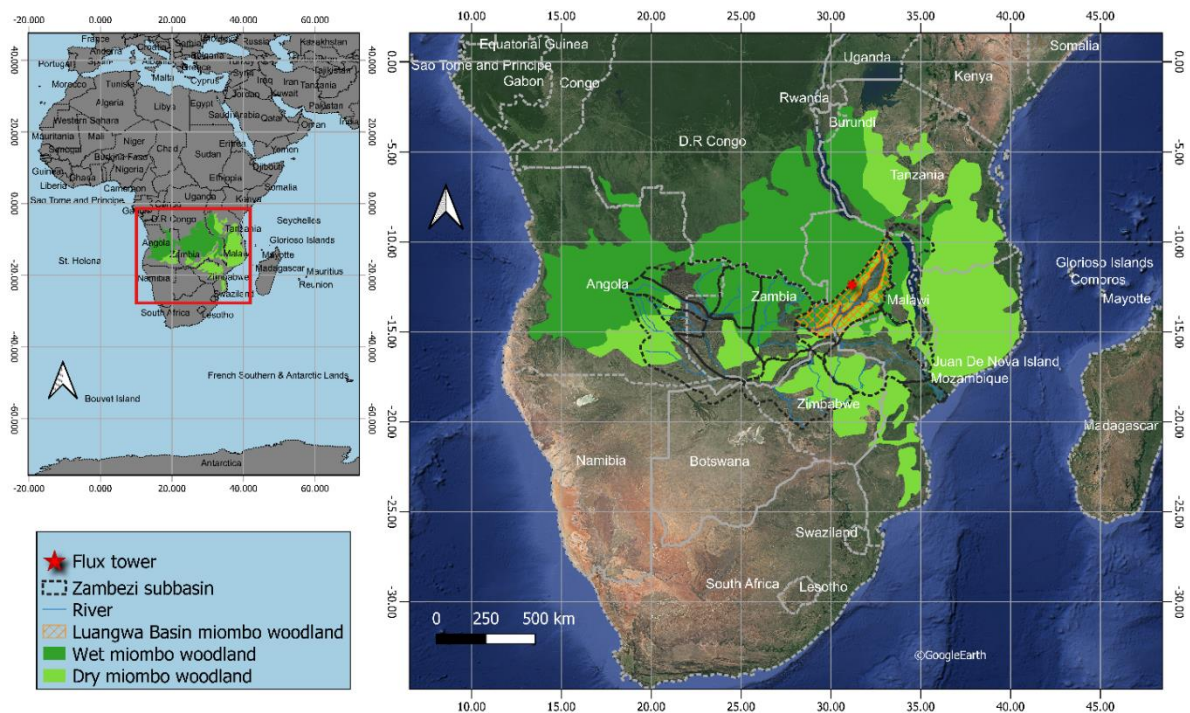


Figure 1.1: The location and extent of the miombo woodland in Africa. Much of the Zambezi River Basin is covered by the miombo woodland. Major rivers in the Zambezi Basin have their sources in the miombo woodland.

Some major rivers, like those in the Zambezi Basin i.e., Zambezi River and its tributaries like the Luangwa and Kafue rivers, have their source in and whose catchment areas are largely covered by miombo woodland. Therefore, the woodland is likely to have significant transboundary impact on water availability due to evaporation, surface run-off and ground water recharge. Water availability consequently affects irrigation and hydro power generation projects placed on some of the rivers i.e., Zambezi River (Beilfuss, 2012).

The uniqueness, compared to other global ecosystems, of the plant-water interactions of the miombo woodland has been highlighted (Tian *et al.*, 2018; Guan *et al.*, 2014; White, 1983), and has been particularly demonstrated by Vinya *et al.*, (2018), Fuller (1999), Frost (1996) and White (1983). Of importance is the adapted endogenous whole-plant control of leaf phenology (i.e., Vinya *et al.*, 2018), simultaneous leaf fall and leaf flush (i.e., Fuller, 1999) and deep rooting which gives ability to the plants to access groundwater resources to buffer the dry season water limitations (Tian *et al.*, 2018; Guan *et al.*, 2014, Savory, 1963). The miombo woodland is heterogeneous with diverse plant species whose phenological response to stimuli is characteristically species dependent (Chidumayo, 2001; Fuller, 1999; Frost, 1996). For instance, leaf fall, leaf flush and leaf colour change are triggered at different times for each species. This means that for the miombo woodland, unlike what obtains in other homogenous woodlands in which the entire woodland is either undergoing leaf fall or leaf flush, the leaf fall and leaf flush occur simultaneously. This results in a woodland canopy that is variable in terms of canopy closure and greenness especially during the dry season. To this effect the miombo woodland has varied canopy closure ranging between 2 to about 70

percent depending on the miombo woodland strata and local environmental conditions such as rainfall, soil type, soil moisture, species composition and temperature (Chidumayo, 2001; Fuller, 1999; Frost, 1996). For the wet miombo woodland with a canopy closure of about 70 percent, at any given time, there is a relatively large woodland canopy surface for radiation/energy interception. The deep rooting in most miombo woodland species (Savory, 1963) provides access to deep soil moisture resources (Fan *et al.*, 2017; Kleidon and Heimann, 1998). The deep rooting miombo woodland green canopy provides an evaporative surface that, in combination with other environmental variables, possibly facilitates continued transpiration even during the driest periods within moisture stress threshold (i.e., Li *et al.*, 2021). The question is whether actual field evaporation reflects this interaction. Additionally, do satellite-based evaporation estimates capture the various phenological transitions and account for this unique miombo woodland species dry season canopy cover–water interaction within the available energy and soil moisture dynamics at play? Regardless the above highlighted importance of the woodland, there exists scant, if any, information on the woodland evaporation dynamics. This is due to lack of flux observation towers in the entire miombo woodland. Furthermore, the studies conducted in the miombo woodland have tended towards the characterisation of woodland plant species, its role as a carbon sink and the social-economic relevance of the ecosystem. Information on the phenology of the ecosystem exists (i.e., Chidumayo *et al.*, 2010; Chidumayo, 2001; Fuller, 1999; Chidumayo and Frost, 1996), but there has been no attempt to characterise energy partitioning and evaporation patterns linking them to the phenology of the ecosystem with access to ground water resources, especially during the water scarce dry season. The above assertions are made with reference to publications in public domain.

1.6 Problem statement

Globally the advent of climate change has pressed demand on the need for efficient and integrated management of available scarce water resources (Giupponi *et al.*, 2017; Savenije *et al.*, 2008) especially in developing countries that are already grappling with adaptation to its impacts (Agrawal *et al.* 2008). Of great importance in the climate adaptation agenda and process is the availability of locally generated information (Agrawal *et al.*, 2008). The role of accurate information to enable generation of appropriate adaptation interventions cannot be overemphasized (Sebestyén *et al.*, 2021; UNFCCC, 2020; Kusangaya *et al.*, 2014). Evaporation is a key in water resources management as it is an important determinant of water availability and consumption (Dimitriadou *et al.*, 2021; Condon *et al.*, 2020; Konapala *et al.*, 2020) by various competing uses. Evaporation is and will continue to be affected by climate change (Yang *et al.*, 2015; Snyder *et al.*, 2011).

With respect to publications in the public domain, field-based information on evaporation in the miombo woodland in sub-Saharan Africa is not available. Furthermore, satellite-based evaporation estimates are not validated with data from the miombo ecosystem. What has happened is that water resources managers arbitrary use satellite-based evaporation estimates without knowing the degree of uncertainty. In most cases choice of satellite-based evaporation estimates to use is based on validation results in non-miombo ecosystems. The

challenge with this satellite-based evaporation estimates choice scenario is that non-miombo ecosystems have different phenology and evaporation to that of the miombo ecosystem. For instance, satellite-based evaporation estimates that performs extremely well in energy limited conditions and homogenous woodland type i.e., in Europe, cannot be assumed to have the same performance in a warm, water limiting and heterogeneous woodland like the miombo woodland.

Overall, the lack of miombo woodland evaporation information means that water resources at various scales i.e., local catchment and transboundary, are being managed using unverified information. This state likely has many negative cascading implications across the water use spectra in the miombo woodland region. The reason for non-availability of evaporation information is because there are currently no flux observation towers in the miombo ecosystem. This scenario, if left unabated, has potential to continue to negatively affect water resources management in the miombo woodland region.

It is important that field estimates of evaporation of the miombo woodland across the many miombo strata and phenophases are made available. This will facilitate deepened understanding of the evaporation dynamics, and at the same time provide information for comparison with satellite-based evaporation products, enabling the selection of an appropriate product to use in a given miombo region basin. This in return will enhance hydrological and climate modelling, consequently resulting in improved efficiency in the overall water resources management standard in the region.

1.7 Research objectives

This thesis is about contributing to the understanding of the evaporation dynamics in Africa's miombo woodland. The focus was deliberately on the dry season, which is characterised by different vegetation phenophases and water availability unique to the miombo woodland. The study sought to contribute to the filling of information gaps with respect to the energy partitioning and the diurnal and phenophase-based evaporation pattern (i.e., trend and magnitude). Additionally, the study sought to establish the extent of agreement between commonly used free of charge satellite-based evaporation estimates with field observations.

Therefore, the specific objectives of this study were:

1. To characterise the phenophase-based changes in the woodland canopy cover of the miombo woodland in relation to the woodland canopy vegetation water content and the woodland canopy temperature using satellite data;
2. To characterise the Bowen ratio of the miombo woodland across the different phenophases in the dry season and the early rainy season;
3. To partition the available energy into sensible and latent heat fluxes across the different phenophases of the miombo woodland in the dry season and early rainy season;

4. Characterise actual evaporation according to the phenophases of the miombo woodland;
5. Compare four commonly used free of charge satellite-based evaporation estimates to field estimates of actual evaporation across the different phenophases of the wet miombo woodland in the dry season and early rainy season;
6. To compare trends and magnitude of commonly used free of charge satellite-based evaporation estimates in the miombo woodland;
7. To compare free of charge satellite-based evaporation estimates to the general annual water balance-based actual evaporation estimates for the Luangwa Basin.

The above objectives were meant to help answer the following questions.

1. What are the changes in the woodland stand canopy cover, canopy vegetation water content and the canopy temperature with respect to the phenology of the miombo woodland?
2. What are the relationships between the woodland stand canopy cover and the canopy vegetation water content and canopy temperature of the miombo woodland?
3. How is the available energy partitioned in the different phenophases of a wet miombo woodland in the dry season and the early rainy season?
4. What is the trend and magnitude of actual evaporation across the phenophases of the wet miombo woodland in the dry season and early rainy season?
5. How do the satellite-based evaporation estimates perform in estimating actual evaporation in the different phenophases of the wet miombo woodland in the dry season and early rainy season?
6. What could be the potential reasons for the behaviour of each satellite-based evaporation estimate in relation to field-based actual evaporation estimates across the different phenophases of the miombo woodland in the dry season and early rainy season?
7. In which phenophases of the miombo woodland do the satellite-based evaporation estimates differ/agree?
8. What could be the contributing factors to the observed differences/agreements of satellite-based evaporation estimates?
9. Do satellite-based evaporation estimates agree with the water balance-based estimates of actual evaporation at the Luangwa Basin scale?

1.8 Thesis structure

The thesis structure is based on the objectives and research questions of the study. Chapter 1 gives the introduction to the concept of phenology. The chapter also highlights available satellite-based evaporation estimates. Field-based evaporation assessment methods are briefly discussed. In chapter 1 the uniqueness of the phenological characteristics of the miombo woodland species is highlighted. The chapter further shows the miombo woodland as an important ecosystem in sub-Saharan Africa's energy, food and water nexus. Under chapter 1 the existing challenges in assessing actual evaporation of the miombo woodland

are discussed. Finally, the importance of this study in bridging the observed challenges is presented.

Chapter 2 characterises the canopy phenology of the miombo woodland in relation to the canopy vegetation water content and the canopy temperature using satellite-based proxies NDII, NDVI, LAI and LST. Literature on the woodland canopy cover in relation to water and temperature for the miombo woodland was also consulted. Chapter 2 is aimed at objective 1 and answers research questions 1 and 2. It was found that canopy cover varied with the changes in the woodland canopy vegetation water content and the canopy temperature across phenophases. It appeared the canopy vegetation water content accounted for more variations in the canopy cover proxies, LAI and NDVI, than the canopy temperature. The lowest woodland canopy cover was observed during the period with the lowest vegetation water content in the dormant phenophase. The question that followed was to investigate if field observations and satellite-based evaporation estimates also followed this trend.

The point scale phenophase-based available energy partitioning into sensible and latent heat fluxes, daily estimates of the actual evaporation and the comparison to free of charge satellite-based evaporation estimates is presented in chapter 3. In this chapter the BR-DTS approach is used to estimate the Bowen ratio at hourly scale across the different phenophases in the dry season and the early rainy season. Using the Bowen ratio, the available energy is partitioned into sensible and latent heat fluxes. Using the energy balance equation, the actual evaporation is estimated diurnally at hourly interval then summed up into daily and 10-day estimates. The 10-day DTS-based actual evaporation estimates are then compared to 10-day values of satellite-based evaporation estimates according to phenophases i.e., green-down, dormant and green-up phenophases. The potential contributing factors to the observed behaviour of each of the satellite-based evaporation estimate is discussed. It appeared the actual evaporation of the wet miombo woodland followed more the changes in available energy than the changes in the canopy cover. Generally, all satellite-based evaporation estimates underestimated actual evaporation in the dormant and green-up phenophases in the dry season and early rainy season. Chapter 3 is directed at objectives 2 to 5 and answers research questions 3 to 5.

In chapter 4 six satellite-based evaporation estimates are compared across different phenophases. This was meant to observe the extent to which satellite-based evaporation estimates differed or agreed, in terms of trend and magnitude, in each phenophase, and what could be the contributing factors. Additionally, the annual water balance approach is used in which basin scale actual evaporation is estimated as a residue of precipitation and runoff. This component of the study was aimed at establishing whether the satellite-based evaporation estimates underestimated/overestimated actual evaporation at basin scale. Chapter 4 is aimed at achieving objectives 6 and 7 and answers research questions 7 - 9. It was observed that major discrepancies among satellite-based evaporation estimates are in the dormant and green-up phenophases of the miombo woodland. Direct integration of the soil moisture component in satellite-based evaporation estimates could be a key factor which contributed to the observed differences in the dry season and early rainy season. When compared to the water balance-based actual evaporation estimates all satellite-based

evaporation estimates underestimates actual evaporation of the Luangwa Basin.

In conclusion chapter 5 discusses the findings in chapters 2, 3 and 4 while chapter 6 provides an overview of the major conclusions and recommendations. Furthermore, chapter 6 looks at the potential areas for further research in order to augment and solidify the understanding of evaporation dynamics in the miombo ecosystem, especially that field estimates of evaporation in this study were focused only on the wet Zambezian miombo woodland. For an overall conclusive overview on the evaporation dynamics there is need to assess actual evaporation of the various miombo woodland strata.

Chapter 2

Canopy phenology of the miombo woodland and its relationship with climate variables



Photograph showing canopy of the miombo woodland and clouds viewed from the flux tower at the Mpika site, Zambia

Image: Henry Zimba

This chapter is based on:

Zimba, H., Coenders-Gerrits, M., Kawawa, B., Savenije, H., Nyambe, I., & Winsemius, H., 2020. Variations in canopy cover and its relationship with canopy water and temperature in the miombo woodland based on satellite data. *Hydrology*, 7(3). doi: 10.3390/hydrology7030058

Chapter 2

“Imiti ikula empanga”

(Small growing trees become a forest)

(African Proverb)

2.1 Introduction

The miombo woodland is Africa's largest tropical seasonal woodland and dry woodland formation spread in 11 countries and covering an area between 2.7 and 3.6 million km² (Gumbo *et al.*, 2018; Frost, 1996). The woodland forms the transition zone between the tropical rainforest and the African Savannah. Being a transition zone, it is probably sensitive to climate change where dry-out could possibly trigger ecosystem shifts. The word miombo is used to describe *Brachystegia*, one of the many species found across the ecosystem. The miombo ecoregion plays a crucial role in the food, water and energy nexus in sub-Saharan Africa and maintain carbon stocks, thus regulating climate (Gumbo *et al.*, 2018; Pelletier *et al.*, 2018; Jew *et al.*, 2016; Munishi *et al.*, 2010). Furthermore, studies (Sutanto *et al.*, 2012; Gerrits, 2010) showed that woodlands, such as the miombo woodland, plays a critical role in the water balance by affecting the land surface water interaction such as precipitation canopy interception and extraction of soil water via the transpiration process. However, rising temperatures, changing precipitation regimes and changes in the amount of carbon dioxide are expected to affect phenology, composition, structure, distribution and succession processes of woodlands (Gumbo *et al.*, 2018; IPCC, 2007). Thus, the relationships of canopy cover with variables such as canopy water and temperature must be well understood and consequently taken into account in climate and hydrological modelling (Wegehenkel, 2009) in the miombo woodland. However, the species composition, richness and heterogeneity (even at local woodland level) (Gonçalves *et al.*, 2017; Giliba *et al.*, 2011; Frost, 1996; Chidumayo, 1987) and the vastness of the miombo ecosystem in sub-Saharan Africa makes it impossible to employ field observations at a scale capable of capturing an acceptable representation of, for instance, the various plant-water and plant-temperature dynamics of the ecosystem. For instance, field data-based studies like Vinya *et al.* (2018) and Chidumayo (2001) only considered a few miombo species out of the many that exist in the miombo ecosystem. Furthermore, in addition to financial limitations, field observations normally are spatially and temporally constrained. This has possibly contributed to the paucity of data on the various aspects of woodland-climate interactions in the miombo ecosystem. The application of satellite based remote sensing techniques in assessing woodland-climate interaction provides a significant and expanded platform for data collection and monitoring of the dynamic state of woodlands, especially for vast transboundary woodlands like the miombo woodland where ground-based methods are virtually not feasible. This is because satellite remote sensing comes with the advantage of area coverage (spatial resolution), regular revisit time (temporal resolution), acquisition of data in a wide range of the electromagnetic spectrum (spectral resolution) and has a high degree of homogeneity. Furthermore, a large number of satellite sensors, with global coverage, are currently generating enormous amounts of data at various resolutions that form the base for both historical and continued monitoring of woodland-climate interactions (Lechne *et al.*, 2020; Lausch *et al.*, 2017; Wang *et al.*, 2010; Wulder & Franklin, 2003). This is even more important for Africa with limited capacity to undertake field measurements.

Some studies, including satellite data-based ones, related to plant-water and plant-temperature interaction have been conducted, in the Savannah woodland in general and miombo woodland in particular (Vinya *et al.*, 2018; Tian *et al.*, 2018; Chidumayo, 2001;

Botta *et al.*, 2000; Jeffers & Boaler, 1966; Woodward, 1988). However, the type of satellite data used and the climate variables considered leave room for further investigations using other freely available satellite data products such as the Moderate Resolution Imaging Spectroradiometer (MODIS). For instance, most previous studies used air temperature and rainfall to understand the plant water and plant-temperature relationships in the miombo woodland. These studies suggested that the miombo woodland is water controlled and that temperature could be a critical determinant of plant distribution (Vinya *et al.*, 2018; Tian *et al.*, 2018; Chidumayo, 2001; Botta *et al.*, 2000; Woodward, 1988; Jeffers & Boaler, 1966). The satellite data-based studies typically used air temperature and Normalised Difference Vegetation Index (*NDVI*) (Rouse *et al.*, 1973) i.e., Chidumayo (2001), the Leaf Area Index (*LAI*), transpiration and Vegetation Optical depth (*VOD*) (i.e., Tian *et al.*, 2018) to understand the relationships. Chidumayo (2001) analysed the relationship between rainfall, minimum and maximum air temperature with the *NDVI*. Chidumayo (2001) observed that combined minimum and maximum temperature accounted for the largest variation (R^2 0.96) in *NDVI* values followed by rainfall ($R^2 = 0.35$). Further, Chidumayo (2001) observed a negative relationship between *NDVI* and maximum temperature. Tian *et al.* (2018) studied seasonal variations in ecosystem-scale plant water storage and their relationship with leaf phenology. They found that in the miombo woodland transpiration co-varied with *LAI* seasonal variations. They further observed that plant water storage played a critical role in “buffering seasonal dynamics of water supply and demand, and sustaining fresh leaves formed before the rain”.

However, climate variables such as Land surface temperature (*LST*), which is the radiative skin temperature of a surface derived from remotely sensed thermal radiation, is increasingly becoming more useful in hydrological modelling, vegetation monitoring, global circulation models-GCM and many more applications (García-Santos *et al.*, 2018; Hulley, 2017; Avdan & Jovanovska, 2016; Sun *et al.*, 2016; Li *et al.*, 2013; Cammalleri & Vogt, 2005; Dash *et al.*, 2002; Jones & Rotenberg, 2001). The surface temperature is regarded as a direct representation of the canopy thermal status due to its interaction with radiation (long wave and short wave) and other biotic and abiotic processes (Jones & Rotenberg, 2001). The *LST* is considered as a significant variable in controlling several environmental factors including the hydrology, carbon cycle and the land surface energy budget (Sun *et al.*, 2016). In the case of the miombo woodland (Mildrexler, Zhao, & Running, 2011) showed that during the dry season, with reduced canopy cover, the *LST* is higher than air temperature in African Savannah woodland. Furthermore, during the period of high moisture (i.e., rainy season) and high canopy cover maximum *LST* is almost 1:1 ratio with the maximum air temperature. The surface in the case of the miombo woodland would largely be the woodland canopy. The discrepancy between *LST* and air temperature in the dry season could possibly render different results from those observed with the use of air temperature. This makes it necessary to understand the *LST* (as proxy for canopy temperature) interaction with canopy cover proxies such as the *LAI* and *NDVI*. Based on increased application of *LST* in vegetation monitoring and climate and hydrological modelling the use of *LST* to understand the canopy cover and canopy temperature relationship in the miombo woodland could be a significant addition to the body of knowledge on the miombo ecosystem.

In the context of plant water assessment using satellite data, Mobasher & Fatemi (2013) showed that there exists strong correlation between equivalent water thickness (ETW) (defined as the weight of water per unit area of leaf) and the Near Infrared (NIR) and Shortwave Infrared (SWIR) wavelengths in the electromagnetic spectrum. Additionally, they showed that band combinations such as ratio and normalized difference had higher regressions with leaf water content. Some satellite data-based indices such as the Normalised Difference Infrared Index (*NDII*) (Fensholt & Sandholt, 2003), a normalised band ratio, have shown capacity as proxy for both the vegetation water content and root-zone storage and is, therefore, being used in hydrological modelling (Sriwongsitanon *et al.*, 2015; Yilmaz, Hunt Jr, & Jackson, 2008; Gao, 1996; Hunt & Rock, 1989; Hardisky, Klemas, & Smart, 1988). When plant water balance is considered, rainfall can generally be assumed as the gross water received in a woodland (Gerrits, 2010; Marin, Bouten, & Sevink, 2000). The vegetation water content and root-zone storage (i.e., as proxied by *NDII*) can be considered more representative of the net water available for use by plants. What is also important is that the *NDII* can be derived from freely available optical satellite data from sensors such as the Moderate Resolution Imaging Spectroradiometer (MODIS). Therefore, instead of the use of the VOD as proxy for vegetation water (Tian *et al.*, 2018) or rainfall to indicate water availability (Chidumayo, 2001) this study used the Normalised Difference Infrared Index (*NDII*) as proxy for the woodland canopy water content.

When it comes to observing canopy cover and vegetation density the *LAI* i.e., the one-sided green leaf area per unit ground surface area in broadleaf canopies (Myneni & Park, 2015) and the *NDVI* (Rouse *et al.*, 1973) i.e., measure of density of vegetation, have been used to assess canopy cover in dry woodlands of Africa and the miombo woodland in particular (Tian *et al.*, 2018; Chidumayo, 2001; Fuller *et al.*, 1997). For instance, Fuller *et al.* (1997) used the radiative transfer model to demonstrate the *NDVI* as a good predictor of canopy cover in the miombo woodland in Zambia. In this study MODIS based *LAI* and the *NDVI* were utilised as proxies for canopy cover.

The premise for the use of the MODIS data is that it is readily available for free, has a near-global spatial coverage (250m-1km) suitable for assessing vegetation dynamics in a vast woodland like the miombo woodland, has a comparatively better temporal scale (1-2 times/day) and can easily be processed with most available imagery computing applications. Other than the availability of raw data MODIS also has several ready to use highly processed products including but not limited to vegetation indices, land surface temperature and evaporation (Cano *et al.*, 2017; Running, 2017; Didanet *et al.*, 2015; Myneni & Park, 2015; Ticehurst *et al.*, 2014; García-Mora, Mas, & Hinkley, 2011; Vermote, Kotchenova & Ray, 2011; Reeves, Zhao, & Running, 2017; Dash *et al.*, 2002). These attributes make MODIS data suitable for application at local, catchment and regional scales in a cheaper and timely manner especially in the African context with limited capacity to deploy field-based assessments.

To better understand the interaction of canopy cover with canopy water content and canopy temperature this study used several statistical approaches. Key among the statistical analyses was the Correlated Component Regression Linear Model (CCR.LM) (Magidson, 2013). The most significant attributes for selecting the CCR.LM was the capacity to account

for multicollinearity in predictor variables and to eliminate less important predictor variables, using the step-down variable reduction approach, based on importance in affecting the response variable. By using the CCR.LM we sought to evaluate which of the two variables i.e., canopy water content (proxied by *NDII*) and canopy temperature (proxied by *LST*) accounted for the most variations in the canopy cover at different time scales and seasons. This was important for comparison with the previous studies that used rainfall and air temperature to analyse the interactions with canopy cover.

This paper, therefore, describes the results of the assessment of the variations in the canopy cover (proxied by the *LAI* and the *NDVI*) and its relationship with the canopy water content (proxied by the *NDII*) and temperature (proxied by the *LST*) in the miombo woodland using MODIS satellite based-data. The objectives of this study were to: (i) to analyse the seasonal and inter-annual patterns in the woodland canopy cover, canopy water content and canopy temperature, (ii) to ascertain correlation of the canopy cover with the canopy water content and the canopy temperature, (iii) to determine the most determinant factor of the variations in the woodland canopy cover between the canopy water content and the canopy temperature in the miombo woodland, and to (iv) to observe if any significant change points and historical trends in the means of the canopy cover, canopy water content and canopy temperature occurred in the period 2009 – 2018. The analysis of change points and historical trends was meant to further understand the relationships between the canopy cover, the canopy water content and canopy temperature in the miombo woodland. The results of the study could be useful to the monitoring of impact of climate change on the miombo woodland phenology.

2.2 Materials and methods

2.2.1 Study site

The miombo woodland is situated within the southern sub-humid tropical zone of Africa with mean annual precipitation and mean annual temperature in the range 710-1365 mm/year and 18.0 - 23.1°C, respectively. In the Luangwa Basin, in Zambia, where the study was focused (Fig. 2.1), the rainy season is between October and April of a hydrological year. The dry season, May to October, is split into the cool dry (May to August) and hot dry (August to October). The rainfall is a result of the movements of the Inter-Tropical Convergence Zone (ITCZ) over Zambia between October and April of a hydrological year (Beilfus, 2012; Timberlake & Chidumayo, 2001; Frost, 1996). The study was centred on miombo woodland at Nsansala and Mutinondo conservancy areas (lat: -12.4°S, long: 31.2°E) in Mpika District which falls in the central Zambebian miombo, in the north western part of the Luangwa Basin (Fig. 2.1). The location is a conservancy with extremely limited and controlled anthropogenic activities.

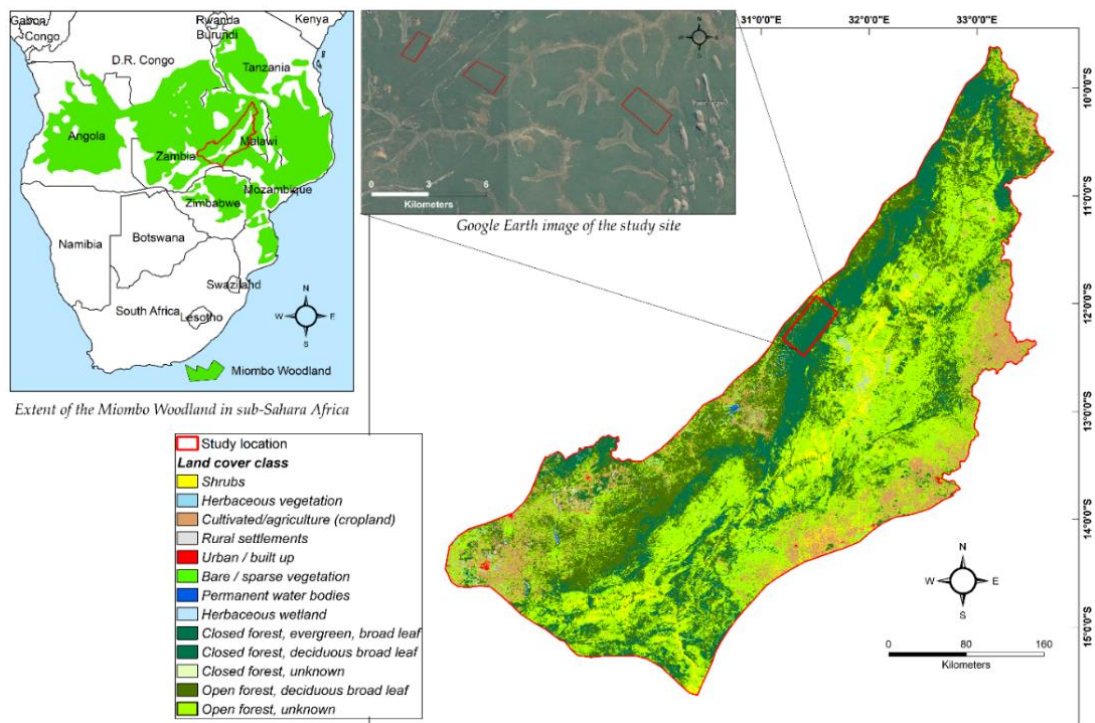


Figure 2.1: Extent of the miombo woodland in sub-Saharan Africa and the Luangwa sub-basin of the Zambezi River Basin showing the miombo woodland study location in Zambia. The studied miombo woodland is located within the central Zambezian miombo woodland, which is the largest miombo subgroup. Map of miombo woodland adapted from the miombo network (miombo Network, 2020). Land cover map was adapted/based on the 2018 Copernicus global land cover map for Africa.

The woodland is largely in its natural state. The central Zambezian miombo is the largest of the four miombo sub-groups the other three being the Angolan miombo, Eastern miombo and the Southern miombo (miombo Network, 2020). According to Frost (1996) Zambia has possibly the highest diversity of trees and is said to be the centre of endemism for *Brachystegia*, with 17 species. The miombo is a heterogeneous woodland of the genus *Brachystegia* with the dominant species in the study location being *Brachystegia longifolia*, *Brachystegia boehmii*, *Brachystegia speciformis* and *Jubenerdia paninculata*. Leaf fall and leaf flush occur in the dry season between May and October (Vinya *et al.*, 2018; Timberlake & Chidumayo, 2001; Frost, 1996; Chidumayo, 1987).

2.2.2 Description of data sets

Climate and hydrological data i.e., modelled precipitation, were retrieved from the National Ocean and Atmospheric Administration (NOAA) Climate Forecast System Reanalysis (CFSR) model which uses satellite data (Saha *et al.*, 2014; Saha *et al.*, 2010) at 19200 m (1/5-deg) spatial resolution and daily temporal resolution using the Climate Engine (<https://clim-engine.appspot.com/climateEngine>). The daily precipitation values were summed into 8-day values to match the temporal resolution of the rest of the data sets. MODIS surface reflectance (MOD09A1/MYD09A1) (Vermote, Kotchenova, & Ray, 2011)

data used to compute the *NDVI* and *NDII* at 8-day temporal scale and 500m spatial resolution was obtained from the climate engine (<http://clim-engine.appspot.com/climateEngine>). MODIS surface reflectance (MOD09A1/MYD09A1) is a 7-band level 3 surface reflectance product with band characteristics as indicated in Table 2.1. Each product pixel contains the best possible level 2 gridded observation during an 8-day period as selected on the basis of high observation coverage, low view angle, absence of clouds or cloud shadow, and aerosol loading. The MOD09A1/MYD09A1 product has been corrected for the effects of atmospheric gases and aerosols (Vermote, Kotchenova, & Ray, 2011).

Table 2.1 Characteristics of the MODerate resolution Imaging Spectroradiometer (MODIS) Terra/Aqua surface reflectance data. NIR = Near-infrared and SWIR = Shortwave infrared

Band No.	Visible Range	Band Centre (nm)	Wavelength Range (nm)	Resolution (m)	Key Applications
B01	Red	648	620–670	500	Absolute land cover transformation, vegetation chlorophyll
B02	NIR-1	858	841–876	500	Cloud amount, vegetation, land cover transformation
B03	Blue	470	459–479	500	Soil/vegetation differences
B04	Green	555	545–565	500	Green vegetation
B05	NIR-2	1240	1230–1250	500	Leaf/canopy differences
B06	SWIR-1	1640	1628–1652	500	Snow/cloud differences
B07	SWIR-2	2130	2105–2155	500	Cloud properties, land properties

The *NDVI* is estimated using the ratio based on the Red (R) and Near Infra-red (NIR) bands in Eq. 2.1 while the *NDII* is estimated using ratios of different values of near infrared reflectance (NIR) and short-wave infrared reflectance (SWIR) as expressed in Eq. 2.2.

$$NDVI = \frac{(NIR - R)}{(NIR + R)} \quad (2.1)$$

$$NDII = \frac{(NIR - SWIR)}{(NIR + SWIR)} \quad (2.2)$$

Satellite data-based Leaf Area Index (LAI) (MCD15A2H/MYD15A2H) (Myneni & Park, 2015) at 8-day interval and 500m spatial resolution were obtained using the Moderate Resolution Imaging Spectroradiometer (MODIS) Global Subset Tool (<https://modis.ornl.gov/cgi-bin/MODIS/global/subset.pl>). The LAI algorithm consists of a main look-up table (LUT) based procedure that exploits spectral information content of the MODIS red (648nm) and near-infrared (NIR) (858 nm) surface reflectances and the back-up algorithm that uses empirical relationships between the *NDVI* and canopy LAI and the Fraction of Absorbed Photosynthetically Active Radiation (FPAR). The MODIS LAI algorithm accounts for sun-sensor geometry. To augment the observations from the LAI and *NDVI* the MODIS phenology data the collection 6 MCD12Q2 (C6 MCD12Q2) (Gray *et al.*, 2019; Friedl *et al.*, 2019; Zhang *et al.*, 2003) was used. The C6 MCD12Q2 derives phenometrics from the 2-band Enhanced Vegetation Index calculated from MODIS nadir bidirectional reflectance distribution function adjusted surface reflectances time series (NBAR-EVI2). Valid vegetation cycles within the series are identified and records

phenometrics for each vegetation cycle (Gray *et al.*, 2019).

LST (MOD11A2 and MYD11A2) (Hulley, 2017) day and night values at 8-day intervals and 1 km spatial resolution were obtained using the MODIS Global Subset Tool (<https://modis.ornl.gov/cgi-bin/MODIS/global/subset.pl>). The Land Surface Temperature (*LST*) and Emissivity daily data are retrieved at 1km pixels by the generalized split-window algorithm. There are uncertainties associated with satellite based *LST* especially during hot humid periods and for a cold and dry atmosphere (Dash *et al.*, 2002). During the rainy season (i.e., hot humid period) *LST* quality information showed that most pixels had data quality pass of below 80 percent. Data from pixels with below 100 percent quality pass was removed and gaps filled by interpolation. However, over 98 percent of the pixels from which data was retrieved in the dry season (i.e., including the cool-dry season) had 100 percent quality pass. The *LST* data was converted from Kelvin to degrees Celsius.

Actual evaporation (E_a) (MOD16A2/MYD16A2) (Running, 2017) at 8-day interval and 500m spatial resolution was also obtained from the climate engine (<https://modis.ornl.gov/cgi-bin/MODIS/global/subset.pl>). The MOD16A2/MYD16A2 uses the Penman-Monteith equation (Monteith, 1965; Penman, 1948) and is a sum of night-time and day-time actual evaporation. It is the sum of the evaporation from the wet canopy surface, the transpiration from the dry canopy surface and the evaporation from the soil surface (Running, 2017). In this study, the term evaporation is used instead of evapotranspiration. This is based on the arguments by Miralles *et al.*, (2020) and Savenije (2004) in which they showed that the term evapotranspiration has limitations and can even be considered as misleading.

All MODIS based data used in this study had quality reports. Based on the quality report all data from pixels with below 100 percent quality pass, especially during the rainy season, were removed and then the gaps were filled by interpolation. The data sets from the MODIS Terra and MODIS Aqua sensors i.e., MOD16A2 and MYD16A2, MCD15A2H and MYD15A2H and also the MOD11A2 and MYD11A2 were summed up per variable and averaged to come up with E_a , *LAI* and *LST* data sets. Polygons for each of the miombo woodland location(s) (Fig. 2.1) were used to extract the required data sets from January 2009 to December 2018. Raw filtered data provided on the global subset tool was used to estimate the 5th and 95th percentiles for the variables. The focus of the study was the dry season and had most pixels with acceptable quality pass of 100 percent.

2.2.3 Study approach

The study evaluated the canopy cover relationship with canopy water content and canopy temperature in the miombo woodland using satellite data. To track and evaluate changes in the woodland canopy cover the *LAI* and *NDVI* were used as proxies for canopy cover (Myneni & Park, 2015; Nielsen *et al.*, 2012; Knyazikhin *et al.*, 1999), the *NDII* as a proxy for canopy water content (Sriwongsitanon *et al.*, 2015; Tucker, 1979; Rouse *et al.*, 1973; The *LAI*, *NDII* and *NDVI* all, in their formulations, make use of the near infrared (NIR) region of the electromagnetic spectrum. In addition, since actual evaporation (E_a) and rainfall are closely linked to the *LAI*, *LST*, *NDII* and *NDVI* (Sun *et al.*, 2016; Yu *et al.*, 2016; Simic, Fernandes, & Wang, 2014; Mildrexler, Zhao, & Running, 2011; Jones & Rotenberg, 2001;

Hunt & Rock, 1989) they were used to augment the observations in the general patterns of the *LAI*, *LST*, *NDII* and *NDVI* but were not included in the statistical analyses as predictor or response variable. Furthermore, the phenology calendar was used to augment the *LAI* and *NDVI* observations. We analysed a 10-year period (2009 – 2018) in order to capture long term variations in the data. In the Luangwa Basin, hydrological year is categorised as the period from September to August. The rainy season is between November and April while the dry season is between May and October (Beilfus, 2012). Three polygons were used to retrieve the data in a 30 km by 30 km (900 km²) area in the miombo woodland at Nsansala and Mutinondo conservancy areas (Fig. 2.1). The conservancy areas were selected due to availability of a dense miombo woodland which is protected and is with minimal anthropogenic disturbances. The data for each variable from the three polygons was merged into one data set per variable and analysed. To avoid mixing variables values from different land cover types (i.e., grassland, bare soil and other woodland types) with miombo woodland the assessment was restricted to a dense miombo woodland (Fig. 2.1). Hence, the assessment was not conducted at the entire miombo ecosystem level in Africa but restricted to this dense miombo woodland in the Luangwa Basin in Zambia.

The statistical analyses included testing for outliers with the Dixon test and Z-score approach, testing for homogeneity and monotonic trends using the Pettit test and the Mann-Kendall trends test, analysis of variations with the Analysis of variance (ANOVA) approach, analysis of correlations was conducted with the Pearson r while the correlated component regression linear model (CCR.LM) was used to understand the influence of predictor variables on response variables. The methods are briefly explained in section 2.2.4 below.

2.2.4 Statistical approaches used to analyse the data

2.2.4.1 Testing for out-liers with the Dixon test

We used the Dixon test (Dixon, 1950) to assess if the data sets contained outliers at either end points i.e., highest and lowest values in the data sets. The Dixon test is a process developed to help ascertain if the greatest value or lowest value of a sample, or the two largest values, or the two smallest ones can be considered as outliers. The test works based on the assumptions that the data correspond to a sample extracted from a population that follows a normal distribution. The null hypothesis is that there are no outliers in the data. The outlier is said to be significant if the test statistic value is lower than the critical value from the Dixon test table. Further examination of data for outliers was conducted with the Z-score analysis approach. The Z-score defines the position of a raw score with reference to its distance from the mean when measured in standard deviation units. The Z-score is positive if the value lies above the mean, and negative if below.

2.2.4.2 Assessing correlation of variables with the Pearson r approach

Pearson's r (Pearson, 1895) is the most commonly used measure of correlation (Helsel & Hirsch, 2002). It is sometimes referred to as the linear correlation coefficient because of its measure of linear association between two variables. Pearson's r is a dimensionless property obtained by standardizing and dividing the distance from the mean by the sample standard deviation. The significance of r is determined by testing whether r

differs from zero. The test statistic is compared to a table of the t distribution with $n-2$ degree of freedom. The Pearson r value ranges between -1 and $+1$ with -1 indicating that the two variables are perfectly negatively linearly related while $+1$ indicates that the two variables are perfectly positively related. The closer the Pearson r value to either -1 or $+1$ the stronger the correlation (Helsel & Hirsch, 2002).

2.2.4.3 Assessing variations in the variables with the RM-ANOVA

The repeated measure analysis of variance (RM-ANOVA) (Helsel & Hirsch, 2002) is a commonly used typical parametric test which helps to ascertain whether samples in more than two groups have the same central value (mean or median) or whether one of the groups has the central value different from others. Reliability of the RM-ANOVA is dependent on the fulfilment of the assumptions that; variables are independent and identically distributed, variable residuals are normally distributed (or approximately normally distributed and the variances of populations are equal. The total variation of all the observations about the overall mean is measured by what is called the total sum of squares. The null hypothesis is that there are no variations in the population means while the alternative hypothesis is that there are variations in the population means. To test for the null hypothesis the F statistic is used. The F statistic is compared with the F distribution with $k - 1$ and $N - k$ degrees of freedom. The F statistic is approximately equal to 1 if the null hypothesis is true but will be larger than 1 if there are differences between the population means. Significance of the variations in the population means is ascertained by the p -value which simply expresses the probability of having the means constant or not constant. If the means are constant or are not further apart the p -value is very large (no significant variations) while if the means are wide or further apart (significant variation exists) the p -value is very small (< 0.00001) (Helsel & Hirsch, 2002).

2.2.4.4 Correlated component regression linear model (CCR.LM)

The correlated component regression (CCR), developed by Magidson, (2013), is an ensemble dimension reduction regression technique which utilises the K correlated components to predict the dependent variable. It is equivalent to the corresponding Naïve Bayes solution for $K = 1$ and equivalent to traditional regression for $K = P$ with P predictors. The application of the Naïve Bayes rule deals with the effects of multicollinearity among predictor variables. In the CCR-linear algorithm the outcome variable Y is predicted by K correlated components, each a linear combination of the predictors X_1, X_2, \dots, X_P . The CCR-linear algorithm is a generalisation of the CCR-logistic and is generally performed in three steps. Step1: The first component S_1 captures the effects of prime predictors which have direct effects on the outcome. It is an average (ensemble) of all 1-predictor effects: Step 2: The second component S_2 , correlated with S_1 , captures the effects of suppressor variables (proxy predictors) that improve prediction by removing extraneous variation from S_1 : Step 3: Estimate the 2-component model using S_1 and S_2 as predictors: The predictions (coefficients of estimates) for Y in the K -component CCR model are obtained from the ordinary least square regression of Y on S_1, \dots, S_k . The regression coefficient for predictor a variable is simply the weighted sum of loadings, where the weights are the

regression coefficients for the components in the K-component model. The step-down variable reduction step for a given K-component model, eliminates the predictor variable that is the least important, where importance is quantified as the absolute value of the variable's standardized coefficient. If a predictor variable is found to have the least absolute value of the standardised coefficient the predictor is excluded and the steps of the CCR estimation algorithm repeated on the reduced set of Predictors. The regression correlation coefficient of determination (R^2) and the Normalised Mean Square Error (NMSE) (Cirillo & Poli, 1993) are used to assess the performance of the CCR.LM in predicting the response variable(s) with a given combination of predictor variables.

2.2.4.5 Testing for homogeneity with Pettit test

To observe if there were any significant abrupt changes (i.e., due to changes in climate, change in land cover type and other factors) in the means of the variables we used the Pettit (1979) homogeneity test. The Pettit Homogeneity test approach is a common non-parametric application in change point detection studies involving hydrological or climate series which are known to be non-normal data (Zimba *et al.*, 2018; Helsel & Hirsch, 2002). The test statistic counts the number of times a member of the first sample exceeds a member of the second sample. The null hypothesis is that the data are homogenous i.e., absence of a change point. The test statistic is said to indicate a significant change point when the associated probability ≤ 0.05 . When a significant change point was found the time series data were divided into two parts at the location of the change point. The Pettit test was then conducted on the time series from which the change was detected to see if any further changes occurred (Helsel & Hirsch, 2002).

2.2.4.6 The Mann-Kendal trends test and the Sens' method

The Mann-Kendall test (Kendall, 1975; Dixon, 1950; Mann, 1945) used in this study was chosen premised on the advantages it possesses over other tests such as being a non-parametric test which does not need the data to be normally distributed and its low sensitivity to abrupt changes due to inhomogeneity in time series data. In general terms, the Mann-Kendall test seeks to establish whether monotonic changes are present in a given set of random values. The test statistic represents the number of positive differences minus the number of negative differences for all the differences between adjacent points in the time series. Positive values indicate an upward trend while negative values indicate a downward trend. The test statistic is used to test the null hypothesis and is a measure of the strength of the trend. The null hypothesis is that there is no trend in the series while the alternative hypothesis is that there is a trend in the series. If the computed *p-value* is greater than the chosen significance level (i.e., alpha level=0.05 used in this study), the null hypothesis is accepted while the alternative hypothesis is accepted if the *p-value* is less than the significance level.

The Sens' method (Sens, 1968) is a non-parametric approach used to estimate magnitude of trends in data time series. The Sens' method can be used in cases where the trend can be assumed to be linear. It estimates the slope of "n" pairs of data. The Sens' estimator of slope is the median value of these *N* values of the slope estimate. To obtain the

slope estimator the N values of the slope estimate are ranked from the smallest to the largest. Lastly, a two tailed test at $100(1 - \alpha)\%$ confidence interval is used to test the slope estimate with a non-parametric technique based on the normal distribution (Salmi *et al.*, 2002)

2.3 Results

2.3.1 Assessment of outliers with the Dixon test and Z-score approach

The assessment for outliers in the data was conducted with the Dixon test. The data was first categorised into sample population of $n \leq 100$ based on the seasons i.e., rainy season and the dry season (categorised into cool-dry and hot dry). The data was then tested for outliers on each category. Table S1, in the supplementary data of Zimba *et al.*, 2020, gives some of the results of the Dixon test. Across seasons no statistically significant (P -value > 0.05) outliers were detected. However, further analysis with the Z-score values showed that some variables had some outliers. These were removed and the gaps filled by interpolation. For instance, Z-score values showed some LAI_{Max} values to be outliers. The LAI_{Max} outliers were lowest values of 1.1 observed on the 7th and 20th of July 2009, 20th and 13th of August 2011 and also on the 13th and 19th July 2012. These observations can possibly be attributed to underestimation by the LAI algorithm as the observations were for shorter periods between two points with higher values on both ends (before and after). Furthermore, these outliers in LAI_{Max} were not linked to any changes in the LST , $NDII$ or $NDVI$ on the same dates or period. For the LST , some outliers were mostly flagged in the rainy season which is possibly due to the associated challenges in assessing the LST in hot-humid environments. The rainy season LST “outliers” could also indicate drought periods during the rainy season though this was discounted based on the counterchecking with rainfall, LAI , $NDII$ and $NDVI$ values for the same dates/period(s). In general, the test for outliers showed that there were no extreme events in the variables examined for the period 2009 – 2018 in the study area.

2.3.2 Pattern observed in phenology, canopy cover, water content and temperature

Based on the phenological observations by collection 6 MCD12Q2 data, shown in Fig. 2.2, it was noticed that senescence (i.e., process of leaf aging) generally occurred between January and March in the rainy season. The green down (i.e., reduction in green colour in leaves due to reduction in chlorophyll) was normally reached between March and May while the dormancy state (i.e., state of temporary metabolic inactivity or minimal activity) was mostly attained between May and July. The green up (i.e., increase in green colour in leaves due to increase in chlorophyll and metabolic activity) was noted to normally start around October in the dry season reaching peak between December and January.

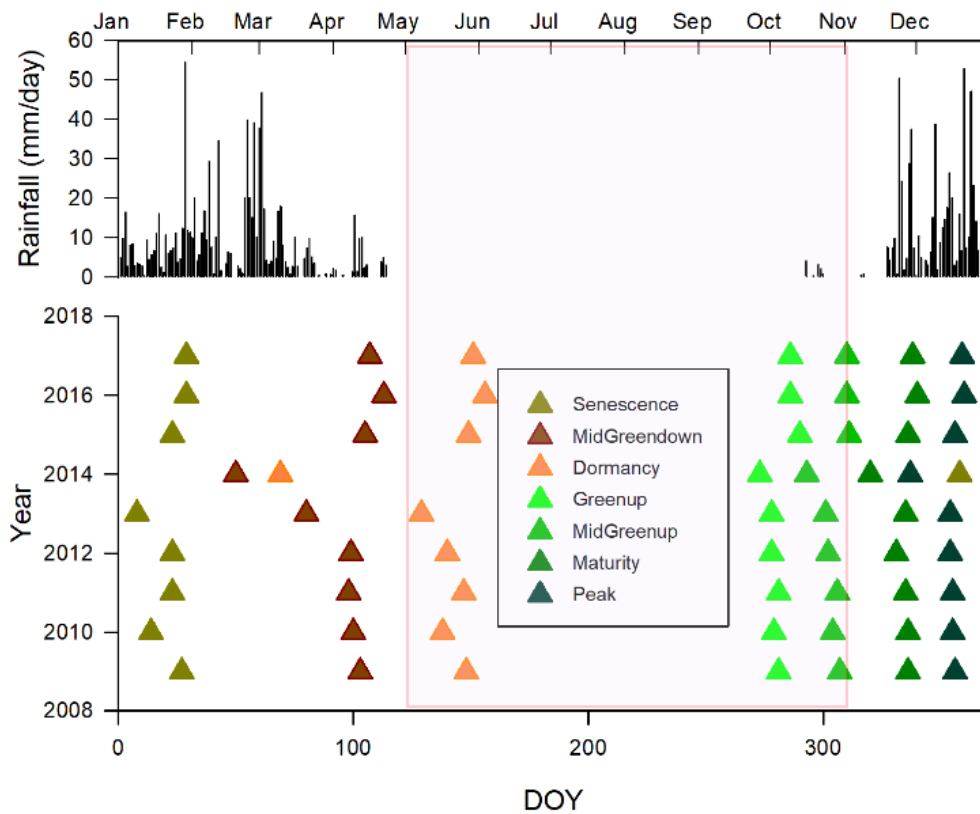


Figure 2.2: Satellite-based phenology calendar at the miombo woodland site in Mpika, Zambia based on the data for the period 2009 to 2017. Shaded box indicates the dry season.

There seemed to be synchronism between the phenology calendar and the changes in canopy cover values (i.e., *LAI* and *NDVI*) and the canopy water content (i.e., *NDII*). Canopy cover peak was observed during the rainy season between January and February (Figs. 2.3a and 2.4) the same period when phenological maturity was attained (Fig. 2.2). Minimum canopy cover was observed during the dry season between August and September during the dormancy state (Figs. 2.2, 2.3a and 2.4). The period January 2017 to May 2019 was used to illustrate the annual temporal patterns in the variables. During this period the canopy cover (proxied by *LAI* and *NDVI*) showed synchronism with the canopy water content and the actual evaporation (Fig. 2.3). A sharp decline in the *LAI*, *NDVI* and E_a were observed at the end of the rainy season in April.

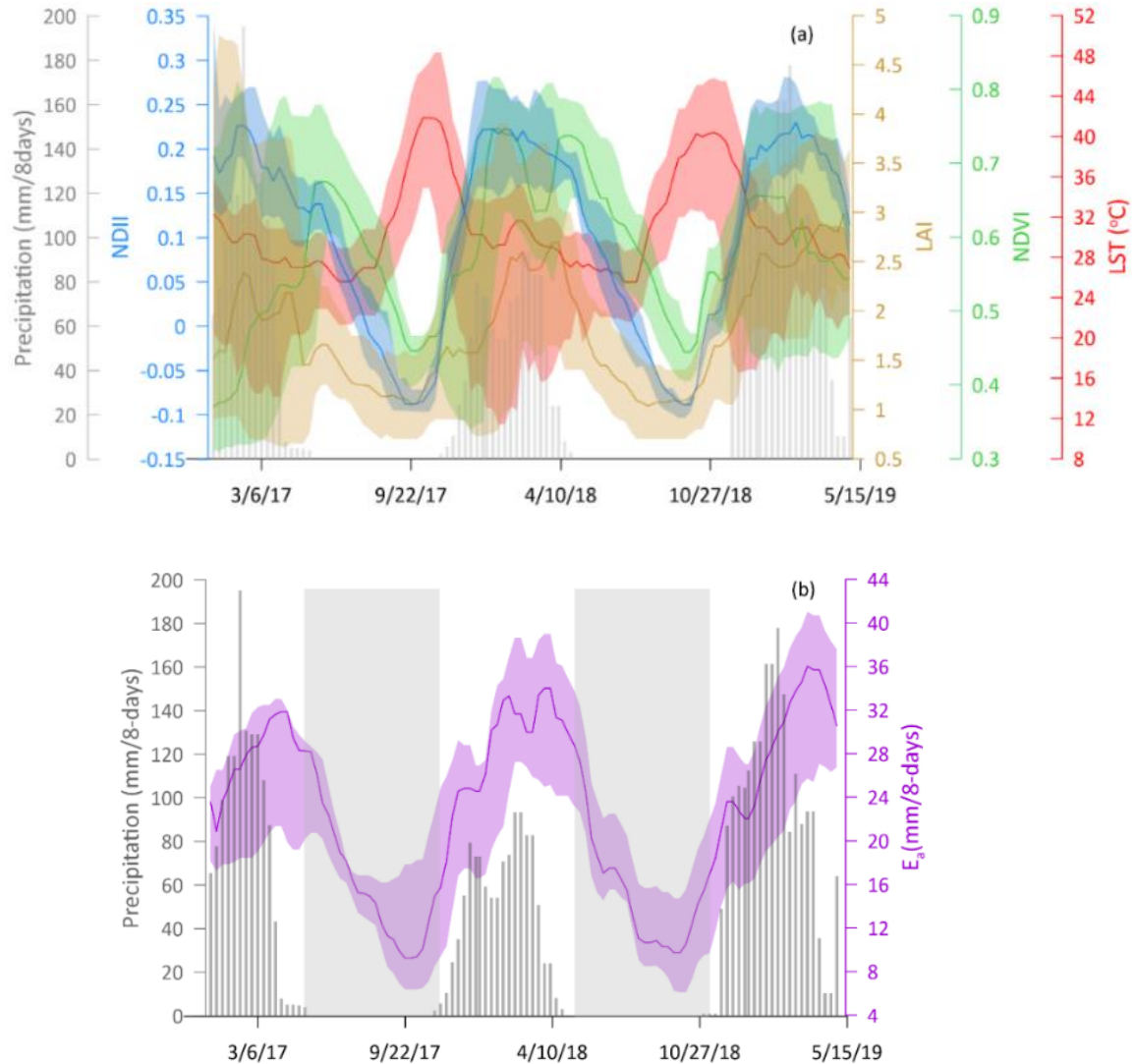


Figure 2.3: Illustration of (a) the seasonal pattern in the means of the 8-day values of the woodland canopy cover (i.e., LAI and NDVI), canopy water content (i.e., NDII) and canopy temperature (i.e., LST) and (b) the seasonal pattern in the means of the 8-day values of actual evaporation (E_a). Shaded area for variables is the 5th and 95th percentiles. The shaded area (grey) is the dry season. The rainy and dry season seasons are clearly delineated with peak values in E_a , LAI, NDII and NDVI observed during the rainy season while lowest values were observed in the dry season. Peak canopy temperature (i.e., LST) value(s) were observed during the dry season.

The start in decline in the variables in Fig. 2.3 coincided with the green-down phenological phase in Fig. 2.2. There appeared to be a time lag of about one to two months between the LAI and the NDVI as to the start in the rise in canopy cover (Fig. 2.3a) in the dry season. Generally, the LAI begun to rise in mid-August while NDVI started at the beginning of October. Start in steady decline in canopy cover (i.e., both LAI and NDVI) was observed in May a month after the end of the rainy season in April (Figs. 2.3a and 2.4) the same period when the vegetation enters the dormancy stage (Figs. 2.2). However, there was a difference

when canopy cover began to increase with maximum *LAI* values indicating mid-August while *NDVI* seemed to show end of October (Fig. 2.4). Peak canopy water content (i.e., *NDII*) was observed in the rainy season between December and February while lowest values were observed in the dry season in September (Fig. 2.4). The peak and lowest canopy water content corresponded with the peak and dormancy stages in the phenology. The canopy water content began to decline in May following the end of the rainy season in April. However, it was surprising that canopy water content (i.e., *NDII*) like canopy cover (i.e., *NDVI*) started to increase in the hot dry season in October before the commencement of the summer rains (Figs. 2.3a and 2.4). However, like with canopy cover, canopy water content started to increase in October before the commencement of the summer rains (Figs. 2.3a and 2.4).

The start in decline in variables in Fig. 2.3 coincided with the green-down phenological phase in Figure 2.2. There appeared to be a time lag of about one to two months between the *LAI* and the *NDVI* as to the start in the rise in canopy cover (Fig. 2.3a) in the dry season. Generally, the *LAI* began to rise in mid-August while *NDVI* started at the beginning of October.

Start in steady decline in canopy cover (i.e., both *LAI* and *NDVI*) was observed in May a month after the end of the rainy season in April (Figs. 2.3a and 2.4) the same period when the vegetation enters the dormancy stage (Fig. 2.2). However, there was a difference when canopy cover began to increase with maximum *LAI* values indicating mid-August while *NDVI* seemed to show end of October (Fig. 2.4). Peak canopy water content (i.e., *NDII*) was observed in the rainy season between December and February while lowest values were observed in the dry season in September (Fig. 2.4). The peak and lowest canopy water content corresponded with the peak and dormancy stages in the phenology. The canopy water content began to decline in May following the end of the rainy season in April. However, it was surprising that canopy water content (i.e., *NDII*) like canopy cover (i.e., *NDVI*) started to increase in the hot dry season in October before the commencement of the summer rains (Figs. 2.3a and 2.4). However, like with canopy cover, canopy water content started to increase in October before the commencement of the summer rains (Figs. 2.3a and 2.4).

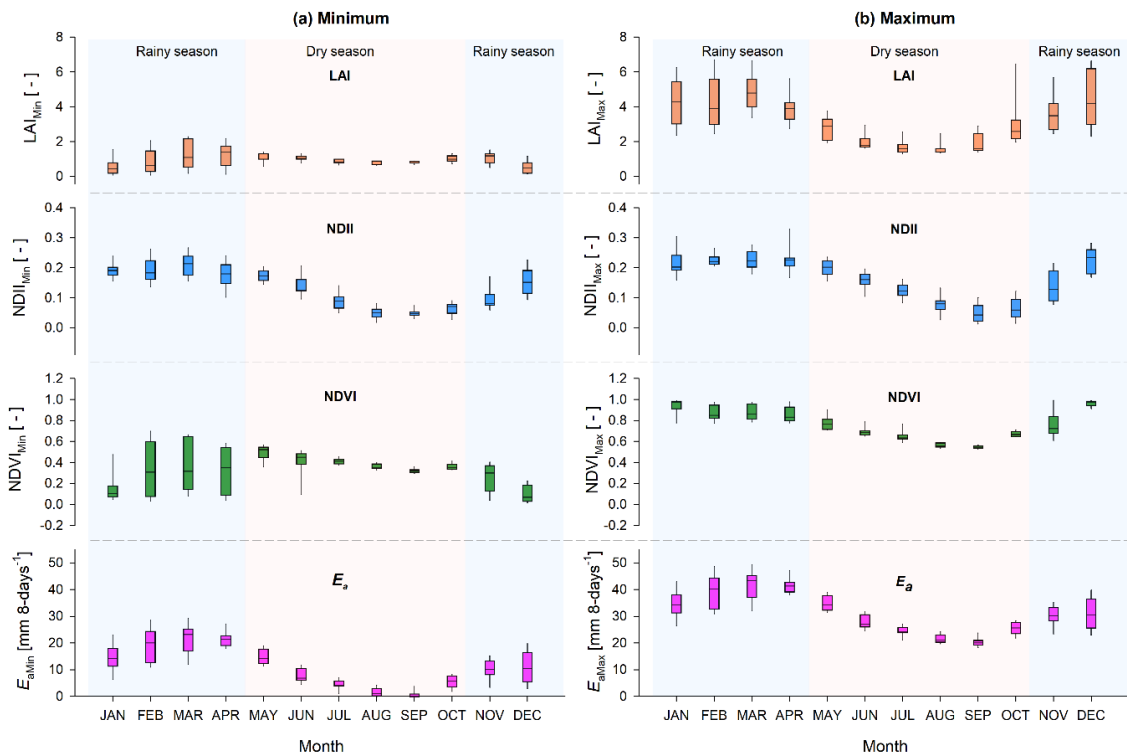


Figure 2.4: 2009–2018 January to December minimum (a) and maximum (b) values of E_a , LAI, NDII, and NDVI. The lowest values were seen during the dry season while peak values were observed in the rainy season. Shaded areas represent the rainy and dry seasons: November–December indicate start of the rainfall, January–February is the peak rainfall period, while March–April is the end of the rainfall season. May–October is the dry season.

The start in decline in variables in Fig. 2.3 coincided with the green-down phenological phase in Fig. 2.2. There appeared to be a time lag of about one to two months between the LAI and the NDVI as to the start in the rise in canopy cover (Fig. 2.3a) in the dry season. Generally, the LAI began to rise in mid-August while NDVI started at the beginning of October.

A start in steady decline in canopy cover (i.e., both LAI and NDVI) was observed in May, one month after the end of April's rainy season (Figs. 2.3a and 2.4), which happens to be the same period when vegetation enters dormancy (Fig. 2.2). However, there was a difference when canopy cover increased with maximum LAI values, indicating mid-August, while NDVI seemed to show at the end of October (Fig. 2.4). Peak canopy water content (i.e., NDII) was observed in the rainy season between December and February, while the lowest values were observed in the dry season in September (Fig. 2.4). The peak and lowest canopy water content corresponded with the peak and dormancy stages in the phenology. The canopy water content declined in May following the end of April's rainy season. However, it was surprising that canopy water content (i.e., NDII) like canopy cover (i.e., NDVI) increased in the hot-dry season in October before the commencement of the summer rains (Figs. 2.3a and 2.4). However, like with canopy cover, canopy water content started to increase in October before the commencement of the summer rains (Figs. 2.3a and 2.4).

The periods for the lowest and highest canopy temperature (i.e., LST) values corresponded with the dormancy and green-up phenological stages (Figs. 2.2 and 2.3a). One important observation was that there seemed to be synchronism between the E_a and the

canopy cover (i.e., LAI and NDVI) and the canopy water content (i.e., NDII) across seasons (Figs. 2.3 and 2.4).

2.3.3 Analysis of the observed patterns with the RM-ANOVA test

The RM-ANOVA results for the comparison between the rainy and dry season values of variables and the inter-annual comparison of the dry season values of variables are shown in Tables 2.2 and Table S2 of supplementary data of Zimba *et al.*, 2020. The LAI, LST, NDII, and NDVI values for the rainy season significantly (p -value < 0.05) differed with the dry season values. The highest values of the LAI were observed in the rainy season, while the lowest values were observed in the dry season. The opposite was true for the LST with the high and lowest values both occurring in the dry season. The differences in terms of the means were 2.32, 2.48 °C, 0.15m and 0.13 for the LAI, LST, NDII, and the NDVI, respectively. The dry season values of the LAI, NDII, and the NDVI significantly (p -value < 0.05) differed across the years (2009–2018), while the LST values did not show significant (p -value = 0.81) differences. However, further analysis involving the all pairwise multiple comparison with the Holm–Sidak method showed that values of variables between some years were not significantly different (Table S3 of supplementary data of Zimba *et al.*, 2020).

Table 2.2. Repeated measure-analysis of variance (RM-ANOVA) test results for variables.

Variable	Rainy Season vs. Dry Season				Dry Season Inter-Annual Variations		
	Mean Diff	DF	F	p -Value	DF	F	p -Value
LAI _{Mean}	2.32	(1,454)	596.62	<0.001	(9,198)	9.41	<0.001
LST _{Mean}	2.48	(1,438)	20.87	<0.001	(9,197)	0.59	0.805
NDII _{Mean}	0.15	(1,458)	485.12	<0.001	(9,192)	11.27	<0.001
NDVI _{Mean}	0.13	(1,454)	306.70	<0.001	(9,192)	7.96	<0.001

Mean Diff = Mean difference, *DF* = Degree of freedom, *F* = Test statistic

2.3.4 Pearson r correlation analysis of the relationship of variables

Minimum, maximum, and mean values of variables were analysed for correlation. Mean values were used to demonstrate the relationships among variables across seasons. Figure 2.5 shows the annual (January–December) correlation plots using mean values of variables. Table 2.3 gives the results of the correlation statistics of variables at annual scale. Detailed correlation statistics for the rainy and dry seasons are shown in the supplementary data (Tables S4–S7 of supplementary data of Zimba *et al.*, 2020). In Figs. 2.3 and 2.5, there seemed to be hysteresis behaviour between LAI_{Mean} and NDII_{Mean}, as well as between LAI_{Mean} and LST_{Mean}, indicating that changes in canopy cover (i.e., LAI_{Mean}) lagged behind changes in canopy water content (i.e., NDII_{Mean}), as well as changes in canopy temperature (i.e., LST_{Mean}). The changes in the canopy cover were not only affected by the canopy water (i.e., NDII_{Mean}) and temperature (i.e., LST_{Mean}) in a given day but by cumulative canopy water and temperature conditions. Generally, canopy cover (i.e., NDVI_{Mean}) showed synchronism with canopy water content (i.e., NDII_{Mean}) throughout the year. Canopy cover (in the case of LAI_{Mean}) only showed strong correlation with canopy temperature during the hot-dry season. Statistically, at the annual scale, the canopy water content (i.e., NDII_{Mean}) relationship with woodland canopy cover (i.e., LAI_{Mean} and NDVI_{Mean}) was strongly positive with $r = 0.78$, 0.97 with p -value < 0.0001 , respectively (Fig. 2.5 and Table 2.3).

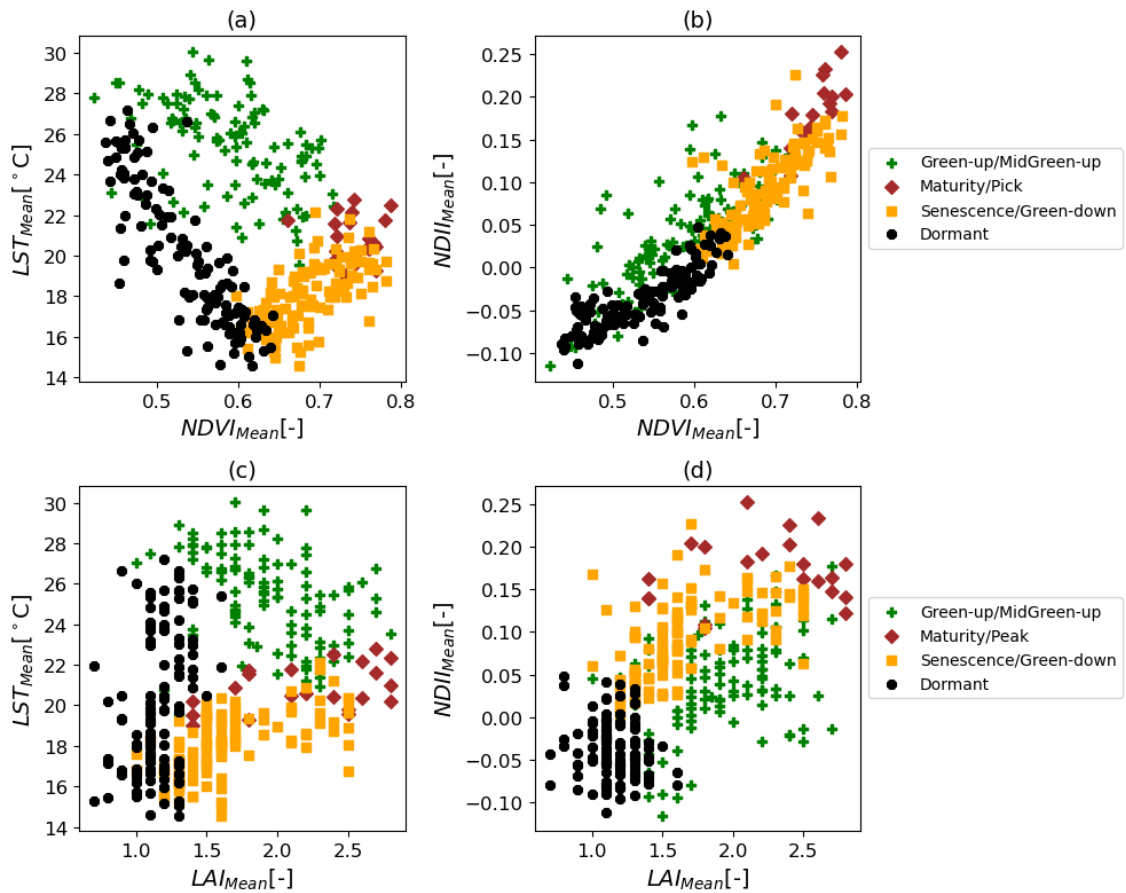


Figure 2.5: Correlation of mean values for the 8-day $NDVI_{Mean}$ and LAI_{Mean} with $NDII_{Mean}$ (a, b), as well as with LST_{Mean} (c, d) at the annual scale. The $NDVI_{Mean}$ shows stronger correlation with canopy water content (i.e., $NDII$) and canopy temperature (i.e., LST) compared to the LAI_{Mean} when used as proxies for canopy cover. LST_{Mean} shows hysteresis with $NDVI_{Mean}$ and LAI_{Mean} while $NDII_{Mean}$ shows hysteresis with LAI_{Mean} .

Table 2.3. Pearson (r) correlation statistics of the minimum, maximum, and mean values of LAI , LST , $NDII$, and $NDVI$ at an annual scale. The LST minimum values showed relatively stronger correlation with minimum values of LAI , $NDII$, and $NDVI$ compared to the maximum and mean values.

Variable	LAI_{Min}	LAI_{Max}	LAI_{Mean}	LST_{Min}	LST_{Max}	LST_{Mean}	$NDII_{Min}$	$NDII_{Max}$	$NDII_{Mean}$	$NDVI_{Min}$	$NDVI_{Max}$	$NDVI_{Mean}$
LAI_{Min}	1.00											
LAI_{Max}	0.20	1.00										
LAI_{Mean}	0.51	0.79	1.00									
LST_{Min}	-0.12	-0.02	-0.08	1.00								
LST_{Max}	-0.11	0.10	0.01	0.94	1.00							
LST_{Mean}	-0.11	0.09	0.01	0.97	0.99	1.00						
$NDII_{Min}$	0.34	0.65	0.75	-0.42	-0.33	-0.33	1.00					
$NDII_{Max}$	0.36	0.70	0.78	-0.24	-0.14	-0.15	0.92	1.00				
$NDII_{Mean}$	0.35	0.69	0.78	-0.37	-0.26	-0.27	0.97	0.96	1.00			
$NDVI_{Min}$	0.35	0.58	0.69	-0.51	-0.43	-0.43	0.97	0.86	0.94	1.00		
$NDVI_{Max}$	0.36	0.62	0.72	-0.38	-0.31	-0.31	0.92	0.93	0.94	0.90	1.00	
$NDVI_{Mean}$	0.35	0.61	0.71	-0.50	-0.41	-0.41	0.96	0.89	0.97	0.98	0.94	1.00

Values in bold are different from 0 with a significance level $\alpha=0.05$,
max= maximum, min = minimum

At rainy and dry season scales, the canopy water content (i.e., $NDII_{Mean}$) versus canopy cover (i.e., LAI_{Mean} and $NDVI_{Mean}$) correlation was strongly positive except for the $NDII$ - LAI relationship, which showed a low coefficient of correlation (i.e., $r = 0.29$ and p -value < 0.008) for the rainy season (Tables S4–S7 of supplementary data of Zimba *et al.*, 2020). However, during the hot-dry season, strong $NDII$ - LAI correlation was observed with $r = 0.70$ and p -value < 0.0001 (Table S7 of supplementary data of Zimba *et al.*, 2020). Generally, the $NDII$ - $NDVI$ correlations were stronger (i.e., $r > 0.75$) across all seasonal scales (Tables S4–S7 of supplementary data of Zimba *et al.*, 2020). Table 2.3 and Tables S4–S7 of supplementary data of Zimba *et al.* (2020) gives statistics of the Pearson r correlation analysis of the woodland canopy temperature (i.e., LST) correlation with the woodland canopy cover (i.e., LAI and $NDVI$). At the annual scale, the woodland canopy cover (i.e., LAI_{Mean} as a proxy) negatively covaried with woodland canopy temperature with $r = -0.11$ and p -value < 0.83 . When canopy cover was proxied by $NDVI$ a negative covariation with canopy temperature of $r = -0.41$ and p -value < 0.0001 was observed. During the rainy season, the LST - $NDVI$ relationship showed a correlation coefficient of $r = -0.44$; and p -value < 0.0001 , while LST - LAI correlation had $r = -0.52$; and p -value < 0.001 . During the dry season (May–October), the LAI - LST correlation was positive but weak and statistically insignificant with $r = 0.04$ and p -value = 0.56. The $NDVI$ - LST correlation was negative but relatively stronger with $r = -0.68$ and p -value < 0.0001 . During the cool-dry season (May–July) the $NDVI$ - LST correlation was positive but relatively weak ($r = 0.26$, p -value < 0.0046), and was the same as the LAI - LST relationship ($r = 0.26$, p -value < 0.0044) (Tables S4–S7 of supplementary data of Zimba *et al.*, 2020). However, the hot-dry season (August–October) showed stronger positive LAI - LST correlation ($r = 0.62$, p -value < 0.0001), while the $NDVI$ - LST relationship was negative ($r = -0.25$, p -value = 0.0097) (Tables S4–S7 of supplementary data of Zimba *et al.*, 2020). Generally, at the annual scale, LST_{Min} values showed relatively stronger correlation with LAI_{Min} and $NDVI_{Min}$ compared to the LST_{Max} and LST_{Mean} values (Table 2.3).

2.3.5 Relationship of the woodland canopy cover with the canopy water content and canopy temperature using the CCR.LM

Figure 2.6, Tables 2.4, 2.5, and Tables S8–S10 of supplementary data of Zimba *et al.* (2020) show results of the CCR.LM. First, regression was conducted with mean values of individual predictor variables and later inputted simultaneously. This was conducted to benchmark the relationship of the LST and $NDII$ with the LAI and $NDVI$ exclusive of the other predictor variable. The second part of the regression was the relationship of the woodland canopy cover (i.e., the LAI and the $NDVI$) with both the woodland canopy water content (i.e., $NDII$) and the woodland canopy temperature (i.e., LST) used simultaneously as predictors. This enabled the assessment of the combined influence of the variables on the variations in the woodland canopy cover. There was no collinearity between the LST and $NDII$. The NMSE and the coefficient of determination (R^2) were used to assess the estimate of the overall deviations between predicted and “observed” values, thus ascertaining the performance of the model. The standardised and unstandardized coefficients ($\hat{\beta}$) were used to analyse which of the input variables (i.e., LST or $NDII$), at each run, had a significant effect on each response variable (i.e., LAI and $NDVI$) at different time scales, i.e., annual and dry season. However, it was observed that whether with the standardised or unstandardized coefficient the $NDII$ showed the most influence on the variations of the LAI and the $NDVI$ (i.e., Fig 2.6) at all intervals of assessment. Consequently, the unstandardised coefficient was used for analysis.

At the annual scale, the $NDII$ as a single variable accounted for 61% ($R^2 = 0.61$) of the variations in LAI and 93% ($R^2 = 0.93$) in $NDVI$.

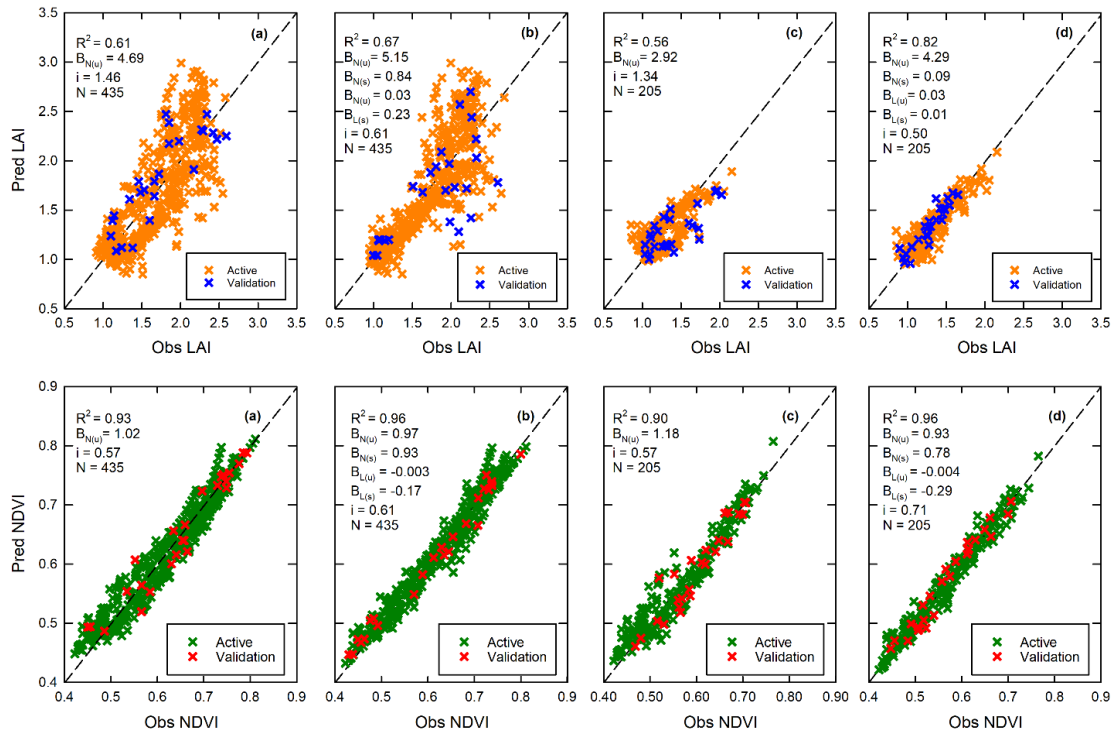


Figure 2.6: First row: Plots of the CCR.LM results at annual scale (January–December) (a, b) and dry season (May–October) (c, d): LAI regression graphs at annual scale (a) with NDII as only predictor variable and (b) with LST and NDII used simultaneously as predictors. LAI regression graphs during the dry season (c) with NDII as only predictor variable and (d) with LST and NDII combined as predictor variables. Second row: Plots of the CCR.LM results at annual scale (January–December) (a, b) and dry season (May–October) (c, d): NDVI regression graphs at annual scale (a) with NDII as only predictor variable and (b) with LST and NDII combined as predictors. NDVI regression graphs during the dry season (c) with NDII as only predictor variable and (d) with LST and NDII used simultaneously as predictor variables. R^2 = coefficient of determination, $B_{N(s)}$ = standardized coefficient of estimate with the NDII, $B_{N(u)}$ = unstandardized coefficient of estimate with the NDII, $B_{L(s)}$ = standardized coefficient of estimate with the LST, $B_{L(u)}$ = unstandardized coefficient of estimate with the LST, i = intercept, N = number of observations.

The LST as a single variable accounted for 13% in the LAI variations and 17% in the NDVI variations (Table 2.4). A combination of the LST with the NDII accounted for about 67% ($R^2 = 0.67$) of the variations in the LAI and 96% ($R^2 = 0.96$) in the NDVI improvements of 9.83% and 3.22%, respectively. Further analysis of the coefficients of estimates showed that the NDII had the most influence on variations in canopy cover with coefficient estimates of $\hat{\beta} = 0.03$, -0.003 and $\hat{\beta} = 5.15$, 0.97 for the LST and the NDII on the LAI and the NDVI, respectively (Fig. 2.6 and Table 2.4). When analysed for the rainy season scale (November–April), the most determinant factor of variations in the canopy cover (i.e., LAI and NDVI) were by single variable interactions.

Table 2.4: CCR.LM coefficients of estimates and goodness of fit statistics (at 95% confidence level) at annual scale with *NDII* and *LST* as predictors. Prediction of *LAI* was improved by about 9.83 percent when *LST* and *NDII* were simultaneously inputted as predictors. *NDVI* prediction improved by 3.22 percent when *LST* and *NDII* were simultaneously used as predictors.

Variable	Predictors: <i>NDII</i> and <i>LST</i>																
	<i>LST</i>					<i>NDII</i>											
	Model	GFS Cv	Model	GFS Cv	N	Model	GFS Cv	Model	GFS Cv	N							
<i>LAI</i>	$\hat{\beta}$	<i>i</i>	R ²	NMSE	$\hat{\beta}$	<i>i</i>	R ²	NMSE	N	$\hat{\beta}$	$\hat{\beta}$	<i>i</i>	R ²	NMSE	N	Diff. R ²	
<i>NDVI</i>	-0.001	1.69	0.13	0.87	4.69	1.46	0.61	0.39	435	0.03	5.15	0.61	0.67	0.33	435	0.06	9.83
	-0.01	0.87	0.17	0.83	1.02	0.57	0.93	0.07	435	-0.003	0.97	0.67	0.96	0.04	435	0.09	3.22

Table 2.5: CCR.LM coefficients of estimates and goodness of fit statistics (at 95% confidence level) during the dry season with *NDII* and *LST* as predictors. Accounting for variations in *LAI* was improved by about 46 percent when *LST* and *NDII* were simultaneously used as predictor variable.

Variable	Predictors - <i>NDII</i> and <i>LST</i>																
	<i>LST</i>					<i>NDII</i>											
	Model	GFS Cv	Model	GFS Cv	N	Model	GFS Cv	Model	GFS Cv	N							
<i>LAI</i>	$\hat{\beta}$	<i>i</i>	R ²	NMSE	$\hat{\beta}$	<i>i</i>	R ²	NMSE	N	$\hat{\beta}$	$\hat{\beta}$	<i>i</i>	R ²	NMSE	N	Diff. R ²	
<i>NDVI</i>	0.001	1.28	0.21	0.79	2.92	1.34	0.56	0.44	205	0.03	4.29	0.5	0.82	0.18	205	0.26	46.43
	-0.01	0.89	0.56	0.44	1.18	0.57	0.90	0.16	205	-0.004	0.93	0.71	0.96	0.04	205	0.11	6.67

Interpretation (Tables 2.4 & 2.5): GFS Cv = Goodness of fit statistics cross validated, *i* = intercept, N = number of observations, *NDVI* = Normalised difference vegetation index, *LST* = Land surface temperature, *LAI* = Leaf area index, NMSE = Normalised mean square error, R² = coefficient of determination and $\hat{\beta}$ = unstandardised coefficient of estimate

For instance, LST as a single variable accounted for 21% of variations in the LAI while interaction between LST and NDII only accounted for 24%. Further, as single variables, the LST and NDII accounted for 50% and 91% of variations in the NDVI, respectively. LST and NDII interaction also accounted for 91% variations in NDVI, the same as the NDII as a single variable (Table S8 of supplementary data of Zimba *et al.*, 2020). For the dry season, the NDII as a single variable accounted for 56% variations in LAI and 90% in NDVI. As a single variable, LST accounted for 21% ($R^2 = 0.21$) variations in LAI and 56% ($R^2 = 0.56$) of the variations in NDVI (Fig. 2.6 and Table 2.5).

During the dry season the combination of LST and NDII as predictor variables accounted for 82% ($R^2 = 0.82$) of the variations in LAI and 96% ($R^2 = 0.96$) in the NDVI (Fig. 2.6 and Table 2.5). Consequently, adding LST to the regression improved the outcomes by 46.43% and 6.67% in the case of LAI and NDVI, respectively (Table 2.5). During the annual time scale, the NDII had the most influence on the variations in the canopy cover, as indicated by the coefficients of estimates $\hat{\beta} = 0.03, -0.004$ and $\hat{\beta} = 4.29, 0.93$ for LST and NDII on LAI and NDVI, respectively (Fig. 2.6 and Table 2.5). The interpretation of the coefficients (i.e., for the dry season), with LAI as a proxy for the canopy cover, is that the amount of change (i.e., $\hat{\beta} = 4.29$) in the canopy cover (i.e., LAI) due to a 1-unit change of canopy water content (i.e., NDII) was higher than the change (i.e., $\hat{\beta} = 0.03$) in the canopy cover (i.e., LAI) due to a 1-unit change in canopy temperature (i.e., LST) (Tables 2.5 and S8–S10 of supplementary data of Zimba *et al.*, 2020). For every one-unit increment in LST during the hot-dry season, the NDVI was reduced by about 0.01, while for every increase in one-unit of NDII, the NDVI increased by about 1.1 (Table S10 of supplementary data of Zimba *et al.*, 2020). The model outputs and overall interpretation for the cool- and hot-dry season analyses (Tables S8–S10 of supplementary data of Zimba *et al.*, 2020) were different than the annual scale results. For the hot-dry season (August–October), the LST, as a single variable, accounted for most variations (35%) in the LAI, while the NDII accounted for most variations (47%) in the NDVI. Furthermore, combination of the LST and NDII as predictors improved accounting for variations in the LAI from about 35% (with either the LST or NDII) to 68% (with the LST and the NDII combined) and NDVI from 48% (with NDII only) to 79% (with the LST and the NDII combined). During the cool-dry season (May–July), LST, as a single variable, had insignificant influence on variations in both LAI and NDVI. On the other hand, the NDII as a single variable accounted for 87% variations in the LAI and 94% in the variations in the NDVI. Thus, a combination of LST and NDII in the cool-dry season did not improve accounting for variations in the LAI and the NDVI (Table S9 of supplementary data of Zimba *et al.*, 2020). Overall, the NDII seemed to account for the most variations in both the LAI and the NDVI across seasons. However, during the dry season, the LST seemed to account for the most variations in the LAI. Further, despite the LST_{Min} showing relatively stronger correlations with the LAI_{Min} and the $NDVI_{\text{Min}}$, there were no significant differences observed between the use of the LST_{Mean} , LST_{Min} , and LST_{Max} in the model. Generally, for the annual (January–December), dry season (May–October), and cool-dry season (May–July) scales, adding the LST to the NDII improved accounting for variations in the canopy cover (i.e., LAI and NDVI as proxies) but at varying magnitudes with the most significant contribution noted in the dry season (Tables 2.5 and S10 of supplementary data of Zimba *et al.*, 2020). Based on the CCR.ML results (Fig. 2.6, Tables 2.4, 2.5, and Tables S8–S10 of supplementary data of Zimba *et al.*, 2020), changes in canopy water content accounted for the largest variations in canopy cover across seasons.

2.3.6 Assessment of abrupt change in variables with the Pettit test

Figure 2.7 and Table 2.6 shows results of the Pettit test at the annual scale (January–December), while Table S11a of supplementary data of Zimba *et al.* (2020) provides the dry season Pettit test results. For the annual scale (January–December), the Pettit test on the 8-day values of variables indicated only three variables—LST (minimum, maximum, and mean), NDII_{Max}, and NDVI_{Max}—to have had abrupt change in mean values between the period 2009 and 2018. Daily rainfall values also showed significant downward abrupt changes in 2012 and 2014, and an upward change was observed in 2016. The mean annual and monthly rainfall values, as well as the rest of the variables—i.e., LAI_{Min}, LAI_{Max}, LAI_{Mean}, NDVI_{Min}, NDVI_{Mean}, NDII_{Min}, and NDII_{Mean}—did not show any significant abrupt changes in the time space 2009–2018 (Tables 2.6 and S11a of supplementary data of Zimba *et al.*, 2020). The LST_{Min}, LST_{Max}, and LST_{Mean} values seemed to have had a significant (p -value < 0.05) abrupt upward change. The NDII_{Max} and NDVI_{Max} seemed to have had a significant (p -value < 0.05) abrupt downward change in the mean values. At the 99% confidence level, the LST_{Min} mean value changed from about 28.30 °C between 2009 and 2012 to 30.04 °C between 2012 and 2018.

Table 2.6. Pettit test results for LAI, LST, NDII and NDVI for the period 2009 -2018.

Variable	Period	Change time	Year	p-value	Alpha level	Conf. Level	Mean from	Mean to	Test decision
LAI _{Min}	2009 - 2018			0.5463	0.05	99%			$p > \alpha$, H0 accepted
LAI _{Max}	2009 -2018			0.6127	0.05	99%			$p > \alpha$, H0 accepted
LAI _{Mean}	2009 -2018			0.5420	0.05	99%			$p > \alpha$, H0 accepted
LST _{Min}	2009 - 2018	4 th Aug	2012	0.0027	0.05	99%	28.3	30.04	$p < \alpha$, H0 rejected
LST _{Max}	2009 -2018	12 th Aug	2012	< 0.0001	0.05	99%	32.79	35.59	$p < \alpha$, H0 rejected
LST _{Mean}	2009 -2018	12 th Aug	2012	< 0.0001	0.05	99%	30.5	32.8	$p < \alpha$, H0 rejected
NDII _{Min}	2009 - 2018			0.0798	0.05	99%			$p > \alpha$, H0 accepted
NDII _{Max}	2009 -2018	16 th May	2016	0.0004	0.05	99%	0.05	0.01	$p < \alpha$, H0 rejected
NDII _{Mean}	2009 -2018			0.0942	0.05	99%			$p > \alpha$, H0 accepted
NDVI _{Min}	2009 - 2018			0.0573	0.05	99%			$p > \alpha$, H0 accepted
NDVI _{Max}	2009 - 2018	9 th May	2010	0.0287	0.05	99%	0.62	0.56	$p < \alpha$, H0 rejected
NDVI _{Mean}	2009 -2018			0.1496	0.05	99%			$p > \alpha$, H0 accepted
Annual R	2009 - 2018			0.3162	0.05	99%			$p > \alpha$, H0 accepted
Monthly R	2009 - 2018			0.8283	0.05	99%			$p > \alpha$, H0 accepted
Daily R	2009 - 2012	4 th April	2012	0.0035	0.05	99%	4.98	3.90	$p < \alpha$, H0 rejected
Daily R	2012 -2014	22 nd April	2014	< 0.0001	0.05	99%	6.14	3.65	$p < \alpha$, H0 rejected
Daily R	2014 -2016	15 th Nov	2016	< 0.0001	0.05	99%	2.48	5.07	$p < \alpha$, H0 rejected

*R = Rainfall

For the same time steps, the LST_{Max} and LST_{Mean} seemed to have changed from about 32.8 to 35.6 °C and from about 30.5 to 32.8 °C, respectively. The NDII_{Max} mean changed from 0.05 between 2009 and 2016 to 0.01 between 2016 and 2018. Except for the daily rainfall data none of the other variables showed further change points after the initial change points. For the dry season scale, the Pettit test showed one-time abrupt change with upward change in the LAI_{Mean} in September, 2013 from LAI_{Mean} value of 1.25 to 1.37, while the NDII_{Max} and the NDVI_{Max} changed

downwards in July from -0.03 to -0.07 and 0.52 to 0.49 , respectively. There was no change in LST.

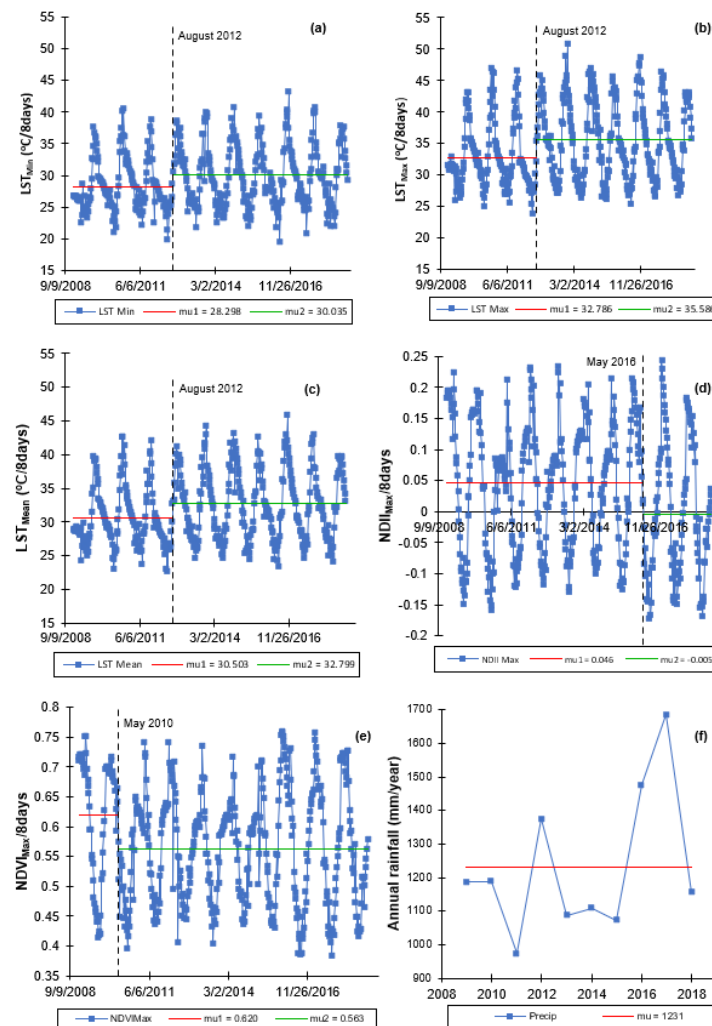


Figure 2.7: Plots of the Pettit test for the 8-day LST_{Min} (a), LST_{Max} (b), LST_{Mean} (c), $NDII_{Max}$ (d), $NDVI_{Max}$ (e), and mean annual rainfall (f) for the period of 2009 to 2018 in the miombo woodland in the Luangwa Basin. Significant upward change in the LST means seemed to have occurred in August 2012. Significant abrupt changes in $NDII_{Max}$ and $NDVI_{Max}$ seem to have occurred in May at the start of the dry season.

2.3.7 Assessment of trends in values of variables with Mann–Kendall trends test

To observe if trends existed in the variables, we performed the Mann–Kendall trends test on all variables. Figure 2.8, Tables 2.7 and S11b of supplementary data of Zimba *et al.* (2020) shows the results of the Mann–Kendall test for the tested variables. From 2009 to 2018, the Mann–Kendall test revealed existence of significant (p -value < 0.05) trends in some variables with the LST_{Min} , LST_{Max} , and LST_{Mean} , indicating an upward trend, while the $NDII_{Max}$ and $NDVI_{Max}$ revealed significant downward trends with p -values of 0.0187 and 0.0022, respectively. At the

alpha level = 0.05, there were significant trends in daily rainfall values (Table 2.7) but no significant trend in the mean monthly and annual values was observed.

Table 2.7. Mann–Kendall trends test results for variables with abrupt change points.

Variable	Mann-Kendall Statistic(S)	Kendall's Tau	Var (S)	<i>p</i> -value	Alpha	Test Interpretation	Nature of Trend
LST_{Min}	8642	0.0819	10850159.33	0.0087	0.05	Reject H0	Upward
LST_{Max}	9305	0.0882	10850163.67	0.0047	0.05	Reject H0	Upward
LST_{Mean}	9709	0.092	10850179.67	0.0032	0.05	Reject H0	Upward
$NDII_{Max}$	-10094	-0.0956	10850248.00	0.0022	0.05	Reject H0	Downward
$NDVI_{Max}$	-7748	-0.0734	10850248.00	0.0187	0.05	Reject H0	Downward
*Rainfall 2009-2018	-86112	-0.0147	4830751280.00	0.2154	0.05	Accept H0	No trend
*Rainfall 2012-2018	-86394	-0.0385	1143571362.00	0.0106	0.05	Reject H0	Downward
*Rainfall 2014-2018	78236	0.0614	492345124.00	0.0004	0.05	Reject H0	Upward
*Rainfall 2016-2018	77711	0.0609	493326659.67	0.0005	0.05	Reject H0	Upward
Annual rainfall	9.0000	0.2000	125.0000	0.4743	0.05	Accept H0	No trend
Monthly rainfall	182	0.0263	191454.67	0.6791	0.05	Accept H0	No trend

Rainfall = Daily rainfall values used

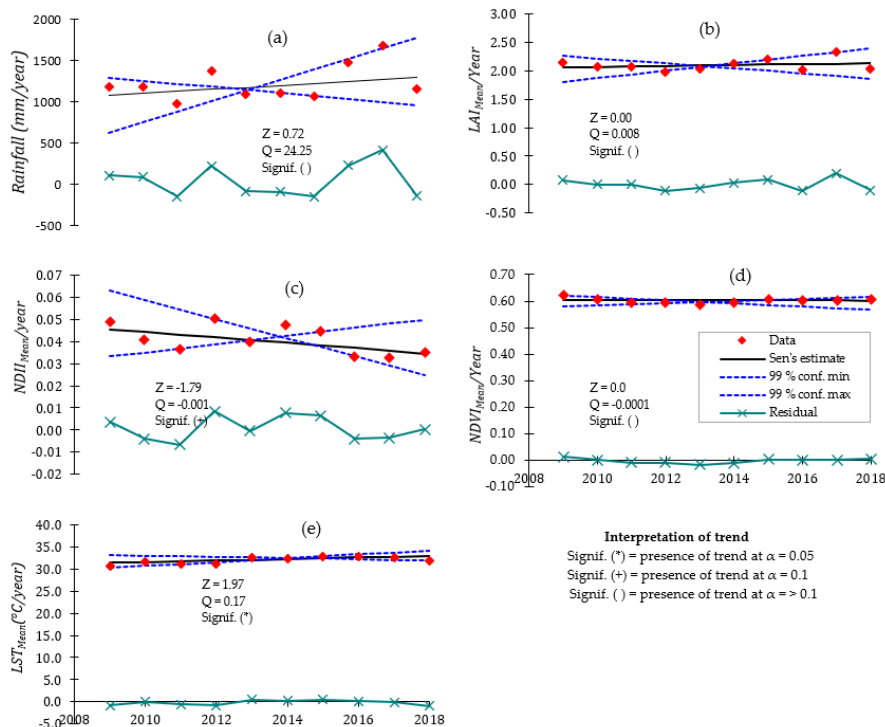


Figure 2.8: Mann–Kendall trends test and the Sens' slope estimates for mean annual rainfall (a), mean annual LAI_{Mean} (b), mean annual $NDII_{Mean}$ (c), mean annual $NDVI_{Mean}$ (d), and mean annual LST_{Mean} (e) for the period of 2009 to 2018. Years with relatively high LST values seem to correspond to years with relatively low rainfall and NDII values.

However, the negative sign in the S-statistic and the Kendall's Tau for the mean monthly and annual rainfall data indicated a general downward movement. The direction of the trend is revealed by the S-statistic and the Kendall's Tau with a positive value indicating an upward trend, and a negative value indicating a downward trend (Table 2.7).

Annual averages of rainfall, LAI, LST, NDII, and NDVI were analysed with the Mann–Kendall and Sens' slope estimate. This was conducted to find out the possible change in the variables per unit of time (i.e., per year) and if these changes showed any relationship(s). Figure 2.8 shows the results of the analyses of the annual average data of variables. The Q is the true slope of linear trend and the Z is the test statistic. It was observed that during the period 2009–2018, rainfall generally increased at a rate of 24.25 mm year⁻¹, which was significant at alpha level > 0.1. The LAI increased at the rate of 0.008 year⁻¹ at alpha level > 0.1. At alpha level 0.1, the NDII reduced at an annual rate of 0.001 year⁻¹, while the NDVI reduced at -0.0001 year⁻¹ at alpha level > 0.1. The most significant rate of change was with the LST, which increased at 0.17 °C year⁻¹ at alpha level 0.05. In essence, at the alpha level of 0.05, only the LST showed a significant annual rate of change. In general, mean LST_{Mean} and LAI_{Mean} increased while NDII_{Mean} and NDVI_{Mean} reduced despite the insignificant (at alpha > 0.1) increase in rainfall.

2.4 Discussion

2.4.1 Variations in canopy cover, canopy water content and canopy temperature

Water and temperature have already been advanced as key variables in the miombo woodland's canopy cover (Vinya *et al.*, 2018; Tian *et al.*, 2018; Chidumayo, 2001; Frost, 1996; Fuller, 1994). However, the studies that used remote sensing-based data such as Chidumayo (2001) and Tian *et al.* (2018) used air temperature, LAI, NDVI, rainfall and the VOD to understand the relationships. In this study satellite-based LST and NDII were used as proxies for the woodland canopy temperature and the woodland canopy water content respectively. Like in the other assessments i.e., Chidumayo (2001) and Tian *et al.* (2018) this study used the LAI and NDVI as proxies for the woodland canopy cover. The observations made in this study in terms of the variations in the woodland canopy cover across seasons were similar to those previously noted by Chidumayo (2001) and Tian *et al.* (2018). The observed variations in the woodland canopy cover during the dry season could be attributed to climatic factors such as rainfall. According to Fuller (1994) and Frost (1996) depending on the amount of rainfall received in the preceding season some miombo species may shed leaves early at the commencement of the dry season in case of low rainfall or may keep leaves late into the dry season in case of high rainfall. These observations are affirmed by the phenology calendar (Fig. 2.2) which show differences in occurrence of phenological stages across years. Further, the ANOVA analyses in this study found statistically significant inter-annual variations in the woodland canopy water content (i.e., NDII) and the woodland canopy cover (i.e., LAI and NDVI). In this study it was observed that the woodland canopy cover is highly correlated and is in sync with canopy water content. These observations, coupled with those by Fuller (1994) and Frost (1996), demonstrate water as a significant woodland canopy cover controlling factor. However, based on the observations in Figs. 2.3 and 2.4 significant woodland canopy cover, as proxied by the LAI and the NDVI, begun to decrease immediately following the end of the rainy season. A plausible explanation for the observed sharp decrease in LAI and NDVI in May could be that the remote sensing LAI and NDVI calculations are based on the 500 m by 500 m spatial resolution (Myneni & Park, 2015) which potentially includes under canopy grass and shrubs. Under canopy grass in the miombo woodland easily dry out at the end of the rainy season when soil moisture reduces (Frost, 1996). Therefore, the observed sharp

decrease in the *LAI* and the *NDVI* in May could be due to wilting and drying of the canopy undergrowth grass and shrubs (Mildrexler *et al.*, 2011) as rainfall would have stopped and soil moisture begun to reduce in the upper layers hence little moisture to sustain grass and shrub turgidity and greenness.

In this study there seemed to be a minimal discrepancy of about one to two months between when the *LAI* and the *NDVI* values begun to rise in the dry season with the *LAI* values appearing to begin rising in August during the dormant stage while the *NDVI* begun to rise between end of September and beginning of October at the start of the green-up stage (Figs. 2.2, 2.3 and 2.4). One plausible explanation for this observation could be that in some miombo woodland species new leaf colour transitions during the dry season. Leaf flush in some miombo woodland species is followed with leaf colour transitions from red to green and occurs at different times for different species with most species undergoing this process between August and October (Vinya *et al.*, 2019; Johnson & Choinski, 1993; Ernst, 1975). The *NDVI* is sensitive to green vegetation thus the colour transitions may affect the values and possibly results in the observed delay. The start in rise in the *NDVI* values in September/October may suggest that that's when the leaf flush or growth of vegetation component occurs which is contrary to the field observations (Vinya *et al.*, 2019; Chidumayo, 2001; Frost, 1996). The start in the rise in the mean *LAI* values in August is likely to be more representative of the occurrence of leaf flush than that of the *NDVI* in September/October. However, the start in rise in *NDVI* values in the dry season correspond with the collection 6 MCD12Q2 start in green-up (Figs. 2.3 and 2.5). This could suggest the *LAI* as being a good proxy for the woodland canopy cover during the dry season than the *NDVI*.

The observed high *LST* values (Fig. 3) in the dry season can be attributed to reduction in the woodland canopy cover (i.e., *LAI*) and the vegetation water content (i.e., *NDII*) (Figs. 2.3 and 2.4). This is because the start in increase in the *LST* values in July when the *LAI* values were towards the lowest could indicate that there is reduced canopy closure which exposes the woodland floor (normally covered with dry leaves and exposed soil) to direct interaction with radiation resulting in increased surface temperature (Jones & Rotenberg, 2001). Furthermore, the *NDII* exhibited zero values in June (Figs. 2.3 and 2.4) which signify that plant water stress is normally attained around this period. *LST* is used as an indicator for plant water stress and drought (Delogu *et al.*, 2018; Cammalleri & Vogt, 2005; Karnieli *et al.*, 2010). Therefore, the start in rise in *LST* in July could also signify plant water stress due to limited water conditions. According to Baldocchi *et al.* (2004) and Mildrexler *et al.* (2011), in the dry season, stomata shut in the savannah trees and the sensible heat fluxes significantly increase. This observation is contrasted by the start in decline in *LST* values in October when the woodland canopy water content (i.e., *NDII*) begun to rise (Figs. 2.3 and 2.4). Most importantly, by October the woodland canopy cover (i.e., *LAI*) and the actual evaporation had increased (Figs. 3 and 4) which imply that there is increase in energy demand (i.e., increase in latent heat fluxes) for evaporation resulting in decline in canopy temperature (i.e., *LST*) (Sun *et al.*, 2016).

2.4.2 Canopy cover relationship with canopy water content and canopy temperature

Contrary to the observations with the air temperature by Chidumayo (2001) this study found that the *LST* accounted for less variation, i.e., 13 percent and 17 percent, in the *LAI* and the *NDVI* respectively compared to the canopy water content at 61 percent and 93 percent in the *LAI* and the *NDVI* respectively. For instance, at the Mpika miombo woodland site Chidumayo (2001) found that rainfall as a single variable accounted for 35 percent of the variations in *NDVI* while a combination of minimum and maximum air temperature accounted for 94 percent of the variations.

However, this study revealed that the woodland canopy water content (i.e., *NDII*), and not the woodland canopy temperature, as a single variable accounted for the largest, i.e., 93 percent, of variations in the *NDVI* annually. However, the combination of the woodland canopy water content (i.e., *NDII*) and the woodland canopy temperature (i.e., *LST*) accounted for the largest variation in canopy cover proxies, i.e., 67 percent in the *LAI* and 96 percent in the *NDVI* (Tables 2.4 and 2.5). For the dry season *LST* as a single variable accounted for 21 percent and 56 percent variations in the *LAI* and the *NDVI* compared to the *NDII* at 56 percent and 90 percent for the *LAI* and the *NDVI* respectively. This observation highlights the significance of surface temperature in observing phenological response during the seasonal drought in the miombo woodland. The observed strong positive correlation between the woodland canopy water content (i.e., *NDII*) and the woodland canopy cover (i.e., *LAI* and *NDVI*) across seasons and the high percentage of accounting for variations in both the *LAI* and *NDVI* could go to augment the role of the vegetation water content in the woodland canopy cover of the miombo woodland. These observations agree with the findings of Tian *et al.* (2018) who demonstrated that plant water storage, as proxied by the *VOD*, strongly covaried with *LAI* and that plant water storage played a critical role in “buffering seasonal dynamics of water supply and demand, and sustaining fresh leaves formed before the rain”. Like demonstrated by Fuller *et al.* (1997) the *NDVI* as proxy for the woodland canopy cover seemed to have better relationship, i.e., higher correlation coefficients, with both the woodland canopy water content and the woodland canopy temperature compared to the *LAI*. Thus, MODIS *NDVI* can act as a better proxy for variations in canopy cover in the miombo woodland in the Luangwa Basin though it might be important to take into account the discrepancies observed in the start in rise of *LAI* and *NDVI* values in the dry season. In previous studies (Sriwongsitanon *et al.*, 2015; Yilmaz *et al.*, 2008; Hardisky *et al.*, 1988) the *NDII* was found to be a good proxy for both vegetation water content and root zone storage. In this study the *NDII* was used as proxy for the woodland canopy water content. It was observed that in the dry season, one to two months before commencement of rainfall, the *NDII* and the E_a values begun to increase (Figs. 3 and 4). This rise in the *NDII* and the E_a cannot possibly be attributed to increased root zone storage but most likely the vegetation own water storage mechanism as espoused by Tian *et al.* (2018), Vinya *et al.* (2018) and Vinya *et al.* (2013).

Generally, the seasonal changes in the canopy cover (as proxied by the *LAI* and the *NDVI*) seem to be in response to the changes in the vegetation water content and the woodland canopy temperature. This behaviour could be a water conservation strategy to deal with stress conditions i.e., reduced water availability and high temperature as has been indicated by field observations by Vinya *et al.* (2018).

2.4.3 Observed abrupt change point(s) and the trends in variables during the 2009 – 2018 period

The Pettit homogeneity test revealed significant upward abrupt change in the 8-day LST_{Min} , LST_{Max} and LST_{Mean} in August 2012. The $NDVI_{Max}$ and the $NDII_{Max}$ showed abrupt downward changes in May 2010 and May 2016 respectively. The change point in the *LST* did not correspond with the change points in the $NDII_{Max}$ and the $NDVI_{Max}$ (Fig. 2.7). Analysis of the mean annual values showed a significant ($\alpha = 0.05$) upward trend in the *LST* increasing at annual rate of $0.17^\circ\text{C year}^{-1}$; the Sens' slope showed the *LAI* and rainfall to generally have been in an upward trend (α level > 0.1) increasing at annual rates of 24 mm/year and 0.008 year^{-1} respectively, while the *NDII* and *NDVI* generally showed a downward trend at α levels 0.1 and >0.1 with annual rates of decrease at 0.001 year^{-1} and 0.0001 year^{-1} respectively (Fig. 2.8). The upward

change in the *LST* could be attributed to several factors including but not limited to; change in land cover i.e. from woodland to cropland or grassland, the uncertainties associated with the estimation of the *LST* especially during the hot-humid periods i.e. in the rainy season, reduction in vegetation water content as a result of a prolonged drought period or reduced rainfall and, data quality (i.e., several outliers in the data) (Jaafar *et al.*, 2020; Sun *et al.*, 2016; Li *et al.*, 2013; Mildrexler *et al.*, 2011; Karnieli *et al.*, 2010). However, in this study it is more likely that the upward abrupt change in the *LST* is a true change. This is because the *LAI* i.e., a proxy for the woodland cover showed a generally upward trend indicating that there were possibly no changes in the woodland land cover. The study site is also a conservancy with extremely limited anthropogenic activities that could result in extensive change in the land cover type. What is more probable, as could be “evidenced” by the generally downward movement in the *NDII* and the *NDVI* (Figs. 2.7 and 2.8) and the daily rainfall values (i.e., as indicated by negative *S* and Kendall Tau values) (Table 2.7), is that the abrupt change and rising trend in the *LST* maybe an indication of the woodland getting drier during the period 2008 – 2018 (Karnieli *et al.*, 2010). Thus, the *LST* maybe a good indicator of temporal changes in the plant water status as a result of changing climatic factors in the miombo ecosystem.

Furthermore, during the period 2009 – 2018 the *NDII* (proxy for canopy water content) did not show any significant (at alpha level 0.05) trend but there was an upward trend in the *LST* (proxy for canopy temperature) with a magnitude of $0.17^{\circ}\text{C year}^{-1}$. However, the upward trend in the *LST* did not result in significant (at alpha level 0.05) downward changes in canopy cover (i.e., proxied by the *LAI* and the *NDVI*). This result augments the observed least determinant factor characterisation of temperature (i.e., *LST*) on the woodland canopy cover as compared to the vegetation water content (i.e., *NDII*).

2.5 Limitations of the study

The satellite-based observations i.e., *LAI*, *LST*, *NDII* and *NDVI* used in the study were not validated with the ground data in the miombo woodland. The E_a values were not direct observations, but model-based and not validated with ground data. The E_a values were based on MODIS MOD16A2 and MYD16A2, which also make use of the other indicators used (i.e., *NDVI/LAI*). Based on the results of this study further investigations should be made using field data to verify these satellite data-based observations.

2.6 Conclusions

The study sought to analyse the relationships between the variations in the woodland canopy cover and the changes in the woodland canopy water content and the woodland canopy temperature at a local miombo woodland using satellite-based data and statistical methods. The study was mainly focused on the dry season. The following conclusions can be drawn from the results:

The woodland canopy cover and the water content were significantly higher during the rainy season while the woodland canopy temperature was significantly higher during the dry season. Over the years, there appears to be no significant difference in dry season canopy temperature. Across seasons, variations in the woodland canopy cover seem to be more strongly associated with the woodland canopy water content than the woodland canopy temperature.

The plant water status, i.e., canopy water content, as a single variable appears to be a major determinant factor of the temporal variation in the woodland canopy cover across seasons, though combination with the woodland canopy temperature appears to significantly improve accounting for variations in the woodland canopy cover during the dry season.

Based on the satellite data analysed in this study, seasonal variations in canopy cover could be a water conservation strategy by miombo plant species as a result of the changes in plant water availability and the woodland canopy temperature.

The satellite-based *LST* and the *NDII* seem to have captured the seasonal variations in the miombo woodland, therefore, they may be good indicators of plant water status in this ecosystem. However, field measurements are needed to determine the degree of correlation with actual physical conditions.

Chapter 3

Phenophase-based comparison of satellite-based evaporation estimates to field observations of a natural woodland: miombo woodland, southern Africa



Photograph showing changes in the canopy attributes across phenophases of the miombo woodland at the Mpika study site, Zambia.

Image: Henry Zimba

This chapter is based on:

Zimba, H. M., Coenders-gerrits, M. A. J., Banda, K. E., Schilperoort, B., Nyambe, I., van de Giesen, N., & Savenije, H. H. G., 2022. Measuring evaporation across canopy phenophases of a natural forest : Miombo forest , Southern Africa. *Hydrol. Earth Syst. Sci. Discuss, October*, 1–23. doi: <https://doi.org/10.5194/hess-2022-303>, in review.

Chapter 3

“Estimating invisible water. Easy as
drinking water?”

(Personal reflection – H.M. Zimba)

3.1 Introduction

Global terrestrial evaporation is about 60 percent of the total incoming precipitation (Miralles *et al.*, 2011a; Van Der Ent *et al.*, 2014). Evaporation in Africa, Asia and south America accounts for 78 percent of this terrestrial evaporation (Miralles *et al.*, 2011a). A general paucity of evaporation flux observation towers exists across the vast spectrum of ecosystems. As a consequence, in most cases several satellite-based evaporation estimates (e.g., GLEAM, MODIS, SSEBop) are used in hydrological modelling and water resources management without validation with field observations from the African ecosystems. In the face of climate change, accurate information on evaporation dynamics in major ecosystems, like the miombo woodland in southern Africa is important in the management of scarce water resources. Some studies have been conducted to validate satellite-based evaporation estimates in Africa (e.g., Blatchford *et al.*, 2020; Dile *et al.*, 2020; Weerasinghe *et al.*, 2020; Ramoelo *et al.*, 2014). However, none of these studies used field observations based on the miombo woodland evaporation.

In southern Africa, the miombo woodland is the largest dry forest formation (Fuller, 1999; Frost, 1996) and the characteristic vegetation cover for many river basins, including the Zambezi Basin. The miombo woodland has unique phenology (Chidumayo, 2001; Fuller, 1999, Frost, 1996) and plant-water interactions that are different from other ecosystems in Africa (Tian *et al.*, 2018; Vinya *et al.*, 2018). For instance, Fuller (1996) conducted an assessment of miombo canopy phenology, i.e., leaf display and canopy closure, in the Luangwa Basin in Zambia. The plots for the assessment included the mopane woodland and the miombo woodland. Both wet miombo (i.e., plateau miombo in Mpika) and dry miombo (i.e., valley areas) in the Luangwa Basin were assessed. The assessment involved field estimates of the normalised vegetation index (NDVI) for leaf display and the upward pointing photographs were used for canopy closure observations. The results showed the plateau miombo with the lowest seasonality in the tree layer with mean range of 40 - 60 % closure over one season. The canopy closure values among the miombo plots ranged between a minimum of 2 % for the scrub miombo to a maximum of 70 % for the plateau miombo. For the plateau miombo, compared to other miombo plots (i.e., scrub and valley miombo) it was observed that there is net zero change in the increase in the canopy closure due to simultaneous leaf fall and leaf flush in the dry season before the commencement of the rains. The leaf fall, leaf flush and the accompanying change in leaf colour occur during what is normally termed the transition period in the dry season (May – October) (Fuller, 1999; Frost, 1996; White, 1983). The leaf fall and leaf flush are species dependent, occurring at different times for each species in the dry season. The flushing of new leaves, weeks to months or more, before commencement of seasonal rainfall is a unique feature of the miombo woodland (Frost, 1996; White 1983). Depending on rainfall received in the preceding rain season, the leaf fall and leaf flush processes may start early in the cool dry season (i.e., in case of low rainfall received) or late (in case of high rainfall received) and may extend into November in the early rainy season (i.e., in the case of high rainfall received) (Fuller, 1999; Frost, 1996; White, 1983). The new young flushed leaves have high leaf water content of about 66% which declines to around 51% as the leaves harden until they are shed in the next season. The osmotic pressure in the flushed leaves in the dry season increases as the leaves harden but declines after the onset of the rains reaching minimum levels in February (Ernst and Walker 1973). Most miombo species are broad leaved with capacity to intercept more radiation than other vegetation types such as the mopane species (Fuller, 1999). Wet miombo woodland canopies intercept between 18-20 % of incoming rainfall annually (i.e., Alexandre, 1977). Most miombo species are deep rooting, beyond 5 metres, with access to deep soil moisture (Savory, 1963). The moisture in miombo woodland soils increases with depth (Chidumayo, 1994;

Jeffers and Boaler 1966; Savory, 1963). Miombo species also have a plant water storage mechanism (i.e., Vinya *et al.*, 2018; Ernst and Walker 1973) that helps to buffer dry season water limitations. The highlighted unique phenological attributes of the miombo species suggests that the miombo woodland gives evaporation feedback incomparable to other ecosystems.

The evaporation dynamics of the miombo woodland and its relationship with the above highlighted phenological characteristics have not been studied. However, given the need for assessing the limited water resources in the ecosystem, there is a clear need for a detailed understanding of the phenophase-based evaporation of the miombo woodland. Yet, estimating evaporation over natural vegetation such as the miombo woodland in southern Africa remains a challenge.

Limitations can be found in all available conventional approaches, such as the eddy covariance (EC) system (Foken, Aubinet, and Leuning, 2012; Jarmain *et al.*, 2009; Savage *et al.*, 1997), lysimeters (Sutanto, Wenninger, and Uhlenbrook, 2012; Teuling, 2018), scintillometry (Dzikiti *et al.*, 2014; Jarmain *et al.*, 2009) and the conventional Bowen ratio (Everson, 2001; Savage *et al.*, 1997; Bowen, 1926). For instance, inability to account for energy fluxes near the observation tower causes energy closure problems in the EC-systems. Site heterogeneities introduces horizontal and vertical advective terms that are impossible to resolve by single point flux tower measurements (Liu *et al.*, 2006). Furthermore, if the optical path is obscured, such as occurs in wet conditions, the EC's optical open-path sensors do not work properly and if the open-path analyzer is wet the evaporation which occurs shortly after a rainfall event is not observed (Coenders-Gerrits *et al.*, 2020; Hirschi *et al.*, 2017). In the case of the two vertical sensor-based Bowen ratio, each sensor has its own errors which are propagated to the Bowen ratio. Additionally, it is difficult to ensure that the two sensors are correctly aligned with each other which results in incorrect Bowen ratio estimates (Angus and Watts, 1984; Spittlehouse and Black, 1980). Jarmain *et al.* (2009) assessed and reported on various conventional methods for estimating evaporation in different land surfaces in south Africa. However, recent advances in the distributed temperature sensing system has expanded possibilities for improved accuracy in energy partitioning and the application of the Bowen ratio for evaporation flux assessment in woodlands (Euser *et al.*, 2014; Schilperoort *et al.*, 2020; Schilperoort *et al.*, 2018). In contrast to the conventional Bowen ratio approach, the Distributed Temperature Sensing Bowen ratio technique (BR-DTS) makes use of several vertical high resolution temperature measurements made with a single fibre optic cable. This eliminates the need for the conventional configuration with two individual sensors at different locations and the associated errors with this type of set up. One section of the fibre optic cable measures the air temperature profile, while a second section, covered in a constantly wetted cloth, measures the wet-bulb temperature profile. The vapour pressure profile can be derived through the psychrometer principle. The DTS technique enables that wet and dry bulb temperature measurements can cover the entire vertical profile through a woodland stand: above the canopy, within the canopy, and under the canopy. This is conducted simultaneously along a single fibre optic cable, thereby facilitating a deepened understanding of the energy partitioning in a woodland (Schilperoort *et al.*, 2020; Schilperoort *et al.*, 2018; Euser *et al.*, 2014). Coenders-Gerrits *et al.* (2020) have suggested that the DTS technique offers opportunities to assess forest energy storage components that are not normally captured when using conventional approaches. The BR-DTS approach provides an avenue for enhanced understanding and increased accuracy in the estimation of forest evaporation. This is notwithstanding the challenges associated with the BR-DTS approach such as the requirement for sufficient ventilation and constant wetting of the fibre optic cable. Despite the highlighted advantages of the BR-DTS approach its major limitation is

that it is a point measurement. Furthermore, compared to the EC method the BR-DTS approach tends to minimally overestimate diurnal latent heat flux (LE) by a mean difference of 18.7 Wm^{-2} (Schilperoort *et al.*, 2018).

For the miombo woodland, the need for field-based actual evaporation estimates is highlighted by the discrepancies in satellite-based evaporation estimates (Zimba *et al.*, 2023 under review). Due to a lack of field-based observations of actual evaporation of the miombo woodland the satellite-based evaporation estimate(s) that are close to field conditions are unknown. Therefore, this study is focused on providing an independent estimation of actual evaporation of the wet miombo woodland that can be used to validate satellite-based evaporation estimates.

In this study field observations were compared to four commonly-used free satellite-based actual evaporation estimates: GLEAM (Martens *et al.*, 2017; Miralles *et al.*, 2011b), MOD16 (Mu *et al.*, 2011), SSEBop (Senay *et al.*, 2013) and WaPOR (FAO, 2018). The satellite-based estimates were selected because they can be obtained free of cost, have comparatively high spatial-temporal resolution, and good spatial coverage (i.e., global in the case of GLEAM, MODIS, SSEBop and continental in the case of WaPOR), and are ready-to-use products with no further processing required. Hence, the focus of our study was on characterising the actual evaporation of the miombo woodland using the BR-DTS approach, and comparing the field observations to the satellite-based evaporation estimates. Consequently, objectives of this study were to:

1. Estimate the actual evaporation of the wet miombo woodland across difference canopy/leaf phenophases to help understand the flux trend and magnitude in the ecosystem,
2. Compare free satellite-based evaporation estimates to the field-based estimates at point scale across the different canopy/leaf phenophases of the wet miombo woodland.

3.2 Materials and methods

3.2.1 Study site

The study was centred on a miombo woodland at the Nsanzala and Mutinondo conservancy areas (lat: -12.38° S , long: 31.17° E) in the Mpika District, northern Zambia in southern Africa (Fig. 3.1). Zambia was selected because it is considered to have the largest diversity in miombo woodland species composition (Frost, 1996; White, 1983). The site in Mpika was chosen because it represents a large area of undisturbed miombo woodland with high heterogeneity in species typical of miombo woodland. The site is also situated in the largest miombo ecosystem component of the wetter central Zambezi miombo (Olson *et al.*, 2001; White, 1983), in the north-western part of the Luangwa Basin (Fig. 3.1). At the study site, species identification and counts within a 250m-by-250m sample plot showed that over 95 percent of the dominant miombo species is semi-deciduous and include: *Brachystegia floribunda*, *Brachystegia longifolia*, *Brachystegia boehmii*, *Brachystegia speciformis*, *Jubenerdia paninculata*, *Uapaca kirkiana*, *Pericopsis angolensis*, *Bauhinia petersenia* and *Uapaca sansibarica*. These are typical miombo species, especially the *Brachystegia floribunda*, found in the wetter Zambezi miombo woodland (Fuller, 1999; White, 1983). The typical characteristics of the miombo species at the site are that they shed off leaves (leaf fall) and also leaf flush during what is termed as the transition period in the dry season (May – October). Frost (1996) indicated that, based on the amounts of rainfall received in the preceding rain season, the leaf-fall and leaf flush processes may start early (i.e., in case of low rainfall received) or late (in case of high rainfall received) and may extend up to November (i.e., in the case of high rainfall received). Elevation ranges between 318 m and 2327 m above sea level (Fig. 3.1 b). The study site has a mean annual rainfall of $1200 \text{ mm year}^{-1}$ and mean annual temperature

of 26 °C. Rainfall is a result of the movement of the intertropical convergence zone (ITCZ) over Zambia. Rainfall period is between October and April while the dry season is between May and October (Hachigonta and Reason, 2006; Chidumayo, 2001). The woodland at the study site is undisturbed by anthropogenic activities due to the site being a conservancy. The major activities in the area are controlled cattle ranching and tourism.

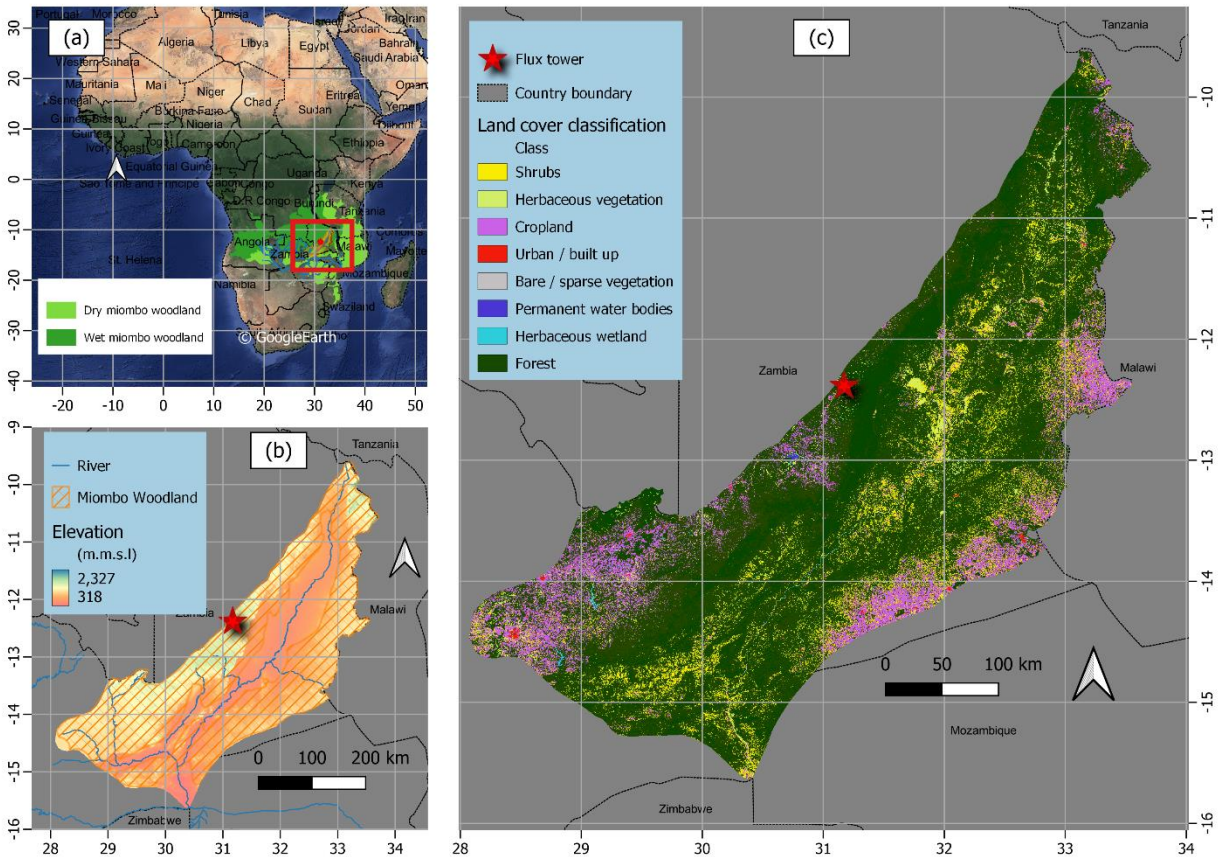


Figure 3.1: Location and extent of the miombo woodland in Africa (a), elevation characterisation in the Luangwa Basin and at the study site in Mpika (b) and land cover classification of the Luangwa Basin (c). The ASTER Digital elevation model was used to depict elevation while the 2019 Copernicus Land cover for Africa was used for land cover characterization.

Controlled burns at the study site are normally conducted in August when the Dambos (wetlands) are dry, and are mainly conducted in the dambo grassland for livestock grazing purposes. The non-burning of the study site ensured the evaporation observations were not influenced by fire activity especially burning of the canopy leaves.

3.2.2 Study approach

3.2.2.1 Characterisation of phenophases at the study site

This study compared estimates of actual evaporation by the BR-DTS method with the Penman-Monteith reference evaporation (Allen *et al.*, 1998) and to four satellite-based evaporation estimates at point scale in the miombo woodland. The observations were conducted for the period

May to December 2021. The study period facilitated assessment of evaporation during the dry season and early rainy season across three different phenophases of the miombo woodland. The phenophases were characterised using satellite-based data (Gray *et al.*, 2019; Zimba *et al.*, 2020) and the climate (rainfall and temperature) and soil moisture-based classification by Chidumayo and Frost (1996). Satellite-based classification uses the changes in canopy greenness to characterise the canopy phenophases (Gray *et al.*, 2019). In this study the Collection 6 MODIS Land Cover Dynamics (MCD12Q2) Product (Gray *et al.*, 2019; Friedl *et al.*, 2019; Zhang *et al.*, 2003) was used to identify the satellite-based phenophases. For the year 2021 eight phenophases were identified using the satellite-based data MCD12Q2 (Fig. 3.2), NDVI, leaf area index (LAI) and photographs from a digital camera (Denver WCT-8010) installed on the flux tower at the study site (see Fig. 3.9 in section 3.3.6). For the climate and soil moisture-based classification Chidumayo and Frost (1996) observed five phenological seasons: warm pre-rainy season, early rainy season, mid-rainy season, late rainy season and the cool dry season (Fig. 3.2). Within these phenological seasons the phenology of miombo species transition through various stages i.e., from leaf fall/leaf flush, growth of stems, flowering to mortality of seed (Chidumayo and Frost, 1996). The satellite-based phenophases can be identified within the climate-based phenological seasons (Fig. 3.2). Based on the period for this study, May – December, five satellite-based phenophases were identified within three climate-based phenological seasons (Fig. 3.2). The identified phenophases based on satellite data were the green-down, mid-green down, dormant, green-up and the mid-green up (Fig. 3.2). For easy of analysis some satellite-based phenophases were merged based on the dominant activity.

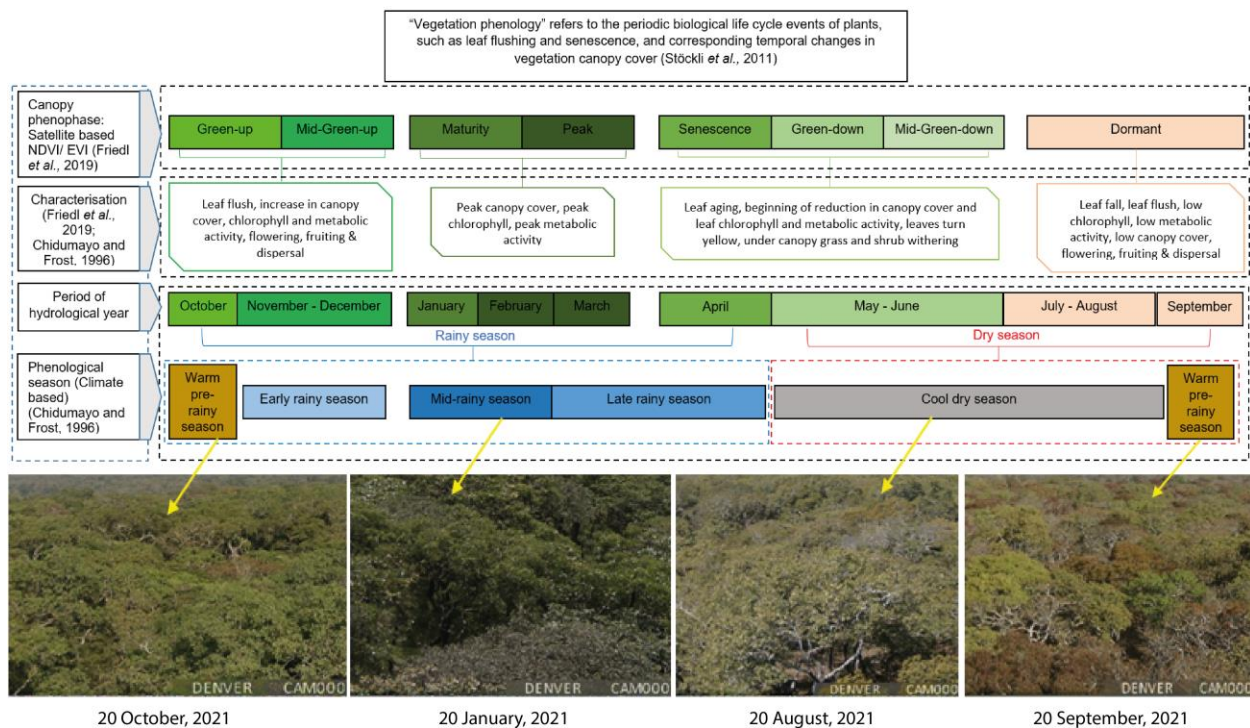


Figure 3.2: Characterisation of canopy phenophases of the miombo woodland in relation to seasonality at the study site. Photographs show the changes in the canopy cover on selected days across phenophases for the year 2021.

For instance, the green-down and mid-green-down were merged together into one green-down phenophase while the green-up and mid-green-up were merged into one green-up phenophase. The established satellite-based phenophases green-down (May–June), dormant (July – September) and green-up (October – December) were in the cool-dry season, warm pre-rainy season and early-rainy season phenological seasons (Fig. 3.2). The detailed characterisation of the phenology of the miombo woodland, particularly in Zambia, can be found in Chidumayo (2001), Fuller (1999), Chidumayo and Frost (1996) and Fuller *et al.* (1996).

3.2.3 Estimating potential evaporation

The Penman-Monteith (PM) equation (i.e., Eq. 6 in Allen *et al.*, 1998) was used to estimate reference evaporation (E_o) from which potential evaporation for the miombo woodland was calculated using Eq. (3.1). All required inputs for the PM equation were obtained at the study site. To obtain potential evaporation for the miombo woodland the crop coefficient (K_c) value of 0.8 was used. The K_c value used was obtained from literature (Hunink *et al.*, 2015). The K_c value was estimated based on the miombo woodland in Mahele, Tanzania. The K_c value for the Mahele region in Tanzania was utilised because it is situated in the wet miombo region receiving rainfall of about 1000 mm year⁻¹, with similar seasonality as the study site in Mpika, Zambia in which rainfall starts late October and ends early May (Hunink *et al.*, 2015). Furthermore, despite its vast expanse there is unexpectedly little variation in miombo woodland species diversity (Chidumayo and Gumbo, 2010). In this study the same K_c value was applied for the dry and the rainy season.

$$E_{c(PM)} = K_c \cdot E_o \quad (3.1)$$

3.2.4 Conventional Bowen ratio energy balance method

The Bowen ratio is the proportion of the sensible (H) to the latent heat flux (LE) of a surface. In simple form the Bowen ratio can be determined by multiplying the psychrometric constant by the ratio of the temperature and vapour pressure gradients as expressed in Eq. (3.2):

$$\beta \approx \gamma \cdot \Delta T_a / \Delta e_a \quad (3.2)$$

where γ is the psychrometric constant (kPaK⁻¹) (Eq. 3.3), ΔT_a is the difference in temperature (K) between two heights and Δe_a is the difference in the actual vapor pressure (kPa) between the same two heights. The psychrometric constant is obtained using the relationship between air pressure and ventilation of the psychrometer as given by Allen *et al.* (1998) in Eq. (3.3):

$$\gamma = 0.0665 \times 10^3 \cdot P_a \quad (3.3)$$

where, P_a is the atmospheric air pressure (kPa).

Despite the simplicity of the approach, the energy balance Bowen ratio method needs to meet several conditions in its application for results to be reliable. For instance, the two levels at which the temperature and vapor pressure are measured must be within the boundary layer of the air flow, which has adjusted to that particular land surface. The measurement site therefore requires

extensive fetch in the upwind direction for the airflow over the land surface, in this case the forest canopy. A fetch of at least 100 times the maximum height of measurement is typically suggested for such measurements (Angus and Watts, 1984).

3.2.5 BR-DTS energy balance approach

The BR-DTS method measures air temperature gradients directly and the vapour pressure gradients are estimated via the wet bulb temperatures using Eq. (3.4):

$$e_{a(T_a)} = e_{s(T_w)} - \gamma(T_a - T_w) \quad (3.4)$$

where $e_{a(T_a)}$ is the actual vapour pressure, $e_{s(T_w)}$ is the saturated vapour pressure, γ is the psychrometric constant, T_a and T_w are the dry bulb and wet bulb temperature. Details on this calculation can be found in Schilperoort *et al.* (2018).

In contrast to the conventional Bowen Ratio Energy Balance, where only the temperature and vapour pressure at two heights are used, the BR-DTS method uses all measuring points between two heights. All dry and wet bulb temperatures within this segment are used to determine the gradients according to a natural logarithmic of the height (Eqs. 3.5 and 3.6):

$$T_{a_{fit}} = a \cdot \ln(z) + b \quad (3.5)$$

$$e_{a_{fit}} = c \cdot \ln(z) + d \quad (3.6)$$

The fitted DTS temperature and actual vapour pressure at 11 m (bottom) and 15.5 m (top) heights above the forest canopy were used to estimate the Bowen ratio following Eqs. (3.7) – (3.9):

$$\beta = \gamma \cdot \frac{\Delta T_{a_{fit}} / \Delta z}{\Delta e_{a_{fit}} / \Delta z} \quad (3.7)$$

in which;

$$\Delta T_{a_{fit}} / \Delta z = T_{a_{fit}}(z=\text{top}) - T_{a_{fit}}(z=\text{bottom}) / (z=\text{top} - z=\text{bottom}) + \Gamma(z) \quad (3.8)$$

and

$$\frac{\Delta e_{a_{fit}}}{\Delta z} = \frac{e_{a_{fit}}(z=\text{top}) - e_{a_{fit}}(z=\text{bottom})}{z=\text{top} - z=\text{bottom}} \quad (3.9)$$

where $\Delta T_{a. fit}$ is the difference in air temperature (K) of the fitted curve between the bottom and top of the height range used for the Bowen ratio, $\Delta e_{a. fit}$ is the difference in actual vapor pressure (kPa) of the fitted curve over the same height as in temperature, Δz is the difference in height (m) between the two points and Γ is the adiabatic lapse rate (normally around 0.01 Km^{-1}). During dry and unsaturated conditions, very small temperature and vapor pressure gradients could result in errors in the Bowen ratio estimates. The use of the lapse rate is recommended in such circumstances (Schilperoort *et al.*, 2018; Barr *et al.*, 1994). In this study the lapse rate was applied throughout the study period following Schilperoort *et al.* (2018). Before fitting the raw DTS data was calibrated following the approach by des Tombe *et al.* (2020).

3.2.6 DTS data quality control

The quality control process followed the demonstration by Schilperoort *et al.* (2018) as shown in Eqs. (3.10) and (3.11). Only diurnal temperature and actual vapour pressure data (i.e., obtained between 06AM and 18PM were considered). This is because night time actual evaporation was not estimated, as it was assumed to be negligible. The correlation coefficient of determination (r^2) values for fitted vapour pressure were used for quality control. The fitted actual vapour pressure with r^2 values below 0.2 and Bowen ratio values approaching -1.1 and -0.9 were removed from the data and gaps filled by the regression method. The coefficients (r^2) for dry and wet bulb temperature were not considered because the high uncertainty in temperature is propagated in vapour pressure.

$$\text{Flag 1: } r^2_{ea,z} > 0.20, \quad (3.10)$$

$$\text{Flag 2: } \beta < -1.1 \text{ or } \beta > -0.9. \quad (3.11)$$

3.2.7 Actual evaporation estimation

Several studies (i.e., Buttar *et al.*, 2018; Euser *et al.*, 2014; Xing *et al.*, 2008; Spittlehouse and Black, 1980) demonstrated the use of the Bowen ratio in combination with the energy balance to assess the latent heat flux. In combination with other energy terms the Bowen ratio energy balance estimate of evaporation (E_β) can be performed using Eq. (3.12):

$$E_\beta = (R_n - M - G_s)/L(1 + \beta) \quad (3.12)$$

where R_n is the net radiation flux (Wm^{-2}), L being the latent heat of vaporization of water (2.45 MJkg^{-1}), G_s is the ground heat flux (Wm^{-2}) and the M is the change in energy storage in the system canopy storage (Wm^{-2}). The ground heat flux in this study was estimated from the net radiation at hourly intervals. For the Penman-Monteith model (Allen *et al.*, 1998), the ground heat flux for hourly (G_{hr}) or shorter periods for reference/growing crop, can be estimated from net radiation (R_n) using Eq. (3.13) during daylight and Eq. (3.14) during night-time periods. However, the G_s for woodlands is different from that of grass or growing crop. Some studies, in different woodlands, found G_s to be between 5 – 24 percent of R_n (i.e., Ma *et al.*, 2017; Van Der Meulen

and Klaassen, 1996; McCaughey, 1982). With reference to observed G_s in different woodlands, this study selected 10 percent of R_n for hourly daytime G_s . The 10 percent was selected because the wet miombo woodland at the study site, at any period of the year, has about 70 percent canopy closure (Fuller, 1999; Frost, 1996). Furthermore, during the dry season (May-October) top soil (0 - 30 cm) moisture, was not expected to vary significantly.

$$G_{hr} = 0.1R_n \quad (3.13)$$

$$G_{hr} = 0.5R_n \quad (3.14)$$

We follow Schilperoort *et al.* (2018) in their observation that the change in canopy storage (M) can be ignored. The E_β was estimated at hourly intervals and then summed up into daily and 10-day values.

3.2.8 Comparison of satellite-based evaporation estimates to field observations

For comparison to satellite-based evaporation estimates, field actual evaporation estimates were aggregated into 10-day and monthly data sets to align with the satellite-based evaporation estimates temporal scales. The native spatial resolutions (Table 3.1) of the satellite-based evaporation estimates were used because these products are mostly applied or used in their native resolution configuration. All satellite-based estimates used in this study can be obtained free of cost and are readily available. In Africa, financial constraints are a resource limitation for field observations. Therefore, to have access to free of cost satellite-based evaporation estimates has significant advantage. Furthermore, in the context of this study, sufficient historical data was available and all satellite-based evaporation estimates are continuously being processed which assures, to a large extent, future availability of data for continued monitoring. Except for the WaPOR, which had a continental spatial extent, the rest of the satellite-based evaporation estimates had global spatial extent. However, all four satellite-based evaporation estimates adequately covered the extent of the miombo woodland, which was the focus of this study. All four satellite-based estimates were accessed online from different platforms as indicated in Table 3.1. Details of the methods for each satellite-based evaporation estimate can be found in the specific documents cited in Table 3.1.

3.2.9 Statistical analysis

The field observations and satellite-based evaporation estimates were compared using the Kendall and Pearson correlation coefficients, correlation coefficient of determination (R^2) (Eq. 3.15), Root Mean Square Error (RMSE) (Eq. 3.16) and the mean bias error (MBE) (Eq. 3.17). These are some of the commonly used techniques for comparing pairs of variables and assessing performance of hydrological models (Helsel *et al.*, 2020). The coefficient of determination measures the strength of relationship between the observed with the modelled values. The relationship between variables is strongest as the R^2 value approaches 1. The RMSE quantifies the deviation of the predicted values from the observed values. The model predictions are more accurate as the RMSE value approaches zero. The mean bias error is the measure of the extent to

which modelled values deviate from observed values and indicates whether there is under or overestimation. The smaller the mean bias error value the less the deviation of the predicted values from the observed values (Helsel *et al.*, 2020). Negative value indicates underestimation while a positive value indicates overestimation.

$$R^2 = 1 - \frac{\sum_{i=1}^n (E_s - \bar{E}_{a(DTS)})^2}{\sum_{i=1}^n (E_{a(DTS)i} - \bar{E}_{a(DTS)})^2} \quad (3.15)$$

$$RMSE = \sqrt{\frac{1}{n} \sum_{i=1}^n (E_{si} - E_{a(DTS)i})^2} \quad (3.16)$$

$$MBE = \frac{1}{n} \sum_{i=1}^n (E_{si} - E_{a(DTS)i}) \quad (3.17)$$

where, $E_{a(DTS)}$ is the BR-DTS-based actual evaporation estimate, $\bar{E}_{a(DTS)}$ is the mean of the BR-DTS-based actual evaporation estimate, E_s is the satellite-based evaporation estimate and n is the number of observations.

Table 3.1. Characteristics of satellite-based evaporation estimates used in this study

Satellite-based evaporation estimate	Spatial coverage	Temporal resolution	Spatial resolution(m)	Estimation approach	Source of input data	Reference	Source of data
GLEAM (V3.6a and v3.6b)	Global	Daily	27700 m	Priestley Taylor equation, Soil moisture stress factor	AMSER-E, LPMRM, MSWEP+MSWX	(Martens <i>et al.</i> , 2017; Miralles <i>et al.</i> , 2011b)	FTP server. Last accessed: 05/06/2022
MOD16v2	Global	8-days	500 m	Penman-Monteith equation, surface conductance model	MODIS	(Mu <i>et al.</i> ,2011)	Climate Engine portal Access: https://app.climateengine.com/climateEngine Last accessed: 05/06/2022
SSEBop	Global	10-days	1000 m	Penman-Monteith equation, ET fractions from T _s estimates	MODIS and GDAS	(Senay <i>et al.</i> , 2013)	Climate Engine portal Access: https://app.climateengine.com/climateEngine Last accessed: 05/06/2022
WaPOR v2	Continental	10-days	250 m	Based on the ETLook model, Penman-Monteith equation, estimates Ea, I and T separately	MODIS	(FAO, 2018; Bastiaanssen <i>et al.</i> , 2012)	WaPOR Portal Access: https://wapor.apps.fao.org/home/WAPOR_2/1 Last accessed: 05/06/2022

3.2.10 Flux observation tower setup

Temperature was measured using a single 3 mm 1 km long white jacket duplex single tube fibre optic cable connected to the DTS machine. The cable's ends were spliced together to loop the signal back making a double ended configuration. Double ended configuration was explained in (van de Giesen *et al.*, 2012). The DTS machine used is the Silixa XT-DTS (Silixa Ltd, 2016) with sensing capabilities as shown in Table A1 in the appendices. A calibration bath was set up in which 10 m of the fibre cable from the DTS was placed in water together with 2 x 2 PT-100 probes for the entire period of the measurements. The DTS was set to take temperature measurements at a 5 minutes interval. The fibre optic cable was firmly secured on a 17.25 m vertical tower (illustrated in Figs. 3.3 and 3.4) following the techniques demonstrated by Euser *et al.* (2014) and Schilperoort *et al.* (2018). One section of the fibre cable (blue line in Fig. 3.3) from the DTS machine was wrapped in cotton cloth (Fig. 3.4 a) starting at the base up to the top of the tower and was always kept wet for estimation of what is known as wet bulb temperature. Separated by a 1 m gap the other section of the fibre cable (red cable in Fig. 3.3) was not wrapped (Fig. 3.4 b) in a cotton cloth and was designated to measure the air temperature. The cloth on the designated wet cable was kept constantly wet by the water that was pumped to the 65-litre tank placed at the top of the tower. The water flow from the water tank to the fibre cable was regulated (roughly 20 litres per day) to ensure a smooth and constant wetting of the cotton cloth.

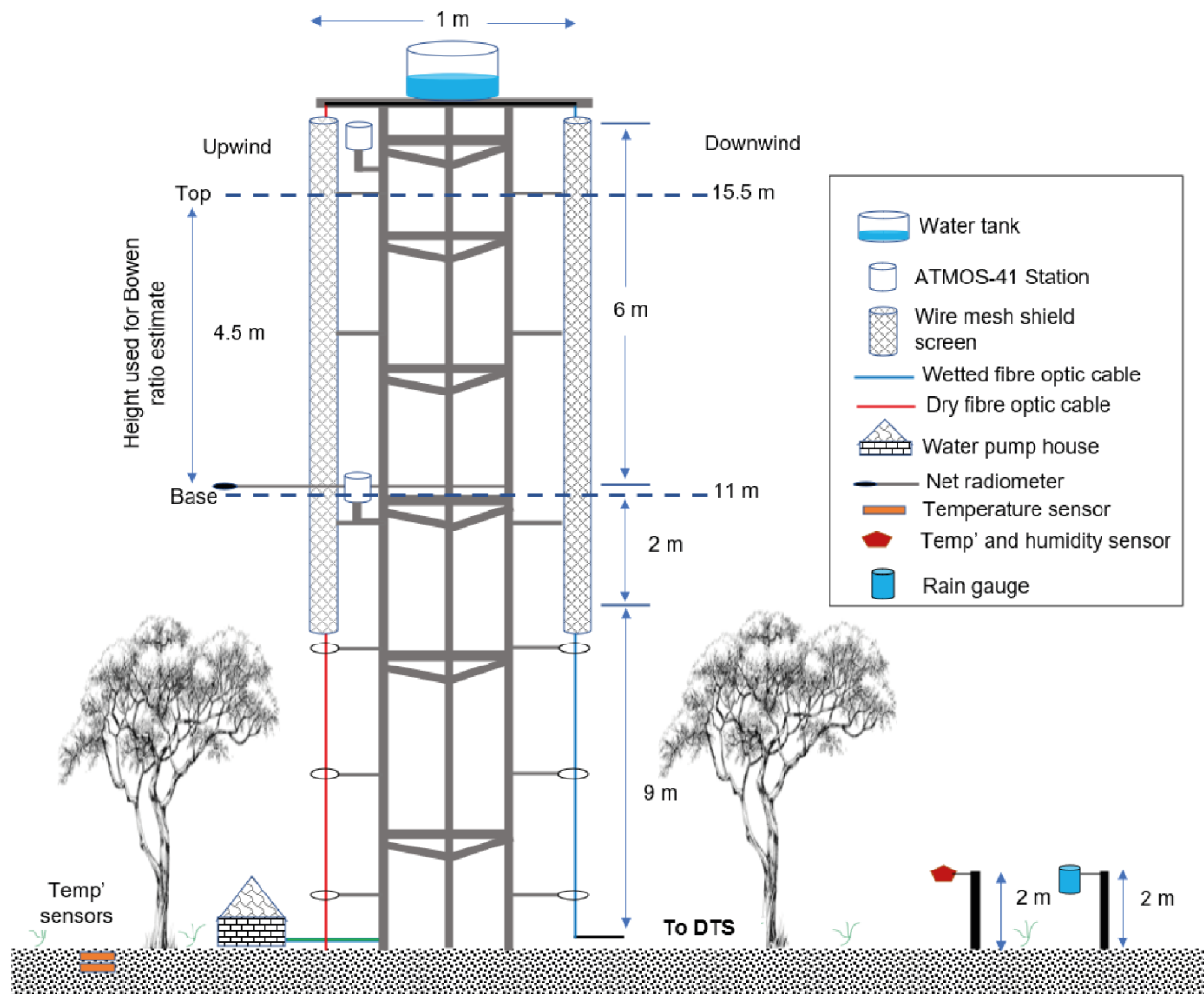


Figure 3.3: Schematic drawing (not to scale) of the field set-up of the observation tower at the wet miombo woodland study site in Mpika, Zambia.

As recommended by Euser *et al.* (2014) the wet cable was placed on the downwind side while the dry cable was placed on the upwind side of the tower. The type of cables arrangement prevented water from the wetted cotton cloth for the wet cable from splashing onto the dry cable. This set up of cables ensured that the dry bulb temperature measurements were not affected. Furthermore, a gap of 1 m also contributed to ensuring that the dry cable was not affected by the water from the wetted cotton cloth. Following the recommendation by Schilperoort *et al.* (2018) both the wet and dry cables were shielded from direct sunlight by 8-meter long two layered wire mesh screens placed above the canopy (Fig. 3.3). A portion of data, within 2 m of the top of the tower, was not included in the assessment because it was assumed to influence the wet cloth/wet cable temperature as the water from the tank above the tower was at a temperature slightly higher than the air temperature.

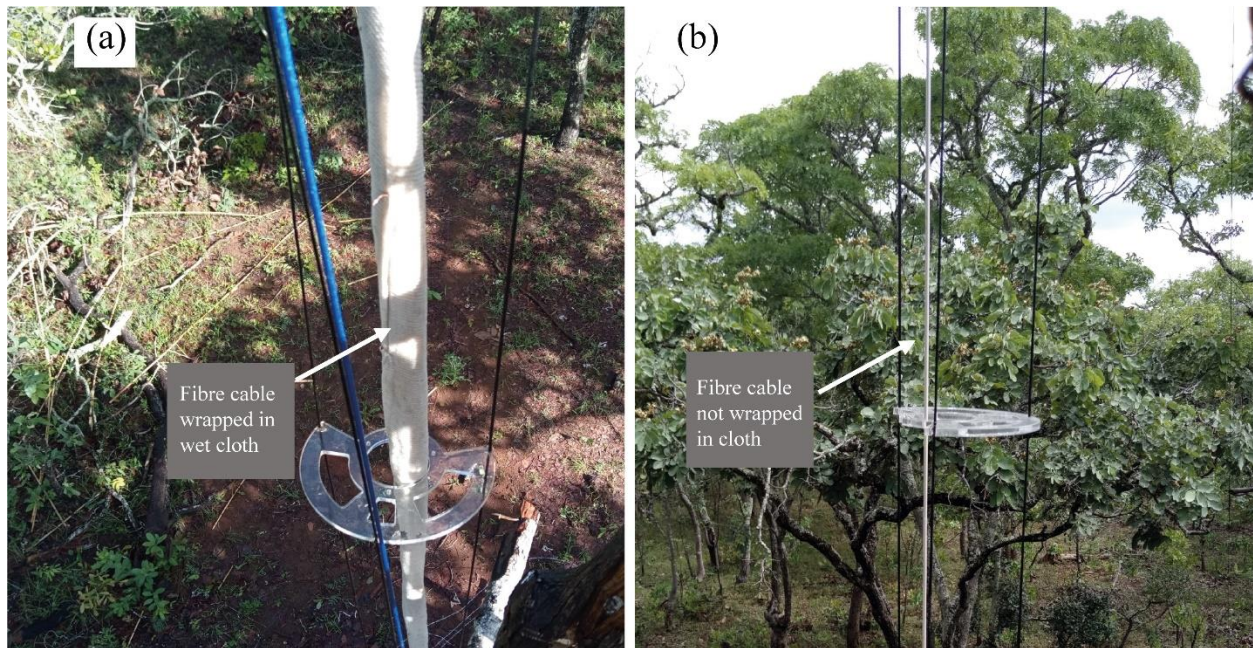


Figure 3.4: Optic fibre cable wrapped in the wet cloth (a) for collecting the wet bulb temperature and (b) optic fibre cable not wrapped in cloth for estimating the dry bulb temperature on the observation tower at Mpika site, Zambia. Under canopy view without screens.

The 2 m length was considered a sufficient length for the temperature of the water from the tank to be uniform with the environment and suitable for measurement of wet bulb temperature. For this study the tower height was 17.25 m and the fetch was beyond 1.7 km. The fetch covered an area with more than 20 km of uninterrupted miombo woodland with typical sporadic small seasonal wet grasslands (Fig. A1 b in the appendices of Zimba *et al.*, 2023). Furthermore, Spittlehouse and Black (1980) showed that greater accuracy in the Bowen ratio measurements could be attained by increasing the separation between, and interchanging the psychrometers. In this study it was ensured that more than 4 metres separation were between the two levels at which the temperature and actual vapour pressure were selected above the canopy.

To obtain the net radiation (R_n , Wm^{-2}) the NR Lite 2 net radiometer (Kipp & Zonen CNR4) was installed at about 2 m above the canopy (that is 11 meters from the ground) (Fig. 3.3). The net radiation was logged at an hourly interval using the Campbell CR10X data logger. With reference to estimates in other ecosystems (i.e., Ma *et al.*, 2017; Van Der Meulen and Klaassen, 1996; McCaughey, 1982) an hourly ground heat flux (G_o , Wm^{-2}) was estimated at 10 percent of the hourly net radiation. The soil moisture was obtained using two HOBOnet ECH2O™ EC-5 soil moisture sensors placed at 5 cm and 30 cm in the soil sub-surface. The Onset HOBO S-THB-M002 smart sensors were used to measure under-canopy air temperature and relative humidity at 2 m above the ground and logged at a 5-minutes interval. Using the Onset HOBO RG2-M – raingauge rainfall was measured at the flux tower site 2 m above ground and away from tree canopies (Fig. 3.3). The rain gauge was logged at a 5-minutes interval.

The air temperature and actual vapour pressure to compare with the DTS measurements were obtained using the METER Group Em60G ATMOS-41 all-in-one weather station sensors. The ATMOS-41 sensors meet standards for the World Meteorological organization (WMO). The

accuracy of the ATMOS-41 is ± 0.6 °C for air temperature at below 40 °C and $\pm 3\%$ for relative humidity. Details on the capabilities of the ATMOS-41 sensors can be found in the manual (Meter Group AG 2020). Characteristics of selected ATMOS-41 sensors are given in Table A2 in the appendices of Zimba *et al.* (2022 under review). Two ATMOS 41 stations were used, placed at 2 m above the canopy (11 meters from the ground) and at 8 meters above the canopy (16.5 meters from the ground) (Fig. 3.3). The ATMOS-41 station sensors were logged at a 5-minutes interval same as the DTS.

3.3 Results and discussion

3.3.1 Evaporation flux foot print/Fetch analysis

The analysis of the evaporation flux foot print was performed using the wind rose (Fig. A1 in the appendices of Zimba *et al.*, (2022 under review)). The wind rose was used to obtain the most frequent and consistent wind direction to help determine which part of the study site had the greatest influence on the evaporation flux. The wind was predominantly coming from the eastern direction with wind speed ranging between 2 – 6 m s⁻¹. The use of the wind direction guided the selection of pixels of satellite-based evaporation estimates for comparison with BR-DTS evaporation estimates $E_{a(DTS)}$. Using the identified predominant wind direction, the fetch/flux footprint equal to 100 times the height (17.25 m) of the observation tower was designed. Thus, the fetch/flux footprint was designed to cover a 1.725 by 1.725 km area (approximately 2 km by 2 km grid).

3.3.2 DTS data quality control

The DTS measurements were conducted from 1 May to 25 December, 2021. Following the quality control processes by Schilperoort *et al.* (2018), DTS data for seven days (2 in June, 2 in August, 2 in September and 1 in October) did not pass the quality test. These data were collected on the days when challenges of keeping the entire wet fibre cable cloth constantly wet were experienced. The data were removed and gaps filled by the linear regression method. Due to challenges with power supply for the DTS machine, six days in December (26th to 31st) were not available for analysis.

3.3.3 Comparison of DTS-based estimates with the ATMOS-41 estimates

DTS estimates of air temperature and actual vapour pressure were compared with the ATMOS41 estimates at 11 m and 16.5 m heights above the forest canopy on the tower (Fig. 3.3). At height 16.5 m the DTS-based estimates and the ATMOS-41-based estimates showed relatively lower correlation ($R^2 = 0.97$; 0.79 for air temperature and actual vapour pressure respectively). However, at 11 m the correlation coefficients ($R^2 = 0.98$; 0.86 for air temperature and actual vapour pressure respectively) were relatively higher (Fig. 3.5 a - d). The lower correlation coefficients at 16.5 m may be explained by the installation of the ATMOS-41 weather stations above the forest canopy that exposed the temperature sensors to direct sunlight in early morning and late afternoon. This influenced the temperature measurements and resulted in deviations in ATMOS-41 air temperature for the two periods. Additionally, the water from the tank on the tower did not always reach the wet bulb temperature at the 16.5 m height resulting the overestimation of the DTS-based

actual vapour pressure. Overall, the DTS and ATMOS-41-based estimates, at both heights, showed good agreement, sufficient for this study. The accuracy properties of the ATMOS-41 are shown in Table A2 in the appendices of Zimba *et al.* (2022 under review).

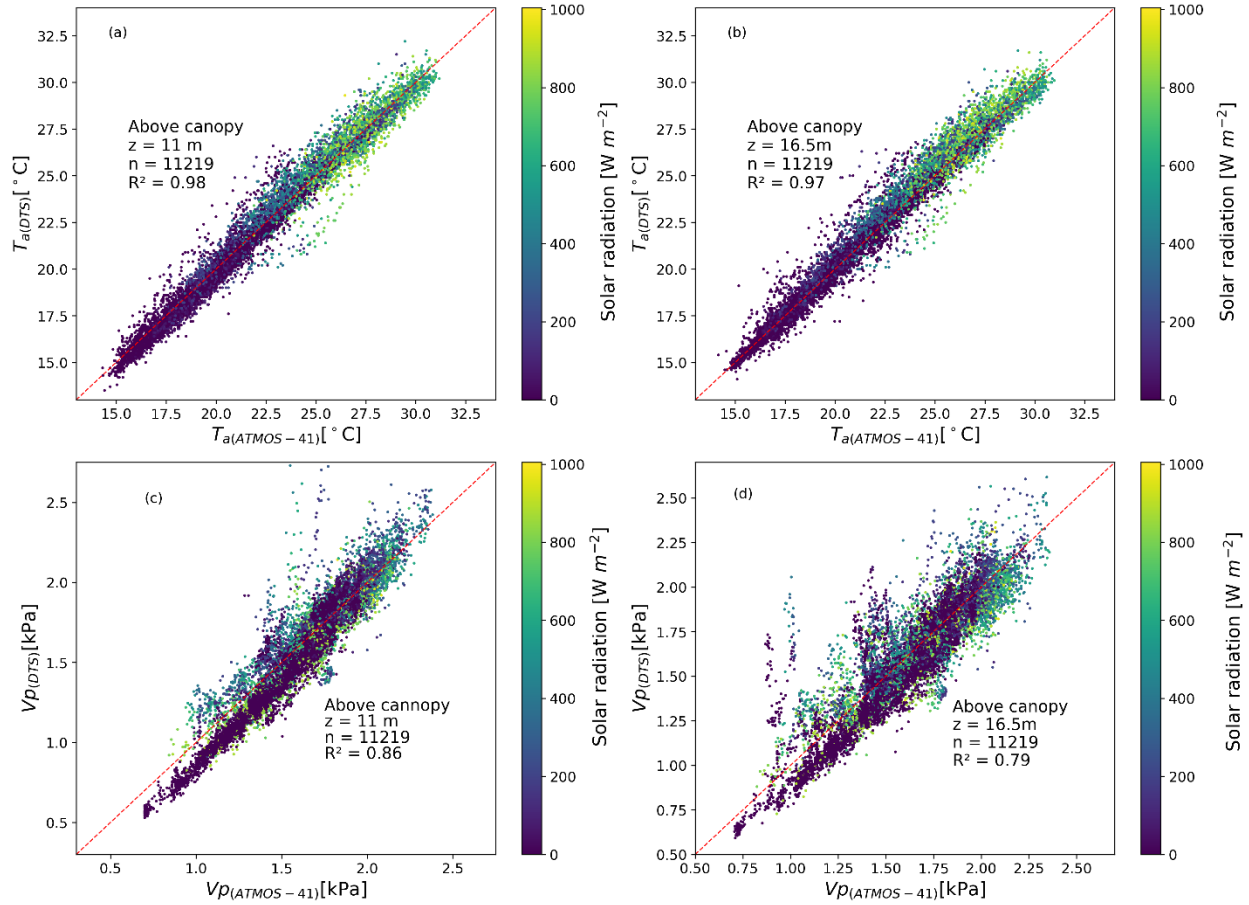


Figure 3.5: Comparison of DTS temperature ($T_{a(DTS)}$) and actual vapour ($VP_{(DTS)}$) measurements with the *ATMOS-41* ($T_{a(ATMOS-41)}$ and $VP_{(ATMOS-41)}$) measurements at 11 m and 16.5 m above the wet miombo woodland canopy at Mpika site, Zambia.

3.3.4 Meteorological conditions

The wind direction was mainly between the North-East and South-East direction (approx. 50 – 110 degrees) (Fig. A1 in the appendices of Zimba *et al.* (2022 under review)). Wind speed (u) ranged between 0.7 - 8 m s⁻¹ with relatively higher speeds observed in the dry season between July and September during the dormant phenophase (Figs. 3.5 and 3.6). Minimum and maximum net radiation (R_N) were observed during the dry season and wet season respectively. The drop in air temperature (T_a) and relative humidity (RH) coincided with reduced soil moisture (SM) in the dormant phenophase in the dry season (Fig. 3.6). T_a ranged between 7 – 32° C. Relative humidity negatively co-varied with T_a and R_N .

Using the DTS-based Bowen ratio (BR_{DTS}), available energy was partitioned into sensible (H) and latent heat (LE) fluxes (Fig. 3.6 and Fig. A2 in the appendices of Zimba *et al.* (2022 under review)). The H and LE co-varied with latent heat predominantly exceeding sensible heat across phenophases. On days with precipitation (P) the H and LE appeared to be equally partitioned.

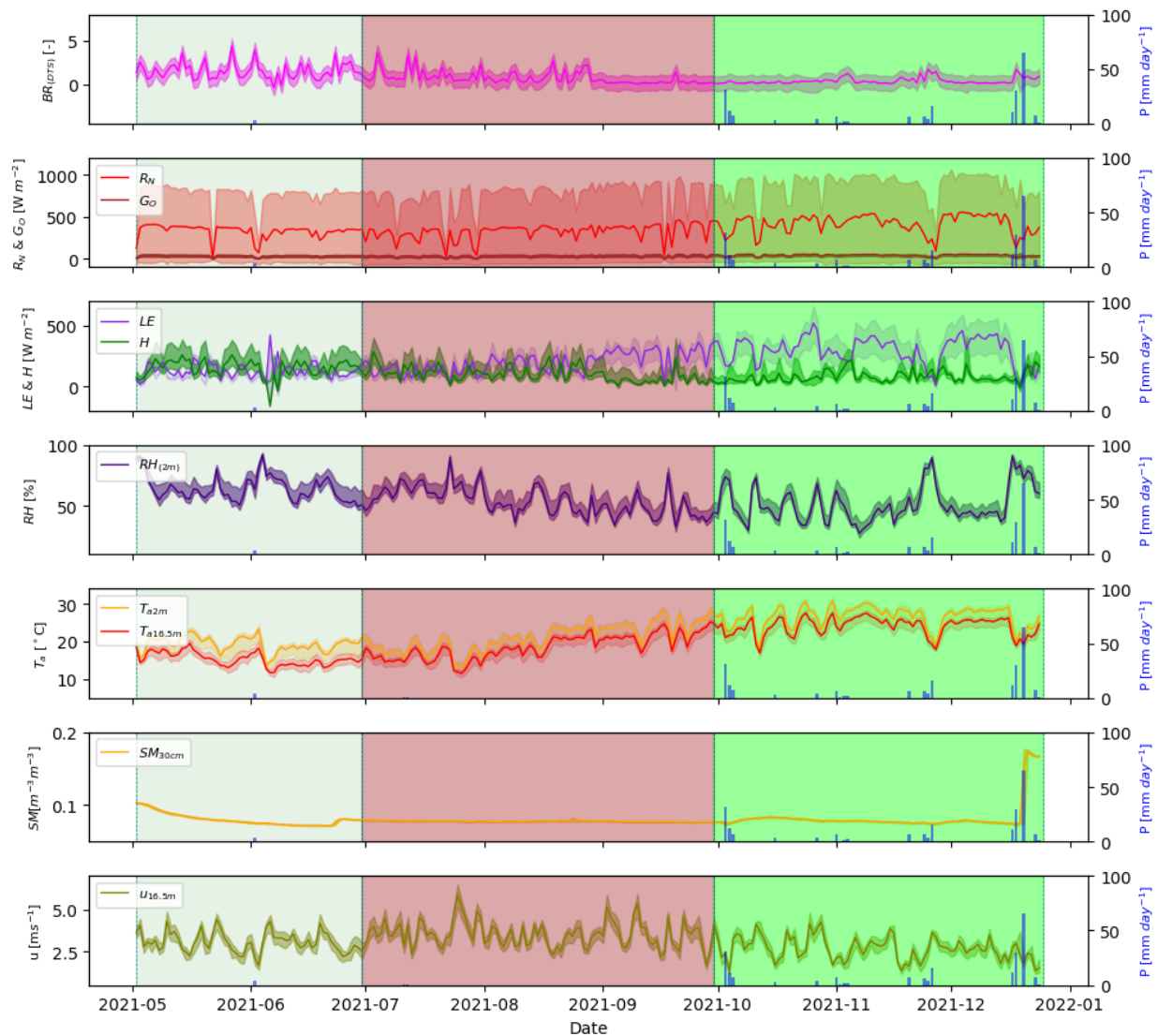


Figure 3.6: Daily diurnal meteorological conditions at the wet miombo woodland study site, Mpika, in the Luangwa Basin for the period May 2021 – December 2021. Shaded area for variables is the standard deviation. Shaded area May-June is the canopy green-down phenophase, July-September is the dormant phenophase and October-December is the green-up phenophase.

3.3.5 Canopy phenophase based Bowen ratio and evaporation trend

During the green-down phenophase the Bowen ratio was highest while air temperature was lowest in a relatively lower net radiation and vapour pressure environment. During the dormant and green-up phenophases the Bowen ratio was lowest while the temperature was highest in

relatively higher net radiation and lower relative humidity conditions (Figs. 3.6, 3.7 and Fig. A2 in the appendices of Zimba *et al.* (2023)). The green-down phenophase (i.e., May-June) showed the lowest air temperature and net radiation (Figs. 3.6 and 3.7) and exhibited the highest mean diurnal Bowen ratio (BR) (i.e., diurnal mean BR ≈ 1.3) indicative of the energy being largely partitioned as sensible heat compared to the dormant (i.e., diurnal mean BR ≈ 0.27) and green-up (i.e., diurnal mean BR ≈ 0.35) phenophases with raised air temperature and net radiation when the energy was mainly partitioned as latent heat (i.e., diurnal mean BR < 0.4) (Figs. 3.6 and 3.7). Alternating energy partitioning was detected across the phenophases as can be seen through the mean Bowen ratio, sensible and latent heat fluxes (Figs. 3.6 and 3.7). Diurnal energy partitioning interchange, across the three phenophases, occurred round 06 AM and 6PM (Fig. 3.7). The study site is situated in a warmer miombo region (Chidumayo and Gumbo, 2010).

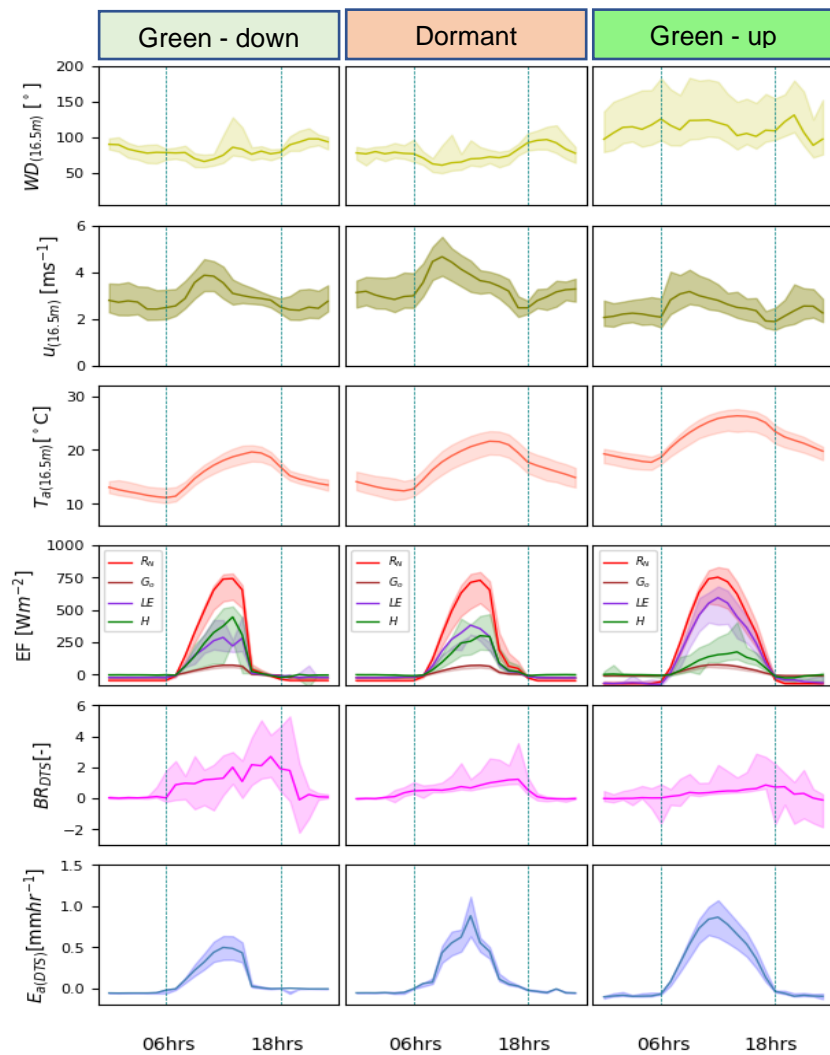


Figure 3.7: Characterisation of the wet miombo woodland canopy phenophase based hourly averages of wind direction (WD), wind speed (u), Energy flux (EF) (net radiation (R_N), ground heat flux (G_o), latent heat flux (LE) and sensible heat flux (H)), Bowen ratio (BR_{DTS}) and actual evaporation ($E_{a(DTS)}$). Shaded area is the standard deviation.

The observed alternating energy partitioning (i.e., Bowen ratio) pattern is similar to what has been observed in warm ecosystems and climates (i.e., Cho *et al.*, 2012) such as the miombo ecosystem. Consequently, diurnal evaporation pattern at the study site is dependent on daily energy partitioning, increasing with net radiation and air temperature (Figs. 3.6 and 3.7).

3.3.6 Comparison of potential evaporation and actual evaporation

$E_{a(DTS)}$ was estimated at diurnal (06 AM – 6 PM) hourly interval and then summed up into daily and dekadal estimates. Overall, daily $E_{c(PM)}$ was higher than $E_{a(DTS)}$ by an average of 17 percent (Fig. 3.8 a). However, under low temperature conditions (i.e., June – July) on some days the $E_{a(DTS)}$ was higher than the $E_{c(PM)}$ (Fig. 3.8 a). In higher air temperature and low canopy cover (i.e., in the dormant phenophase August and September), $E_{c(PM)}$ was higher than $E_{a(DTS)}$. The soil water limitations and changes in leaf colour (Fig. 3.9 and Fig. A3 in the appendices of Zimba *et al.* (2022 under review)) may have resulted in significantly higher $E_{c(PM)}$ compared to $E_{a(DTS)}$.

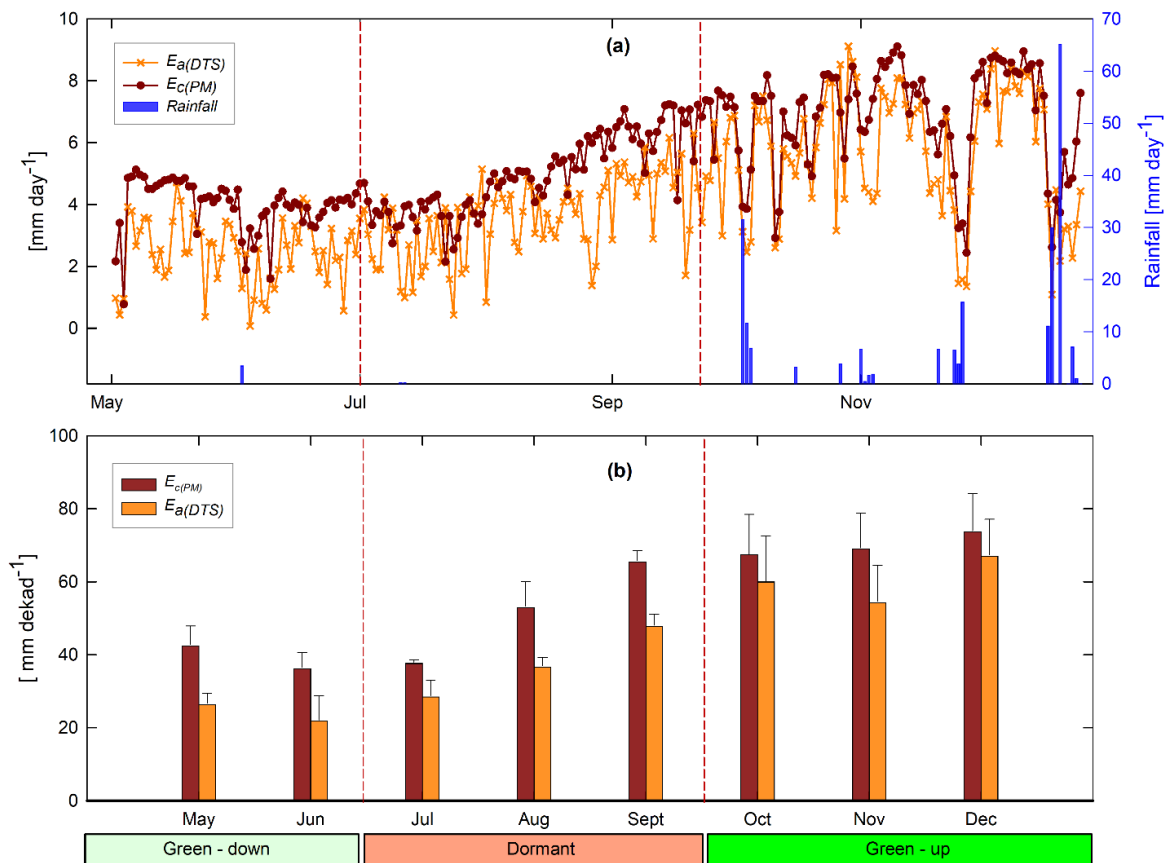


Figure 3.8: (a) May – December 2021 daily (6AM - 6PM) estimates of evaporation $E_{a(DTS)}$ using the *BR-DTS* and $E_{c(PM)}$ using the *PM*. (b) Comparison of dekadal evaporation estimates between $E_{a(DTS)}$ estimates and $E_{c(PM)}$ ($E_c = K_c \cdot E_o$). Overall, at dekadal scale the $E_{c(PM)}$ is relatively higher than $E_{a(DTS)}$ (b).

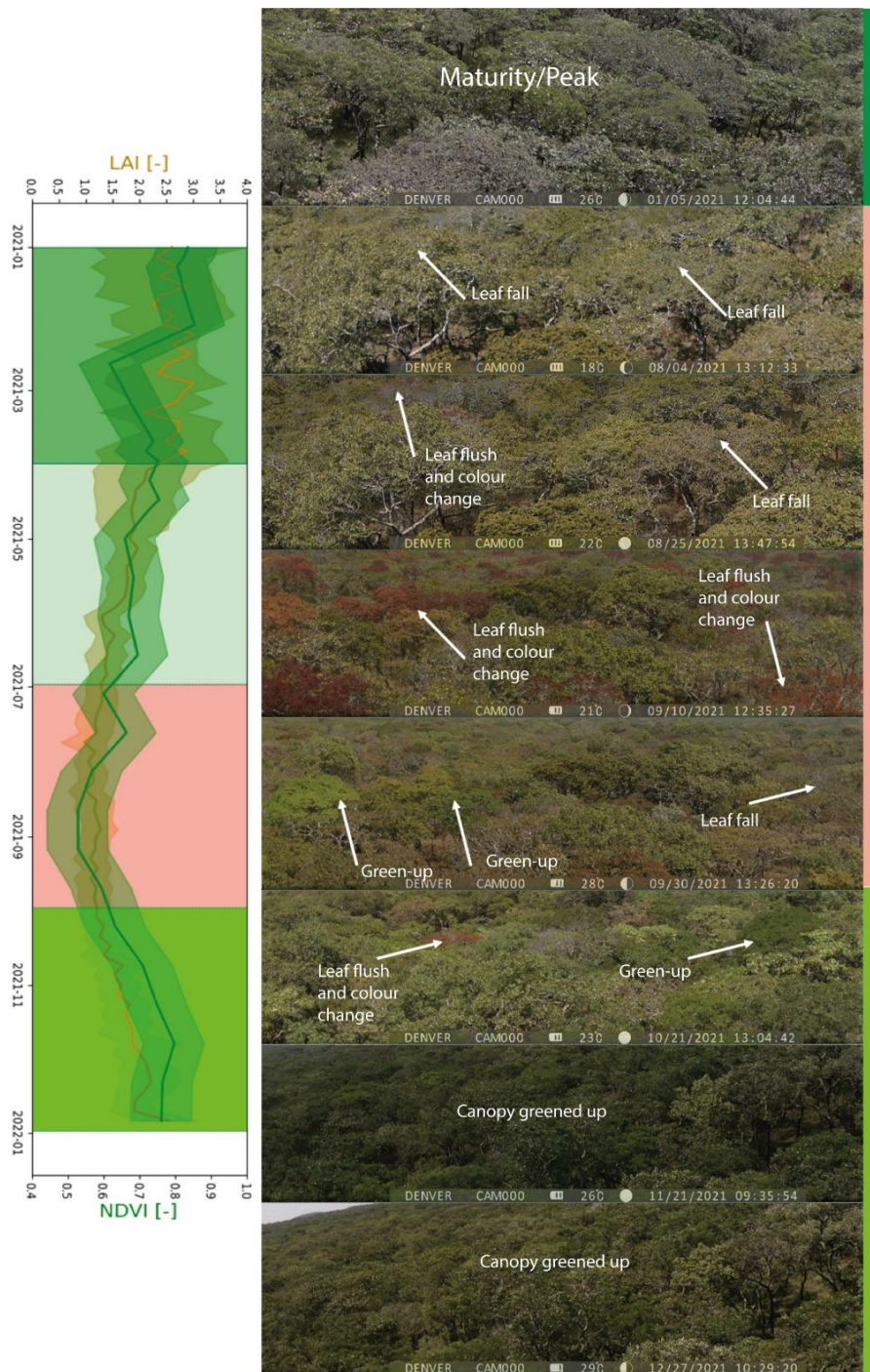


Figure 3.9: Selected aerial view images of the upwind direction (East direction) above the canopy from the flux tower across phenophases from January-December 2021. Shaded boxes are the phenophases: Peak/maturity (January-March), senescence/green-down (April-June), dormant (July – September) and green-up (October – December). The satellite-based *NDVI* and *LAI* appear to agree with the changes in the canopy cover. Shading in variables *LAI* and *NDVI* is the minimum and maximum values.

The $E_{a(DTS)}$ and $E_{c(PM)}$ showed similar behaviour (i.e., trend and magnitude) across canopy phenophases with strong correlation ($r = 0.95$) at decadal scale (Fig. 3.8 b and Table A4 in the appendices of Zimba *et al.* (2022 under review)). For both $E_{a(DTS)}$ and $E_{c(PM)}$, significant variations (i.e., coefficients of variations and standard deviations) in evaporation estimates were observed in the green-up phenophases (i.e., October – December) (Fig. 3.8 b, Table A3 in the appendices of Zimba *et al.* (2022 under review)). The high coefficients of variations in the magnitude of actual evaporation in the dormant and green-up phenophases could have been caused by changes in both meteorological conditions and forest canopy cover characteristics such as leaf fall, leaf flush and leaf colour (i.e., Figs. 3.6 and 3.9).

The $E_{a(DTS)}$ appeared to follow the trend of available energy (i.e., net radiation, air temperature) (i.e., Kendall's tau (τ) from 0.09 to 0.6) instead of the changes in forest canopy cover (i.e., Kendall's tau (τ) from 0.09 to 0.2) (Figs. 3.6 and 3.10). For instance, the lowest $E_{a(DTS)}$ was observed during the lowest net radiation and air temperature in June while the highest $E_{a(DTS)}$ was observed during the period with highest net radiation in the green-up phenophase. In the dormant phenophase, the $E_{a(DTS)}$ increased as NDVI reduced ($\tau = -0.22$). The upward trend in the dormant $E_{a(DTS)}$ even when forest canopy cover (i.e., NDVI) reduced may have been caused by the access to deep soil moisture and vegetative water storage (Tian *et al.*, 2018; Vinya *et al.*, 2018) by plants that had either not started the leaf fall or those that already acquired new leaves and had greened up (Fig. 3.9). The leaf fall and leaf colour transitions (i.e., Fig. 3.9 and Fig. A3 in the appendices of Zimba *et al.* (2022 under review)) in some wet miombo species, at any given time, across the three phenophases, is compensated by the leaf flush and greening up process in other species, which ensures that about 70% evaporative surface (i.e., canopy closure) (Fuller, 1999, Frost, 1996 and Fig. 3.9) is available at any period of the year.

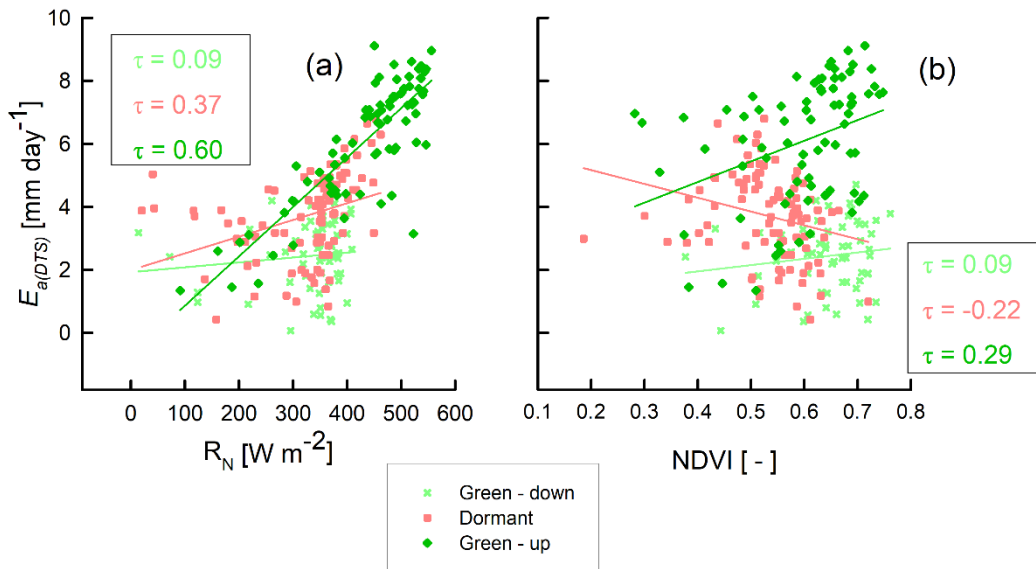


Figure 3.10: Kendall correlation of $E_{a(DTS)}$ with R_N and NDVI in the Green-down, Dormant and Green-up phenophases of the miombo woodland at Mpika site, Zambia.

The canopy cover percentage increases as the phenophases transition from dormant to the peak phenophase (i.e., Fig. 3.9 and Fig. A3 in the appendices of Zimba *et al.* (2022 under review)). Zimba *et al.* (2020) showed that August/September and not June, had the highest plant water stress (i.e., lowest NDII (Sriwongsitanon *et al.*, 2015)). June showed the lowest net radiation and air temperature (Fig. 3.6). However, $E_{a(DTS)}$ for August/September was higher than that for June. This $E_{a(DTS)}$ trend and magnitude of actual evaporation demonstrates available energy, coupled with adapted physiological processes, as the possible main driver(s) of the evaporation of the miombo woodland during the dormant phenophase (in the cool dry season and warm pre-rainy season).

In the green-up phenophase, $E_{a(DTS)}$ increased with increase in net radiation and NDVI ($\tau = 0.60; 0.29$ respectively) (Fig. 3.10). The highest net radiation and air temperature were observed in the green-up phenophase (Fig. 3.6). The NDII values (i.e., vegetation water content) started to rise in September (Zimba *et al.*, 2020). The increase in the $E_{a(DTS)}$ from July was sustained through October to December (green-up phenophase) (Fig. 3.8), before the commencement of stable rains. The NDII trend (Zimba *et al.*, 2020) in the green-up phenophase may have been as a result of the increased canopy cover as proxied by the LAI and NDVI (Fig. 3.9) facilitated by the plants access to deep soil moisture/ground water after the leaf flush. The $E_{a(DTS)}$ green-up phenophase trend could have been caused by increased canopy cover, access to deep soil moisture and high available energy. The marginal drop of $E_{a(DTS)}$, in November, at the start of the rain season, could be attributed to the drop in net radiation and air temperature (Fig. 3.6) influenced by cloud cover and rainfall activity (Fig. 3.8a). During increased rainfall activity, atmospheric water demand may have been lowered as relative humidity increased while net radiation reduced (Fig. 3.6). The same explanation holds for the $E_{a(DTS)}$ estimates in December.

3.3.7 Comparison of satellite-based evaporation estimates to field observations

3.3.7.1 Comparison of temporal trend and magnitude

Among the four satellite-based evaporation estimates, only the WaPOR showed similar trend to field observations across the three phenophases from May to December with strong correlation coefficients ($r = 0.85, 0.83$ with $E_{a(DTS)}$ and $E_{c(PM)}$ respectively) (Fig. 3.11 and Table A4 in the appendices of Zimba *et al.* (2022 under review)). This was followed by SSEBop ($r = 0.51, 0.58$ with $E_{a(DTS)}$ and $E_{c(PM)}$ respectively), while MOD16 showed the weakest correlation ($r = 0.01, -0.01$ with $E_{a(DTS)}$ and $E_{c(PM)}$ respectively). In contrast, GLEAM showed a negative correlation with both $E_{a(DTS)}$ and $E_{c(PM)}$ observations ($r = -0.53, -0.48$ with $E_{a(DTS)}$ and $E_{c(PM)}$ respectively) (Fig. 3.11 and Table A4 in the appendices of Zimba *et al.* (2022 under review)). With an exception of WaPOR, diversion from observed $E_{a(DTS)}$ and $E_{c(PM)}$ begun in July at the commencement of the rise in air temperature and net radiation, increased wind speed and the beginning of the dormant phenophase (i.e., typified by leaf fall, leaf flush and leaf colour change activities (Figs. 3.6, 3.9 and 3.11)). Surprisingly, GLEAM appeared to substantially underestimate actual evaporation during the dormant and green-up phenophases (in the cool-dry season and warm pre-rainy season) (Fig. 3.2 and Fig. 3.11).

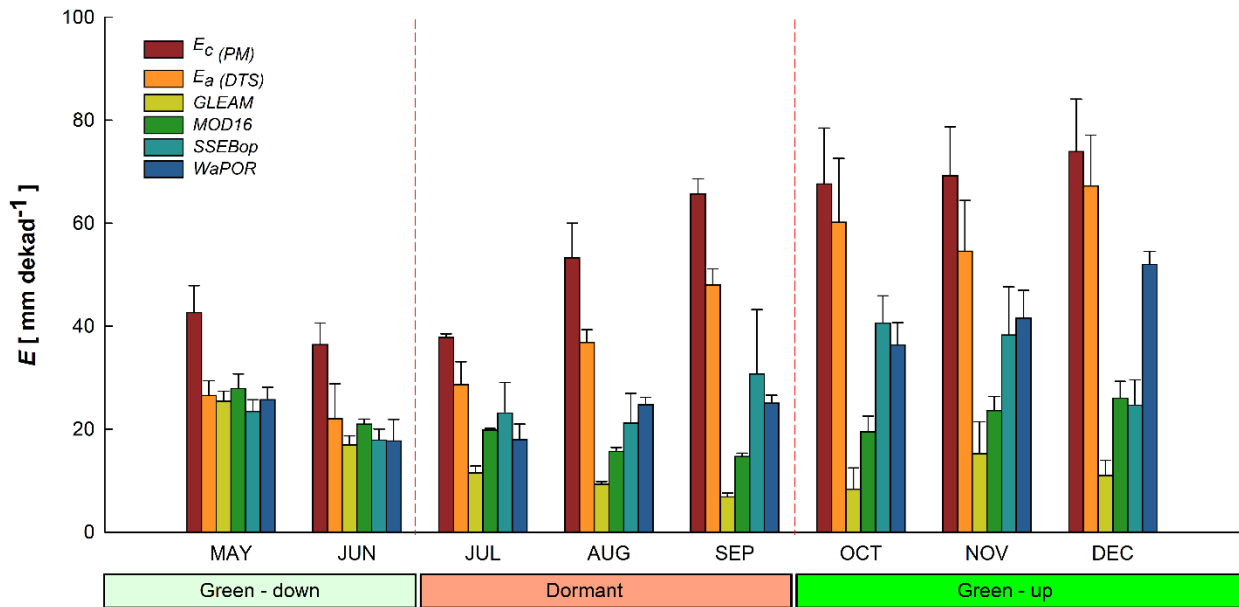


Figure 3.11: Bar graphs with standard deviation error bars comparing dekadal averages of $E_a(DTS)$ and $E_c(PM)$ with satellite-based evaporation estimates from May – December 2021. The WaPOR shows a similar trend to both $E_a(DTS)$ and $E_c(PM)$.

3.3.7.2 Phenophase-based cumulative estimates and coefficients of variations of estimates

Between 1st May to 20th December, 2021, observed actual evaporation $E_a(DTS)$ was about 24 percent lower than the estimated potential evaporation $E_c(PM)$ (Table 3.2). The largest difference (approximately 130 mm) between $E_c(PM)$ and $E_a(DTS)$ was in the water limited dormant phenophase in the dry season proper.

Table 3.2. Comparison of the 2021 monthly cumulative evaporation for the wet miombo woodland, Mpika, Zambia

Product	Phenophase mean actual evaporation estimate (mm phenophase ⁻¹)				Satellite-based estimate % lower than $E_a(DTS)$	Satellite-based estimate % lower than $E_c(PM)$
	Green-down	Dormant	Green-up	Total		
$E_a(DTS)$	146.62	341.75	479.47	967.83		
$E_c(PM)$	237.86	471.32	558.88	1268.06		
GLEAM	128.22	84.69	94.25	307.16	68.26	75.78
MOD16	147.44	152.14	182.75	482.33	50.16	61.96
SSEBop	124.99	226.72	287.05	638.76	34.00	49.63
WaPOR	131.40	204.93	338.64	674.97	30.26	46.77

Over the same period, cumulative average GLEAM actual evaporation was about 76 percent lower than potential evaporation and 68 percent lower than $E_{a(DTS)}$. MOD16 was about 62 percent lower than potential evaporation and 50 percent lower than actual evaporation $E_{a(DTS)}$. The SSEBop was about 50 percent lower than potential evaporation and 34 percent lower than actual evaporation $E_{a(DTS)}$. WaPOR was about 46 percent lower than potential evaporation and 30 percent lower than actual evaporation $E_{a(DTS)}$ (Table 3.2). The green-down phenophase showed the least differences between satellite-based evaporation estimates and field observations (Table 3.2). Overall, the four satellite-based estimates underestimated actual evaporation across the forest canopy phenophases (Fig. 3.11 and Table 2). However, in the green-down all four satellite-based estimates showed similar behaviour (i.e., trend and magnitude) with the $E_{a(DTS)}$ (Fig. 3.11 and Table 3.2).

The green-down phenophase showed the lowest coefficient of variation among the four satellite-based evaporation estimates (Fig. 3.12). The low coefficient of variation coupled with the low underestimation in the green-down phenophase showed that satellite-based estimates are closer to miombo woodland actual evaporation in conditions of high forest canopy cover and high soil moisture content in the sub-surface. The dormant and green-up phenophases showed large underestimation and large coefficients of variation among the satellite-based estimates (Table 3.2 and Fig. 3.12). The underestimation during the green-up phenophase may be caused by difficulty of modelling interception, especially in October and November at the beginning of the rain season.

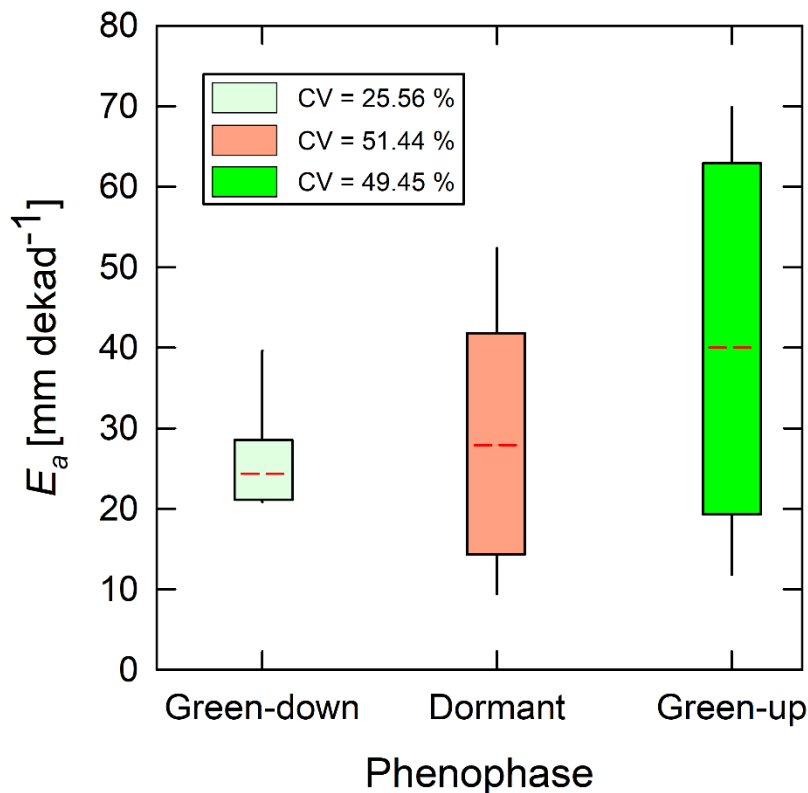


Figure 3.12: Box plots showing variations in satellite-based evaporation estimates at dekad scale across phenophases. Dotted red line is the mean for each phenophase. Coefficients of variation (CV) of satellite-based evaporation estimates were largest during the dormant and green-up phenophases.

The significant variations in dormant phenophase actual evaporation estimates showed that satellite-based evaporation estimates have difficulty estimating evaporation of the miombo woodland in conditions with low canopy cover (with associated changes in leaf display characteristics), both high and low available energy, and low soil moisture content in the upper layers of the soil. If canopy transpiration is not coupled with access to deep soil moisture beyond 250 cm, as is the case with GLEAM (as explained in section 3.4.1), satellite-based estimates are likely to underestimate actual evaporation in the dormant phenophase of the miombo woodland.

3.3.7.3 Performance statistics of satellite-based estimates with reference to BR-DTS estimates

Overall, for the eight-month period, the WaPOR showed the lowest underestimation (i.e., MBE), had the highest correlation coefficient and lowest RMSE. The WaPOR was followed by the SSEBop and then MOD16. The GLEAM showed the lowest estimates, high RMSE and largest MBE. Only the WaPOR consistently showed positive correlation (r) with field observations across the three phenophases (Fig. 3.13a). The underestimations were mainly associated with the dormant and green-up phenophase (Fig. 3.11), as can be seen from the uncertainty RMSE and MBE values (Fig. 3.13 b, c). Therefore, for satellite-based estimates, it appears the dormant and green-up phenophases are the most difficult to assess. The SSEBop and WaPOR estimates appeared closer to dry season miombo woodland actual evaporation than the MOD16 and GLEAM. The behaviour, in terms of trend and magnitude, of satellite-based evaporation estimates in relation to field observations of the miombo woodland actual evaporation may be attributed to individual satellite product characteristics.

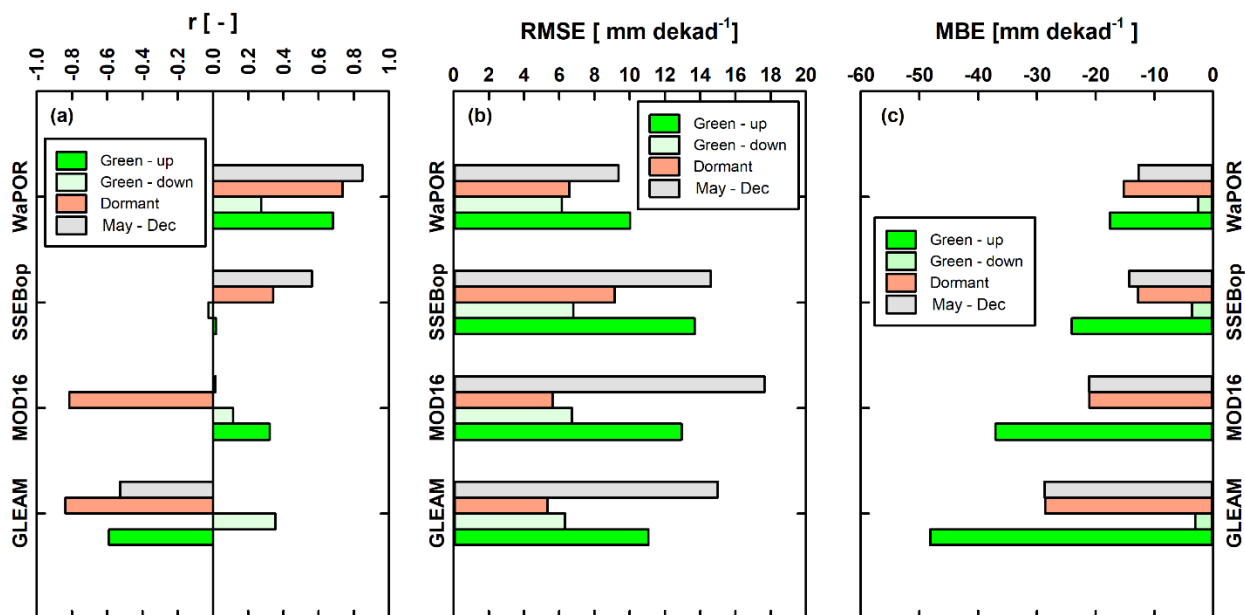


Figure 3.13: (a) statistics of the correlation of $E_{a(DTS)}$ with satellite-based estimates and (b, c) statistics of uncertainty in satellite-based evaporation estimates with reference to $E_{a(DTS)}$ for each phenophase and for the entire study period May-December, 2021.

3.3.8 Potential causes of the discrepancies between $E_a(DTS)$ and satellite-based estimates

3.3.8.1 Global Land Evaporation Amsterdam Model (GLEAM)

GLEAM has four modules that are used to obtain actual evaporation. The modules include the potential evaporation, rainfall interception, soil and stress modules. The potential evaporation module uses the Priestly and Taylor equation, and is driven by observed surface meteorology. The interception module is based on the Gash analytical model, and is driven by observed precipitation. The soil module is a multi-layer model driven by observed precipitation and satellite surface soil moisture. The stress module is based on semi-empirical relation to root zone soil moisture and the vegetation optical depth (VOD) (Martens *et al.*, 2017; Miralles *et al.*, 2011b).

GLEAM's green-down phenophase behaviour was similar to both field observations and other satellite-based evaporation estimates. However, GLEAM's behaviour, in low soil moisture and low forest canopy cover dormant phenophase, was different, both in terms of trend and magnitude. This showed GLEAM's sensitivity to changes in the sub-surface moisture dynamics. GLEAM soil module only takes into account 250 cm of the sub-surface soil moisture that is linked to observed precipitation. GLEAM drainage algorithm does not take into account horizontal and upward moisture fluxes beyond 250 cm depth. This implies that GLEAM is fully based on net precipitation, thereby not taking into account the groundwater fluxes that are not related to precipitation. At the study site, and the miombo woodland in general, the green down and dormant phenophases occurs in the dry season. The soil moisture (i.e., at 30 cm) begins to decline in March at the end of the rain season but stays relatively unchanged throughout the dry season (Fig. 6). However, the moisture residue at 30 cm subsurface is higher during the green-down phenophase as compared to the dormant and start of the green-up phenophases (Fig. 3.6 and Chidumayo, 2001). Studies (e.g., Gumbo *et al.*, 2018; Tian *et al.*, 2018; Vinya *et al.*, 2018; Guan *et al.*, 2014; Frost, 1996; Savory, 1963) showed that miombo species have vegetative water storage mechanisms as well as deep (beyond 5 m depth in some species) and extensive lateral rooting system providing accessing to ground water resources. This explains the behaviour of field observations which showed a rise in evaporation during the dormant and green-up phenophases in the dry season. The rise in GLEAM actual evaporation in October could be attributed to the interception, due to rainfall activity, and the sporadic rise in soil moisture in October (Fig. 3.6). This validates GLEAM's dependence on net precipitation for actual evaporation assessment. In increased solar radiation and canopy cover (i.e., leaf area index (LAI)) conditions, i.e., in October at the study site, a small amount of precipitation is likely to result in high interception, and only begins to reduce as precipitation increases. This shows that the GLEAM interception module, aided by the use of good quality rainfall product, i.e., Multi-Source Weighted-Ensemble Precipitation (MSWEP), is responsive in the miombo woodland.

The overall driving factor of GLEAM's actual evaporation estimates, with reference to the $E_a(DTS)$ in this study, might be the accuracy of the vegetation fraction product used in GLEAM, in this case the Global Vegetation Continuous Fields product (MOD44B). Since the evaporative flux components (i.e., interception loss, soil evaporation and transpiration as well as potential evaporation estimates) are all based on the vegetation fraction cover, the accuracy of the vegetation fraction product is a key factor in the overall accuracy (in relation to the miombo ecosystem) of the estimated actual evaporation for each land cover. The GLEAM is based on four land cover classifications that include bare soil, low vegetation (i.e., grass), tall vegetation (i.e., trees), and open water (i.e., lakes). Misclassification of the land cover type will have a cascaded effect on several components of the model, including the interception loss estimation and the multiplicative stress factor which influences the estimation of the various evaporation components in the model.

Additionally, the coarse spatial resolution (Table 3.1) could have contributed to the magnitude of GLEAM actual evaporation estimates as shown in section 3.4.5 of this study. It is also possible that the Priestley-Taylor equation used in GLEAM underestimates evaporation for the miombo woodland in the cool-dry season and warm pre-rainy season. This is because the other satellite-based evaporation estimates which uses the Penman-Monteith equation (Table 3.1) appear to underestimate less compared to GLEAM during these two periods.

3.3.8.2 MODerate resolution Imaging Spectroradiometer (MOD16)

The MOD16 evaporation algorithm is based on the Penman-Monteith equation (Monteith, 1965). The model computes actual evaporation as a summation of plant evaporation (canopy interception and transpiration) and soil evaporation utilising both remote sensing and meteorological inputs (Mu *et al.*, 2011). In the green-down phenophase MOD16 showed similar behaviour, in terms of trend and magnitude, with $E_{a(DTS)}$. However, in the dormant phenophase MOD16 had a different trend from $E_{a(DTS)}$ and underestimated actual evaporation. In the green-up phenophase MOD16 showed a trend similar to $E_{a(DTS)}$ but underestimated evaporation. Potential evaporation ($E_{c(PM)}$) and actual evaporation ($E_{a(DTS)}$) showed lowest evaporation estimates in June (Figs. 3.8 and 3.11). In contrast, the MOD16 showed September with the lowest estimates of actual evaporation (Fig. 3.11). This was two months delay. During the dormant phenophase (i.e., dry season proper) miombo woodland actual evaporation is through the transpiration process. At Mpika's miombo woodland site, Zimba *et al.* (2020) showed lowest LAI and NDVI values in August and September respectively. The MOD16 actual evaporation trend agreed with the vegetation indices, LAI and NDVI. However, net radiation and air temperature started to increase in July (Fig. 3.6). At the Mpika miombo woodland, Zimba *et al.* (2020) showed long-term average, 2009-2020, NDVI of about 0.5 in July. The July NDVI value was indicative of presence of green health vegetation. Furthermore, the normalised difference infrared index (NDII) indicated that lowest soil moisture and maximum plant water stress was reached in August/September (i.e., Sriwongsitanon *et al.*, 2015; Zimba *et al.*, 2020). Additionally, miombo species dry season plant water interactions have been sufficiently highlighted (e.g., Gumbo *et al.* 2018; Tian *et al.* 2018; Vinya *et al.* 2018; Frost 1996, Savory, 1963). Therefore, the start in increase in air temperature and net radiation (indicative of available energy) in July is before the plants are highly water stressed, and might be the correct start in rise in actual evaporation as depicted by $E_{a(DTS)}$, SSEBop and WaPOR. Consequently, if the MOD16 energy balance module is not well adjusted for the miombo woodland it may be the reason for downward dormant phenophase trend of evaporation estimates.

The key MOD16 component during the dormant and early green-up phenophase is the plant transpiration module driven by land cover/LAI, net radiation, air pressure, air temperature and relative humidity. The canopy/stomata conductance thresholds are the link between the highlighted drivers and the assessed plant transpiration. The MOD16 energy balance module and canopy conductance may not be appropriately configured for the miombo ecosystem. This could explain why the MOD16 trend and magnitude of actual evaporation estimates differed from field observations. Furthermore, for the MOD16 the use of the relative humidity and vapour pressure difference as proxies for soil moisture maybe a source of uncertainty in estimating transpiration (Novick *et al.*, 2016). Direct integration of soil moisture into the MOD16 algorithm appeared to improve the accuracy of actual evaporation estimates (Brust *et al.*, 2021). Additionally, daily MOD16 evaporation is a summation of both day and night evaporation. $E_{a(DTS)}$ was estimated at

hourly scale between 06AM and 6PM. Actual evaporation ($E_{a(DTS)}$) values for day time only (about 12 hours) were different from 24-hour averages for MOD16.

3.3.8.3 Operational Simplified Surface Energy Balance (SSEBop)

The SSEBop is based on the energy balance, distinguishing between hot and cold pixels to estimate evaporation. The SSEBop actual evaporation is calculated using an evaporation fraction that is based on the hot/dry and cold limiting conditions. To obtain actual evaporation the evaporation fraction is multiplied with the crop coefficient (K_c) and potential evaporation (E_o) (Senay *et al.*, 2013). The SSEBop appeared to have a similar behaviour, both trend and magnitude, with $E_{a(DTS)}$ during the green-down phenophase but these differed during the dormant and green-up phenophases in August and December. The SSEBop is sensitive to solar radiation/temperature and thus, effectively responded to the changes in these variables (i.e., net radiation and air temperature) as they started to rise in July. The marginal drop in evaporation in August could be due to the leaf shedding processes that exposed the dry leaf and grass covered forest floor to more interaction with radiation resulting in increased temperature. The increased soil surface temperature was interpreted by SSEBop as non-evaporative surface. Furthermore, the drop in the SSEBop actual evaporation in August could have been caused by the relatively (i.e., compared to the MOD16 and the WaPOR) coarser spatial resolution (i.e., 1 km), the heterogeneity in the leaf fall and leaf flush trend, and the bush burns that normally occur during this period (Gumbo *et al.*, 2018; Frost, 1996). Additionally, the energy balance-based SSEBop doesn't explicitly consider soil moisture dependency and assumes that the variations in satellite-based land surface temperature and vegetation indices such as the NDVI accounts for the soil moisture (Senay *et al.*, 2013). The challenge with the use of the proxies for soil moisture in surface energy balance models is that these are unable to fully account for changes in other factors that may influence sensible heat fluxes (Gokmen *et al.*, 2012). To improve on the accuracy of estimation of water and energy fluxes in regions with recurrent plant water stress, i.e., miombo woodland, Gokmen *et al.* (2012) suggested that the soil moisture be integrated in the surface energy balance models. The SSEBop underestimation of actual evaporation in December could be attributed to two factors; cloud cover and the uncertainties associated with estimating land surface temperature (LST) in hot humid conditions (Dash *et al.*, 2002). There is increased cloud cover and rainfall activity in December that affects the quality of the satellite LST product. The SSEBop is based on clear sky net radiation balance principle (Senay *et al.*, 2013). Zimba *et al.* (2020) indicated that the quality pass for the satellite-based MODIS LST product at the study site was below 80 percent during the rainy season (i.e., December).

With reference to the $E_{a(DTS)}$ the underestimation by the SSEBop could be attributed to several factors, including the quality of the satellite LST product used and the overpass time of the MODIS satellite over the study site. The SSEBop daily evaporation estimates includes the night time. $E_{a(DTS)}$ estimates were between 6AM and 6 PM. The differences in the time intervals results in different daily actual evaporation averages contributing to the observed discrepancy. This is even more important when the 10AM and 1 PM overpass time for MODIS Terra and Aqua is considered. The overpass time affects the minimum and maximum LST estimation which influences estimated SSEBop actual evaporation.

3.3.8.4 Water Productivity through Open access Remotely sensed derived data (WaPOR)

The WaPOR is the only one of the four satellite-based evaporation estimates which showed similar trend with $E_{a(DTS)}$ across phenophases and had very strong correlation ($r = 0.85$) (Fig. 3.11 and Table A4 in the appendices of Zimba *et al.* (2022 under review)). However, WaPOR substantially underestimated actual evaporation in the dormant and green-up phenophases. WaPOR is based on satellite estimates from the modified Penman-Monteith (P-M) ETLook model which has been adapted to remote sensing inputs (Blatchford *et al.*, 2020; FAO, 2018). The actual evaporation is estimated based on seven data components which include precipitation, surface albedo, solar radiation, NDVI, soil moisture stress, land cover and weather data. The WaPOR actual evaporation is a summation of interception, soil evaporation and canopy transpiration. In the WaPOR transpiration is coupled via the root zone soil moisture content while soil evaporation is coupled via the top soil moisture content. The Net radiation is split into soil and canopy net radiation. This implies that increase in LAI exponentially reduces available soil net radiation and increases canopy net radiation. The LAI is derived from the NDVI. The WaPOR estimates canopy resistance and establishes the coupled response of soil moisture and LAI on transpiration. The land cover data is used to generate vegetation type dependent stomata conductance thresholds. In the WaPOR, the classes in the land cover data are used to estimate soil and canopy roughness, while the NDVI is used to account for seasonal variations during the growing season (Blatchford *et al.*, 2020). In estimating the soil and canopy aerodynamic resistance, the WaPOR includes buoyancy turbulence using the Monin-Obukhovi similarity theory. The accuracy of the land cover product used influences the thresholds for stomata conductance and other land cover type related components of the model. The use of relatively high spatial resolution Copernicus land cover product in the WaPOR, which has high forest classification accuracy, contributes to its ability to capture the vegetation type, which coupled with appropriate parameterisation of the stomata conductance and other vegetation related variables, appeared to correctly model the trend of the actual evaporation of the miombo woodland.

Unlike GLEAM, the WaPOR is not a product of a full net precipitation-based model. The ETLook model takes into account the vegetation type interaction with the sub-soil moisture content. The soil moisture stress module appeared to correctly model the miombo species interactions with soil moisture across the three phenophases. Most importantly, WaPOR correctly characterised actual evaporation trend in the dormant phenophase, which the other three satellite-based estimates did not. Both $E_{a(DTS)}$ and WaPOR are dependent on correctly partitioning available energy into sensible and latent heat fluxes. Therefore, the WaPOR energy balance module correctly partitioned energy fluxes in the miombo woodland across the three phenophases. The various inputs and processes in the WaPOR, as described above, may explain why it showed the same trend as the field observation and had lower underestimation of actual evaporation. Just like in GLEAM, MOD16 and SSEBop the underestimation by WaPOR could have been partly due to the differences in the daily time intervals for the estimation of actual evaporation, as well as the quality of the net radiation product used in the model. The WaPOR is estimated over a 24-hour (day) period while $E_{a(DTS)}$ was estimated between 06AM and 6 PM.

3.3.9 Possible causes of the $E_{a(DTS)}$ overestimation

It appeared that the spatial resolution of satellite-based estimates was of influence, as the underestimation was clearly observable, with reference to each satellite-based evaporation estimate's spatial scale. The correlation coefficient of -0.87 (Fig. 3.14) implies that the finer the spatial resolution the higher the actual evaporation estimates. Therefore, the finer the spatial

resolution the lower the underestimation (Fig. 3.12 and Table 3.2). This indicates that at finer spatial resolutions, higher than the WaPOR's 250 m, the underestimation of actual evaporation is likely to be reduced. However, the results are statistically insignificant since the p -value > 0.05 and, SSEBop's higher estimates than the MOD16 may suggest that other factors other than the spatial resolution were of greater influence on the estimated evaporation.

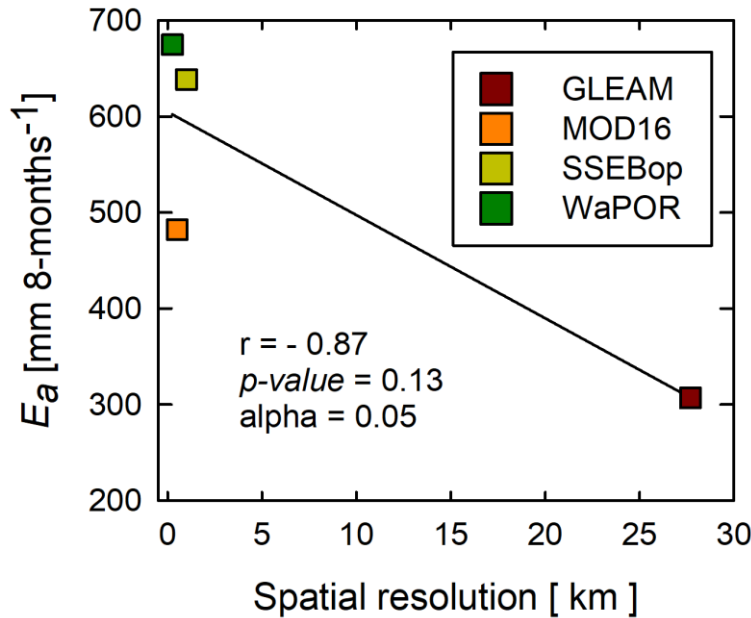


Figure 3.14: Point scale-based correlation of spatial resolution with estimates of actual evaporation of satellite-based evaporation estimates.

Furthermore, the ground heat flux (G_o) used in the $E_{a(DTS)}$ estimates was taken as 10 percent of the diurnal net radiation, based estimates found in other forests (i.e., Ma *et al.*, 2017; Van Der Meulen and Klaassen, 1996; McCaughey, 1982). The miombo woodland phenology is different from other ecosystems. It is possible that the G_o was underestimated, and may have contributed to the higher $E_{a(DTS)}$, as compared to the satellite-based evaporation estimates of the GLEAM, MOD16, SSEBop and WaPOR.

Another source of overestimation by the $E_{a(DTS)}$ could be the overestimation of the latent heat flux (LE) due to difficulties in flux tower instrumentation. Diurnal high temperature in the dry season (i.e., the dormant and green-up phenophases), coupled with the challenge of the constant wetting of the fibre cable for attaining wet bulb temperature, could have resulted in overestimation of the actual vapour pressure, and consequently underestimated the Bowen ratio. Underestimating the Bowen ratio could have resulted in overestimating diurnal latent heat flux, therefore, overestimating the diurnal hourly actual evaporation. This suggestion agrees with the observation by Schilperoort *et al.* (2018) which showed that, compared to the EC approach, the BR-DTS method slightly overestimated diurnal LE by a mean difference of 18.7 Wm^{-2} .

However, using the water balance approach, Zimba *et al.* (2023 under review) showed that

satellite-based estimates generally underestimated actual evaporation in the heterogeneous woodland, but largely miombo woodland covered, Luangwa Basin. Therefore, the outcome of this study's comparison of point-based field observations with satellite-based estimates, agreed with the larger picture at the Luangwa Basin scale. Consequently, the trend and magnitude of satellite-based evaporation estimates, across various miombo strata, are likely to be the same as what this current study has observed. Nevertheless, to consolidate the observations of this study, further studies, such as this one, are needed in the different miombo woodland stratifications in Africa.

3.4 Conclusions and recommendations

The study characterised evaporation across three forest canopy phenophases of the miombo woodland at point scale using the BR-DTS approach. Consequently, four satellite-based evaporation estimates were compared to the field observations. Major conclusions from our study are that:

Despite the dry season challenge with consistently wetting the fibre optic cable, the BR-DTS approach can be used to successfully estimate actual evaporation across different canopy phenophases of the miombo woodland.

The actual evaporation trends appeared to be rather more closely associated with the available energy for evaporation than the changes in the characteristic canopy cover dynamics during the three phenophases. This is because across the three phenophases analysed, actual evaporation had higher correlation with the net radiation trend than the changes in canopy cover (proxied by the NDVI). The actual evaporation estimates in the three phenophases are likely to be more representative of the evaporation of the miombo woodland plants. For instance, the total NDVI/LAI during the dormant and green-up phenophases in the cool-dry season and warm pre-rainy season can largely be attributed to miombo plants. This is because in the three phenophases the non-deep rooting understory and field layer components such as grasses and shrubs normally dry out. However, for a comprehensive analysis it is important that evaporation for the period with the highest LAI and NDVI (January – March) is assessed.

Coupling the canopy transpiration with the root zone storage, taking into account the vertical upward (beyond 2.5 m) and horizontal soil moisture flux is likely to improve satellite-based dry season actual evaporation estimates of the miombo woodland. This is because during the dry season, i.e., dormant phenophase in the cool dry and warm pre-rainy seasons, field-based actual evaporation estimates were higher than satellite-based evaporation estimates. The trend and magnitude of the actual evaporation of the miombo woodland in the dry season is linked to the developed dry season water stress buffering mechanism i.e., leaf fall, leaf flush, plant water storage and deep rooting access to deep soil moisture including ground water.

Phenology plays a role in satellite-based actual evaporation estimates of the miombo woodland. This is evidenced by the phenophase dependent variations (i.e., coefficients of variation) in satellite-based evaporation estimates. Some phenophases (i.e., dormant and green-up) had higher coefficients of variation in actual evaporation estimates compared to the green-down phenophase.

Compared to field observations ($E_{a(DTS)}$) all satellite-based evaporation estimates underestimated actual evaporation. However, this result could have been influenced by the $E_{a(DTS)}$ assessment time intervals, errors in flux tower instrumentation, spatial resolution of satellite-based estimates, and the ground heat flux used in the $E_{a(DTS)}$ estimates.

Consequently, of the four satellite products considered in this study, only the WaPOR showed the same trend as field observations of the actual evaporation of the miombo woodland across the three phenophases. The WaPOR also showed the least underestimation. For the wet miombo woodland, as was represented by this study site, and limited to the four satellite-based estimates assessed, the WaPOR represents a better choice for use across the assessed miombo phenophases. With inference based on the WaPOR, it appears that satellite-based estimates made at a scale that takes into account the local variations in the input variables might give better results.

There is need for observations, such as found in the current study, to be conducted in the drier miombo landscapes and to compare the results. This is because this study was conducted in the wet miombo woodland; therefore, it is possible that the phenological response to changes in hydrological regimes in the drier miombo woodland will differ from the observations at the Mpika site.

Chapter 4

On the importance of phenology in the evaporative processes of the miombo woodland: Could it be why satellite-based evaporation estimates differ?



Photograph showing a portion of the Luangwa River in the dry season
Image: Henry Zimba

This chapter is based on

Zimba, H., Coenders-Gerrits, M., Banda, K., Hulsman, P., van de Giesen, N., Nyambe, I., and Savenije, H. H. G., 2023. On the importance of phenology in the evaporative process of the miombo woodland: Could it be why satellite-based evaporation estimates differ? *Hydrol. Earth Syst. Sci. Discuss.* [preprint], <https://doi.org/10.5194/hess-2023-39>, in review.

Chapter 4

“A river doesn’t flow through the forest without felling the trees.”

(African proverb)

4.1 Introduction

“Vegetation phenology” refers to the periodic biological life cycle events of plants, such as leaf flushing and senescence, and corresponding temporal changes in vegetation canopy cover (Stöckli *et al.*, 2011; Cleland *et al.*, 2007). Plant phenology and climate are highly congruent (Pereira *et al.*, 2022; Niu *et al.*, 2013; Cleland *et al.*, 2007). Woodland plant phenological responses to trigger elements, such as temperature, hydrological and day light regimes, include among others leaf fall and leaf flush, budburst, flowering and variation in photosynthetic activity due to changes in chlorophyll levels (Pereira *et al.*, 2022; Niu *et al.*, 2013; Cleland *et al.*, 2007). The phenological responses are species-dependent and are controlled by adapted physiological properties (i.e., Lu *et al.*, 2006). Plant phenology controls the access to critical soil resources such as nutrients and water (Nord and Lynch, 2009). The phenological response influences plant canopy cover and affects plant-water interactions. For instance, the phenophases associated variations in canopy leaf display, i.e., due to leaf fall and leaf flush, influences how much radiation is intercepted by plants (Shahidan, Salleh, and Mustafa, 2007). Intercepted radiation influences canopy conductance. In water limited conditions, at both individual species and woodland scales, leaf fall reduces canopy radiation interception while leaf flush and the consequent increase in canopy cover increases canopy radiation interception leading to increased transpiration (Snyder and Spano, 2013) controlled by available moisture storage, both vegetative and root zone. Canopy cover and its interactions with atmosphere carbon dioxide through the photosynthetic and autotrophic respiration processes influences transpiration. Ultimately, plant phenological response to changes in the trigger elements influences woodland transpiration and actual evaporation (i.e., Marchesini *et al.*, 2015).

Evaporation in woodland surfaces accounts for a significant portion of the water cycle over the terrestrial land mass (Sheil, 2018; Van Der Ent *et al.*, 2014; Gerrits, 2010; Van Der Ent *et al.*, 2010). Miralles *et al.* (2020) defined evaporation as “the phenomenon by which a substance is converted from its liquid into its vapour phase, independently of where it lies in nature”. Likewise, instead of the often-used term 'evapotranspiration', in this study the term evaporation is used for all forms of terrestrial evaporation, including transpiration by leaves, evaporation from intercepted rainfall by vegetation and woodland floor, soil evaporation, and evaporation from stagnant open water and pools (Miralles *et al.*, 2020; Savenije, 2004). Understanding the characteristics of evaporation, such as interception and transpiration, in various woodland ecosystems is key to monitoring the climate impact on woodland ecosystems, for hydrological modelling and the management of water resources at various scales (Kleine *et al.*, 2021; Bonnesoeur *et al.*, 2019; Roberts, (undated)). One of the key aspects to enable this understanding is the knowledge of the woodland phenological interaction with climate variables and seasonal environmental regimes (i.e., Zhao *et al.*, 2013). Plant phenology influence environmental variables differently across the diverse ecosystems globally (Forrest *et al.*, 2010; Forrest & Miller-Rushing, 2010; Kramer *et al.*, 2000) therefore requiring better understanding at a local or regional level with minimal variations. Yet, evaporation of natural woodlands, especially in African ecosystems, with respect to phenological phases are poorly characterised. This is largely because the development of measuring instruments and models has mainly focused on understanding the phenological response of agricultural crops to climate variables and seasons. Furthermore, phenological studies have mainly focused on mid-latitude regions which excludes other regions such as Africa (Snyder *et al.*, 2013; Schwartz, 2013). It is important to account for woodland phenology interaction with climate variables and seasons when characterizing evaporation in woodlands. This is because, for instance, accounting for phenological phases in evaporation models increases the predictive power

(i.e., Forster *et al.*, 2022).

The miombo woodland in sub-Saharan Africa is a heterogeneous woodland with a unique and complex phenology adapted to dry season conditions such as leaf shedding, deep rooting with access to ground water resources, and vegetation (i.e., stem) water storage (Vinya *et al.*, 2018; Tian *et al.*, 2018; Guan *et al.*, 2014; Chidumayo, 2001; Frost, 1996; Chidumayo and Fuller, 1996). Leaf flushing also occurs before the commencement of seasonal rainfall (Chidumayo, 1994; Fuller and Prince, 1996). While at individual species level the entire tree canopy can be leafless or changing leaf colour this does not occur at woodland canopy level due to heterogeneity in species composition and varied species response to phenological stimuli. The miombo woodland canopy cover varies with phenophases. These phenological attributes influence the evaporation process (Forster *et al.*, 2022; Snyder *et al.*, 2013; Schwartz, 2013).

Evaporation is land cover dependent i.e., evaporation from an open water body, woodland and grassland (Han *et al.*, 2019; Liu & Hu, 2019; Wang *et al.*, 2012). Different satellite-based evaporation estimates give different evaporation estimates depending on the landcover (i.e., Global Land Evaporation Amsterdam Model (GLEAM) (Martens *et al.*, 2017; Miralles *et al.*, 2011); Moderate-resolution Imaging Spectrometer (MODIS) MOD16) (Running *et al.*, 2019; Mu *et al.*, 2011; Mu *et al.*, 2007); Operational Simplified Surface Energy Balance (SSEBop) (Senay *et al.*, 2013); and Water Productivity through Open access of Remotely sensed derived data (WaPOR) (FAO, 2018)). There is currently no publication in the public domain showing how various satellite-based evaporation estimates compare in the miombo woodland, especially with a focus on the miombo phenology across climatic seasons. Yet, the usage of satellite-based evaporation estimates in the management of water resources globally and in Africa is on the increase (García *et al.*, 2016; Zhang *et al.*, 2016; Makapela, 2015). However, because of the absence or scarce field observations and extremely limited validation, it is impossible to know which satellite-based evaporation estimates are close to actual physical conditions of the miombo ecosystem. In most cases, the choice for a satellite-based evaporation product is based on validation results in non-miombo ecosystems. This product choice scenario is a challenge in that non-miombo ecosystems have a different phenology and evaporation to that of the miombo ecosystem. For instance, satellite-based evaporation estimates that performs extremely well in energy limited conditions and homogeneous woodlands, e.g., in Europe, cannot be assumed to have the same performance in a warm, water limiting and heterogeneous woodland such as the miombo.

Therefore, this study was formulated in order to contribute to the bridging of the gap in information on satellite-based evaporation estimates performance in different phenophases of the miombo woodland. We focused on the Luangwa sub-basin in the larger Zambezi Basin, one of the largest river basins in the miombo ecosystem. The Luangwa Basin was chosen because it is situated in a sparsely gauged region (Beilfuss, 2012), where it is essential that management of water resources is based on reliable information, for various competing uses, i.e. hydropower, agriculture, wildlife, industrial and domestic (WARMA, 2022). The Luangwa Basin is located in both dry (i.e., southern miombo woodlands) and wet (i.e., central Zambezian miombo woodlands) miombo. The central Zambezian miombo woodland is the largest of the four miombo woodland sub-groups, the other three being the Angolan miombo woodland, eastern miombo woodland, and the southern miombo woodland (Frost, 1996; White, 1983). The Luangwa Basin is also located in Zambia, argued to have the highest diversity of miombo woodland trees and considered centre of endemism for the miombo woodlands *Brachystegia* species (Frost, 1996). These attributes suggest a catchment that provides a fair representation of the miombo woodlands conditions and an appropriate site for this type of study.

Therefore, the aim of this study was two-fold:

- (i) Compare the temporal trend and magnitude of six free of charge satellite-based evaporation estimates across different phenophases of the miombo woodland.
- (ii) Compare satellite-based evaporation estimates to the water balance-based actual evaporation estimates for the Luangwa Basin scale.

4.2 Materials and Methods

4.2.1 Study approach

The study used both satellite-based data and field observations. Firstly, the study sought to find out if satellite-based evaporation estimates performed differently in the different phenophases of the miombo woodland. To achieve this the canopy phenology of the miombo woodland was understood using satellite-based proxies leaf area index (LAI), the normalised difference vegetation index (NDVI) and photographs taken above a flux tower at a known miombo woodland site for the period January – December, 2021. The phenophases were identified using both satellite-based data and the ecological phenological seasons classified based on literature from the miombo woodland. The satellite-based evaporation estimates were then compared to each other in relation to the identified canopy phenophases of the miombo woodland. The trend and magnitude of satellite-based evaporation estimates across the different phenophases of the miombo woodland were observed. The comparison of the satellite-based evaporation estimates was conducted at pixel scale and at the Luangwa Basin miombo woodland scale. This was performed in order to observe if the trend and magnitude of each satellite-based evaporation estimate is in tandem with the phenology-water interactions of the miombo woodland species across different phenological seasons.

Secondly, point scale observations in the wet miombo woodland (Zimba *et al.*, 2022 under review) showed that satellite-based evaporation estimates underestimate actual evaporation of the wet miombo woodland in phenophases in the dry season and early rainy season in the Luangwa Basin. However, the Luangwa Basin has a heterogenous land cover which include substantially mopane woodland and grasslands. The question was whether the heterogenous nature of the Luangwa Basin would give a different result from what has been observed at point scale in a wet miombo woodland. This question was answered by the use of the annual water balance approach in which the basin scale actual evaporation is estimated as the difference between basin rainfall and run-off.

A 12-year period from 2009 – 2020 was used for the assessments. This period was chosen because of data availability and was sufficient to capture long-term seasonal, monthly and annual variations in the actual evaporation of the basin. The proceeding sections elaborates the methods.

4.2.2 Study site

The Luangwa is a sub-basin in the larger Zambezi Basin in sub-Saharan Africa in Zambia with spatial extent of about 159,000 km² (Beilfuss, 2012; World Bank, 2010). Based on the miombo woodland delineation by White (1983) and the vegetation map shown in Ryan *et al.* (2016) as given in Fig. 4.1 (c) about 75 percent of the total Luangwa Basin land mass is covered by the miombo woodland, both dry and wet miombo. Additionally, the 2019 Copernicus land cover classification (Fig. A1 in the appendices of Zimba *et al.* (2023 under review)), with 80 percent user accuracy and woodland classification accuracy of about 75% (Buchhorn *et al.*, 2020; Martins *et al.*, 2020), indicates that 77 percent of the total basin area is woodland (dense and open woodland) which is largely miombo woodland.

Elevation ranges between 329 – 2210 m above mean sea level with the central part generally a valley. miombo woodland, both dry and wet, is generally in the upland (Fig. 4.1b). The Luangwa River, 770 km long, and its tributaries drain the basin (Beilfuss, 2012). The Luangwa Basin is scarcely gauged. This has resulted in a paucity of data on various hydrological aspects such as rainfall and discharge. The basin is located in a climate environment characterised by a well-delineated wet season, from October to April and a dry season, May to October. Furthermore, the dry season is split into the cool-dry (May to August) and hot dry (August to October) seasons. The movements of the inter-tropical convergence zone (ITCZ) over Zambia between October and April dominate the rainfall activity in the basin. The basin has a mean annual precipitation of about 970 mm yr^{-1} , potential evaporation of about 1560 mm yr^{-1} , and river runoff reaches about 100 mm yr^{-1} (Beilfuss, 2012; World Bank, 2010). The key character of the miombo woodland species is that they shed off old leaves and acquire new ones during the period May to October in the dry season. Depending on the amounts of rainfall received in the preceding rain season the leaf fall and leaf flush processes may start early (i.e., in case of low rainfall received) or late (in case of high rainfall received) and may continue up to November (i.e., in the case of high rainfall received) (Frost, 1996).

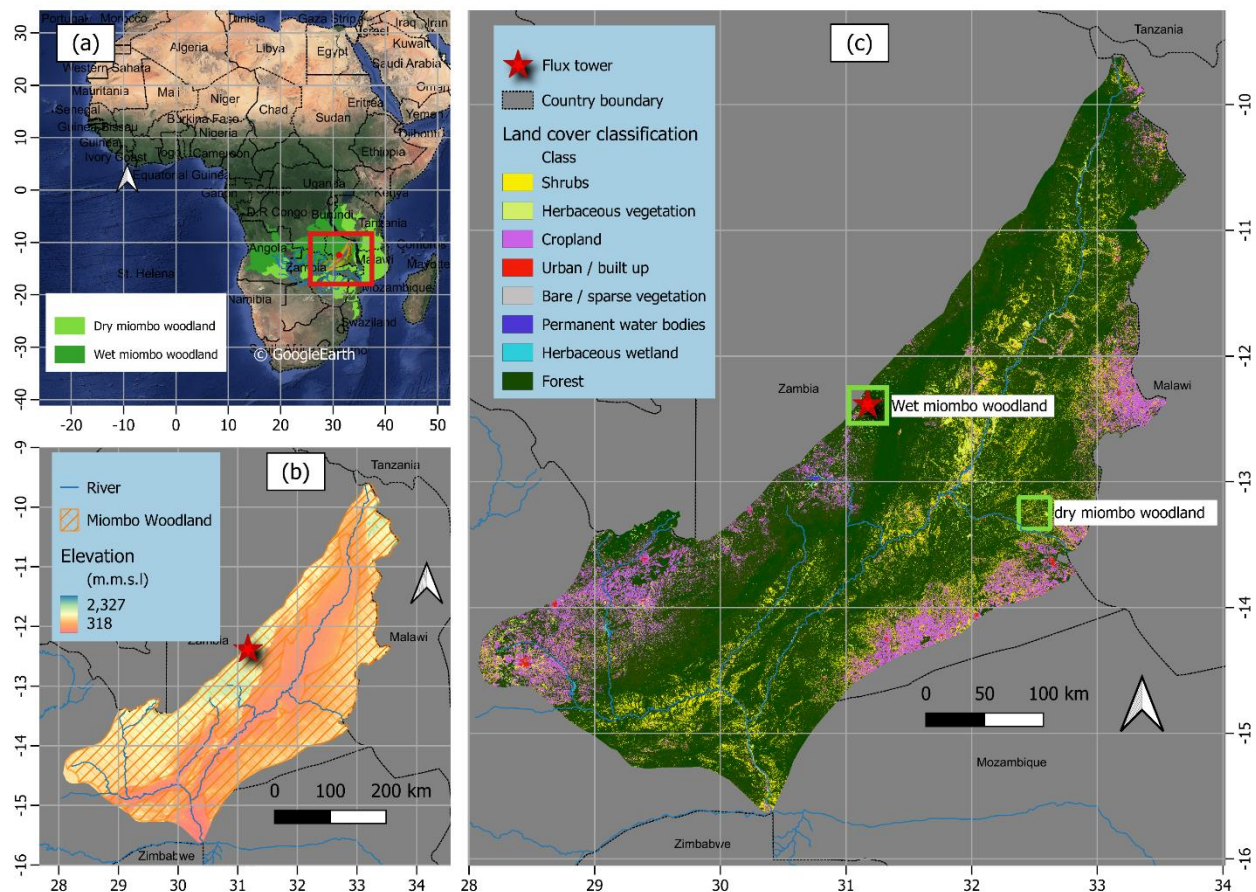


Figure 4.1: (a) Spatial extent of the miombo woodland in Africa and the location of the Luangwa Basin in Zambia. (b) Spatial distribution of elevation ASTER digital elevation model (DEM) and the extent of the miombo woodland in the Luangwa Basin. (c) Land cover characterisation of the Luangwa Basin based on the Copernicus land cover classification.

4.2.3 Classification of phenophases of the miombo woodland and assessment of phenological conditions

The satellite-based LAI and NDVI have been used as proxies to observe phenological conditions such as the canopy biomass formation, changes in the canopy closure (i.e., through leaf fall and leaf flush), and changes in canopy chlorophyll conditions (i.e., Guan *et al.*, 2014; Santin-Janin *et al.*, 2009; Chidumayo, 2001; Fuller, 1999). In this study the satellite-based LAI and NDVI were used as proxy for observing changes in phenological conditions of the miombo woodland across different phenological seasons. For the LAI the NASA's MCD15A3H product with a four-day temporal resolution and 500 m spatial resolution was used. The MODIS MOD09GQ.006 (Vermote and Wolfe, 2015) surface reflectance bands 1,5 and 6 were used to estimate the NDVI at daily temporal resolution and 250 m spatial resolution using the band ratio method. The daily NDVI values were then averaged into four-day values in order to have the same temporal resolution as the LAI.

The phenophases were characterised using satellite-based data (Friedl *et al.*, 2019; Gray *et al.*, 2019; Zimba *et al.*, 2020; Zang *et al.*, 2003) and the climate (rainfall and temperature) and soil moisture-based classification by Chidumayo and Frost (1996). Satellite-based classification uses the changes in canopy greenness to characterise the canopy phenophases (Friedl *et al.*, 2019; Gray *et al.*, 2019; Zang *et al.*, 2003).

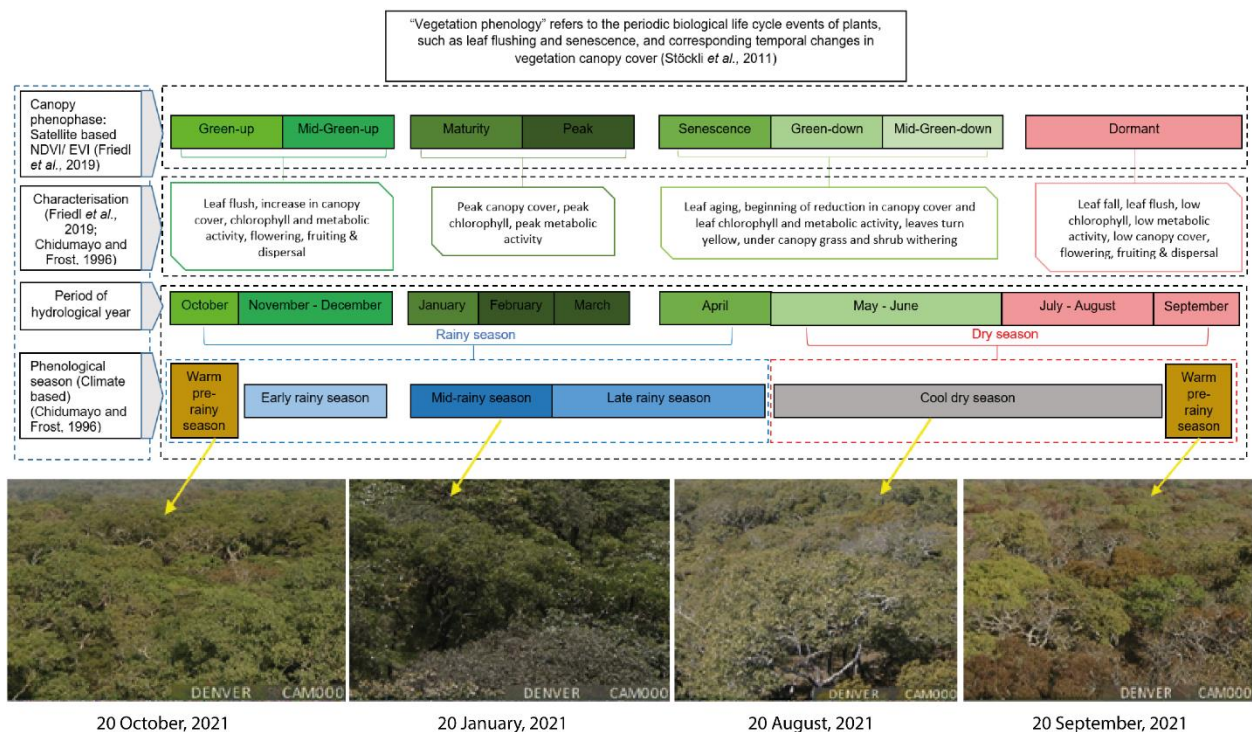


Figure 4.2: Characterisation of canopy phenophases of the miombo woodland in relation to seasonality for the Luangwa Basin. Photographs show the changes in the canopy cover on selected days across different phenophases of a wet miombo woodland for the year 2021.

In this study the Collection 6 MODIS Land Cover Dynamics (MCD12Q2) Product (Friedl *et al.*, 2019; Gray *et al.*, 2019) was used to identify the satellite-based phenophases. For the year 2021 eight phenophases were identified using the satellite-based data MCD12Q2 (Fig. 4.2), NDVI, LAI and photographs obtained using a digital camera (Denver WCT-8010) installed on the flux tower at a miombo woodland in Mpika, Zambia (see Fig. 4.7 in section 4.3.2). The satellite-based phenophases include: green-up, mid-green up, maturity, peak, senescence, green-down, and mid-green down and dormant. For ease of analysis the phenophases were merged into four groups based on dominant activity in each phase. For the climate and soil moisture-based classification Chidumayo and Frost (1996) observed five phenological seasons: warm pre-rainy season, early rain season, mid-rainy season, late rainy season and the cool dry season (Fig.4. 2). Within these phenological seasons the phenology of miombo species transition through various stages i.e., from leaf fall/leaf flush, growth of stems, flowering to mortality of seed (Chidumayo and Frost,1996). The satellite-based phenophases can be identified within the climate-based phenological seasons (Fig. 4.2).

4.2.4 Delineation of the miombo woodland components used in this study

The comparison of satellite-based evaporation estimates was performed at two levels: pixel level at known dry miombo woodland and wet miombo woodland locations, and at entire miombo woodland scale in the Luangwa Basin. Firstly, a pixel-based comparison was performed by using undisturbed known wet and dry miombo woodland locations (Figs. 4.1 and 4.3). The focus on a known wet miombo woodland enabled comparison of the field observations of the changes in canopy cover using digital camera images to the satellite-based LAI and NDVI for the year 2021.

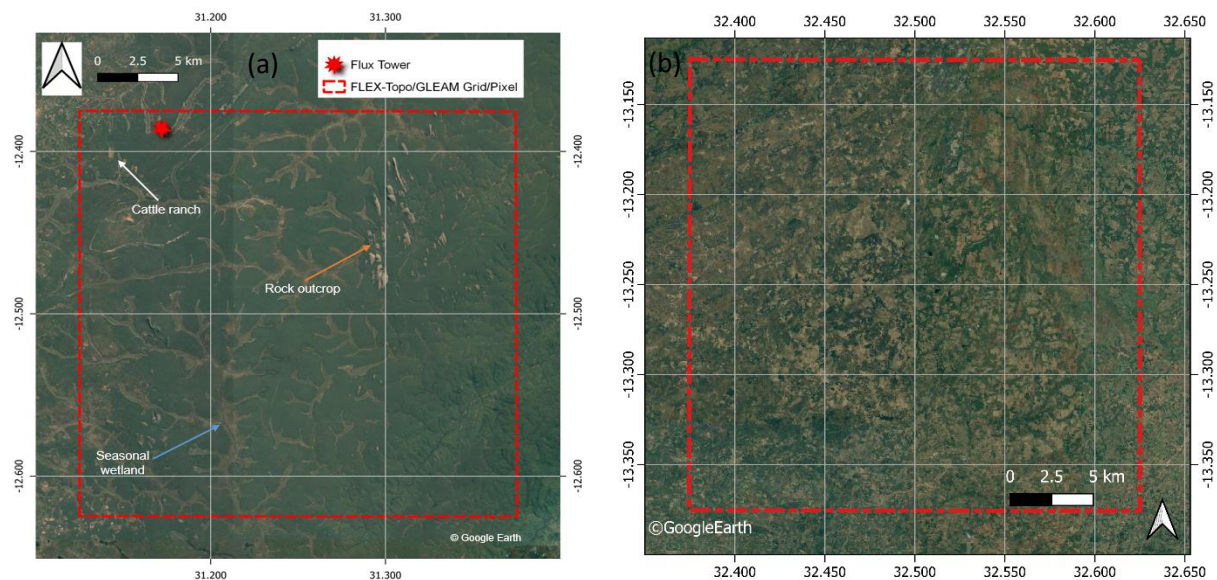


Figure 4.3: The wet (a) and dry (b) miombo woodland locations used for comparison of satellite-based evaporation estimates at FLEX-Topo and GLEAM spatial resolution (approximately 27.7 km by 27.7 km). The dotted red line is the actual location of the FLEX-Topo and GLEAM pixels. Seasonal wetlands are typical miombo ecosystem features.

The pixel-based comparison used actual location of FLEX-Topo and GLEAM pixels with original spatial resolutions (approximately 27.7 by 27.7 km) (Fig. 4.3). For MOD16, SSEBop, TerraClimate and WaPOR, the mean of actual evaporation estimates in all the pixels within the dotted red square (Fig. 4.3) were used. Secondly, the delineation of typical miombo woodland regions as conducted by White (1983) and the vegetation map shown in Ryan *et al.* (2016) (see Fig. 4.1 a,b) were used to delineate the miombo woodland in the Luangwa basin. The delineated miombo woodland in the Luangwa Basin excluded the mopane woodland, mixed woodland as well as the large water bodies like dams. This delineation (as shown in Fig. 4.1) ensured that only the areas classified as typical miombo woodland (Ryan *et al.*, 2016; White, 1983) were considered.

4.2.5 Satellite-based evaporation estimates used in the study

Compared to other ecosystems, Pelletier *et al.* (2018) and Tian *et al.* (2018) observed that miombo woodland species exhibit distinct behaviour (i.e., woodland canopy display and the vegetation water content) during the dry season. To this effect this study compared the behaviour (i.e., trend and magnitude) of six satellite-based evaporation estimates across the different phenophases of the miombo woodland with emphasis on the dry season. This was conducted in order to observe existence of discrepancies in monthly temporal trends and magnitude of satellite-based evaporation estimates under changing phenological seasons. The six satellite-based evaporation estimates consisted of: 1) FLEX-Topo (Hulsman *et al.*, 2021; Hulsman *et al.*, 2020; Savenije, 2010); 2) Thornthwaite-Mather Climatic water balance model (TerraClimate) (Abatzoglou *et al.*, 2018); 3) Global Land Evaporation Amsterdam Model (GLEAM) (Martens *et al.*, 2017; Miralles *et al.*, 2011); 4) Moderate-resolution Imaging Spectrometer (MODIS) MOD16 (Running *et al.*, 2019; Mu *et al.*, 2011; Mu *et al.*, 2007); 5) Operational Simplified Surface Energy Balance (SSEBop) (Senay *et al.*, 2013) and 6) Water Productivity through Open access of Remotely sensed derived data (WaPOR) (FAO, 2018). These products were selected purely because they are free of charge and easily accessible from various platforms and have an archive of historical data with appropriate temporal and spatial resolutions. Furthermore, excluding FLEX-Topo, the other five satellite-based estimates cover the entire miombo woodland of Africa. Except for FLEX-Topo and GLEAM (with spatial resolution of 27.7 km), these products have high spatial resolution (i.e., 500 m, 1000 m, 4000 m and 250 m for MOD16, SSEBop, TerraClimate and WaPOR respectively) and temporal resolution (daily, 8-day, dekadal and monthly respectively), which attributes were deemed suitable for this study. The original spatial resolutions of the six satellite-based evaporation estimates were used. This was because these products are normally applied as is, in their original resolutions. Resampling the spatial resolutions to a standard resolution was thought to be problematic as it would have introduced unknown and unquantifiable errors, regardless the extent resampled. For detailed explanations on the models for the satellite-based estimates used in this study kindly refer to the cited literature above and Table 4.1.

Table 4.1. Characteristics of satellite products used in the study

Variable	Product name	Time Period	Spatial coverage/Location	Temporal resolution	Spatial resolution	Reference	Source of data
Precipitation and temperature	CFRSR v2	2009 - 2020	Global	Daily	19.2 km	(Saha <i>et al.</i> , 2014; Saha <i>et al.</i> , 2010)	Climate Engine portal
	CHIRPS	2009 - 2020	Global	Daily	4.8 km	(Funk <i>et al.</i> , 2015)	https://app.climateengine.com/climateEngine
	ERA5	2009 - 2020	Global	Daily	24	(Hersbach <i>et al.</i> , 2017)	Climate Engine portal
LAI	TerraClimate	2009 - 2020	Global	Monthly	4 km	(Abatzoglou <i>et al.</i> , 2018)	Climate Engine portal
LAI	MODIS MCD15A3H v6	2021	Global	4-Day	0.5 km	(Myneni, Knyazikhin & Park, 2015)	Climate Engine portal
NDVI	MODIS MOD09GA v6	2021	Global	Daily	0.5 km	(Vermote & Wolfe, 2015)	Climate Engine portal
Runoff	Observations	1960-1992	159,000 km ²	Daily	N/A		WARMA, Zambia
Runoff	TerraClimate	1960 - 2020	Global	Monthly	4 km	(Abatzoglou <i>et al.</i> , 2018)	Climate Engine portal
Net radiation	CFRSR v2	2009-2020	Global	Daily	19.2 km	(Saha <i>et al.</i> , 2014; Saha <i>et al.</i> , 2010)	Climate Engine portal
Soil moisture (25 cm)	CFRSR v2	2009 -2020	Global	Daily	19.2 km	(Saha <i>et al.</i> , 2014; Saha <i>et al.</i> , 2010)	Climate Engine portal
Specific humidity	CFRSR v2	2009 - 2020	Global	Daily	19.2 km	(Saha <i>et al.</i> , 2014; Saha <i>et al.</i> , 2010)	Climate Engine portal
Digital elevation model (DEM)	ASTER GDEM v3	N/A	Global	N/A	30m	(Abrams and Chippen, 2019)	NASA GIOVIS portal
Land cover map	Copernicus CGLS-LC100 v3	2019	Global	Annual	100m	(Buchhorn <i>et al.</i> , 2020)	Google Earth Engine
Actual evaporation	FLEX-Topo	2009 - 2020	Catchment	Daily	27.7 km	(Hulsman <i>et al.</i> , 2021; Hulsman <i>et al.</i> , 2020; Savenije, 2010)	ZAMSECUR Project – Delft Technical University
	GLEAM (v3.2a)	2009 -2020	Global	Daily	27.7 km	(Martens <i>et al.</i> , 2017; Miralles <i>et al.</i> , 2011)	GLEAM FTP server
	MOD16v2	2009 -2020	Global	8-Day	0.5 km	(Running <i>et al.</i> , 2019; Mu <i>et al.</i> , 2011)	Climate Engine portal; Global subsets tool; MODIS/VIRS Land Products
Actual evaporation	SSEBop	2009 -2020	Global	Monthly	1 km	(Senay <i>et al.</i> , 2013).	Climate engine portal
	TerraClimate	2009 -2020	Global	Monthly	4 km	(Abatzoglou <i>et al.</i> , 2018)	Climate engine portal
	WAPOR v2. (ETLook)	2009 -2020	Continental	10-Day	0.25 km	(FAO, 2018)	WAPOR Portal

4.2.6 Basin water balance–based actual evaporation

In cases where spatially distributed measurements are not available, as is the case with large basins and more importantly in the Luangwa Basin, the use of the water balance approach is an acceptable approach (i.e., Weerasinghe *et al.*, 2020; Liu *et al.*, 2016). The general annual water balance was conducted in order to have a general outlook on the performance of the satellite-based evaporation estimates at basin level.

The general basin annual average water balance-based evaporation ($E_{a(wb)}$) is estimated using Eq. (4.1) where over-year storage change is neglected.

$$E_{a(wb)} = P - Q \quad (4.1)$$

where, P is the annual average catchment precipitation in mm year^{-1} and Q is annual average discharge in mm year^{-1} . The precipitation and discharge information for the water balance approach were selected and used as explained below.

4.2.7 Satellite-based precipitation products

The challenge posed by using satellite precipitation data in African catchments is that most, if not all, satellite precipitation products are geographically biased towards either underestimation or overestimation, despite some of them having good correlation with ground observations (i.e., Macharia *et al.*, 2022; Asadullah *et al.*, 2008; Dinku *et al.*, 2007). The lack of adequate ground precipitation observations makes it difficult to validate, as well as correct, the product(s) biases with a good degree of certainty. There is not a single precipitation product that can be said to perform better across African landscapes and southern Africa in particular (i.e., Macharia *et al.*, 2022). There is no guarantee any of the precipitation products are spatially representative of a basin that is about 159,000 square kilometres with varying topographical attributes. Using an ensemble of precipitation products is said to reduce errors and therefore, recommended (i.e., Asadullah *et al.*, 2008). To this extent, for the general water balance, this study used annual mean of four satellite precipitation products. The four precipitation products are the Climate Forecasting System Reanalysis (CFSR), Climate Hazards Group Infra-Red Precipitation with Station data (CHIRPS), ECMWF Reanalysis v5 (ERA5) and TerraClimate (Table 4.1). These products were selected purely based on availability and the fact that they had desirable spatial and temporal resolutions as given in Table 4.1.

4.2.8 Runoff data

Reliable monthly basin-scale field observations of run-off were only available for the period 1961 -1992 and not for the study period 2009 – 2020. Monthly modelled TerraClimate run-off data (Abatzoglou *et al.*, 2018) was available for the period 1958 – 2020. Compared to field observations TerraClimate run-off data was significantly higher during the peak rainfall period of January-February. At annual scale TerraClimate overestimated run-off data but strongly correlated ($r = 0.83$) with field observations (Fig. 4.4a). Based on the correlation of annual TerraClimate run-off data with field observations a linear regression equation was formulated to help generate extended near field observations time series for the period 2009-2020. TerraClimate run-off data was used as predictor variable. The TerraClimate run-off data was used because of availability free of cost and with relatively fine temporal and spatial resolution (monthly and 5 km respectively) (Table 4.1).

Firstly, the field observations run-off data and TerraClimate run-off data for the period 1960 - 1992 were split into two segments, 1960 - 1972 and 1980 - 1992. The run-off data for the period 1981 -1992 was used as training data to generate a linear equation with the TerraClimate run-off data as the predictor variable (Fig. 4.4b). The generated linear equation was validated using the 1961-1972 TerraClimate run-off data as a predictor variable (Fig. 4.4c). The predicted 1961-1972 run-off data with the TerraClimate run-off data as a predictor variable was then compared to the field observations for the same period (Fig. 4.4 c). The performance statistics of the equation showed $R^2 = 0.68$, $RMSE = 27.90 \text{ mm year}^{-1}$ and mean bias error (MBE) = $21.89 \text{ mm year}^{-1}$ (Fig. 4.4 c). The validation results of the regression equation were deemed sufficient for this study. The linear regression equation was then used to generate near field observations run-off data for the period 2009 – 2020 with TerraClimate run-off data for the same period as the predictor variable (Fig. 4.4 d). Generally, both observed and extended (with TerraClimate data) annual runoff was, on average, 11 percent of annual satellite-based precipitation. The near field observations extend run-off data was then used in the water balance approach, as explained in section 4.2.5, to estimate actual evaporation at basin level.

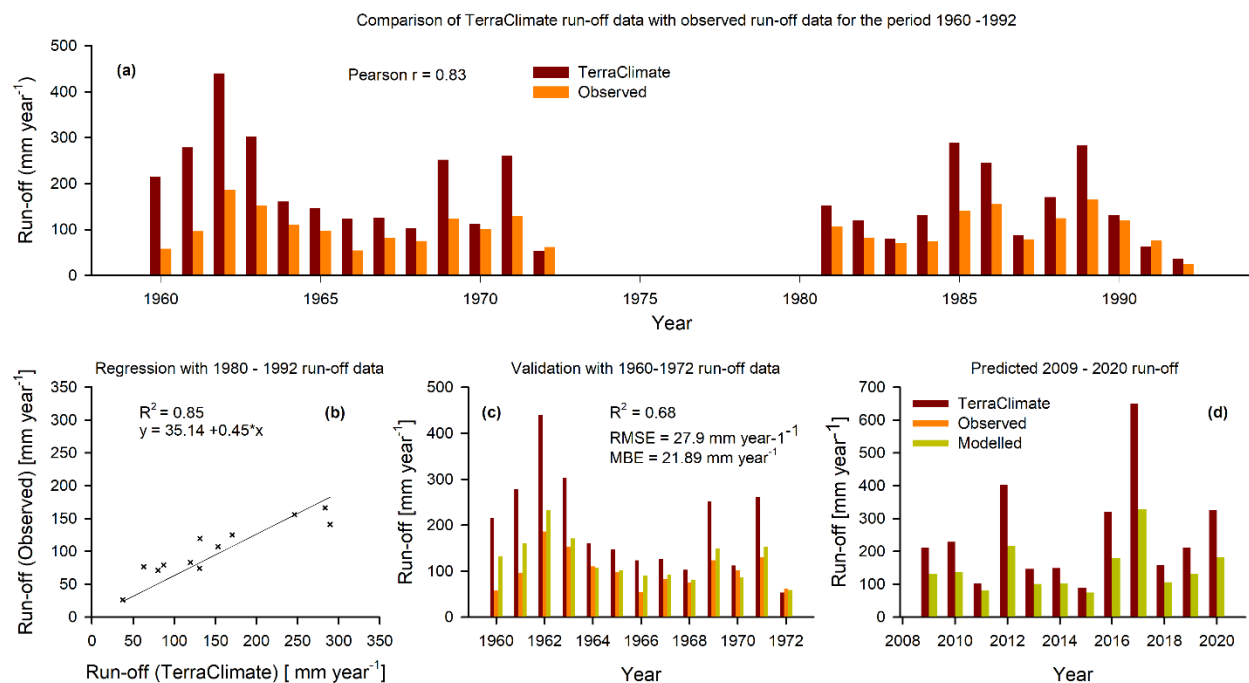


Figure 4.4: Procedure for extending near field observations run-off data for the period 2009-2020 using the TerraClimate run-off data as the predictor.

4.2.9 Field observations of miombo woodland canopy phenology

To observe changes in canopy cover in the miombo woodland, a Denver WCT-8010 digital camera was installed on a tower above the canopy of a known wet miombo woodland in Mpika (Fig. 4.1). This was conducted to obtain field imagery to compare with the temporal trend of satellite-based LAI and NDVI, and the satellite-based evaporation estimates trend across different

phenophases. In addition, the fish-eye lens was used to obtain under-canopy images of differences in canopy leaf display among miombo woodland species. The photographs were acquired for the period January – December 2021.

4.2.10 Statistical analyses

The coefficient of variation C_v (%) in Eq. (4.2) (Helsel *et al.*, 2020) was used to understand the extent to which the satellite-based evaporation estimates varied among each other across phenophases. Furthermore, the analysis of variance (ANOVA) (Helsel *et al.*, 2020) and all pairwise multiple comparison procedures with the Tukey Test (Helsel *et al.*, 2020) was performed. Correlation among satellite-based evaporation estimates was assessed at monthly and annual scales using the Kendal correlation test (Helsel *et al.*, 2020). To establish the extent to which the satellite-based evaporation estimates underestimated or overestimated evaporation, relative to E_{wb} , the mean bias (Eq. 4.3) was used.

$$C_v = \frac{\sigma}{\mu} \quad (4.2)$$

where σ is the standard deviation and μ is the mean of the observations. The higher the C_v value, the larger the standard deviation compared to the mean, which implies greater variation among the variables.

$$MBE = \frac{1}{n} \sum_{i=1}^n (E_{s_i} - E_{a(wb)_i}) \quad (4.3)$$

where n = number of observations, $E_{a(wb)}$ = water balance-based actual evaporation time series and E_s is the satellite-based evaporation estimates time series. The smaller the mean bias value (positive or negative), the less the deviation of the predicted values from the observed values (Helsel *et al.*, 2020).

4.3 Results and discussion

4.3.1 Basin scale miombo woodland climate and phenological trend(s)

Figure 4.5 shows Luangwa Basin miombo woodland aggregated 2009-2020 average NDVI and CFSR data climate conditions; net radiation (R_N), air temperature (T_a), specific humidity (SH), soil moisture (SM) and precipitation (P).

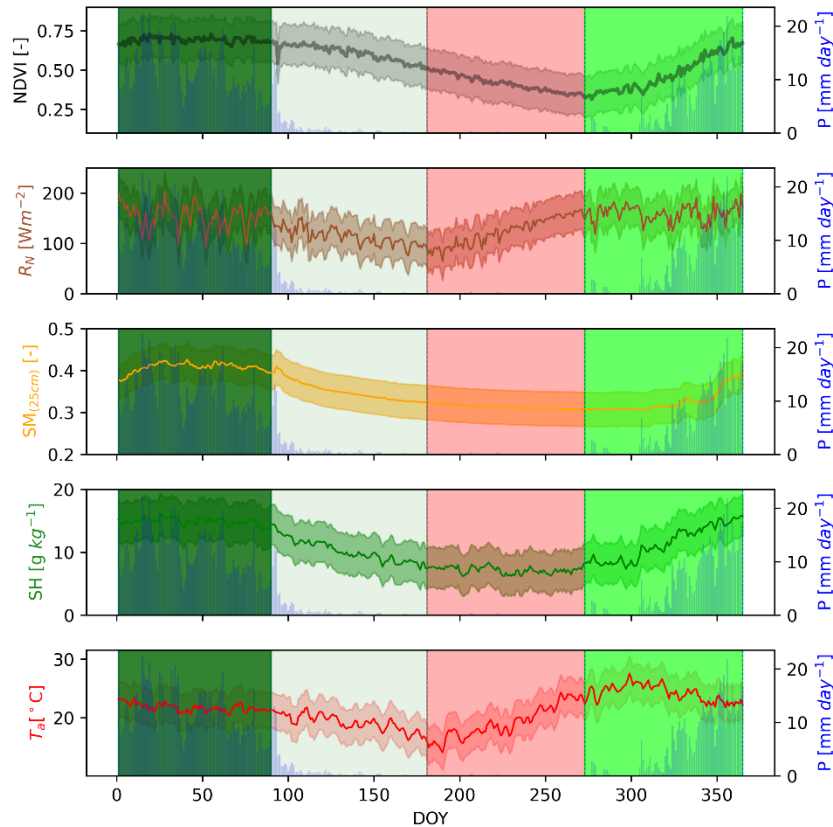


Figure 4.5: Luangwa Basin miombo woodland aggregated 2009-2020 daily climate and phenological conditions NDVI, net radiation (R_N), precipitation (P), soil moisture (SM), specific humidity (SH) and air temperature (T_a). The shaded areas represent the aggregated phenophases as used in this study: January – March is the peak/maturity, April – June is the senescence/Green-down, July – September is the Dormant and October – December is the green-up/mid-green-up phenophase. Shaded area for variables is the standard deviation.

The peak climate and phenological variables values were observed in the early and mid-rainy seasons during the green-up and maturity/peak phenophases. The lowest values in climate and phenological variables were observed in the cool dry season during the green-down and dormant phenophases. Climate variables net radiation, air temperature, specific humidity covaried (positively or negatively) with the NDVI (proxy for canopy phenology) depending on the phenophase (Fig. 4.5 and Table A1 in the appendices of Zimba *et al.* (2023 under review)). The strong correlation between climate and phenology (i.e., NDVI and air temperature/soil moisture) in the miombo woodland (Table A1 in the appendices of Zimba *et al.* (2023 under review)) agreed

with observations made by Chidumayo (2001) and in other ecosystems (Pereira *et al.*, 2022; Niu *et al.*, 2013; Cleland *et al.*, 2007).

4.3.2 Observed phenological conditions in the miombo woodland

The canopy closure is varied, ranging between 2 percent to about 70 percent in the shrub, dry miombo woodland and wet miombo woodland (Fuller, 1999). Therefore, depending on location and dominant species, exposure of the understory, field and ground layers to incident solar radiation, through the canopy is substantial (Figs. 4.6, Chidumayo, 2001; Fuller, 1999). The field layer during the rainy season mainly comprises green grass (Fig. 4.6b and Chidumayo, 2001). Therefore, total LAI and NDVI in the rainy season phenophases can be largely attributed to both the field layer i.e., grass, understory and the tree layer i.e., shrubs and tree canopy (i.e., Fig. 4.4b and Chidumayo, 2001). In the dry season the grass in the field layer and some understory non-deep rooting shrubs dry out (Fig. 4.4a and Chidumayo, 2001, Fuller, 1999). Therefore, the changes in total LAI and NDVI in the phenophases in the dry season can largely be attributed to the changes in the tree layer of the miombo species (i.e., Fig 4.6a, Fig. 7 and Chidumayo, 2001).



Figure 4.6: Dry season (a) and rainy season (b) tree layer, understory and field layer conditions at the wet miombo woodland site in Mpika, Zambia. Images taken on 29th September and 23rd December, 2021.

The LAI and NDVI were used as proxies for observing the changes in the canopy cover across different phenophases of the miombo woodland. At pixel scale the spatial distribution and mean values of the LAI and NDVI for the wet miombo woodland differed with that for the dry miombo woodland (Fig. 4.8a). This is due to the differences in the miombo woodland species composition and distribution at each site. Furthermore, there are differences in soil type, soil moisture, temperature, nutrients, rainfall and canopy closure at the two sites (i.e., Chidumayo, 2001; Fuller, 1999). However, trends in the NDVI and LAI across different phenophases of the miombo woodland at the two sites were significantly similar (Pearson $r = 0.73$ for LAI and NDVI respectively) (Fig. 4.8b). Highest LAI and NDVI, both in the dry miombo woodland and wet miombo woodland, were observed in the maturity/peak phenophases during the mid-rainy season (January – March) (Figs. 4.5, 4.7 & 4.8b). This period for peak LAI and NDVI (Figs. 4.7 and 4.8) agrees with Chidumayo (2001) who observed that peak green biomass in the miombo woodland occur anytime between January and May.

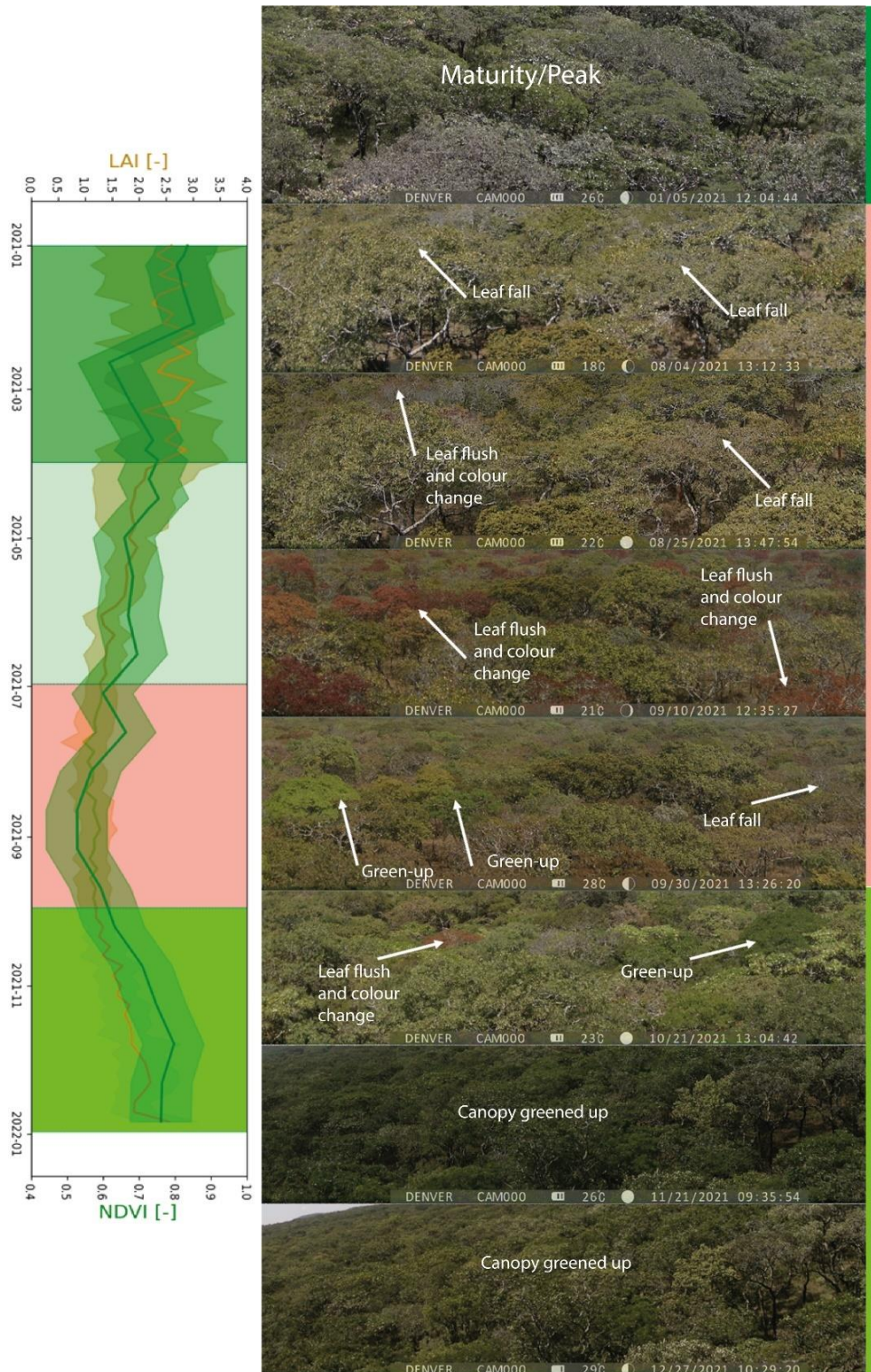


Figure 4.7: Temporal trend of MODIS *LAI*, *NDVI*, and the wet miombo woodland canopy display trend for the year 2021 at Mpika study site. Shaded area are phenophases: January – March is the Maturity/Peak; April-June is the Senescence/Green-down; July-September is the Dormant while October – December is the green-up. Shaded area for variables is the standard deviation.

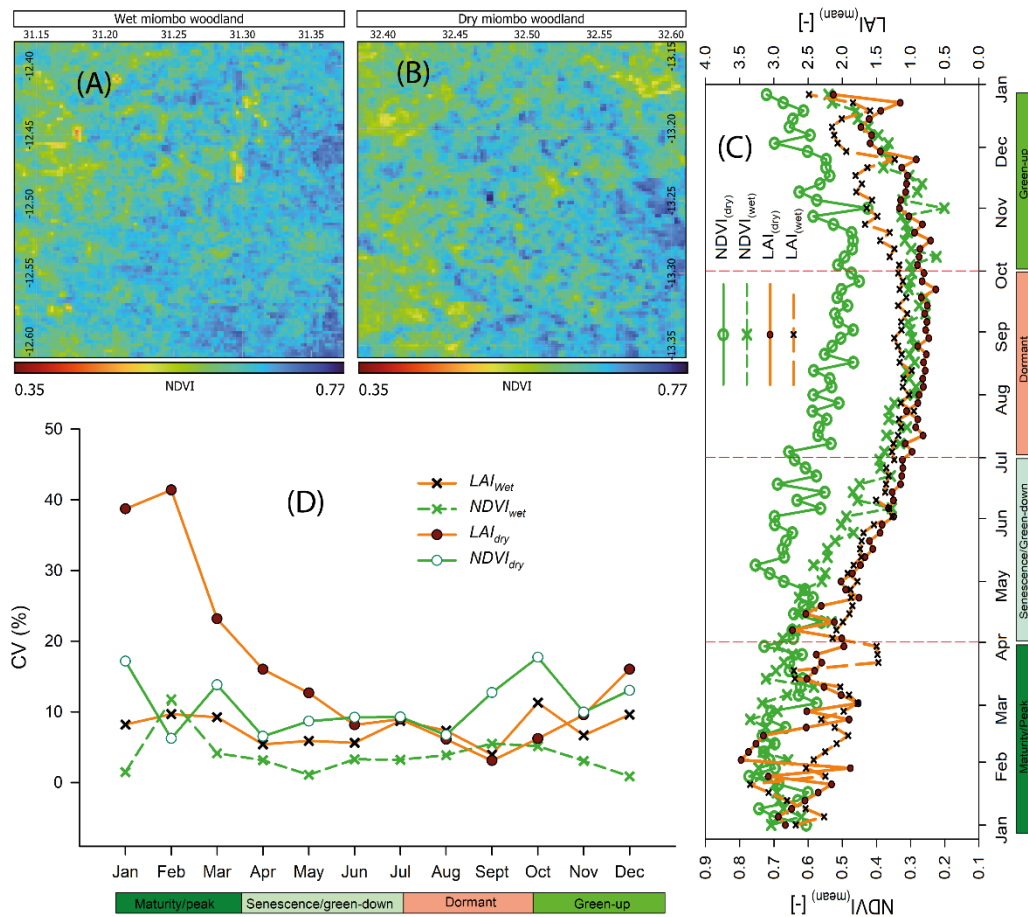


Table 4.2. Dormant phenophase CV correlation

Variables	LAI _(wet)	NDVI _(wet)	LAI _(dry)	NDVI _(dry)
LAI _(wet)	1			
NDVI _(wet)	-1.00	1		
LAI _(dry)	0.98	-0.98	1	
NDVI _(dry)	-0.75	0.75	-0.59	1

Figure 4.8: Spatial distribution of NDVI at the (a) wet miombo woodland and (b) dry miombo woodland site for the period January-December, 2021. Coefficients of variation in the LAI and NDVI values at the wet miombo woodland and dry miombo woodland in the Luangwa Basin in Zambia for the year 2021.

The lowest LAI and NDVI were observed in the dormant phenophase in August/September during the warm pre-rainy season (Figs. 4.5, 4.7 & 4.8). The leaf fall, leaf flush and changes in colour of the leaves intensifies in the August-September period (Fig. 4.7, Chidumayo, 2001; Chidumayo and Fuller, 1996; Fuller, 1999). The intensified leaf fall, leaf flush and leaf colour changes may also explain the increased variations in the NDVI in August-September (Fig. 4.8d). Table 4.2 shows the correlation coefficients of the coefficients of variations in NDVI and LAI values for the

dry miombo woodland and wet miombo woodland. The coefficients of variation in LAI and NDVI values for the wet and dry miombo woodland were only similar for the dormant phenophase (Pearson $r = 0.98$ and 0.75 for the LAI and NDVI respectively (Fig. 4.8). The similarity in the coefficients of variations of estimates for the dry miombo woodland and wet miombo woodland LAI and NDVI in the dormant phenophases may be due to the plants at the two sites undergoing similar phenological processes leaf fall and leaf flush. In the dormant phenophase the grass component would have dried out leaving largely the tree component (i.e., miombo woodland canopy). The coefficients of variation in LAI values in July and August in wet miombo woodland can be attributed to increased leaf fall activity (Fig. 4.8). Fuller (1999) observed that in the wet miombo woodland the simultaneous occurrence of the leaf fall and leaf flush, in August and September, among miombo woodland species resulted in net zero change in the canopy closure. The net zero change increase in canopy closure may explain the observed low coefficient of variation in the LAI values in September (Fig. 4.8). The substantially high coefficient of variations in LAI and NDVI values, for both dry miombo woodland and wet miombo woodland, during the mid-rainy season in the maturity/peak phenophases mainly can be attributed to two factors. Firstly, the increase in the growth of the green biomass of the woodland which occur anytime between January and May (Chidumayo, 2001, Fuller, 1999) and the effect of cloud cover on the quality of the satellite-based LAI and NDVI products (Vermote and Wolfe, 2015; Zang *et al.*, 2003). Furthermore, the differences in the canopy closure between the dry miombo woodland and wet miombo woodland (Fuller, 1999) may be the reason for differences between the coefficients of variations in LAI and NDVI values in the maturity/peak and senescence\green phenophases. For instance, the dry miombo woodland which has a lower canopy closure compared to the wet miombo (Fuller, 1999) is likely to have a higher grass component. Additionally, the differences in miombo woodland species composition, distribution of rainfall, soil type and soil moisture, among other variables, may result in varied phenological differences between the dry miombo woodland and wet miombo woodland (Chidumayo, 2001; Fuller, 1999). However, unlike in the other phenophases, there appeared strong correlations (Table 4.2) in the variations in LAI and NDVI values in the dry miombo woodland and wet miombo woodland in the dormant phenophase.

The simultaneous occurrence of leaf fall and leaf flush (i.e., Fig. 4.9) is one of the phenological attributes that distinguishes the miombo woodland from other woodlands (Fuller, 1999; White, 1983). The leaf fall and leaf flush in the dry season (Figs. 4.7 and 4.9) occur many weeks and even months before the start of the rains. The growth of the new leaves in the dry season is sustained by both access to deep soil moisture, including ground water, and the adapted plant water storage mechanisms (i.e., Tian *et al.*, 2018; Vinya *et al.*, 2018; Fuller, 1999; Savory, 1963). The leaf fall and leaf flush occur simultaneously (i.e., Fig. 4.9) and results in net zero change increase in canopy closure in the dry season in wet miombo woodland (i.e., miombo woodland site in Mpika) (Fig. 4.9 and Fuller, 1999). The balance in the leaf fall and leaf flush may explain the lower coefficient of variation in LAI values in September in both dry miombo woodland and wet miombo woodland.

Therefore, in the dormant phenophase and the early green up in October, when the total LAI and NDVI can largely be attributed to the miombo woodland plants, the variations in the trend in the changes in phenology appear to be similar in both dry miombo woodland and wet miombo woodland though at different rates (Fig.4.8).

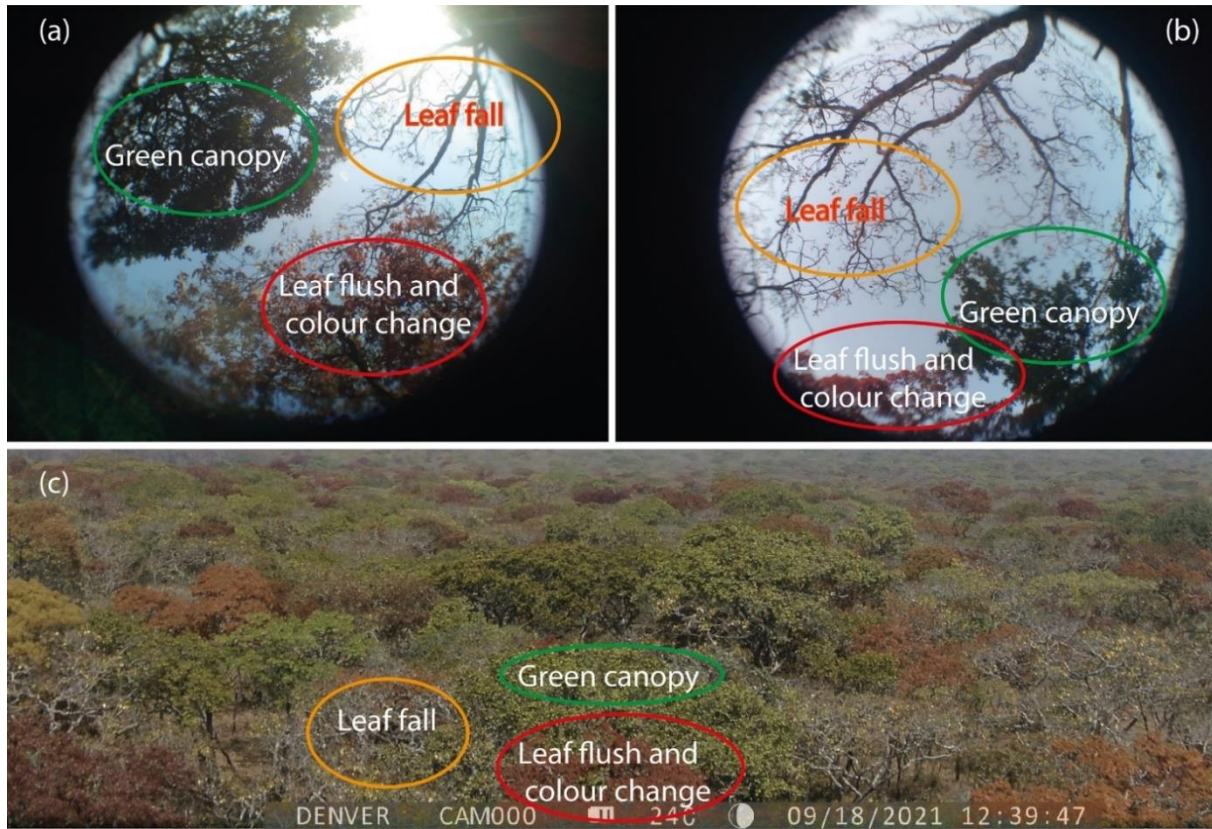


Figure 4.9: Heterogeneity in leaf fall and leaf flush activities among miombo woodland species: observed from under the canopy (a, b) and as observed above the canopy (c). Images taken at the wet miombo woodland site in Mpika, Zambia. Images taken on 18 September, 2021.

4.3.3 Phenophase-based difference in satellite-based evaporation estimates

Figure 4.10 shows results for the comparison at (a) pixel(s) with wet miombo woodland, (b) pixel(s) with dry miombo woodland and (c) miombo woodland at basin scale. Across different phenophases the trend and magnitude of satellite-based evaporation estimates at pixel and basin scales appeared similar (Table A1 in the appendices of Zimba *et al.* (2023 under review)). The coefficients of variations for the dry miombo woodland and wet miombo woodland (Fig. 4.11) strongly correlated ($r = 0.95$). This correlation coefficient implies that the trend in satellite-based evaporation estimates at the dry miombo woodland and wet miombo woodland were similar (Fig. 4.11).

Substantial differences in satellite-based evaporation estimates, at both pixel level in wet miombo woodland, dry miombo woodland and at the Luangwa Basin miombo woodland scale, were observed during the green-up ($C_v = 28.23$; 30.06; 22.63 percent respectively) and dormant phenophase ($C_v = 36.72$; 58.87; 39.98 percent respectively) (Figs. 4.10, 4.11 and Table A2 in the appendices of Zimba *et al.* (2023 under review)). The green-up phenophase is at the commencement of the rain season with high canopy cover (i.e., mean NDVI between 0.5 and 0.7) and highest net radiation (i.e., 150 Wm^{-2}). The dormant phenophase is during the driest part of the year with the lowest moisture in the topsoil, least woodland canopy cover (i.e., $\text{NDVI} \approx 0.5$) but, compared to the senescence/green-down phenophase, with increasing net radiation and air temperature (Fig. 4.5).

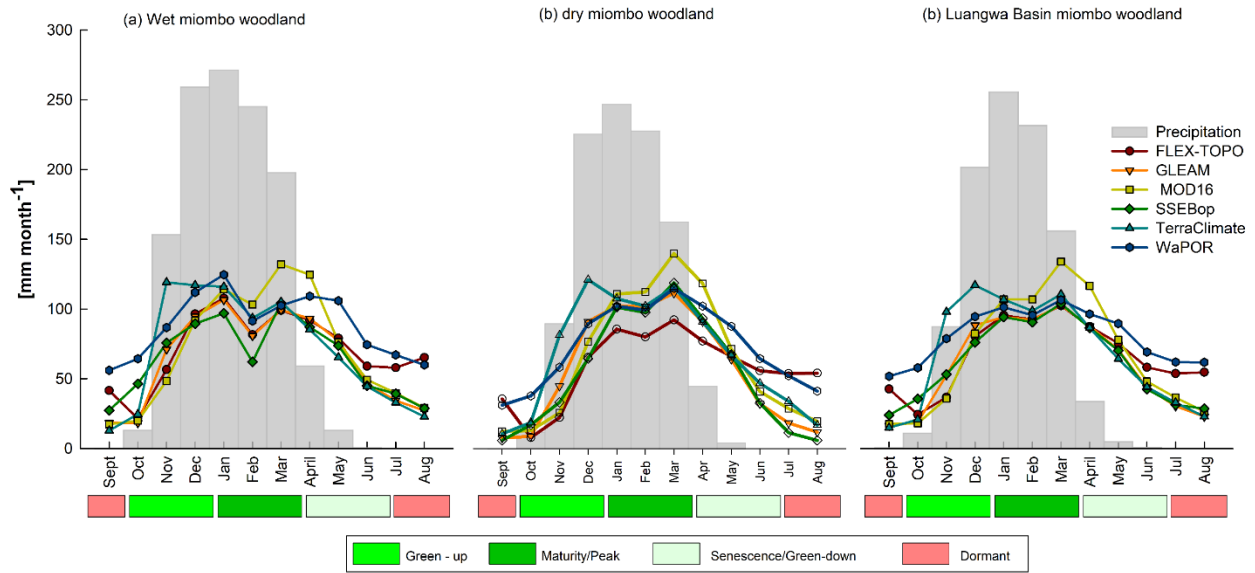


Figure 4.10: Comparison of aggregated 2009-2020 mean estimates of actual evaporation of satellite-based evaporation estimates (a) at wet miombo woodland, (b) dry miombo woodland, and (c) delineated Luangwa Basin miombo woodland across hydrological year (September – August) in the Luangwa Basin.

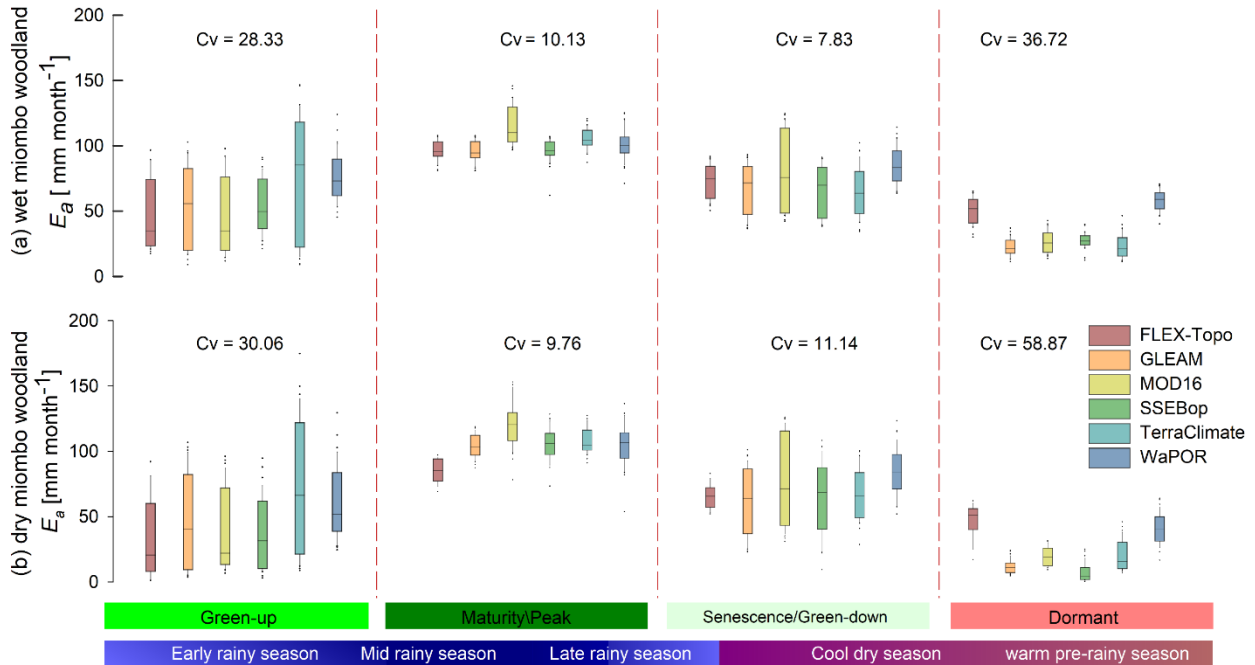


Figure 4.11: Comparison of satellite-based evaporation estimates across phenophases based on hydrological year (a) in wet miombo woodland and (b) in dry miombo woodland. Most variations in actual evaporation estimates among the satellite-based evaporation estimates were observed in the dormant and green up phenophases.

What is important to note is that, unlike during the maturity/peak and senescence/green down phenophases, the total LAI and total NDVI during the dormant and green-up phenophases can largely be attributed to the tree layer (i.e., miombo woodland canopy) (Chidumayo, 2001; Chidumayo and Frost, 1996). The implication is that the dormant and green-up phenophases are likely to be more representative of the evaporation of the miombo woodland than the other phenophases in the rainy season when the grass component substantially increases. Compared to the maturity/peak and the senescence/green-down phenophases, the dormant and green-up phenophases showed higher variations in evaporation estimates and lower correlation among satellite-based evaporation estimates (Fig. 4.11 and Table A1 in the appendices of Zimba *et al.* (2023 under review)). The substantial differences in satellite-based evaporation estimates during the dormant and green-up phenophases suggests that it is more challenging to estimate evaporation of the miombo woodland in low soil moisture in the upper layers, changing canopy phenology and high available energy conditions.

4.3.4 All pairwise multiple comparison of satellite-based evaporation estimates at Luangwa Basin miombo woodland scale

Tables A3 and A4 in the appendices of Zimba *et al.* (2023 under review) shows results of the ANOVA and all pairwise multiple comparison of satellite-based evaporation estimates. In the dormant phenophase the trend and magnitude of FLEX-Topo and WaPOR were significantly (p -value > 0.05) similar to each other but significantly (p -value < 0.05) different from the other satellite-based estimates. In the same phenophase GLEAM and MOD16 showed similar trend and magnitude. SSEBop was significantly different from MOD16 and TerraClimate. The rest of the comparisons did not show significant differences in trend and magnitude of satellite-based evaporation estimates. During the green-up phenophase there were no significant (p -value > 0.05) differences between GLEAM estimates and FLEX-Topo and WaPOR estimates. However, the TerraClimate and WaPOR were significantly different (p -value < 0.05) from other estimates. In the maturity/peak phenophase MOD16 was significantly (p -value < 0.05) from the other satellite-based evaporation estimates. During the same period GLEAM, SSEBop and WaPOR were significantly different from at least one other satellite-based estimate. During the senescence/green-down phenophase the WaPOR significantly differed with FLEX-Topo, GLEAM, SSEBop and TerraClimate while the rest of the comparison showed similarity in trend and magnitude among satellite-based evaporation estimates. Across phenophases WaPOR appeared to be the most significantly different satellite-based evaporation estimate followed by FLEX-Topo, MOD16 and TerraClimate (Fig. 4.12).

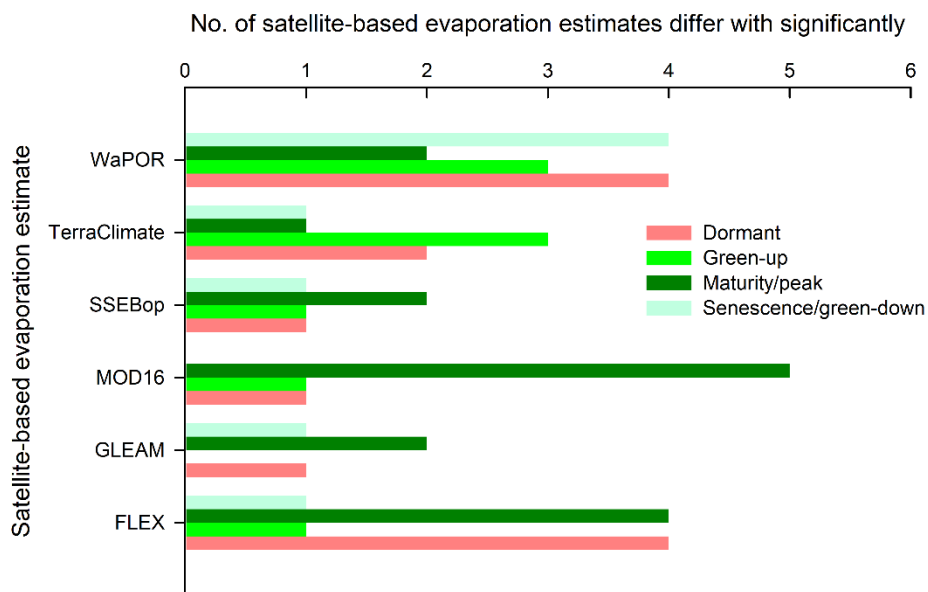


Figure 4.12: Number of times each satellite-based evaporation estimate was significantly different to one or more other estimates in each phenophase at Luangwa Basin miombo woodland scale

4.3.5 Variations within each climate, LAI, NDVI and satellite-based evaporation

Variations in within satellite-based evaporation estimates were higher in the green-up and senescence/green-down phenophases (Fig. 4.13a). These two phenophases are at the boundaries of the dry season into the mid-rainy season (in case of green-up phenophase) and the rainy season into the dry season (in the case of the senescence/green-down phenophase). The variations in the rainfall in these two phenophases (Fig. 13b) likely explains the variations within each satellite-based evaporation estimates. Additionally, there were more variations in the NDVI values across phenophases than there were variations in the LAI values (Fig. 4.13b). The low variations in the LAI may be due to the tree layer in the Luangwa Basin miombo woodland experiencing no significant seasonality especially in the wet miombo woodland (i.e., Fuller, 1999). Furthermore, the simultaneous occurrence of leaf fall and leaf flush in the dry season phenophases facilitates a varied canopy closure of up to 70 percent as was observed (Fuller, 1999) in the miombo woodland in the Luangwa Basin.

It appears that at the boundaries of the commencement and end of the rainy season, green-up and senescence/green-down phenophases, there is high variations (i.e., high standard deviation values) in within satellite-based evaporation estimates (Fig. 4.13a). The possible explanation for the high standard deviations could be the high variations in the amounts of rainfall received during these two boundaries (Fig. 13b). During the maturity/peak phenophase the rains are consistent while the dormant phenophase has no rainfall. It appears the rainfall interception could be a key driver of the differences in satellite-based evaporation estimates of the phenophases in the rainy season. For instance, field observations showed that wet miombo woodland canopies intercepted up to 18-20 percent of rainfall annually (i.e., Alexandre, 1977). In the cool dry season and warm pre-rainy season, in the dormant phenophase, it appears there is consistency in each satellite-based evaporation estimates (Fig. 4.13 a). Yet, this is the phenophase when the largest differences are

observed between the various satellite-based evaporation estimates. It is also the phenophase when the total LAI and total NDVI can be largely attributed to the tree layer (i.e., canopy of the miombo woodland). By implication, this is the phenophase when the satellite-based evaporation estimates can largely, if not entirely, be attributed to the transpiration of the miombo woodland species.

The maturity/peak phenophase had highest rainfall (above 200 mm/month), highest canopy cover (i.e., NDVI > 0.6), highest soil moisture and net radiation of above 150 W m² (Figs. 4.5, 4.7 and 4.10). However, the total LAI and total NDVI in these two phenophases is largely attributed to various components such as the tree layer (i.e., miombo woodland canopy), understory (i.e., shrubs) and the field layer (i.e., grass component) (Chidumayo, 2001; Chidumayo and Frost, 1996).

The highest coefficients of variations in satellite-based evaporation estimates were observed in the dormant and green-up phenophases. The dormant phenophase in the cool-dry season and warm pre-rainy phenological season is the driest part of the year. This is also the phenophase with the most physiologically adapted changes in the canopy display characteristics. During this phenophase the actual evaporation is mainly, if not entirely, through transpiration

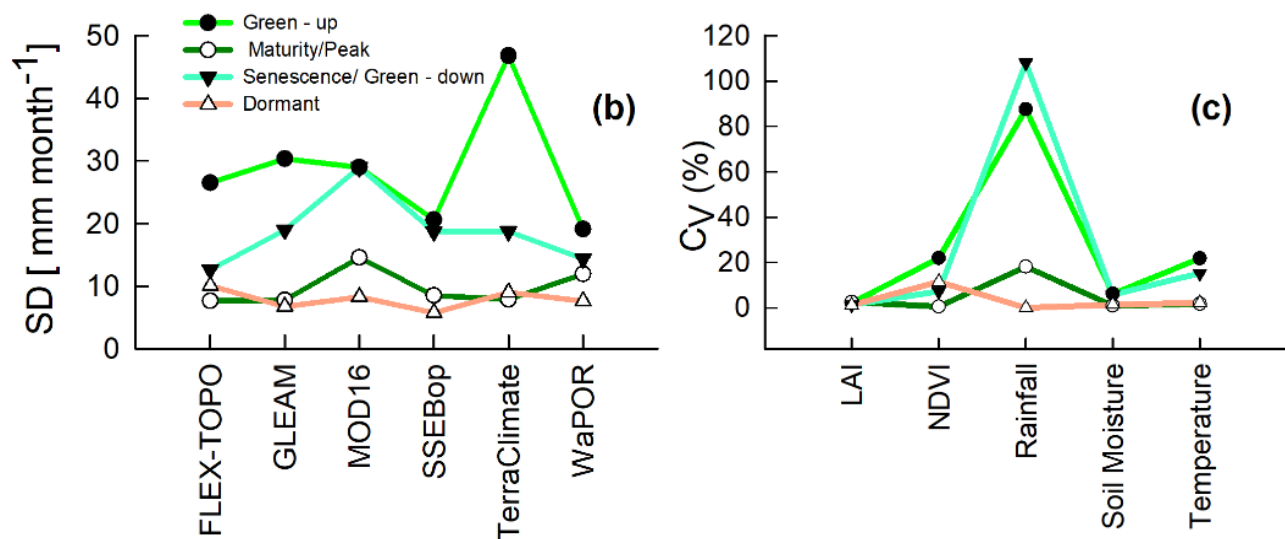


Figure 4.13: Standard deviations (SD) (a) showing within satellite-based evaporation estimate variations across phenophases and (b) coefficients of variation (C_v) in estimates for climate and phenological variables across phenophases at Luangwa Basin miombo woodland scale.

4.3.6 Differences in spatial distribution of satellite-based evaporation estimates and the potential contributing factors

Figure 4.14 shows spatial-temporal distribution of satellite-based actual evaporation estimates across different phenophases for the hydrological year 2019/2020. The comparison was based on the entire Luangwa Basin, including non-miombo regions. Generally, substantial differences in the spatial distribution of actual evaporation were observed in the dormant and green-up phenophases (Fig. 4.14). During the dormant phenophase, all six estimates appeared to show higher actual evaporation in upland miombo areas than in other land cover types (Fig. 4.14)

(refer to Fig. 4.1 and Fig. A1 in the appendices of Zimba *et al.* (2023 under review) for extent of the cover of the miombo woodland in the Luangwa Basin).

Substantial differences in the spatial-temporal distribution of satellite-based evaporation estimates were observed in the dormant and green-up phenophases. The two phenophases were characterised by low (cool dry season) and high (warm pre-rainy and early rainy season) available energy conditions (i.e., net radiation) (Fig. 4.5). The key adapted phenological and physiological characteristics during the two phenophases include the leaf fall, leaf flush, leaf colour change, vegetation water storage, and the deep rooting with access to deep soil moisture (including ground water) (Vinya *et al.*, 2018; Fuller, 1999; Frost, 1996; Savory, 1963).

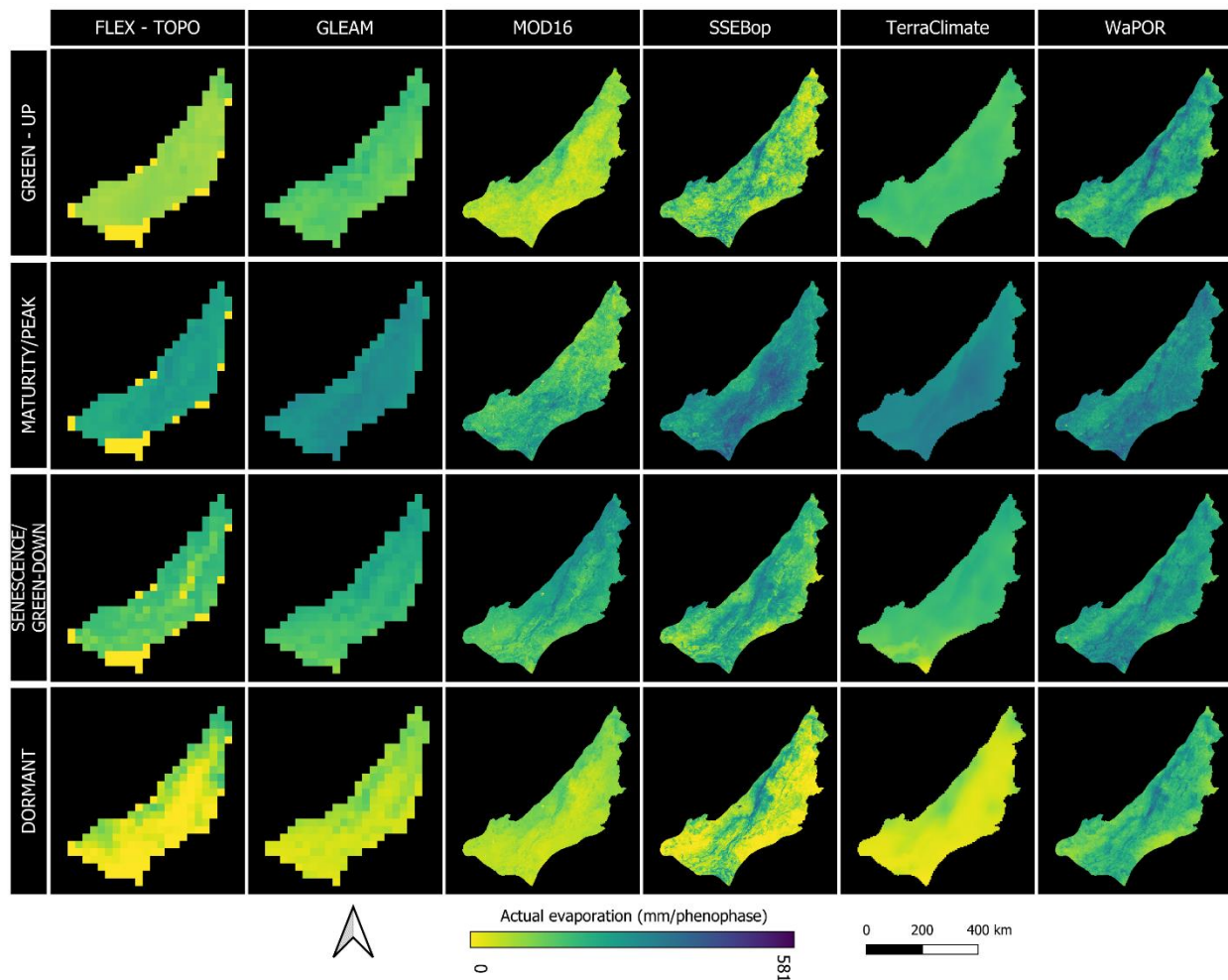


Figure 4.14: Spatial-temporal distribution of satellite-based evaporation estimates across different vegetation phenophases of the Luangwa Basin for the hydrological year 2019-2020.

In the dry season evaporation in the miombo woodland is through the transpiration process. The transpiration is influenced by the above highlighted adapted phenological and physiological characteristics (i.e., Marchesini *et al.*, 2015; Snyder and Spano, 2013). It appears that satellite-based evaporation estimates from models whose structure, processes and inputs take into account

the highlighted phenological and physiological attributes in the dry season and early rainy season, especially the access to deep soil moisture, are likely to have the accurate trend and magnitude of evaporation of the miombo woodland.

Some studies have shown that direct integration of soil moisture rather than the use of proxies improves the accuracy of actual evaporation estimates (Brust *et al.*, 2021; Novick *et al.*, 2016). For instance, transpiration in the FLEX-Topo and WaPOR (ETLook model) is coupled with the rootzone soil moisture using an integrated approach. The all pairwise comparison showed the trend and magnitude of FLEX-Topo and WaPOR estimates were not significantly (p -value > 0.05) different (in both dry miombo woodland and wet miombo woodland) in the dry season. GLEAM only takes into account 2.5m of the sub-surface moisture linked to observed precipitation. TerraClimate uses the plant-extractable water capacity of soil for soil moisture input. However, the challenge with the plant-extractable water capacity of soil is in selecting the rooting depth. The soil moisture in the miombo woodland tend to increase with depth. Some miombo plants are deep rooting (beyond 5 metres) with ability to tap into ground water sources. The energy balance-based SSEBop does not explicitly consider soil moisture dependency and assume that the variations in satellite-based land surface temperature and vegetation indices such as the NDVI accounts for the soil moisture (Senay *et al.*, 2013). The challenge with the use of the proxies for soil moisture in surface energy balance models is that these are unable to fully account for changes in other factors that may influence sensible heat fluxes (Gokmen *et al.*, 2012). To improve on the accuracy of estimation of water and energy fluxes in regions with recurrent plant water stress, i.e., miombo woodland, Gokmen *et al.* (2012) suggested that the soil moisture be integrated in the surface energy balance models. For the MOD16 the use of the relative humidity and vapour pressure difference as proxies for soil moisture maybe a source of uncertainty in estimating transpiration (Novick *et al.*, 2016). Direct integration of soil moisture into the MOD16 algorithm appeared to improve the accuracy of actual evaporation estimates (Brust *et al.*, 2021). The quality of the soil moisture product(s), rooting depth and whether the model structure accounts for vegetation interaction with ground water possibly contributed to the differences observed in the trend, magnitude and the spatial distribution of satellite-based evaporation estimates of the miombo woodland.

Additionally, among many other contributing factors, the land cover product as a model input in satellite-based evaporation estimates may largely explain the observed differences in both temporal and spatial distribution of evaporation. For instance, the MOD16 heavily relies on a global land-cover product (Gray *et al.*, 2019; Running *et al.*, 2019) which had shown to misclassify certain land cover types and showed low user accuracy in certain regions (i.e., Leroux *et al.*, 2014). The WaPOR uses the Copernicus land cover product, but adds the distinction between irrigated and rain-fed areas (FAO, 2018). For the vegetation fraction, the GLEAM uses the MODIS MOD44B product (Martens *et al.*, 2017; Miralles *et al.*, 2011). Different vegetation types have different phenology and physiological attributes (i.e., Lu *et al.*, 2006) which influence how actual evaporation is estimated. Miombo woodland's dry season evaporation mainly occurs through plant transpiration, which is dependent on the landcover type, and is driven by root zone water availability and climate variables such as net radiation, air pressure, wind speed, air temperature and relative humidity. The link between the drivers and the plant transpiration are the rooting depth and stomata conductance thresholds which are vegetation type dependent (ie., Urban *et al.*, 2017; Wehr *et al.*, 2017; Tuzet, 2011). Therefore, dissimilarities in the land cover products and their associated accuracy limitations possibly reflect in differences in the spatial-temporal distribution of the satellite-based actual evaporation estimates.

Furthermore, the differences observed in satellite-based evaporation estimates during the green-up, maturity/peak and the senescence/green-down phenophases may be more related to the ability of the models to effectively account for rainfall interception. For instance, field observations showed that wet miombo woodland canopies intercepted up to 18-20 percent of rainfall annually (i.e., Alexandre, 1977). As earlier mentioned above the accuracy of the vegetation cover product influences the classification of the various vegetation types. Misclassification of the miombo woodland would result in inaccurate estimation of rainfall interception. The differences in the set up of the rainfall interception modules/models may also contribute to these differences in satellite-based evaporation estimates.

4.3.7 Comparison of satellite-based evaporation estimates to the water balance-based actual evaporation estimates

Figure 4.15 shows the results of the temporal comparison of satellite-based evaporation estimates with the water balance-based evaporation estimates at Luangwa Basin scale for the period 2009-2019. This comparison included non-miombo areas. All satellite-based evaporation estimates showed insignificant correlation (p -value > 0.05) with the water balance-based actual evaporation (E_{wb}) (Table A3 in the appendices of Zimba *et al.* (2023 under review)). The poor correlation could be due to the uncertainties in the precipitation and run-off data used in the study.

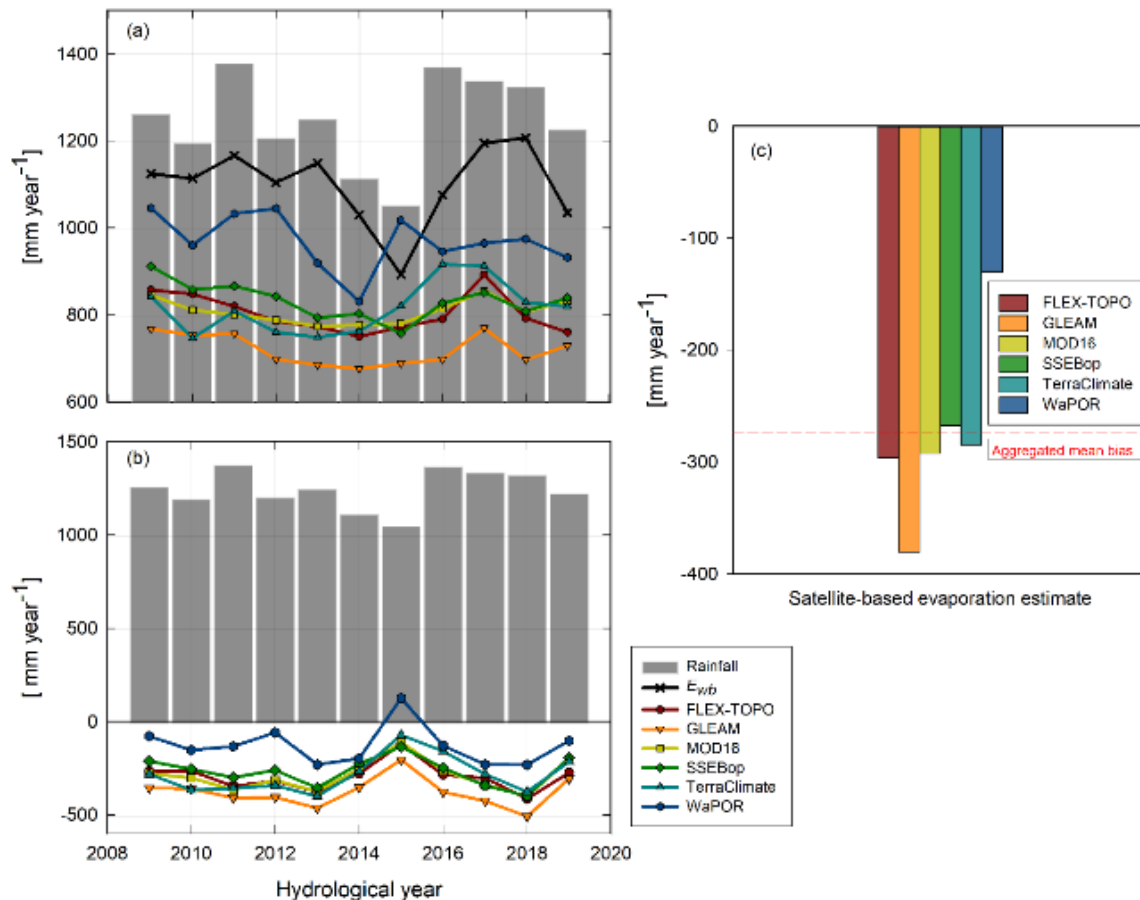


Figure 4.15: (a) Comparison of satellite-based evaporation estimates to the water balance-based estimates of actual evaporation for the Luangwa Basin and (b, c) the results of the bias assessment.

Compared to the E_{wb} estimates, all six satellite-based evaporation estimates underestimated actual evaporation (Fig. 4.15). Potential reasons for the underestimation include the quality of the precipitation product(s) used in this study. It is possible the precipitation was overestimated resulting in overestimating the actual evaporation with the water balance equation. To the contrary the extended run-off time series with the TerraClimate could have been overestimated resulting in underestimating the water balance-based actual evaporation at basin scale. The assumption of overestimation of the extended run-off data is based on the validation results of the linear equation, used to extend the run-off time series, which showed $RMSE = 27 \text{ mm year}^{-1}$ and $MBE = 21 \text{ mm year}^{-1}$.

In any given year, the WaPOR appeared to have the least underestimation with an aggregated mean bias of 120 mm year^{-1} , while the GLEAM had the largest underestimation with an aggregated mean bias of 370 mm year^{-1} . Only the SSEBop and the WaPOR showed a below average aggregated annual mean bias (in dotted red line) (Fig. 4.15 c). The aggregated mean is the average of all six satellite-based evaporation estimates. At basin scale, it appeared there was no statistically significant correlation ($r = -0.63$; $p\text{-value} = 0.18$; $\alpha = 0.05$) between spatial resolution of satellite-based evaporation estimates and evaporation estimates of each product (Fig. 4.16). For instance, the TerraClimate, with a coarser spatial resolution, compared to finer spatial resolution products MOD16 and SSEBop, showed similar bias estimates. The MOD16 had a higher spatial resolution than the SSEBop, but underestimated more. The FLEX-Topo had a coarser spatial resolution than the MOD16 and the SSEBop but exhibited higher estimates in the dormant phenophases (July-September) (Figs. 4.10 and 4.11). The lack of a clear significant relationship, between spatial resolution and actual evaporation estimates (Fig. 4.16) may imply that, other factors such as the heterogeneity in the land cover (i.e., miombo woodland, mopane woodland, cropland, settlements etc), differences in model structure, processes and model inputs (as highlighted in Zimba *et al.* (2022 under review)) may be the largest contributing factors of the observed differences in the actual evaporation estimates at basin scale.

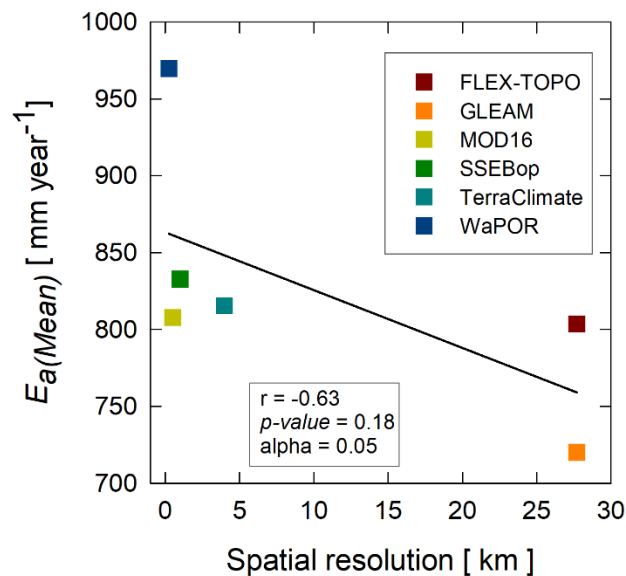


Figure 4.16: Basin scale correlation of actual evaporation estimates with spatial resolution of satellite-based evaporation estimates.

However, unlike the observations for the wet miombo woodland by Zimba *et al.* (2022 under review) the underestimation of actual evaporation at basin scale by satellite-based evaporation estimates cannot be entirely attributed to the difficulty of estimating evaporation of the miombo woodland. The evaporation of other vegetation types, i.e., mopane woodland, that are also found in the Luangwa Basin have not been investigated. What the basin scale water balance-based comparison suggests is that the satellite-based evaporation estimates underestimate actual evaporation even in other non-miombo woodland landscapes. However, this suggestion needs to be investigated because it's possible the satellite-based evaporations would behave differently in each landscape or land surface such as grassland, shrubland, wetland. Therefore, the extent to which each land surface i.e., miombo and mopane woodlands, contribute to the actual evaporation of the Luangwa Basin need to be investigated. For a more comprehensive understanding of the evaporation of the miombo there is need for the assessment of the phenology of each vegetation type and the accompanying potential influence on the evaporation dynamics of the Luangwa Basin.

Nevertheless, the results of this study agreed with Weerasinghe *et al.* (2020) who showed that most satellite-based evaporation estimates generally underestimated evaporation across African basins though SSEBop and WaPOR showed mixed behaviour of both underestimating and overestimating. In this study, in comparison to other satellite-based evaporation estimates, the SSEBop and WaPOR appeared to have lower underestimations. The lower underestimation by SSEBop and the WaPOR agreed with the point scale field observations for the wet miombo woodland (Zimba *et al.*, 2022 under review) and suggests the two estimates could be close to field actual evaporation of the Luangwa Basin.

4.4 Conclusions and recommendations

The study sought to find out the extent to which satellite-based evaporation estimates were similar to each other across the different phenophases of the miombo woodland. The study also sought to establish the potential underlying factor(s) for the discrepancies. Furthermore, the study compared the satellite-based actual evaporation estimates to the annual general water balance-based actual evaporation estimates at basin scale. This helped to establish whether the heterogeneity in the landscape at the Luangwa Basin scale would give a different result to that observed at point scale in the wet miombo woodland. The following were the conclusions:

- (i) Satellite-based evaporation estimates appeared to have difficulty estimating evaporation in the dormant and green-up phenophases. This was evidenced by the large differences (i.e., coefficients of variations) in satellite-based evaporation estimates observed during these phenophases. The limited understanding and lack of representation in models of the typical traits of the phenology of the miombo woodland and its interaction with climate variables, including the access to deep soil moisture stocks (and possibly to ground water), is what could have contributed to the poor correlation among satellite-based evaporation estimates.
- (ii) The canopy cover of the wet miombo woodland in the dry season remained relatively high, green and healthy ($LAI \approx 0.6$; $NDVI \approx 0.5$) with capacity for continued transpiration. This may have been aided by the species dependent variations in time for the leaf fall and leaf flush activities, and the physiologically adapted characteristics of the miombo woodland species such as access to deep soil

moisture and vegetation water storage. Therefore, satellite-based evaporation estimates that are better equipped to account for the physiological attributes of the wet miombo woodland and the interactions with climate variables during the dormant and green-up phenophases are likely to provide more accurate actual evaporation estimates.

- (iii) Satellite-based evaporation estimates appear to have similar (i.e., low coefficients of variation in estimates) trend and magnitude during the maturity, peak, senescence and green-down phenophases in the rainy season and at the end of the rainy season. This may suggest that it is easier to assess satellite-based evaporation of the miombo woodland during phenophases with high canopy cover/canopy closure, available energy and soil moisture. However, during these phenophases the total LAI and NDVI cannot entirely be attributed to the miombo woodland plants as the grass component is high.
- (iv) All satellite-based evaporation estimates appeared to underestimate actual evaporation at basin scale. Although this result appeared to agree with the point-based field observations in a wet miombo woodland the underestimation cannot be entirely be attributed to the challenges of estimating actual evaporation in the miombo woodland because the basin is composed of several other landscapes such as the mopane woodland and grasslands. To understand the extent to which each landscape contributes to the actual evaporation of the basin there is need for landscape dependent evaporation in the basin like what was conducted for the wet miombo woodland. Landscape dependent evaporation assessment can facilitate improved accuracy in satellite-based evaporation estimates.
- (v) At basin scale, the spatial resolution of satellite-based evaporation estimates appeared to be statistically insignificant in estimating the actual evaporation. With an exception of the WaPOR, which had the finest spatial resolution, the FLEX-Topo, MOD16, SSEBop and TerraClimate estimates had relatively similar magnitude of estimates despite having varying spatial resolutions. For example, in the senescence/green-down and dormant phenophases, FLEX-Topo, a product with a coarser resolution showed higher estimates of evaporation compared to products with relatively finer resolutions like MOD16, SSEBop and TerraClimate. Additionally, the SSEBop, with a coarser resolution, relative to MOD16, showed lower underestimation. These observations suggested that, among other factors, the heterogeneity in the land surface, model structure, processes and inputs may influence more the satellite-based evaporation estimates of the miombo woodland.
- (vi) Overall, significant differences in satellite-based evaporation estimates of the miombo woodland appeared to be phenophase dependent. This suggests that phenology of the miombo woodland may have influence on the satellite-based evaporation estimates. Therefore, understanding the phenology of the miombo woodland and its interaction with soil moisture and climate variables, and accounting for these in the model structure, processes and inputs, might improve satellite-based evaporation estimates for this complex ecosystem.

- (vii) Consequently, field observations of evaporation across the different phenophases of the miombo woodland are needed in order to establish the correct characteristics of the actual evaporation. This information can be used to help improve satellite-based evaporation assessments in the Luangwa Basin and the miombo region as whole.

Chapter 5

Synthesis



Photograph showing the roots of miombo woodland species beyond 2.5 m at the Mpika site, Zambia
Image: Henry zimba

This chapter is based on:

- Zimba, H., Coenders-Gerrits, M., Banda, K., Hulsman, P., van de Giesen, N., Nyambe, I., and Savenije, H. H. G., 2023. On the importance of phenology in the evaporative process of the miombo woodland: Could it be why satellite-based evaporation estimates differ? *Hydrol. Earth Syst. Sci. Discuss.* [preprint], <https://doi.org/10.5194/hess-2023-39>, in review.
- Zimba, H. M., Coenders-gerrits, M. A. J., Banda, K. E., Schilperoort, B., Nyambe, I., van de Giesen, N., & Savenije, H. H. G., 2022. Measuring evaporation across canopy phenophases of a natural forest : Miombo forest , Southern Africa. *Hydrol. Earth Syst. Sci. Discuss.*, October, 1–23. doi: <https://doi.org/10.5194/hess-2022-303>, in review.
- Zimba, H., Coenders-Gerrits, M., Kawawa, B., Savenije, H., Nyambe, I., & Winsemius, H., 2020. Variations in canopy cover and its relationship with canopy water and temperature in the miombo woodland based on satellite data. *Hydrology*, 7(3). doi: 10.3390/hydrology7030058

Chapter 5

“Storms make trees take deeper roots”

(Dolly Parton)

5.1 Introduction

This study used both field observations and satellite products. The focus of the study was on understanding the evaporation dynamics in relation to the phenology of the miombo woodland. The phenology was understood mainly using satellite-based data complimented with information from literature in public domain (i.e., Chidumayo, 2001; Frost, 1996; Fuller, 1999) and the photographs taken using a cameral installed on the flux observation tower. In the absence of field measurements of woodland canopy leaf area index, woodland canopy temperature and woodland canopy vegetation water content, the use of satellite data proxies was performed with assumptions. The assumptions are here highlighted in order to contextualise the findings and the accompanying implications of the study. Thereafter, the evaporation trend and quantities at both point and basin scale as they relate to the phenology are discussed.

5.2 Limitations of using satellite products for phenology analysis

The first limitation is with the assumption that the total LAI, NDII, NDVI and LST were entirely attributed to miombo woodland canopy. This assumption was made because the study on canopy phenology focused on a wet miombo woodland, known to have canopy closure of up to 70 percent at any period of year. However, miombo woodland is characterised by understory and field layer vegetation such as emerging miombo species, shrubs and grass. Grass and shallow rooting shrubs normally dry out during the dry season proper (May – October), though in some places the grass shots in August/September (or earlier) after the wild fires that normally occur during this period (Chidumayo, 2001; Fuller, 1999). Furthermore, leaf fall, in the dry season, entails the woodland floor is covered by dry leaves as well as bare soil. In such circumstances the satellite-based total LAI, NDII, NDVI and LST includes that for the above-described understory and grass components. In this study the understory and grass components were assumed insignificant in the dry season. This is because, the observations on canopy phenology were based on plots sampled from a wild life conservancy area with minimal and controlled anthropogenic activities including bush fires. Furthermore, the plateau miombo is less seasonal (Fuller, 1999) with species found at the study site mainly broadleaved with minimal seasonal variations in canopy closure (Fuller, 1999).

The constraint of cloud cover, especially in the rainy season, has been highlighted in chapter 2 of this thesis. Other than limiting the number of days with clear sky, use of satellite products with quality pass of below 100 percent, but above 80 percent, entails introduction of some degree of error in the estimates of the satellite proxies. No field measurements of the LAI, NDVI, vegetation water content or canopy temperature were conducted. Therefore, the degree to which these satellite products agree with field conditions of the miombo woodland is unknown. However, information from literature (i.e., Vinya *et al.*, 2018; Chidumayo, 2001; Fuller, 1999, Frost, 1996) on the miombo phenology, coupled with the cameral images taken at the miombo woodland at Mpika site appeared to agree with trends in satellite products, LAI and NDVI.

5.3 Relationship of the LAI and NDVI with the LST and NDII

The canopy cover is proxied by both the LAI and the NDVI. The canopy temperature and canopy vegetation water content relationship with changes in canopy cover proxied by LAI appeared to be non-linear across all phenophases. This speaks to the observation that the wet miombo woodland shows little variation in canopy cover across phenophases including in the dry

season (Fuller, 1999; Frost, 1996). At woodland stand level this result showed that there are no significant changes in the woodland total LAI (i.e., woodland canopy cover) to warrant establishment of a clear linear relationship. Furthermore, this result speaks to the heterogeneity nature of the miombo woodland species pointed out by Chidumayo (2001). However, at individual miombo woodland tree species level, the result might be different as the leaf fall at this level is significant with the entire individual canopy being leafless (i.e., Fig. 4.9; Fuller, 1999) at some point. Therefore, at wet miombo woodland stand level it appeared changes in canopy vegetation water content and canopy temperature does not result in significant changes in the woodland canopy cover as proxied by the LAI. The dry season woodland canopy NDVI values were indicative of a continuously photosynthetically active woodland. The heterogeneity in the species composition at woodland level implies that the leaf fall and leaf colour transitions at individual plant species level do not occur at the same. Therefore, the woodland canopy at any given point during the dry season is a combination of different individual plant species phenology which ensures up to about 70 percent canopy closure (Fuller, 1999). Fuller (1999) observed that herbaceous and woody (i.e., miombo woodland species) vegetation phenology was largely in phase within plots but varied across plots. Fuller (1999) suggested that the variations could be as a result of resources available at individual sites in a given landscape.

However, when the NDVI was used as proxy for woodland canopy cover, distinct linear relationships were observed between woodland canopy cover and the canopy vegetation water content and canopy temperature. This is because, unlike the LAI that helps to understand the area facet of the canopy, the changes in the NDVI also helps to observe the changes in chlorophyll i.e., leaf/canopy greenness over time. What was observed is that, with an exception of the green-up and maturity phenophases during the rainy season, canopy temperature showed significant distinct linear relationships with the NDVI during the senescence and dormant phenophases. This means that during periods of abundant water and high leaf/canopy chlorophyll content, symbolic of increased metabolism in plants, the woodland stand canopy cover - temperature relationship is non-linear. Again, this observation at woodland stand level may be different from the relationships at individual plant species canopy/leaf level. On the other hand, the canopy vegetation water content showed significant strong linear relationships with woodland canopy cover across phenophases. Water is utilised in the photosynthetic process. Thus, this was seen in the positive linear relationship between the NDII and the NDVI across phenophases.

Overall, the canopy phenology of the miombo woodland in terms of leaf fall, leaf flush and photosynthetic activity during the dry season showed strong correlation with changes in water and temperature. This affirms the strong correlation that exists between water availability and temperature with plant phenology (Pereira *et al.*, 2022; Niu *et al.*, 2013; Cleland *et al.*, 2007).

5.4 The miombo woodland canopy phenology, energy partitioning and the observed evaporation trend

This study is about understanding the evaporation dynamics in the miombo woodland with respect to adapted phenological and physiological characteristics. Central to this understanding is the characterisation of the phenology and evaporation in relation to climate variables that are known to influence both phenological and evaporative processes. Plant phenology influences plant-energy interaction and facilitates access to both vegetative and root zone moisture storage (Vinay *et al.*, 2018; Nord *et al.*, 2009) that, coupled with various species dependent physiological processes (i.e., Lu *et al.*, 2006), determines the evaporation dynamics of a woodland (Snyder *et al.*, 2013). In this study it appears that understanding the phenophase based plant-water and plant-

energy interaction is crucial to ascertaining the appropriate trend and magnitude of evaporation in the miombo woodland.

In Chapter 3 it was observed that miombo woodland plants phenology-energy interaction and phenology-water interaction influence evaporation trend. The woodland canopy cover interactions with canopy vegetation water content and woodland canopy temperature observed in Chapter 2 helps to understand the behaviour of evaporation in Chapter 3. It appeared that there is an interchange in the dominant determinant of evaporation for the rainy and dry season phenophases. During the green-down and dormant phenophases in the dry season the woodland canopy cover (i.e., proxied by the LAI and NDVI) and the vegetation water content (i.e., proxied by the NDII) are relatively high but in a downward trajectory reaching lowest values in August-September. The LAI and NDVI values for the green-down phenophase were indicative of availability of green and health woodland canopy. The NDII values for the green-down phenophase were indicative of availability of sufficient woodland canopy vegetation water content and root zone storage. Actual evaporation is a representation of simultaneous occurrence of energy and water (Stephenson, 1990). In the green-down phenophase the net radiation was high in May but lowest in June. Actual evaporation, as determined using the DTS approach, was in the downward trajectory only during the lowest energy green-down phenophase (May-June) with lowest values of actual evaporation observed in the month of June which had the lowest available energy. The month of May, with relatively higher solar radiation than June, had relatively higher evaporation. There was enough green and healthy woodland canopy (i.e., as proxied by the LAI and NDVI values) that was able to intercept more radiation for evaporation (Figs. 3.9 and 4.5). There was also relatively higher soil moisture and vegetative water content but the available energy was lowest. Therefore, during green-down phenophase the available energy and not water availability appeared to be the dominant limiting factor of evaporation. This is further augmented by the energy partitioning during the green-down phenophase that showed a larger portion of the available energy being partitioned as sensible heat (H) (Figs. 3.6 and 3.7). Additionally, relatively low wind speeds (Fig. 3.7) during the green-down phenophase influences evaporation.

Canopy leaf fall, leaf flush and the accompanying leaf colour transitions, occurred largely in the dormant phenophase. This was exhibited through continued decline in the LAI and NDVI values reaching lowest values in August for the LAI and September for the NDVI. The NDII also showed a declining trajectory with lowest values observed in September. On the contrary woodland canopy temperature and available energy (i.e., LST and net radiation) and the observed actual evaporation were on an increasing trajectory throughout the phenophase. The observed actual evaporation in July, at the commencement of the dormant phenophase, was higher than that of June in the green down-phenophase with relatively higher woodland canopy cover and vegetation water content. Actual evaporation took on a rising trajectory despite the dormant phenophase being the driest part of the year. During this period, it appeared the reduction in the available evaporative surface, i.e., through leaf fall and leaf colour change, and the resulting overall reduction in canopy vegetative water storage are the main limiting factors of evaporation. The observations that some miombo woodland species have extensive lateral and deep rooting system capable of accessing ground water resources during the dry season entails that it is mainly the changes in the canopy cover, due to the leaf fall, leaf flush and leaf colour transitions coupled with the plant physiological interaction with driving factors such as radiation and wind speed, that influenced the evaporation process during the dormant phenophase. This could explain why the actual evaporation kept rising as the canopy cover increased through leaf flush even without the rains or horizontal/vertical changes in root zone storage. This observation could go towards

validating the miombo species at the study site having access to both vegetative storage and ground water resources in the dry season, especially that the site is in the high rainfall wet miombo woodland region, with accompanying seasonal wetlands within the fetch of the flux observation tower. Increasing canopy cover of new leaves implies increasing canopy interception of radiation which, with access to both vegetative and ground water storage, could result in increased actual evaporation. Canopy biomass formation i.e., leaf flush/leaf growth which occur in the dry season requires water, which in the dry season can only come from vegetative storage and root zone/ground water storage.

5.5 On the comparison of satellite-based evaporation estimates in the miombo woodland

This study endeavoured to compare performance of some commonly used satellite-based evaporation estimates in a largely miombo woodland covered river basin the Luangwa. Firstly, the satellite-based estimates were compared to each other. This comparison was meant to observe the similarity in trend and magnitude of satellite-based evaporation estimates. Secondly, the satellite-based evaporation estimates were compared to the water balance-based evaporation estimates at basin scale. The comparison of satellite-based evaporation estimates to the water balance-evaporation was meant to verify if the underestimation of actual evaporation by satellite-based evaporation estimates, observed at point scale, also occurred at basin scale in a heterogenous landscape. Chapter 4 shows the results of the comparison.

Results of this study showed that major differences in satellite-based evaporation estimates were in the dormant and green-up phenophases in the dry season and early rainy season. The main evaporative processes of the miombo woodland during these two phenophases are: transpiration in the dormant and early green-up phenophases, transpiration and rainfall interception (i.e., canopy interception) in the late green-up phenophase as the rains commence. The key determinants of transpiration in the dry season are the rooting depth of plants, moisture storage in the root zone, ground water storage (including depth of ground water table) and a photosynthetically active canopy. Optimizing rooting depth than the use of the standard one metre has been shown to increase transpiration in landscapes with a dry season (Kleidon and Heimann, 1998). Modifying rooting depth can improve energy flux simulations at both field scale and regional scale (Liu *et al.*, 2020). Rooting depth has been shown to be sensitivity to local soil water profiles determined by precipitation infiltration depth and ground water table depth from below (Fan *et al.*, 2017). Soil moisture in the miombo woodland increases with depth (i.e., Chidumayo, 2001). As earlier discussed, some miombo woodland species are deep rooting, beyond 5 metres. Therefore, one of the potential causes of the observed differences in satellite-based evaporation estimates could be the rooting depth.

Additionally, direct integration of soil moisture rather than the use of proxies has been shown to improve the accuracy of actual evaporation estimates (Brust *et al.*, 2021; Novick *et al.*, 2016). Some of the satellite-based evaporation estimates used in this study such as MOD16 and SSEBop use proxies for soil moisture. The challenge with the use of the proxies, i.e., NDVI, for soil moisture, for instance in surface energy balance models, is that these are unable to fully account for changes in other factors that may influence sensible heat fluxes (Gokmen *et al.*, 2012). The miombo woodland is located in a high available energy landscape. Woodlands, with the

associated phenology, influence energy partitioning (i.e., Yuan *et al.*, 2021; McGloin *et al.*, 2019; Grandgirard *et al.*, 2002). Therefore, correct partitioning of miombo woodland available energy into, for instance, sensible and latent heat fluxes may be a key to improving accuracy of satellite-based evaporation estimates, especially in the phenophases in the dry season. In a woodland that has a varied canopy closure of up to 70 percent at any given time of the year, coupled with the root zone storage that does not show significant changes in the dry season, energy partitioning into sensible and latent heat fluxes appears to be a key factor in appropriate actual evaporation assessment. Integration of energy partitioning may partly explain the trend of WaPOR which appeared to agree with the point-based field observation of actual evaporation of the wet miombo woodland.

Furthermore, the use of the relative humidity and vapour pressure difference as proxies for soil moisture in MOD16 may be a source of uncertainty in estimating transpiration (Novick *et al.*, 2016). However, direct integration of soil moisture into the MOD16 algorithm appeared to improve the accuracy of actual evaporation estimates (Brust *et al.*, 2021). Consequently, to improve on the accuracy of estimation of water and energy fluxes in regions with recurrent plant water stress, i.e., miombo woodland, Gokmen *et al.* (2012) suggested that the soil moisture be integrated in the surface energy balance models.

The quality of land cover products or their proxies used for satellite-based evaporation estimates may explain the observed differences in the spatial-temporal distribution of satellite-based evaporation across different phenophases. This is because use of land cover products with low woodland classification accuracy in satellite data-based evaporation modelling may result in significant errors. These errors could arise due to incorrect parameterisation of land cover dependent attributes such as stomata conductance thresholds. Therefore, the robustness of different land cover products in evaporation modelling, especially for the miombo region should be explored.

This study showed that there is strong correlation between the spatial resolution and the magnitude of satellite-based evaporation estimates. Therefore, a spatial scale that is capable of taking into account heterogeneity in landscape is likely to improve actual evaporation estimates of the miombo woodland. Fine spatial resolution allows for isolation and capture of actual evaporation of specific land surfaces with minimal overlaps. For instance, WaPOR has a continent spatial coverage and spatial resolutions of 100m and 250m. These attributes contributed to the WaPOR accounting for heterogeneity in the landscape and could be the reason for the lower underestimation of actual evaporation.

5.6 Opportunities and challenges with using the DTS approach in an African landscape

While the use of the BR-DTS approach provides numerous opportunities for deepened understanding of the energy fluxes in the African woodland ecosystems, it comes with its own challenges. The BR-DTS approach requires uninterrupted power and water supply. This is a challenge in most African environments, with one of the solutions requiring additional power supply setup such as solar power. The additional cost implications, that is besides the cost of the DTS equipment, are significant depending on the location of the land surface to be assessed.

The difficulty in attaining the wet bulb temperature due to high temperatures, especially in the dry season, is likely to result in errors and underestimation of the Bowen ratio. Underestimating

the Bowen ratio would result in errors in the partitioning of the available energy and the actual evaporation. Adding screen shields, as a solution to overcoming high temperatures, comes with its own shortcomings that could result in additional errors. However, insulating the water tank(s) for water supply to the wet cable could limit the impact of the high temperatures.

Chapter 6

Conclusions and recommendations



Photograph showing the roots of a Miombo species beyond 2.5 m at the Mpika study site, Zambia.
Image: Henry Zimba

This chapter is based on:

- Zimba, H., Coenders-Gerrits, M., Banda, K., Hulsman, P., van de Giesen, N., Nyambe, I., and Savenije, H. H. G., 2023. On the importance of phenology in the evaporative process of the miombo woodland: Could it be why satellite-based evaporation estimates differ? *Hydrol. Earth Syst. Sci. Discuss.* [preprint], <https://doi.org/10.5194/hess-2023-39>, in review.
- Zimba, H. M., Coenders-gerrits, M. A. J., Banda, K. E., Schilperoort, B., Nyambe, I., van de Giesen, N., & Savenije, H. H. G., 2022. Measuring evaporation across canopy phenophases of a natural forest : Miombo forest , Southern Africa. *Hydrol. Earth Syst. Sci. Discuss.*, October, 1–23. doi: <https://doi.org/10.5194/hess-2022-303>, in review.
- Zimba, H., Coenders-Gerrits, M., Kawawa, B., Savenije, H., Nyambe, I., & Winsemius, H., 2020. Variations in canopy cover and its relationship with canopy water and temperature in the miombo woodland based on satellite data. *Hydrology*, 7(3). doi: 10.3390/hydrology7030058

Chapter 6

“In a forest of a hundred thousand trees, no two leaves are alike. And no two journeys along the same path are alike”

(Paulo Coelho)

6.1. Introduction

The preceding chapters have given account of the various aspects of the plant-water interaction and evaporation dynamics of the miombo woodland. The goal of this study was to understand evaporation dynamics across the different phenophases of the miombo woodland, and to observe if satellite-based evaporation estimates are correct. This chapter gives the main conclusions and the outlook for assessments of the evaporation of the miombo woodland.

6.2 Canopy cover relationship with the vegetation water content and temperature

Woodland stand canopy cover relationships with vegetation water content and temperature are season and phenophase dependent. For observing the relationship between the woodland canopy phenology and climate variables the use of the NDVI, as a proxy, appears to show a clearer relationship than when the LAI is used. The lack of a clear linear relationship between the vegetation water content (proxied by the NDII), the woodland canopy temperature (proxied by the LST) and the woodland canopy cover when proxied by the LAI consolidates the observation that across seasons there is little variation in the woodland canopy closure of the wet miombo woodland. The water availability, proxied by the NDII as vegetation water content, appears to be a more significant influencing factor of the variations in the values of the NDVI, proxy for canopy cover, of the miombo woodland than the woodland canopy temperature (proxied by LST). This is because across climatic seasons and canopy phenophases the vegetation water content (proxied by the NDII), as a single variable or in combination with temperature, accounts for more variations in the values of the NDVI (proxy for canopy cover) of the miombo woodland than the woodland canopy temperature (proxied by the LST).

6.3 Phenophase-based evaporation of the miombo woodland

6.3.1 Observed evaporation dynamics of the miombo woodland

In chapter 3 the Bowen ratio is first estimated at hourly interval using the DTS approach. Using the energy balance equation, the Bowen ratio is used to partition available energy ($R_N - G_o$) into H and LE . Furthermore, actual evaporation is estimated at hourly interval and then summed up into daily and dekadal values. Four satellite-based evaporation estimates are then compared to the observed actual evaporation. The potential contributing factors to the observed trend and magnitude of satellite-based evaporation estimates in relation to field observations are then discussed. The following conclusions are made:

Across phenophases, the wet miombo woodland, represented by the study site at Mpika, experiences alternating energy partitioning. This interchange occurs around 06:07 AM and 17:18 PM. This means that during day time the available energy is largely partitioned as LE while at night it is partitioned as H . This agrees with the observed energy partitioning trend in other miombo woodland like warm ecosystems and climates. In low energy phenophases like the green-down (May-June) available energy is mainly partitioned as H while in high energy (i.e., high net radiation) phenophases like the dormant and green-up, available energy is largely partitioned as LE . In low energy phenophases, i.e., green down in the cool-dry season, with relatively higher woodland canopy cover/closure (i.e., NDVI, LAI) and high vegetation water content (i.e., NDII), it appears that daily actual evaporation is more constrained by available energy than water availability. During the dormant and early green-up phenophases, it appears that access to moisture

in deeper soils and potential access to ground water, make the canopy cover (evaporative surface) of the miombo woodland a key driver of the evaporation flux. This is because actual evaporation during the dormant phenophase is likely limited by the species dependent phenological changes such as leaf fall and leaf flush as well as the leaf colour changes. The species dependent leaf fall, and leaf colour changes reduces the available evaporative surface which increases as more miombo woodland plants flush and green up. These changes in the canopy display occur as the available energy for evaporation continue to increase.

There is need for a similar study such as the one in Chapter 3 to be conducted in the dry miombo woodland and to compare the results. It would be interesting to investigate the magnitude of the transpiration of the dry miombo woodland and wet miombo woodland in the dry season with changes in soil moisture at different depths and the variations in canopy cover (leaf fall, leaf flush and leaf colour change).

6.4 Why do satellite-based estimates behave the way they do?

6.4.1 Direct integration of soil moisture and optimisation of the rooting depth may improve satellite-based evaporation estimates

The phenophase-based comparison of satellite-based evaporation estimates at pixel scale in dry miombo woodland and wet miombo woodland and at Luangwa Basin miombo woodland scale showed similar results. In all three scenarios substantially high coefficients of variation in actual evaporation estimates among satellite-based evaporation estimates were observed in the water limited, high temperature and low woodland canopy cover conditions in the dormant phenophase. Coefficients of variation in actual evaporation estimates were also substantially high in the green-up phenophase at the boundary between the dry season and the rainy season. The lowest coefficients of variation in actual evaporation estimates were observed in water abundant, high temperature, high leaf chlorophyll content and high woodland canopy cover during the maturity/peak phenophase. The high coefficients of variation in actual evaporation estimates, among satellite-based evaporation estimates, in the dormant and green-up phenophases, points to the challenge of estimating the actual evaporation of the miombo woodland in the dry season and early rainy season. The same scenario emerged as was observed at point scale, with reference to field observations, in which satellite-based evaporation estimates which directly integrate soil moisture in their algorithm appeared to have higher estimates of actual evaporation in the dormant phenophase in the dry season. For instance, the FLEX-Topo and WaPOR integrate soil moisture in their algorithms. Compared to each other the FLEX-Topo and WaPOR appeared to have no statistically significant ($p\text{-value} > 0.5$) differences in their trends and mean estimates of actual evaporation in the dormant phenophase in the dry season. Compared to the FLEX-Topo and WaPOR the other four satellite-based evaporation estimates, GLEAM, MOD16, SSEBop and TerraClimate showed statistically significant ($p\text{-value} < 0.05$) differences in the trend and mean estimates of actual evaporation in the dormant phenophase in the dry season. Considering the highlighted canopy phenology and the associated physiological adaptation of the miombo woodland plants in the dry season the direct integration of the soil moisture in the algorithms and optimising the rooting depth is likely to improve the accuracy of the satellite-based evaporation estimates.

6.4.2 Rainfall interception likely a major component during the rainy season

Rainfall interception of the miombo woodland is likely to be a cause for the differences in satellite-based evaporation estimates in the phenophases in the rainy season. For instance wet miombo woodland intercepts between 17-20 percent of rainfall annually. The values for the rainfall interception for the dry miombo woodland are unknown. Among many factors, differences in the algorithms and inputs for rainfall interception estimation are likely to be a source of the differences in satellite-based evaporation estimates in the rainy season. For instance, in the maturity/peak during the mid-rainy season, compared to the other five satellite-based evaporation estimates, the MOD16 appeared to have significantly ($p\text{-value} < 0.05$) higher estimates of actual evaporation. The rainfall interception module of MOD16 is different from that of FLEX-Topo, GLEAM and WaPOR. It is possible that the rainfall interception module of MOD16 is more responsive to the miombo woodland phenology than the other modules. It is also possible that the rainfall interception module of MOD16 is inaccurate. Therefore, there is need for field observations of rainfall interception of the miombo woodland and to compare these to satellite-based estimates.

6.4.3 Satellite-based evaporation estimates likely underestimates evaporation in other landscapes of the Luangwa Basin

Compared to the general annual water balance-based actual evaporation all six satellite-based evaporation estimates underestimated actual evaporation of the Luangwa Basin. The implication of this observation is that satellite-based evaporation estimates likely underestimate actual evaporation even in non-miombo woodland landscapes such as the mopane woodland that are also part of the larger Luangwa Basin vegetation landscape. However, for a comprehensive overview, there is need for land-cover type based assessments of actual evaporation in the Luangwa Basin.

6.4.4 The spatial resolution of the satellite-based evaporation estimates may not be a key factor for estimating evaporation of the miombo woodland and the other landscapes of the Luangwa Basin

At both point and basin scale-based assessments, there was a negative linear relationship between the spatial resolution of satellite-based evaporation estimates and the estimated actual evaporation. Satellite-based evaporation estimates with fine spatial resolutions showed lower underestimates compared to those with coarser resolutions. The implication is that the finer the spatial resolution the lower the underestimation. However, at both assessment scales (pixel and basin), the linear relationships between the spatial resolutions and the evaporation estimates were statistically insignificant (i.e., $p\text{-value} > 0.05$). The reason for this outcome is exhibited in that some satellite-based evaporation estimates with relatively coarser spatial resolutions, i.e., SSEBop at both point and basin scale and TerraClimate at basin scale, underestimated less compared to MOD16 which had a finer spatial resolution. Furthermore, at basin scale a coarser resolution estimate FLEX-Topo and WaPOR with a finer resolution showed similar magnitude of actual evaporation in the dormant phenophase in the dry season. The implication of this observation is that other factors (i.e., heterogeneity in the landscape, model structure, processes and inputs) influence more the estimated actual evaporation rather than the spatial resolutions of the satellite-based evaporation estimates. Consequently, it appears that satellite-based estimates at finer spatial resolution with the structure, processes and inputs that couple canopy transpiration with the root zone storage, taking into account the vertical upward (beyond 2.5 m) and horizontal moisture flux

as well as the canopy phenological changes, are likely to provide actual evaporation estimates that reflect actual conditions of the miombo woodland. This is demonstrated by the WaPOR estimates which appears to include these aspects in simulating actual evaporation.

6.4.5 The need for land cover-based assessment of actual evaporation for the Luangwa Basin

The field-based actual evaporation assessment was conducted in the wet miombo woodland. It is possible that the phenological response to changes in hydrological and climate regimes in the drier miombo woodland are different from the observations at the Mpika site. Therefore, there is need for similar observations to be performed in the drier miombo woodland and to compare the results. However, this thesis has demonstrated the importance of understanding and incorporating the canopy phenology and dry season physiological adaptation (i.e., deep rooting) of the miombo woodland in modelling actual evaporation. Additionally, for basins with heterogeneous woodland types like the Luangwa, it is important to conduct actual evaporation assessments in the different vegetation types. This is likely to give a more representative understanding of basin scale evaporation dynamics. However, this study has provided a foundation on which other studies can build towards a more comprehensive understanding of the actual evaporation dynamics in this unique ecosystem.

6.5 Outlook

From the available literature in the public domain, this study appears to be the first attempt at providing independent field data-based energy partitioning and actual evaporation estimates across different canopy cover phenophases of the miombo woodland. Therefore, this study provides a basis on which other studies on actual evaporation in the miombo woodland can build. The miombo woodland is a diverse and vast ecosystem with many strata, that require several field investigations in order to establish a clearer picture of the actual evaporation dynamics. One study, in one location in a vast ecosystem like the miombo, cannot be used as representative of all actual evaporation trends. This is because the phenological response to climate variables could be different across the different strata of the miombo woodland.

In this vein, application of the BR-DTS approach to investigate actual evaporation in the miombo woodland provides many opportunities as well as challenges. The BR-DTS approach currently provides an expanded avenue for understanding woodland energy partitioning in a more detailed manner than any other approach. Applying this technology would make available information that is key for climate and hydrological modelling in a region that has an urgent need for adaptation to climate change, and requires information for management of scarce water resources. The continued application of the BR-DTS approach in African ecosystems entails opportunity to find solutions to the challenges encountered and therefore, providing avenue for continued improvement in the application of the DTS technology in African conditions.

It appears direct integration of soil moisture in algorithms and optimisation of the rooting depth would improve the accuracy of estimates of transpiration of the miombo woodland. It would be interesting to observe how after taking into account these two aspects the satellite-based estimates compare to field observations.

References

- Abatzoglou, J. T., Dobrowski, S. Z., Parks, S. A., & Hegewisch, K. C., 2018. TerraClimate, a high-resolution global dataset of monthly climate and climatic water balance from 1958-2015. *Scientific Data*, 5, 1–12. doi:10.1038/sdata.2017.191
- Abrams, M., & Crippen, R., 2019. ASTER Global DEM (Digital Elevation Mode) - Quick Guide for V3. *California Institute of Technology*, 3(July), 10.
- Allen, R. G., Tasumi, M., Morse, A., Trezza, R., Wright, J. L., Bastiaanssen, W., Kramber, W., Lorite, I., & Robison, C. W., 2007. Satellite-Based Energy Balance for Mapping Evapotranspiration with Internalized Calibration (METRIC)—Applications. *Journal of Irrigation and Drainage Engineering*, 133(4), 395–406. doi: 10.1061/(asce)0733-9437(2007)133:4(395)
- Allen, R. G., L. S. Pereira, D. Raes, and M. Smith., 1998. “FAO Irrigation and Drainage Paper No. 56 - Crop Evapotranspiration,” no. 56.1998.
- Alexandre, J., 1977. Le bilan de l’eau dans le miombo (forêt claire tropicale). *Bulletin de la Société Géographie du Liège* 13, 107-126.
- Agrawal, A., Perrin, N., Norton, A., Mearns, R., Duarte, M., Gambarelli, G., Mcsweeney, C., Siegel, P., Ribot, J., Adger, N., Carey, E., Kornak, R., Labonne, J., Miller, D., & Ahmad, N., 2008. *The Role of Local Institutions in Adaptation to Climate Change 1. Executive summary the role of local governance and institutions in livelihoods adaptation to climate change.* 734–764.
- Anderson, M. C., Norman, J. M., Diak, G. R., Kustas, W. P., & Mecikalski, J. R., 1997. A two-source time-integrated model for estimating surface fluxes using thermal infrared remote sensing. *Remote Sensing of Environment*, 60(2), 195–216. doi: 10.1016/S0034-4257(96)00215-5
- Angus, D. E., & Watts, P. J., 1984. Evapotranspiration - How good is the Bowen ratio method? *Agricultural Water Management*, 8(1–3), 133–150. doi: 10.1016/0378-3774(84)90050-7.
- Arsyad, U., & Wahyuni., 2019. The characteristics of infiltration in natural forest in teaching forest of Hasanuddin University University at Maros Regency. *IOP Conference Series: Earth and Environmental Science*, 270(1). doi: 10.1088/1755-1315/270/1/012004.
- Asadullah, Anita, Neil McIntyre, and Max Kigobe., 2008. “Evaluation of Five Satellite Products for Estimation of Rainfall over Uganda.” *Hydrological Sciences Journal* 53 (6): 1137–50. <https://doi.org/10.1623/hysj.53.6.1137>.
- Avdan, U., & Jovanovska, G., 2016. Algorithm for Automated Mapping of Land Surface Temperature Using LANDSAT 8 Satellite Data. *Journal of Sensors*, 2016, 1-8. Retrieved from <http://dx.doi.org/10.1155/2016/1480307>.

- Bastiaanssen, W. G. M., Cheema, M. J. M., Immerzeel, W. W., Miltenburg, I. J., & Pelgrum, H., 2012. Surface energy balance and actual evapotranspiration of the transboundary Indus Basin estimated from satellite measurements and the ETLook model. *Water Resources Research*, 48(11)
- Bastiaanssen W.G.M., M. Meneti, R.A. Feddes, & Holtslag, a a M., 1998. A remote sensing surface energy balance algorithm for land (SEBAL). *J. Hydrol.*, 212–213(January), 198–212.
- Baldocchi, D. D., Xu, L., & Kiang, N., 2004. How plant functional-type, weather, seasonal drought, and soil physical properties alter water and energy fluxes of an oak-grass savanah and annual grassland. *Agricultural and Forest Meteorology*, 123, 13 - 39. doi:10.1016/j.agrformet.2003.11.006
- Barr, A. G., King, K. M., Gillespie, T. J., Den Hartog, G. & Neumann, H. H., 1994. A comparison of bowen ratio and eddy correlation sensible and latent heat flux measurements above deciduous forest. *Boundary-Layer Meteorol.* 71, 21–41.
- Beilfus, R., 2012. *A Risky Climate for Southern African Hydro: Assessing hydrological risks and consequences for the Zambezi River Basin Dams*. International Rivers.
- Blatchford, Megan L., Chris M. Mannaerts, Sammy M. Njuki, Hamideh Nouri, Yijian Zeng, Henk Pelgrum, Steven Wonink, and Poolad Karimi., 2020. “Evaluation of WaPOR V2 Evapotranspiration Products across Africa.” *Hydrological Processes* 34 (15): 3200–3221. <https://doi.org/10.1002/hyp.13791>.
- Botta, A., Viory , N., Ciais, P., Friedlingstein, P., & Monfray, P., 2000. A global prognostic scheme of leaf onset satellite data. *Global change Biology*, 6, 709-725.
- Bonnesoeur, Vivien, Bruno Locatelli, Manuel R. Guariguata, Boris F. Ochoa-Tocachi, Veerle Vanacker, Zhun Mao, Alexia Stokes, and Sarah Lan Mathez-Stiefel., 2019. “Impacts of Forests and Forestation on Hydrological Services in the Andes: A Systematic Review.” *Forest Ecology and Management* 433 (June 2018): 569–84. <https://doi.org/10.1016/j.foreco.2018.11.033>.
- Bowen, I. S., 1926. “The Ratio of Heat Losses by Conduction and by Evaporation from Any Water Surface.” *Physical Review* 27 (6): 779–87. <https://doi.org/10.1103/PhysRev.27.779>.
- Brust, C., Kimball, J. S., Maneta, M. P., Jencso, K., He, M., & Reichle, R. H., 2021. Using SMAP Level-4 soil moisture to constrain MOD16 evapotranspiration over the contiguous USA. *Remote Sensing of Environment*, 255(January), 112277. doi: 10.1016/j.rse.2020.112277, 2021
- Buchhorn, M., Smets, B., Bertels, L., De Roo, B., Lesiv, M., Tsendbazar, N.E., Linlin, L., Tarko, A., 2020. “Copernicus Global Land Service: Land Cover 100m: Version 3 Globe 2015-2019: Product User Manual.” Zenodo, Geneve, Switzerland. <https://doi.org/10.5281/zenodo.3938963>.

- Buttar, Noman Ali, Hu Yongguang, Abdul Shabbir, Imran Ali Lakhari, Ikram Ullah, Asad Ali, Muhammad Aleem, and Muhammad Asim Yasin., 2018. "Estimation of Evapotranspiration Using Bowen Ratio Method." *IFAC-PapersOnLine* 51 (17): 807–10. <https://doi.org/10.1016/j.ifacol.2018.08.096>.
- Cammalleri, C., & Vogt, J., 2005. On the Role of Land Surface Temperature as Proxy of Soil Moisture Status for Drought Monitoring in Europe. *Remote Sensing*, 7, 16849–16864.
- Cano, E., Denux, J.-P., Bisquert, M., Hubert-Moy, L., & Chéret, V., 2017. Improved forest-cover mapping based on MODIS time series and landscape stratification. *International Journal of Remote Sensing*, 38(7), 1865–1888. Retrieved from <https://doi.org/10.1080/01431161.2017.1280635>
- Chidumayo, Emmanuel N., and Davison J. Gumbo., 2010. *The Dry Forests and Woodlands of Africa: Managing for Products and Services. The Dry Forests and Woodlands of Africa: Managing for Products and Services.* <https://doi.org/10.4324/9781849776547>.
- Chidumayo, E. N., & Frost, P., 1996. Population biology of miombo trees. In *The miombo in transition: woodlands and welfare in Africa*, Campbell, B. (ed.). Bogor (Indonesia): CIFOR, ISBN 979-8764-07-2.
- Chidumayo, E. N., 2001. Climate and Phenology of Savanna Vegetation in Southern Africa. *Journal of Vegetation Science*, 12(3), 347. doi: 10.2307/3236848
- Chidumayo, E. N., 1994. Phenology and nutrition of miombo woodland trees in Zambia. *Trees*, 9(2), 67–72. doi: 10.1007/BF00202124
- Chidumayo, E. N., 1987. Species structure in Zambian Miombo woodland. *Journal of Tropical Ecology*(3), 109 - 118.
- Cho, Jaeil, Taikan Oki, Pat J.F. Yeh, Wonsik Kim, Shinjiro Kanae, and Kyoichi Otsuki., 2012. "On the Relationship between the Bowen Ratio and the Near-Surface Air Temperature." *Theoretical and Applied Climatology* 108 (1–2): 135–45. <https://doi.org/10.1007/s00704-011-0520-y>.
- Cho, Jaeil, Taikan Oki, Pat J.F. Yeh, Wonsik Kim, Shinjiro Kanae, and Kyoichi Otsuki., 2012. "On the Relationship between the Bowen Ratio and the Near-Surface Air Temperature." *Theoretical and Applied Climatology* 108 (1–2): 135–45. <https://doi.org/10.1007/s00704-011-0520-y>.
- Cirillo, M., & Poli, A. A., 1993. On the use of the Normalised Mean Square Error in evaluating dispersion model performance. *Atmospheric environment*, 12A(15), 2427 - 2434.
- Cleland, E. E., Chuine, I., Menzel, A., Mooney, H. A., & Schwartz, M. D., 2007. Shifting plant phenology in response to global change. *Trends in Ecology and Evolution*, 22(7), 357–365. doi: 10.1016/j.tree.2007.04.003

- Cleland, Elsa E., Isabelle Chuine, Annette Menzel, Harold A. Mooney, and Mark D. Schwartz., 2007. "Shifting Plant Phenology in Response to Global Change." *Trends in Ecology and Evolution* 22 (7): 357–65. <https://doi.org/10.1016/j.tree.2007.04.003>.
- Cleland, Elsa E., Isabelle Chuine, Annette Menzel, Harold A. Mooney, and Mark D. Schwartz., 2007. "Shifting Plant Phenology in Response to Global Change." *Trends in Ecology and Evolution* 22 (7): 357–65. <https://doi.org/10.1016/j.tree.2007.04.003>.
- Coenders-Gerrits, M., Schilperoord, B., & Jiménez-Rodríguez, C., 2020. Evaporative Processes on Vegetation: An Inside Look. In J. T. Van Stan II, E. Gutmann, & J. Friesen (Eds.), *Precipitation Partitioning by Vegetation: A Global Synthesis* (pp. 35–48). Cham: Springer International Publishing. doi: 10.1007/978-3-030-29702-2_3
- Condon, L. E., Atchley, A. L., & Maxwell, R. M., 2020. Evapotranspiration depletes groundwater under warming over the contiguous United States. *Nature Communications*, 11(1). doi: 10.1038/s41467-020-14688-0
- Dash, P., F. M. Göttsche, F. S. Olesen, and H. Fischer., 2002. "Land Surface Temperature and Emissivity Estimation from Passive Sensor Data: Theory and Practice-Current Trends." *International Journal of Remote Sensing* 23 (13): 2563–94. <https://doi.org/10.1080/01431160110115041>.
- Delogu, E., Boulet, G., Olioso, A., Garrigues, S., Brut, A., Tallec, T., . . . Lagouarde, J.-P., 2018. Evaluation of the SPARSE Dual-Source Model for Predicting Water Stress and Evapotranspiration from Thermal Infrared Data over Multiple Crops and Climates. *Remote sensing*, 10(1806), 1-20. doi:10.3390/rs10111806
- Didan, K., Munoz, A. B., Solano, R., & Huete, A., 2015. *MODIS Vegetation Index User's Guide (MOD13 Series)*. Arizona: The University of Arizona.
- Dile, Y. T., Ayana, E. K., Worqlul, A. W., Xie, H., Srinivasan, R., Lefore, N., You, L., & Clarke, N., 2020. Evaluating satellite-based evapotranspiration estimates for hydrological applications in data-scarce regions: A case in Ethiopia. *Science of the Total Environment*, 743, 140702. doi: 10.1016/j.scitotenv.2020.140702
- Dimitriadou, S., & Nikolakopoulos, K. G., 2021. Evapotranspiration trends and interactions in light of the anthropogenic footprint and the climate crisis: A review. *Hydrology*, 8(4). doi: 10.3390/hydrology8040163
- Dinku, T., P. Ceccato, E. Grover-Kopec, M. Lemma, S. J. Connor, and C. F. Ropelewski., 2007. "Validation of Satellite Rainfall Products over East Africa's Complex Topography." *International Journal of Remote Sensing* 28 (7): 1503–26. <https://doi.org/10.1080/01431160600954688>.
- Dixon, W. J., 1950. Analysis of extreme values. *Annals of mathematics and statistics*, 21, 488 - 506.

- Dzikiti, S., Jovanovic, N. Z., Bugan, R., Israel, S., & Le Maitre, D. C., 2014. Measurement and modelling of evapotranspiration in three fynbos vegetation types. *Water SA*, 40(2), 189–198. doi: 10.4314/wsa.v40i2.1.
- Ent, R. J. Van Der, L. Wang-Erlandsson, P. W. Keys, and H. H.G. Savenije., 2014. “Contrasting Roles of Interception and Transpiration in the Hydrological Cycle – Part 2: Moisture Recycling.” *Earth System Dynamics* 5 (2): 471–89. <https://doi.org/10.5194/esd-5-471-2014>.
- Ent, Rudi J. Van Der, Hubert H.G. Savenije, Bettina Schaepli, and Susan C. Steele-Dunne., 2010. “Origin and Fate of Atmospheric Moisture over Continents.” *Water Resources Research* 46 (9): 1–12. <https://doi.org/10.1029/2010WR009127>.
- Ernst, W., 1975. Variation in the mineral content of leaves of trees in miombo woodland in South Central Africa. *Journal of Ecology*, 63 , 801-807.
- Ernst, W. and Walker, B.H.: Studies on the hydration of trees in miombo woodland in South Central Africa. *Journal of Ecology* 61, 667-673, 1973.
- Euser, T, W M J Luxemburg, C S Everson, M G Mengistu, A D Clulow, and W G M Bastiaanssen., 2014. “A New Method to Measure Bowen Ratios Using High-Resolution Vertical Dry and Wet Bulb Temperature Profiles.” *Hydrology and Earth System Sciences* 18 (6): 2021–32. <https://doi.org/10.5194/hess-18-2021-2014>.
- Everson, C. S., 2001. The water balance of a first order catchment in the montane grasslands of South Africa. *Journal of Hydrology*, 241(1–2), 110–123. doi: 10.1016/S0022-1694(00)00376-0, 2001.
- FAO., 2020. Global Forest Resources Assessment 2020. In Global Forest Resources Assessment 2020. Rome: FAO. doi: 10.4060/ca8753en.
- FAO., 2018. *WaPOR Database Methodology: Level 1 Data. Remote Sensing for Water Productivity Technical Report: Methodology Series*. http://www.fao.org/fileadmin/user_upload/faoweb/RS-WP/pdf_files/Web_WaPOR-beta_Methodology_document_Level1.pdf.
- Fan, Y., Miguez-Macho, G., Jobbágy, E. G., Jackson, R. B., & Otero-Casal, C., 2017. Hydrologic regulation of plant rooting depth. *Proceedings of the National Academy of Sciences*, 114(40), 10572–10577. doi: 10.1073/pnas.1712381114
- Fensholt, R., & Sandholt , I., 2003. Derivation of a shortwave infrared stress index from MODIS near- and shortwave infrared data in a semiarid environment. *Remote sensing of the environment*, 87, 111–121. doi:10.1016/j.rse.2003.07.002
- Foken, T., Aubinet, M., & Leuning, R., 2012. In M. Aubinet et al. (eds.), *Eddy Covariance: A Practical Guide to Measurement and Data Analysis*, Springer Atmospheric Sciences, DOI 10.1007/978-94-007-2351-1 1, © Springer Science+Business Media B.V. 2012

- Foken, T., 2008. The energy balance closure problem: An overview. *Ecological Applications*, 18(6), 1351–1367. doi: 10.1890/06-0922.1
- Forster, M. A., Kim, T. D. H., Kunz, S., Abuseif, M., Chulliparambil, V. R., Srichandra, J., & Michael, R. N., 2022. Phenology and canopy conductance limit the accuracy of 20 evapotranspiration models in predicting transpiration. *Agricultural and Forest Meteorology*, 315(December 2021), 108824. doi: 10.1016/j.agrformet.2022.108824.
- Forrest, J., Inouye, D. W., & Thomson, J. D., 2010. Flowering phenology in subalpine meadows: Does climate variation influence community co-flowering trends? *Ecology*, 91(2), 431–440. doi: 10.1890/09-0099.1
- Forrest, J., & Miller-Rushing, A. J., 2010. Toward a synthetic understanding of the role of phenology in ecology and evolution. *Philosophical Transactions of the Royal Society B: Biological Sciences*, 365(1555), 3101–3112. doi: 10.1098/rstb.2010.0145
- Frost, P., 1996. The ecology of miombo woodlands. In B. Campbel (ed.) , *The Miombo in Transition: Woodlands and Welfare in Africa* (pp. 11 -57). Borgo, Inconductedsia: Centre for International Forestry Research.
- Friedl, M., Gray, J., Sulla-Menashe, D., 2019. MCD12Q2 MODIS/Terra+Aqua Land Cover Dynamics Yearly L3 Global 500m SIN Grid V006 [Data set]. NASA EOSDIS Land Processes DAAC. Accessed 2023-03-30 from <https://doi.org/10.5067/MODIS/MCD12Q2.006>
- Fuller, Douglas O., 1999. “Canopy Phenology of Some Mopane and Miombo Woodlands in Eastern Zambia.” *Global Ecology and Biogeography* 8 (3–4): 199–209. <https://doi.org/10.1046/j.1365-2699.1999.00130.x>.
- Fuller, D. O., Prince, S. D., & Astle, W. L., 1997. The influence of canopy strata on remotely sensed observation of savannah woodlands. *International Journal of remote sensing*, 18, 2985 - 3009.
- Fuller, Douglas O., and Stephen D. Prince., 1996. Rainfall and Foliar Dynamics in Tropical Southern Africa: Potential Impacts of Global Climatic Change on Savanna Vegetation. *Climatic Change* 33 (1): 69–96. <https://doi.org/10.1007/BF00140514>.
- Fuller, D. O., 1994. *Folia phenology of vegetation in South Central Africa and its relevance to climate change*. College Park: The University of Maryland.
- Funk, C., Peterson, P., Landsfeld, M., Pedreros, D., Verdin, J., Shukla, S., Husak, G., Rowland, J., Harrison, L., Hoell, A., & Michaelsen, J., 2015. The climate hazards infrared precipitation with stations - A new environmental record for monitoring extremes. *Scientific Data*, 2, 1–21. doi: 10.1038/sdata.2015.66
- García, L., Rodríguez, J. D., Wijnen, M., & Pakulski, I., 2016. *Earth Observation for Water Resources Management: Current Use and Future Opportunities for the Water Sector*. Washington, DC 20433: Washington, DC: World Bank. doi: 10.1596/978-1-4648-0475-5

- García-Mora, T. J., Mas, J.-F., & Hinkley, E. A., 2011. Land cover mapping applications with MODIS: a literature review. *International Journal of Digital Earth*, 1 -25. doi:10.1080/17538947.2011.565080
- García-Santos, V., Cuxart, J., Martínez-Villagrasa, D., Jiménez, M. A., & Simó, G., 2018. Comparison of Three Methods for Estimating Land Surface Temperature from Landsat 8-TIRS Sensor Data. *Remote Sensing*, 10(1450), 1 - 13. doi:doi:10.3390/rs10091450
- Gajic, B., Dugalic, G., Sredojevic, Z., & Tomic, Z., 2008. Effect of different vegetation types on infiltration and soil water. Supplement : Proceedings of the VII . Alps-Adria Scient. *Cereal Research Communications*, 36(June 2008).
- Gao, B. C., 1996. *Remote Sensing of the Environment*, 58, 257–266. doi:10.1016/S0034-4257(96)00067-3
- García, Luis, Juan Diego Rodríguez, Marcus Wijnen, and Inge Pakulski., 2016. *Earth Observation for Water Resources Management: Current Use and Future Opportunities for the Water Sector*. Washington, DC 20433: Washington, DC: World Bank. <https://doi.org/10.1596/978-1-4648-0475-5>.
- Gerrits, A.M.J., 2010. The role of interception in the hydrological cycle. Dissertation Delft University of Technology. ISBN: 978-90-6562-248-8 <http://resolver.tudelft.nl/uuid:7dd2523b-2169-4e7e-992c-365d2294d02e>
- Gerrits, A. M. J., Savenije, H. H. G., Veling, E. J. M., & Pfister, L., 2009. Analytical derivation of the Budyko curve based on rainfall characteristics and a simple evaporation model. *Water Resources Research*, 45(4). doi: 10.1029/2008WR007308
- Gerrits, A. M. J., Savenije, H. H. G., Hoffmann, L., & Pflster, L., 2007. New technique to measure forest floor interception - An application in a beech forest in Luxembourg. *Hydrology and Earth System Sciences*, 11(2), 695–701. doi: 10.5194/hess-11-695-2007
- Giesen, Nick van de, Susan C. Steele-Dunne, Jop Jansen, Olivier Hoes, Mark B. Hausner, Scott Tyler, and John Selker., 2012. “Double-Ended Calibration of Fiber-Optic Raman Spectra Distributed Temperature Sensing Data.” *Sensors (Switzerland)* 12 (5): 5471–85. <https://doi.org/10.3390/s120505471>.
- Giupponi, C., & Gain, A. K., 2017. Integrated water resources management (IWRM) for climate change adaptation. *Regional Environmental Change*, 17(7), 1865–1867. doi: 10.1007/s10113-017-1173-x
- Giliba, R. A., Boon, E. K., Kayombo, C. J., Musamba, E. B., Kashindye, A. M., & Shayo , P. F., 2011. Species Composition, Richness and Diversity in Miombo Woodland of Bereku Forest Reserve, Tanzania. *Journal of Biodiversity*, 2(1), 1-7. doi:10.1080/09766901.2011.11884724

- Gokmen, M., Vekerdy, Z., Verhoef, A., Verhoef, W., Batelaan, O., & van der Tol, C.: Integration of soil moisture in SEBS for improving evapotranspiration estimation under water stress conditions. *Remote Sensing of Environment*, 121, 261–274. doi: 10.1016/j.rse.2012.02.003, 2012
- Gonçalves, F. M., Revermann, R., Gomes, A. L., Aidar, M. P., Finckh, M., & Juergens, N., 2017. Tree Species Diversity and Composition of Miombo Woodlands in South-Central Angola: A Chronosequence of Forest Recovery after Shifting Cultivation. *International Journal of Forestry Research*, 2017, 1 -14. doi:<https://doi.org/10.1155/2017/6202093>
- Grandgirard, Julie, Denis Poinot, Liliane Krespi, Jean Pierre Nénon, and Anne Marie Cortesero., 2002. “Costs of Secondary Parasitism in the Facultative Hyperparasitoid *Pachycrepoideus Dubius*: Does Host Size Matter?” *Entomologia Experimentalis et Applicata* 103 (3): 239–48. <https://doi.org/10.1023/A>.
- Gray, J., Sulla-Menashe, D., & Friedl, M. A., 2019. *User Guide to Collection 6 MODIS Land Cover Dynamics (MCD12Q2) Product*. NASA EOSDIS Land Processes DAAC.
- Gray, J., D. Sulla-Menashe, and M. A. Friedl., 2019. “MODIS Land Cover Dynamics (MCD12Q2) Product.” *User Guide Collection 6* 6: 8. https://modis-land.gsfc.nasa.gov/pdf/MCD12Q2_Collection6_UserGuide.pdf.
- Guan, K., Eric F. Wood, D. Medvigy, John. Kimball, Ming. Pan, K.K. Caylor, J. Sheffield, Xiangtao. Xu, and O.M. Jones., 2014. “Phenology of African Savannas and Woodlands” 119: 1652–69. <https://doi.org/10.1002/2013JG002572>.
- Guerschman, J. P., Scarth, P. F., McVicar, T. R., Renzullo, L. J., Malthus, T. J., Stewart, J. B., Rickards, J. E., & Trevithick, R., 2015. Assessing the effects of site heterogeneity and soil properties when unmixing photosynthetic vegetation, non-photosynthetic vegetation and bare soil fractions from Landsat and MODIS data. *Remote Sensing of Environment*, 161, 12–26. doi: 10.1016/j.rse.2015.01.021
- Gumbo, , J. D., Dumas-Johansen, , M., Muir, G., Boerstler, F., & Xia, Z., 2018. *Sustainable management of Miombo woodlands – Food security, nutrition and wood energy*. Rome, Italy: Food and Agriculture Organization of the United Nations.
- Hachigonta, S., and C. J.C. Reason., 2006. “Interannual Variability in Dry and Wet Spell Characteristics over Zambia.” *Handbook of Environmental Chemistry, Volume 5: Water Pollution* 32 (1): 49–62. <https://doi.org/10.3354/cr032049>.
- Han, J., Zhao, Y., Wang, J., Zhang, B., Zhu, Y., Jiang, S., & Wang, L., 2019. Effects of different land use types on potential evapotranspiration in the Beijing-Tianjin-Hebei region, North China. *Journal of Geographical Sciences*, 29(6), 922–934. doi: 10.1007/s11442-019-1637-7
- Hardisky, M. A., Klemas, V., & Smart, R. M., 1988. The Influence of Soil Salinity, Growth Form, and Leaf Moisture on the Spectral Radiance of *Spartina alterniflora* Canopies. *Photogrammetric Engineering and Remote Sensing* , 49(1), 77-83.

- Helsel, D. R., R. M. Hirsch, K.R. Ryberg, S.A. Archfield, and E.J. Gilroy., 2020. “Statistical Methods in Water Resources Techniques and Methods 4 – A3.” *USGS Techniques and Methods*.
- Helsel, D. R., & Hirsch, R. M., 2002. Statistical Methods in Water Resources. In U. G. SURVEY, *Hydrologic Analysis and Interpretation* (pp. 1-524). Washington: U.S. GEOLOGICAL SURVEY. Retrieved from <http://water.usgs.gov/pubs/twri/twri4a3/>
- Hersbach, H., Bell, B., Berrisford, P., Hirahara, S., Horányi, A., Muñoz-Sabater, J., Nicolas, J., Peubey, C., Radu, R., Schepers, D., Simmons, A., Soci, C., Abdalla, S., Abellan, X., Balsamo, G., Bechtold, P., Biavati, G., Bidlot, J., Bonavita, M., De Chiara, G., Dahlgren, P., Dee, D., Diamantakis, M., Dragani, R., Flemming, J., Forbes, R., Fuentes, M., Geer, A., Haimberger, L., Healy, S., Hogan, R.J., Hólm, E., Janisková, M., Keeley, S., Laloyaux, P., Lopez, P., Lupu, C., Radnoti, G., de Rosnay, P., Rozum, I., Vamborg, F., Villaume, S., Thépaut, J-N., 2017: Complete ERA5 from 1979: Fifth generation of ECMWF atmospheric reanalyses of the global climate. Copernicus Climate Change Service (C3S) Data Store (CDS). (Accessed on 06-06-2021)
- Higgins, S, I., and Scheiter, S., 2012. “Atmospheric CO 2 Forces Abrupt Vegetation Shifts Locally, but Not Globally.” *Nature* 488 (7410): 209–12. <https://doi.org/10.1038/nature11238>.
- Hirschi M, Michel D, Lehner I, Seneviratne S I., 2017. A site-level comparison of lysimeter and eddy covariance flux measurements of evapotranspiration. *Hydrol Earth Syst Sci* 21(3):1809–1825. <https://doi.org/10.5194/hess-21-1809-2017>
- Hulley, G., 2017. MYD21A2 MODIS/Aqua Land Surface Temperature/3-Band Emissivity 8-Day L3 Global 1km SIN Grid V006. NASA EOSDIS Land Processes DAAC. Retrieved from <https://doi.org/10.5067/MODIS/MYD21A2.006>
- Hulsman, P., Hrachowitz, M., and Savenije, H. H.G., 2021. “Improving the Representation of Long-Term Storage Variations With Conceptual Hydrological Models in Data-Scarce Regions.” *Water Resources Research* 57 (4). <https://doi.org/10.1029/2020WR028837>.
- Hulsman, P., Winsemius, H.C., Michailovsky, C. I., Savenije, H.H.G., and Hrachowitz, M., 2020. “Using Altimetry Observations Combined with GRACE to Select Parameter Sets of a Hydrological Model in a Data-Scarce Region.” *Hydrology and Earth System Sciences* 24 (6): 3331–59. <https://doi.org/10.5194/hess-24-3331-2020>.
- Hunt , J. E., & Rock , B. N., 1989. Detection of changes in leaf water content using near and middle-infrared reflectances. *Remote sensing of the environment*(30), 43–54. doi:doi:10.1016/0034-4257(89)90046-1
- Hunink, J.E. , Terink, W, Contreras, S, Droogers P., 2015. “Scoping Assessment of Erosion Levels for the Mahale Region, Lake Tanganyika, Tanzania.” Vol. 31. www.futurewater.nl.

- IPCC: Climate Change., 2007. *Synthesis report In Contribution of Working Groups I, II and III to the Fourth Assessment Report of the Intergovernmental Panel on Climate Change*. Geneva: IPCC, 2007.
- Jarmain, C., Everson, C. S., Savage, M. J., Mengistu, M. G., Clulow, A. D., Walker, S., & Gush, M. B., 2009. *Refining tools for evaporation monitoring in support of water resources management, SA Water Research Commission, Report No. 1567/1/08, (Issue 1567)*.
- Jaafar, S.W.M.W., Maulud, K.N.A., Kamarulzaman, M.A.M., Raihan, A., Sah, S.M., Ahmad, A., Saad, M.S.N., Azmi, A.T.M., Syukri, N.K.A.J., Khan, W.R., 2020. The Influence of Deforestation on Land Surface Temperature—A Case Study of Perak and Kedah, Malaysia. *Forests* 2020, 11, 670.
- Jeffers, J. N., & Boaler, S. B., 1966. Ecology of a miombo site. Lupa North Forest Reserve, Tanzania. I. Weather and plant growth , 1962–64'. *Ecology*, 54, 447–463.
- Jew, E. K., Dougill, A. J., Sallu, S. M., O'Connell, J., & Benton, T. G., 2016. Miombo woodland under threat: Consequences for tree diversity and carbon storage and carbon storage. *Forest Ecology and Management*(361), 144 - 153.
- Jiménez-Rodríguez, C. D., Coenders-Gerrits, M., Wenninger, J., Gonzalez-Angarita, A., & Savenije, H., 2020. Contribution of understory evaporation in a tropical wet forest during the dry season. *Hydrology and Earth System Sciences*, 24(4), 2179–2206. doi: 10.5194/hess-24-2179-2020
- Johnson , J. M., & Choinski, J. S., 1993. The spring flush in Zimbabwe's miombo woodland. *Zimbabwe Science News*, 27, 3-6.
- Jones, H. G., & Rotenberg, E., 2001. Energy, Radiation and Temperature Regulation in Plants. *Encyclopedia of life sciences*, 1-7. doi:doi: 10.1038/npg.els.0006130
- Kalma, J. D., McVicar, T. R., & McCabe, M. F., 2008. Estimating land surface evaporation: A review of methods using remotely sensed surface temperature data. *Surveys in Geophysics*, 29(4–5), 421–469. doi: 10.1007/s10712-008-9037-z
- Karnieli, A., Agam, N., Pinker, R.T., Anderson, M., Imhoff, M.L., Gutman, G.G., Panov, N., Goldberg, A., 2010. Use of NDVI and Land Surface Temperature for Drought Assessment: Merits and Limitations. *J. Clim.* 23, 618–633.
- Kendall, M. G., 1975. Rank correlation measures. London: Charles Griffin.
- Kleine, L., Tetzlaff, D., Smith, A., Dubbert, M., & Soulsby, C., 2021. Modelling ecohydrological feedbacks in forest and grassland plots under a prolonged drought anomaly in Central Europe 2018–2020. *Hydrological Processes*, 35(8). doi: 10.1002/hyp.14325.
- Kleidon, A., & Heimann, M., 1998. A method of determining rooting depth from a terrestrial biosphere model and its impacts on the global water and carbon cycle. *Global Change Biology*, 4(3), 275–286. doi: 10.1046/j.1365-2486.1998.00152.x

- Knyazikhin, Y., Glassy, J., Privette, L. J., Tian, Y., Lotsch, A., Zhang, Y., . . . Running, W. S., 1999. *MODIS Leaf Area Index (LAI) and Fraction of Photosynthetically Active Radiation Absorbed by Vegetation (FPAR) Product (MOD15) Algorithm Theoretical Basis Document*. USGS. Retrieved from <http://eosps0.gsfc.nasa.gov/atbd/modistables.html>.
- Konapala, G., Mishra, A. K., Wada, Y., & Mann, M. E., 2020. Climate change will affect global water availability through compounding changes in seasonal precipitation and evaporation. *Nature Communications*, 11(1), 1–10. doi: 10.1038/s41467-020-16757-w.
- Kramer, K., Leinonen, I., and Loustau, D., 2000. “The Importance of Phenology for the Evaluation of Impact of Climate Change on Growth of Boreal, Temperate and Mediterranean Forests Ecosystems: An Overview.” *International Journal of Biometeorology*. <https://doi.org/10.1007/s004840000066>.
- Kusangaya, S., Warburton, M. L., Archer, E., Garderen, V., & Jewitt, G. P. W., 2014. Impacts of climate change on water resources in southern Africa : A review. *Physics and Chemistry of the Earth*, 67–69, 47–54. doi: 10.1016/j.pce.2013.09.014
- Lakshmi, V., 2004. The role of satellite remote sensing in the prediction of ungauged basins. *Hydrological Processes*, 18(5), 1029–1034. doi: 10.1002/hyp.5520
- Lausch, A., Erasmi, S., King, D. J., Magdon, P., & Heurich, M., 2017. Understanding Forest Health with Remote Sensing-Part II—A Review of Approaches and Data Models. *Remote sensing*, 9(129), 1 - 33. doi:10.3390/rs9020129.
- Lawley, V., Lewis, M., Clarke, K., & Ostendorf, B., 2016. Site-based and remote sensing methods for monitoring indicators of vegetation condition: An Australian review. *Ecological Indicators*, 60, 1273–1283. doi: 10.1016/j.ecolind.2015.03.021
- Lechne, A. M., Foody, G. M., & Boyd, D. S., 2020. Applications in Remote Sensing to Forest Ecology and Management. *One Earth*, 405 - 412. doi:<https://doi.org/10.1016/j.oneear.2020.05.00>
- Leroux, L., Jolivot, A., Bégué, A., Lo Seen, D., and Zoungrana, B., 2014. “How Reliable Is the MODIS Land Cover Product for Crop Mapping Sub-Saharan Agricultural Landscapes?” *Remote Sensing* 6(9):8541–64. doi: 10.3390/rs6098541.
- Lillesand, M. T., Kiefer, W. R., & Chipman, W. J., 2015. Remote Sensing and Image Interpretation. 7th Edition. In *Photogrammetric Engineering & Remote Sensing* (Seventh Ed, Vol. 81, Issue 8). River Street, Hoboken, NJ 07030-5774, (201) 748- 6011, New York: John Wiley & Sons, Inc. doi: 10.14358/PERS.81.8.615
- Li, H., Ma, X., Lu, Y., Ren, R., Cui, B., & Si, B., 2021. Growing deep roots has opposing impacts on the transpiration of apple trees planted in subhumid loess region. *Agricultural Water Management*, 258(June), 107207. doi: 10.1016/j.agwat.2021.107207

- Li, Z. L., Tang, B. H., Wu, H., Ren, H., Yan, G., Wan, Z., Trigo, I. F., & Sobrino, J. A., 2013. Satellite-derived land surface temperature: Current status and perspectives. *Remote Sensing of Environment*, 131, 14–37. doi: 10.1016/j.rse.2012.12.008
- Liu, M., Hu, D., 2019. Response of Wetland Evapotranspiration to Land Use/Cover Change and Climate Change in Liaohe River Delta, China. *Water*; 11(5):955. <https://doi.org/10.3390/w11050955>
- Liu, Wenbin, Lei Wang, Jing Zhou, Yanzhong Li, Fubao Sun, Guobin Fu, Xiuping Li, and Yan Fang Sang., 2016. “A Worldwide Evaluation of Basin-Scale Evapotranspiration Estimates against the Water Balance Method.” *Journal of Hydrology* 538: 82–95. <https://doi.org/10.1016/j.jhydrol.2016.04.006>.
- Liu H., Randerson J.T., Lindfors J., Massman W.J., Foken T., 2006. Consequences of incomplete surface energy balance closure for CO₂ fluxes from open-path CO₂/H₂O infrared gas analysers. *Boundary-Layer Meteorol* 120, 65-85
- Lu, P., Yu, Q., Liu, J., & Lee, X., 2006. Advance of tree-flowering dates in response to urban climate change. *Agricultural and Forest Meteorology*, 138(1–4), 120–131. doi: 10.1016/j.agrformet.2006.04.002
- Ma, X., Feng, Q., Su, Y., Yu, T., and Jin, H., 2017. “Forest Evapotranspiration and Energy Flux Partitioning Based on Eddy Covariance Methods in an Arid Desert Region of Northwest China.” *Advances in Meteorology* 2017. <https://doi.org/10.1155/2017/1619047>.
- Macharia, D, Fankhauser, K., Selker. S. J., Neff. C. J., and Thomas, A. E., 2022. “Validation and Intercomparison of Satellite-Based Rainfall Products over Africa with TAHMO In Situ Rainfall Observations.” *Journal of Hydrometeorology* 23 (7): 1131–54. <https://doi.org/10.1175/JHM-D-21-0161.1>.
- Magidson, J., 2013. Correlated Component Regression: Re-thinking Regression in the Presence of Near Collinearity: In: Abdi H., Chin W., Esposito Vinzi V., Russolillo G., Trinchera L. (eds) *New Perspectives in Partial Least Squares and Related Methods*. In *New Perspectives in Partial Least Squares and Related Methods* (Vol. 56). New York, NY: Springer, . doi:https://doi.org/10.1007/978-1-4614-8283-3_3.
- Makapela, L., 2015. *Review and Use of Earth Observations and Remote Sensing in Water Resource Management in South Africa : Report to the Water Research Commission*.
- Mann, H. B., 1945. Nonparametric test against trend. *Econometrica*, 13, 245 - 259.
- Marchesini, V. A., Fernández, R. J., Reynolds, J. F., Sobrino, J. A., & Di Bella, C. M., 2015. Changes in evapotranspiration and phenology as consequences of shrub removal in dry forests of central Argentina. *Ecohydrology*, 8(7), 1304–1311. doi: 10.1002/eco.1583
- Marin, C., Bouten, W., & Sevink, J., 2000. Gross rainfall and its partitioning into throughfall, stemflow and evaporation of intercepted water in four forest ecosystems in western Amazonia. *Journal of Hydrology* , 237, 40–57.

- Martens, B., Miralles, G.D., Lievens, H., Schalie, V.R., De Jeu, A. M. R., Fernández-Prieto, D., Beck, E. H., Dorigo, A.W., and Verhoest, E.C.N., 2017. "GLEAM v3: Satellite-Based Land Evaporation and Root-Zone Soil Moisture." *Geoscientific Model Development* 10 (5): 1903–25. <https://doi.org/10.5194/gmd-10-1903-2017>.
- Martins, P.J., Trigo, I., and Freitas, C.S., 2020. "Copernicus Global Land Operations "Vegetation and Energy" "CGLOPS-1." *Copernicus Global Land Operations*, 1–93. <https://doi.org/10.5281/zenodo.3938963>.
- McCabe, M.F.; Miralles, D.G.; Holmes, T.R.H.; Fisher, J.B., 2019. Advances in the Remote Sensing of Terrestrial Evaporation. *Remote Sens.* **2019**, *11*, 1138. <https://doi.org/10.3390/rs11091138>
- McCabe, M. F. and Wood, E. F., 2006. 'Scale influences on the remote estimation of evapotranspiration using multiple satellite sensors', *Remote Sensing of Environment*, 105(4), pp. 271–285. doi: 10.1016/j.rse.2006.07.006.
- McCaughey, H. J., 1982. "Spatial Variability of Net Radiation and Soil Heat Flux Density on Two Logged Sites at Montmorency, Quebec." *Journal of Applied Meteorology* 21: 777–87. <https://www.ptonline.com/articles/how-to-get-better-mfi-results>.
- McGloin, R., Šigut, L., Fischer, M., Foltýnová, L., Chawla, S., Trnka, M., Pavelka, M., and Marek, V.M., 2019. "Available Energy Partitioning During Drought at Two Norway Spruce Forests and a European Beech Forest in Central Europe." *Journal of Geophysical Research: Atmospheres* 124 (7): 3726–42. <https://doi.org/10.1029/2018JD029490>.
- Meter Group AG., 2020. "Atmos 41." *Manual*. München. http://library.metergroup.com/Manuals/20635_ATMOS41_Manual_Web.pdf.
- Meulen, M. W.J. Van Der, and W. Klaassen., 1996. "Soil Heat Flux Measurements in an Open Forest." *Physics and Chemistry of the Earth* 21 (3 SPEC. ISS.): 101–5. [https://doi.org/10.1016/S0079-1946\(97\)85568-1](https://doi.org/10.1016/S0079-1946(97)85568-1).
- Mildrexler, D. J., Zhao, M., & Running, S. W., 2011. A global comparison between station air temperatures and MODIS land surface temperatures reveals the cooling role of forests. *Geophysical Research*, 116, 1-15. doi:1029/2010JG001486
- Miombo Network., 2020. Retrieved from <http://www.miombonetwork.org>. Date accessed: January 30, 2020.
- Miralles, D. G., Brutsaert, W., Dolman, A. J., & Gash, J. H., 2020. On the use of the term 'Evapotranspiration'. *Water Resources Research* 56 (11). <https://doi.org/10.1029/2020WR028055>.
- Miralles, D. G., Jiménez, C., Jung, M., Michel, D., Ershadi, A., McCabe, M. F., Hirschi, M., Martens, B., Dolman, A. J., Fisher, J. B., Mu, Q., Seneviratne, S. I., Wood, E. F., & Fernández-Prieto, D., 2016. The WACMOS-ET project - Part 2: Evaluation of global terrestrial evaporation data sets. *Hydrology and Earth System Sciences*, 20(2), 823–842. doi: 10.5194/hess-20-823-2016

- Miralles, D. G., R. A.M. De Jeu, J. H. Gash, T. R.H. Holmes, and A. J. Dolman., 2011 (a). “Magnitude and Variability of Land Evaporation and Its Components at the Global Scale.” *Hydrology and Earth System Sciences* 15 (3): 967–81. <https://doi.org/10.5194/hess-15-967-2011>.
- Miralles, D.G., Holmes, T.R.H., de Jeu, R.A.M., Gash, J.H., Meesters, A.G.C.A., Dolman, A.J.: Global land-surface evaporation estimated from satellite-based observations, *Hydrology and Earth System Sciences*, 15, 453–469, doi: 10.5194/hess-15-453-2011, 2011(b).
- Mobasheri, M. R., & Fatemi, S. B., 2013. Leaf Equivalent Water Thickness assessment using reflectance at optimum wavelengths. *Theoretical and Experimental Plant Physiology*, 25(3), 196-202.
- Monteith, J. L., 1965. Evaporation and environment. *Symposium of the Society for Experimental Biology*, 19, 205-234.
- Mu, Q., Zhao, M., and Running, W.S., 2011. Improvements to a MODIS Global Terrestrial Evapotranspiration Algorithm. *Remote Sensing of Environment* 115 (8): 1781–1800. <https://doi.org/10.1016/j.rse.2011.02.019>.
- Mu, Q., Heinsch, A.F., Zhao,M., and Running.W.S., 2007. Development of a Global Evapotranspiration Algorithm Based on MODIS and Global Meteorology Data. *Remote Sensing of Environment* 111 (4): 519–36. <https://doi.org/10.1016/j.rse.2007.04.015>.
- Munishi, P. K., Mringi, S., Shirima, D. D., & Linda, K. S., 2010. The role of the Miombo Woodlands of the Southern Highlands of Tanzania as carbon sinks. *Journal of Ecology and the Natural Environment*, 2(12), 261-269. Retrieved from <http://www.academicjournals.org/jene>
- Myneni, R., & Park, Y. K., 2015. *MCD15A2H MODIS/Terra+Aqua Leaf Area Index/FPAR 8-day L4 Global 500m SIN Grid V006*. NASA EOSDIS Land Processes DAAC. Retrieved from <https://doi.org/10.5067/MODIS/MCD15A2H.006>
- Neinavaz, E., Schlerf, M., Darvishzadeh, R., Gerhards, M., & Skidmore, A. K., 2021. Thermal infrared remote sensing of vegetation: Current status and perspectives. *International Journal of Applied Earth Observation and Geoinformation*, 102(July), 102415. doi: 10.1016/j.jag.2021.102415
- Nielsen, D., Miceli-Garcia, J. J., & Lyon, D. J., 2012. Canopy cover and Leaf Area Index Relationships. *Agronomy Journal*, 104(6), 1569 -1573.
- Niu,S., Fu,Y., Gu,L., and and Luo, Y., 2013. Temperature Sensitivity of Canopy Photosynthesis Phenology in Northern Ecosystems. Pp. 503–19 in *Phenology: An Integrative Environmental Science*, edited by M. D. Schwartz.
- Nord, E. A., & Lynch, J. P., 2009. Plant phenology: A critical controller of soil resource acquisition. *Journal of Experimental Botany*, 60(7), 1927–1937. doi: 10.1093/jxb/erp018

- Novick, K. A., Ficklin, D. L., Stoy, P. C., Williams, C. A., Bohrer, G., Oishi, A. C., Papuga, S. A., Blanken, P. D., Noormets, A., Sulman, B. N., Scott, R. L., Wang, L., & Phillips, R. P., 2016. The increasing importance of atmospheric demand for ecosystem water and carbon fluxes. *Nature Climate Change*, 6(11), 1023–1027. doi: 10.1038/nclimate3114.
- Olson, D. M., Dinerstein, E., Wikramanayake, E. D., Burgess, N. D., Powell, G. V. N., Underwood, E. C., D'Amico, J. A., Itoua, I., Strand, H. E., Morrison, J. C., Loucks, C. J., Allnutt, T. F., Ricketts, T. H., Kura, Y., Lamoreux, J. F., Wettengel, W. W., Hedao, P., & Kassem, K. R., 2001. Terrestrial ecoregions of the world: A new map of life on Earth. *BioScience*, 51(11), 933–938. doi: 10.1641/0006-3568(2001)051[0933:TEOTWA]2.0.CO;2
- Pagán, B.R., Maes, W.H.; Gentine, P., Martens, B., Miralles, D.G., 2019 Exploring the Potential of Satellite Solar-Induced Fluorescence to Constrain Global Transpiration Estimates. *Remote Sens.* 2019, 11, 413. <https://doi.org/10.3390/rs11040413>
- Pearson, K., 1895. Notes on regression and inheritance in the case of two parents. *Proceedings of the Royal Society of London*, 58, 240–242.
- Pelletier, J., Paquette, A., Mbindo, K., Zimba, N., Siampale, A., Chendauka, B., Siangulube, F., & Roberts, J. W., 2018. Carbon sink despite large deforestation in African tropical dry forests (miombo woodlands). *Environmental Research Letters*, 13(9). doi: 10.1088/1748-9326/aadc9a
- Penman, H. L., 1948. Natural evaporation from open water, bare soil, and grass. *Proceedings of the Royal Society A: Mathematics, Physical and engineering sciences*, 120-146. Retrieved from <https://doi.org/10.1098/rspa.1948.0037>
- Pereira, C. C., Boaventura, M. G., Cornelissen, T., Nunes, Y. R. F., & de Castro, G. C., 2022. What triggers phenological events in plants under seasonal environments? A study with phylogenetically related plant species in sympatry. *Brazilian Journal of Biology*, 84(March). doi: 10.1590/1519-6984.257969
- Peterson, D. L., Aber, J. D., Matson, P. A., Card, D. H., Swanberg, N., Wessman, C., & Spanner, M., 1988. Remote sensing of forest canopy and leaf biochemical contents. *Remote Sensing of Environment*, 24(1), 85–108. doi: 10.1016/0034-4257(88)90007-7
- Pettit, A. N., 1979. A non-Parametric approach to the change-point problem. *Journal of Royal Statistical Society. Series C (Applied statistics)*, 28(2), 126 - 135. doi:10.2307/2346729
- Priestley C.H.B., Taylor R.J., 1972. On the assessment of surface heat flux and evaporation using large- scale parameters. *Monthly Weather Review*, 100: 81-92.
- Quemada, C., Pérez-Escudero, J. M., Gonzalo, R., Ederra, I., Santesteban, L. G., Torres, N., & Iriarte, J. C., 2021. Remote sensing for plant water content monitoring: A review. *Remote Sensing*, 13(11), 1–37. doi: 10.3390/rs13112088.
- Ramoelo, A., Dzikitani, S., Van Deventer, H., Maherry, A., Cho, M. A., & Gush, M., 2015. Potential to monitor plant stress using remote sensing tools. *Journal of Arid Environments*, 113, 134–144. doi: 10.1016/j.jaridenv.2014.09.003.

- Ramoelo, A., Majozi, N., Mathieu, R., Jovanovic, N., Nickless, A., Dzikiti, S., 2014. Validation of Global Evapotranspiration Product (MOD16) using Flux Tower Data in the African Savanna, South Africa. *Remote Sens.* 2014, 6, 7406-7423.
<https://doi.org/10.3390/rs6087406>
- Reeves, M. C., Zhao, M., & Running, S. W., 2006. Applying improved estimates of MODIS productivity of characterize grassland vegetation dynamics. *Rangeland Ecology and Management*, 59, 1 - 10.
- Roberts, J. M., (undate.). The role of forests in the hydrological cycle. In *Forests and forest plants: Vol. III*. Retrieved from <https://www.eolss.net/sample-chapters/c10/E5-03-04-02.pdf>
- Rouse, W. J., Haas, R. H., Schell, A. J., & Deering, D. W., 1973. Monitoring vegetation systems in the great plains with ERTS. *Remote sensing centre*, 309 - 317.
- Running, S. Q., 2017. *MOD16A2 MODIS/Terra Net Evapotranspiration 8-Day L4 Global 500m SIN Grid V006*. NASA EOSDIS Land Processes DAAC. Retrieved from <https://doi.org/10.5067/MODIS/MOD16A2.006>
- Running, W.S., Mu, Q., Zhao, M., Moreno, A., 2019. “User ’ s Guide MODIS Global Terrestrial Evapotranspiration (ET) Product NASA Earth Observing System MODIS Land Algorithm (For Collection 6).”
- Ryan, M.C., Pritchard, R., McNicol, I., Owen, M., Janet A. Fisher, A.J., and Lehmann, C., 2016. “Ecosystem Services from Southern African Woodlands and Their Future under Global Change.” *Philosophical Transactions of the Royal Society B: Biological Sciences* 371 (1703). <https://doi.org/10.1098/rstb.2015.0312>.
- Ryu, Y., Baldocchi, D. D., Black, T. A., Detto, M., Law, B. E., Leuning, R., Miyata, A., Reichstein, M., Vargas, R., Ammann, C., Beringer, J., Flanagan, L. B., Gu, L., Hutley, L. B., Kim, J., McCaughey, H., Moors, E. J., Rambal, S., & Vesala, T., 2012. On the temporal upscaling of evapotranspiration from instantaneous remote sensing measurements to 8-day mean daily-sums. *Agricultural and Forest Meteorology*, 152(1), 212–222. doi: 10.1016/j.agrformet.2011.09.010
- Saha, , S., Moorthi, S., Wu, X., Wang, J., & Coauthors., 2014. The NCEP Climate Forecast System Version 2. *Journal of Climate*, 27, 2185–2208. doi:10.1175/JCLI-D-12-00823.1
- Saha, , S., Moorthi, S., Pan, H., Wu., X., Wang, J., & Coauthors., 2010. The NCEP Climate Forecast System Reanalysis. *Bulletin of the American Meteorological Society*, 91, 1015–1057. doi:10.1175/2010BAMS3001.1
- Salmi, T., Määttä, A., Anttila, P., Ruoho-Airola, T., & Amnell, T., 2002. *Detecting trends of annual values of atmospheric pollutants by the Mann-Kendall test and the Sens' slope estimates: The excel template application Makesens*. Helsinki: Finnish Meteorological Institute.

- Santin-Janin, H., M. Garel, J. L. Chapuis, and D. Pontier., 2009. "Assessing the Performance of NDVI as a Proxy for Plant Biomass Using Non-Linear Models: A Case Study on the Kerguelen Archipelago." *Polar Biology* 32 (6): 861–71. <https://doi.org/10.1007/s00300-009-0586-5>.
- Savage, M.J., Everson, C.S., Metelerkamp, B.R., 1997. Evaporation measurement above vegetated surfaces using micrometeorological techniques, SA Water Research Commission, Report No. 349/1/97
- Savenije, H. H.G., 2010. "HESS Opinions 'Topography Driven Conceptual Modelling (FLEX-Topo).'" *Hydrology and Earth System Sciences* 14 (12): 2681–92. <https://doi.org/10.5194/hess-14-2681-2010>.
- Savenije, H. H. G., & Van der Zaag, P., 2008. Integrated water resources management: Concepts and issues. *Physics and Chemistry of the Earth*, 33(5), 290–297. doi: 10.1016/j.pce.2008.02.003.
- Savenije, H. H. G., 1997. Determination of evaporation from a catchment water balance at a monthly time scale. In *Hydrology and Earth System Sciences* (Vol. 1, Issue 1, pp. 93–99). doi: 10.5194/hess-1-93-1997
- Savenije, H.H.G., 2004. "The Importance of Interception and Why We Should Delete the Term Evapotranspiration from Our Vocabulary." *Hydrological Processes* 18 (8): 1507–11. <https://doi.org/10.1002/hyp.5563>.
- Senay, G.B., Savoca, M. E., M. A. Maupin, J. F. Kenny, and C. A. Perry., 2013. "Actual Evapotranspiration Modeling Using the Operational Simplified Surface Energy Balance (SSEBop) Approach." *U.S Geological Survey Scientific Investigations Report 2013–5126*, no. January: 16 p. <http://pubs.usgs.gov/sir/2013/5126>.
- Savory B. M., 1963. "Rooting Habits of Important Miombo Species." Ndola.
- Sebestyén, V., Czvetkó, T., & Abonyi, J., 2021. The Applicability of Big Data in Climate Change Research: The Importance of System of Systems Thinking. *Frontiers in Environmental Science*, 9(March), 1–26. doi: 10.3389/fenvs.2021.619092
- Sens, P. K., 1968. Estimates of the regression coefficient based on Kendall' Tau. *American Statistical Association*, 63(324), 1379-1389. doi:10.2307/2285891
- Schilperoort, B., Coenders-Gerrits, M., Jiménez Rodríguez, C., van der Tol, C., van de Wiel, B., & Savenije, H., 2020. Decoupling of a Douglas fir canopy: a look into the subcanopy with continuous vertical temperature profiles. *Biogeosciences*, 17(24), 6423–6439. doi: 10.5194/bg-17-6423-2020
- Schilperoort, B., Coenders-Gerrits, M., Luxemburg, W., Rodríguez, J. C., Vaca, C.C., and Savenije, H., 2018. "Technical Note: Using Distributed Temperature Sensing for Bowen Ratio Evaporation Measurements." *Hydrology and Earth System Sciences* 22 (1): 819–30. <https://doi.org/10.5194/hess-22-819-2018>.

- Schwartz, D.M., 2013. Phenology: An Integrative Environmental Science. Edited by Mark D. Schwartz (Ed.), *Phenology: An Integrative Environmental Science*. (Second Edi). Dordrecht: Springer Netherlands. https://doi.org/10.1007/978-94-007-6925-0_27.
- Shahidan, M. F., Salleh, E., & Mustafa, K. M. S., 2007. Effects of tree canopies on solar radiation filtration in a tropical microclimatic environment. *Sun, Wind and Architecture - The Proceedings of the 24th International Conference on Passive and Low Energy Architecture, PLEA 2007, November*, 400–406.
- Shefali, A., 2013. Principles of Remote Sensing. In *Introductory Remote Sensing Principles and Concepts* (Vol. 11, Issue 3, pp. 31–85). Routledge. doi: 10.4324/9780203714522-9
- Sheil, D., 2018. Forests, atmospheric water and an uncertain future: the new biology of the global water cycle. *Forest Ecosystems*, 5(1). doi: 10.1186/s40663-018-0138-y
- Silixa Ltd., 2016. Silixa XT-DTS Hardware Manual Version 1.3., issued 2016. www.silixa.com.
- Simic, A., Fernandes, R., & Wang, S., 2014. Assessing the Impact of Leaf Area Index on Evapotranspiration and Groundwater Recharge across a Shallow Water Region for Diverse Land Cover and Soil Properties. *Journal of Water Resource and Hydraulic Engineering*, 3(4), 60-73.
- Snyder, L.R., and Spano, D., 2013. Phenology and Evapotranspiration. In *Phenology: An Integrative Environmental Science*, edited by Mark D. Schwartz, Second, 521–28. Milwaukee.
- Snyder, R. L., Moratiel, R., Song, Z., Swelam, A., Jomaa, I., & Shapland, T., 2011. Evapotranspiration response to climate change. *Acta Horticulturae*, 922(May 2021), 91–98. doi: 10.17660/ActaHortic.2011.922.11
- Spittlehouse, D. L., and T. A. Black., 1980. Evaluation of the Bowen Ratio/Energy Balance Method for Determining Forest Evapotranspiration. *Atmosphere - Ocean* 18 (2): 98–116. <https://doi.org/10.1080/07055900.1980.9649081>.
- Sriwongsitanon, N., Gao, H., Savenije, H. H., Maekan, E., Saengsawang, S., & Thianpopirug, S., 2015. The Normalized Difference Infrared Index (NDII) as a proxy for soil moisture storage in hydrological modelling. *Hydrology and Earth System Sciences*, 12, 8419–8457. doi:10.5194/hessd-12-8419-2015
- Stisen, S., Jensen, K. H., Sandholt, I., & Grimes, D. I. F., 2008. A remote sensing driven distributed hydrological model of the Senegal River basin. *Journal of Hydrology*, 354(1–4), 131–148. doi: 10.1016/j.jhydrol.2008.03.006
- Su, Z., 2002. The Surface Energy Balance System (SEBS) for estimation of turbulent heat fluxes. *Hydrology and Earth System Sciences*, 6(1), 85–100. doi: 10.5194/hess-6-85-2002

- Sun, Z., Wang, Q., Batkhishig, O., & Ouyang, Z., 2016. Relationship between Evapotranspiration and Land Surface Temperature under Energy- and Water-Limited Conditions in Dry and Cold Climates. *Advances in Meteorology*, 2016, 1-9. Retrieved from <http://dx.doi.org/10.1155/2016/1835487>
- Sutanto, S. J., Wenninger, J., Coenders-Gerrits, A. M., & Uhlenbrook, S., 2012. Partitioning of evaporation into transpiration, soil evaporation and interception: a comparison between isotope measurements and a HYDRUS-1D model. *Hydrology and Earth System Sciences*, 16, 2605–2616. doi:10.5194/hess-16-2605-2012
- Sutanto, S J, J Wenninger, and S Uhlenbrook., 2012. Partitioning of Evaporation into Transpiration, Soil Evaporation and Interception: A Combination of Hydrometric Measurements and Stable Isotope Analyses. *Hydrology and Earth System Sciences Discussions* 9 (3): 3657–90. <https://doi.org/10.5194/hessd-9-3657-2012>.
- Stephenson, L.N., 1990. “Climatic Control of Vegetation Distribution : The Role of the Water Balance Published by : The University of Chicago Press for The American Society of Naturalists Stable URL : <Http://Www.Jstor.Org/Stable/2462028>.” *The American Naturalist* 135 (5): 649–70.
- Stöckli, R., T. Rutishauser, I. Baker, M. A. Liniger, and A. S. Denning., 2011. “A Global Reanalysis of Vegetation Phenology.” *Journal of Geophysical Research: Biogeosciences* 116 (3): 1–19. <https://doi.org/10.1029/2010JG001545>.
- Tang, R., Li, Z. L., & Sun, X., 2013. Temporal upscaling of instantaneous evapotranspiration: An intercomparison of four methods using eddy covariance measurements and MODIS data. *Remote Sensing of Environment*, 138, 102–118. doi: 10.1016/j.rse.2013.07.001
- Teuling, J.A., 2018. “A Forest Evapotranspiration Paradox Investigated Using Lysimeter Data.” *Vadose Zone Journal* 17 (1): 170031. <https://doi.org/10.2136/vzj2017.01.0031>
- Tian, F., Wigneron, J. P., Ciais, P., Chave, J., Ogée, J., Peñuelas, J., Ræbild, A., Domec, J. C., Tong, X., Brandt, M., Mialon, A., Rodriguez-Fernandez, N., Tagesson, T., Al-Yaari, A., Kerr, Y., Chen, C., Myneni, R. B., Zhang, W., Ardö, J., & Fensholt, R., 2018. Coupling of ecosystem-scale plant water storage and leaf phenology observed by satellite. *Nature Ecology and Evolution*, 2(9), 1428–1435. doi: 10.1038/s41559-018-0630-3
- Ticehurst, C., Guerschman, P. J., & Yun, C., 2014. The Strengths and Limitations in Using the Daily MODIS Open Water Likelihood Algorithm for Identifying Flood Events. *Remote sensing*, 6, 11791-11809. doi:10.3390/rs61211791
- Timberlake, J., & Chidumayo, E., 2001. *Miombo eco-region vision report*. Bulawayo: Biodiversity Foundation for Africa.
- Tombe, B. des, Schilperoort, B. and Bakker, M., 2020. ‘Estimation of temperature and associated uncertainty from fiber-optic raman-spectrum distributed temperature sensing’, *Sensors (Switzerland)*, 20(8). doi: 10.3390/s20082235.

- Tucker, C. J., 1979. Red and Photographic Infrared Linear Combination for Monitoring Vegetation. *Remote Sensing of the Environment*, 8, 127–150.
- Tuzet, A. J., 2011. Stomatal Conductance, Photosynthesis, and Transpiration, Modeling. in *Encyclopedia of Agrophysics. Encyclopedia of Earth Sciences Series* (ed. Gliński, J., Horabik, J., Lipiec, J.) 855–858. doi:10.1007/978-90-481-3585-1_213.
- UNFCCC., 2020. *Data for adaptation*. Bonn, Germany: UNFCCC. Retrieved from <https://unfccc.int>
- Urban, J., Ingwers, M. W., McGuire, M. A. & Teskey, R. O., 2017. Increase in leaf temperature opens stomata and decouples net photosynthesis from stomatal conductance in *Pinus taeda* and *Populus deltoides* x *nigra*. *J. Exp. Bot.* **68**, 1757–1767.
- Van Der Ent, R. J., Wang-Erlandsson, L., Keys, P. W., & Savenije, H. H. G., 2014. Contrasting roles of interception and transpiration in the hydrological cycle – Part 2: Moisture recycling. *Earth System Dynamics*, 5(2), 471–489. doi: 10.5194/esd-5-471-2014
- Van Der Ent, Rudi J., Savenije, H. H. G., Schaeffli, B., & Steele-Dunne, S. C., 2010. Origin and fate of atmospheric moisture over continents. *Water Resources Research*, 46(9), 1–12. doi: 10.1029/2010WR009127
- van de Giesen, N., Steele-Dunne, S. C., Jansen, J., Hoes, O., Hausner, M. B., Tyler, S., & Selker, J., 2012. Double-ended calibration of fiber-optic raman spectra distributed temperature sensing data. *Sensors (Switzerland)*, 12(5), 5471–5485. doi: 10.3390/s120505471
- Van Der Meulen, M. W. J. & Klaassen, W., 1996. Soil heat flux measurements in an open forest. *Phys. Chem. Earth* **21**, 101–105.
- Vermote, E., Wolfe, R., 2015. MOD09GA MODIS/Terra Surface Reflectance Daily L2G Global 1kmand 500m SIN Grid V006
- Vermote, E. F., Kotchenova, S. Y., & Ray,, J. P., 2011, February 11. *MODIS Surface Reflectance User's Guide*,. Retrieved from <http://modis-sr.ltdri.org>: at: <http://modis-sr.ltdri.org>
- Vinya, R., Malhi, Y., Brown, N. D., Fisher, J. B., Brodribb, T., & Aragão, L. E., 2018. Seasonal changes in plant–water relations influence trends of leaf display in Miombo woodlands: evidence of water conservative strategies. *Tree Physiology*, 39, 04–112. doi:doi:10.1093/treephys/tpy062
- Vinya, R., Malhi, Y., Fisher, J. B., Brown, N., Brodribb, T. J., & Aragao, L. E., 2013. Xylem cavitation vulnerability influences tree species' habitat preferences in Miombo woodlands. *Oecologia*, 173(3), 711-720. doi:10.1007/s00442-013-2671-2
- WARMA., 2022. “Catchments for Zambia.” Luangwa Catchment. <http://www.warma.org.zm/catchments-zambia/luangwa-catchment-2/>.

- Wan, Z., & Hulley, S. H., 2015. *MYD11A2 MODIS/Aqua Land Surface Temperature/Emissivity 8-Day L3 Global 1km SIN Grid V006*. NASA EOSDIS Land Processes DAAC. Retrieved from <https://doi.org/10.5067/MODIS/MYD11A2.006>
- Wang, S., Pan, M., Mu, Q., Shi, X., Mao, J., Brümmer, C., Jassal, R. S., Krishnan, P., Li, J., & Andrew Black, T., 2015. Comparing evapotranspiration from eddy covariance measurements, water budgets, remote sensing, and land surface models over Canada. *Journal of Hydrometeorology*, 16(4), 1540–1560. doi: 10.1175/JHM-D-14-0189.1
- Wang, S., Fu, B. J., Gao, G. Y., Yao, X. L., & Zhou, J., 2012. Soil moisture and evapotranspiration of different land cover types in the Loess Plateau, China. *Hydrology and Earth System Sciences*, 16(8), 2883–2892. doi: 10.5194/hess-16-2883-2012
- Wang, K., Franklin, S. E., Guo, X., & Cattet, M., 2010. Remote Sensing of Ecology, Biodiversity and Conservation: A Review from the Perspective of Remote Sensing Specialists. *Sensors*, 10, 9647–9667. doi:10.3390/s101109647
- Wegehenkel, M., 2009. Modeling of vegetation dynamics in hydrological models for the assessment of the effects of climate change on evapotranspiration and groundwater recharge. *Advances in Geosciences*(21), 109–115. Retrieved from www.adv-geosci.net/21/109/2009/
- Weerasinghe, I, Bastiaanssen, W., Mul, M., Jia, L., and Griensven, A., 2020. Can We Trust Remote Sensing Evapotranspiration Products over Africa. *Hydrology and Earth System Sciences* 24 (3): 1565–86. <https://doi.org/10.5194/hess-24-1565-2020>.
- Wehr, R., Commane, R., Munger, J. W., Mcmanus, J. B., Nelson, D. D., Zahniser, S. M., Saleska, R. S., and Wofsy, C. S., 2017. “Dynamics of Canopy Stomatal Conductance, Transpiration, and Evaporation in a Temperate Deciduous Forest, Validated by Carbonyl Sulfide Uptake.” *Biogeosciences* 14(2):389–401. doi: 10.5194/bg-14-389-2017.
- Weishampel, J. F., Ranson, K. J., & Harding, D. J., 1996. *Remote sensing of forest canopies*. Published by: Marie Selby Botanical Gardens Inc. Stable URL : <http://www.jstor.com/stable/41759918>. Linked references are available on J. 17(1), 6–14.
- White, F., 1983. *The Vegetation of Africa*. Paris: UNESCO.
- Woodward, F. I., 1988. Temperature and the distribution of plant species. *Symposium of the Society for Experimental Ecology*, 42, 59–75.
- World Bank., 2010. *The Zambezi River Basin: A Multi-Sector Investment Opportunities Analysis - Basin Development Scenarios*. World Bank. © World Bank. <https://openknowledge.worldbank.org/handle/10986/2959> License: CC BY 3.0 IGO
- Wulder, M. A., & Franklin, S. E., 2003. Remote Sensing of Forest Environments, Introduction. In In: *Wulder M.A., Franklin S.E. (eds) Remote Sensing of Forest Environments*. Boston, MA: Springer. doi:https://doi.org/10.1007/978-1-4615-0306-4_1

- Xing, Z., Chow, L., Meng, F., Rees, W. H., Steve, L., and Monteith, J., 2008. Validating Evapotranspiration Equations Using Bowen Ratio in New Brunswick, Maritime, Canada. *Sensors* 1: 412-428. <https://doi.org/10.3390/s8010412>.
- Yang, H., Luo, P., Wang, J., Mou, C., Mo, L., Wang, Z., Fu, Y., Lin, H., Yang, Y., & Bhatta, L. D., 2015. Ecosystem Evapotranspiration as a Response to Climate and Vegetation Coverage Changes in Northwest Yunnan, China. *PLOS ONE*, 10(8), e0134795. doi: 10.1371/journal.pone.0134795
- Yilmaz, M. T., Hunt Jr, E. R., & Jackson, T. J., 2008. Remote sensing of vegetation water content from equivalent water thickness using satellite imagery. *Remote sensing of the environment*, 112, 2514-2522.
- Yu, L., Zeng, Y., Su, Z., Cai, H., & Zheng, Z., 2016. The effect of different evapotranspiration methods on portraying soil water dynamics and ET partitioning in a semi-arid environment in Northwest China. *Hydrology and Earth System Sciences*, 20, 975–990. doi:10.5194/hess-20-975-2016
- Yuan, K., Zhu, Q., Zheng, S., Zhao, L., Chen, M., Riley, J. W., Cai, X., 2021. Deforestation Reshapes Land-Surface Energy-Flux Partitioning. *Environmental Research Letters* 16 (2). <https://doi.org/10.1088/1748-9326/abd8f9>
- Zhang, F., & Zhou, G., 2019. Estimation of vegetation water content using hyperspectral vegetation indices : a comparison of crop water indicators in response to water stress treatments for summer maize. *BMC Ecology*, 1–12. doi: 10.1186/s12898-019-0233-0
- Zhang, K., Kimball, S. J., and Running, W. S., 2016. A Review of Remote Sensing Based Actual Evapotranspiration Estimation. *Wiley Interdisciplinary Reviews: Water* 3 (6): 834–53. <https://doi.org/10.1002/wat2.1168>.
- Zhang, X., Friedl, M. A., Schaaf, C. B., Strahler, A. H., Hodges, J. C. F., Gao, F., Reed, B. C., & Huete, A. 2003. Monitoring vegetation phenology using MODIS. *Remote Sensing of Environment*, 84(3), 471–475. doi: 10.1016/S0034-4257(02)00135-9, 2003.
- Zhao, M., Peng, C., Xiang, W., Deng, X., Tian, D., Zhou, X., Yu, G., He, H., and Zhao, Z., 2013. “Plant Phenological Modeling and Its Application in Global Climate Change Research: Overview and Future Challenges.” *Environmental Reviews* 21 (1): 1–14. <https://doi.org/10.1139/er-2012-0036>.
- Zhao, M., Peng, C., Xiang, W., Deng, X., Tian, D., Zhou, X., Yu, G., He, H., & Zhao, Z., 2013. Plant phenological modeling and its application in global climate change research: Overview and future challenges. *Environmental Reviews*, 21(1), 1–14. doi: 10.1139/er-2012-0036
- Zimba, H., Coenders-Gerrits, M., Banda, K., Hulsman, P., van de Giesen, N., Nyambe, I., and Savenije, H. H. G., 2023. On the importance of phenology in the evaporative process of the miombo woodland: Could it be why satellite-based evaporation estimates differ? *Hydrol. Earth Syst. Sci. Discuss.* [preprint], <https://doi.org/10.5194/hess-2023-39>, in review.

- Zimba, H., Coenders, M., Schilperoort, B., Savenije, Hubert H.G., van de Giesen, N., 2022. *ZAMSECUR Project Field Data Mpika, Zambia*. 4TU.ResearchData. doi: <https://doi.org/10.4121/19372352.v2>
- Zimba, H. M., Coenders-gerrits, M. A. J., Banda, K. E., Schilperoort, B., Nyambe, I., van de Giesen, N., & Savenije, H. H. G., 2022. Measuring evaporation across canopy phenophases of a natural forest : Miombo forest , Southern Africa. *Hydrol. Earth Syst. Sci. Discuss*, October, 1–23. doi: <https://doi.org/10.5194/hess-2022-303>, in review.
- Zimba, H., Coenders-Gerrits, M., Kawawa, B., Savenije, H., Nyambe, I., & Winsemius, H., 2020. Variations in canopy cover and its relationship with canopy water and temperature in the miombo woodland based on satellite data. *Hydrology*, 7(3). doi: [10.3390/hydrology7030058](https://doi.org/10.3390/hydrology7030058)
- Zimba, H., Kawawa, B., Chabala, A., Phiri, W., Selsam, P., Meinhardt, M., & Nyambe, I., 2018. Assessment of trends in inundation extent in the Barotse Floodplain, upper Zambezi River Basin: A remote sensing-based approach. *Journal of Hydrology: Regional Studies*, 15, 149–170. doi: [10.1016/j.ejrh.2018.01.002](https://doi.org/10.1016/j.ejrh.2018.01.002)

ACKNOWLEDGEMENTS

Some say they are “self-made”. I have a different opinion. No single individual who has become anything or has achieved anything of significance is “self-made”. If no evidence exists to support my opinion, this thesis, is certainly then, the first evidence to completely decant the “self-made” notion from the bank of public opinion. This dream has been turned into reality through the efforts of many individuals and institutions. My name appears on the cover of this thesis, but only as a representative “face” through which the efforts of many can be seen. There are no words good enough to express my sincere gratitude.

I am forever indebted to Prof Hubert Savenije, Dr Miriam Coenders-Gerrits and Dr Kawawa Banda for their invaluable contribution to the realization of this dream. Prof. Savenije, I will never forget the first day we met in Lusaka, Zambia. From afar you called my name and gladly welcomed me as if you knew me for a long time. You made me feel so comfortable in your presence when I had no right to be. In that moment I realised that I just experienced a different kind of greatness. That realization was cemented in each day we met. In each time you shared your thoughts with me. In each time you affirmed me. In the days when I doubted myself, I always found comfort and the will to move forward knowing you believed in me. It was an underserved honour to have been your student. To Dr Coenders-Gerrits, there are no words good enough to describe your leadership in this whole process. You showed me an example of what an excellent daily supervisor is meant to be. It was an awesome privilege to be supervised by you. You always knew when I was in self-doubt mode, and provided the necessary assurance and guidance. I always looked forward to the bi-weekly supervisory meetings because I knew I would come out with solutions. Thanks for showing me around the water section laboratory(s). That was the first time I moved around to see the various aspects of the department. Dr Banda, you know how grateful I am. Thanks for being there for me. Thanks for the long chats, assurances and guidance. This work wouldn't have been possible without you. To you, Prof Savenije, Dr Coenders and Dr Banda, here is my sincere pledge. I will emulate the example(s) you showed me. I promise to show the same kindness and commitment you accorded me to all that will come in my path. I will do for them that which you have done for me. You have planted a fruit tree. I pledge to be fruitful to the benefit of many in my country, and hopefully beyond.

Bart, thanks a lot for your contribution to this work. You were there from the start. We selected the study site in Mpika together. You taught me how to use the DTS machine and provided code. Thanks for the times we shared discussing the results. I learned a lot from you.

Petra, thank you for running the FLEX-Topo and discussing the DTS and GLEAM results. Your insights on the various aspects of the study were very helpful. The various discussions we had helped shape this thesis.

Sylvia and Felix, thanks a lot for being a part of this work. The long drives to and from Mpika, Zambia, were made bearable by your presence. I always looked forward to the lively night discussions while preparing our meals. Thanks for your help with field work activities.

Céaser, thank you for your insights on how to set up the flux tower and the ATMOS weather stations. That was really helpful.

Prof Nick, thanks for insights on the DTS and the ATMOS weather stations. The

discussions were extremely helpful.

Ivar, thanks a lot for showing me the Netherlands. The tour of Rotterdam was amazing. You knew I love football and my support for Ajax Football Club. Thanks for taking me to watch the Ajax vs Sparta Rotterdam game in Amsterdam. The “three little birds” always plays in mind each time I watch Ajax play on television. It was amazing we found ourselves on Sky Sports. That was beyond amazing. At least I know a little bit more about the Netherlands. Thanks to you.

Many thanks to Nsanzala conservancy in Mpika, Zambia, for hosting this research at their farm house. The proprietor of Nsanzala conservancy, Mr. Kangwa, thank you for providing lodging space for the research team for the entire period of the study. Thank you for providing security and maintaining the flux tower site. The farm manager, Mr. Siabili, thank you for helping with tree species identification and counting. Those long walks and talks about the presence of stray lions from the national park, encountering deadly snakes and hyenas were extremely scary, yet interesting. Thanks for showing me how to handle naughty moles which constantly broke the optic fibre cable.

I am forever grateful to the ZAMSECUR project and the Netherlands organisation for scientific research, for the scholarship that enabled this work. Thanks for enabling a dream. Thanks for making a valuable contribution to the understanding of evaporation in the miombo woodland of southern Africa. The region is one step in the right direction as regards the management of water resources. I am thankful to the government of the Republic of Zambia, Ministry of Agriculture, for allowing me to follow my dreams. I know I have become a valuable citizen. I hope to be of use to my country in solving some of the challenges in the agriculture and water sectors.

Finally, thanks to my lovely wife (Meyah) and children (Rione, Thelgy and Yahwéné) for enduring many days, weeks and months without my presence. Thank you for your love and support. You kept me sane through-out the duration of this work. I am grateful to Jehovah for you. To Him who holds all things together by the power of His word. In Him we live, move and have our being.

Therefore, there is no such a thing as a “self-made” person. We are all a product of collaborative effort by individuals, families, communities and institutions.

CURRICULUM VITAE**Henry MUSONDA ZIMBA**

27 th September, 1979	Born at Malole in Kasama, Zambia
1985 – 1993	St John’s and Chimba primary schools, Kasama.
1994 – 1998	St Clements secondary school
2001 – 2004	Bachelor of Science in Natural resources management University of Zambia
2007 – 2010	Agricultural Officer Ministry of Agriculture, Zambia
2010 – present	Senior Agricultural Officer Ministry of Agriculture, Zambia
2012-2013	Post-graduate Diploma in integrated water resources management University of Zambia, Zambia
2014 – 2016	Master of Science in integrated water resources management University of Zambia, Zambia
2018 – present	Doctoral candidate Delft University of Technology, Netherlands
2022 – present	Post -Doc researcher University of Zambia, Zambia

LIST OF PUBLICATIONS

First author – peer reviewed

Zimba, H., Coenders-Gerrits, M., Kawawa, B., Savenije, H., Nyambe, I., & Winsemius, H. (2020). Variations in canopy cover and its relationship with canopy water and temperature in the miombo woodland based on satellite data. *Hydrology*, 7(3). doi: 10.3390/HYDROLOGY7030058

Zimba, H., Kawawa, B., Chabala, A., Phiri, W., Selsam, P., Meinhardt, M., & Nyambe, I. (2018). Assessment of trends in inundation extent in the Barotse Floodplain, upper Zambezi River Basin: A remote sensing-based approach. *Journal of Hydrology: Regional Studies*, 15, 149–170. doi: 10.1016/j.ejrh.2018.01.002

First author – under peer review

Zimba, H. M., Coenders-gerrits, M. A. J., Banda, K. E., Schilperoort, B., Nyambe, I., van de Giesen, N., & Savenije, H. H. G. (2022). Measuring evaporation across canopy phenophases of a natural forest: Miombo forest, Southern Africa. *Hydrol. Earth Syst. Sci. Discuss*, October, 1–23. doi: <https://doi.org/10.5194/hess-2022-303>

Zimba, H., Coenders-Gerrits, M., Banda, K., Hulsman, P., van de Giesen, N., Nyambe, I., and Savenije, H. H. G.: On the importance of phenology in the evaporative process of the Miombo Woodland: Could it be why satellite-based evaporation estimates differ?, *Hydrol. Earth Syst. Sci. Discuss*. [preprint], <https://doi.org/10.5194/hess-2023-39>, in review, 2023.

Co-author – Peer reviewed

Fritz Kleinschroth, Kawawa Banda, **Henry Zimba**, Stefaan Dondeyne, Imasiku Nyambe, Simon Spratley, R. Scott Winto. (2022). Drone imagery to create a common understanding of landscapes, *Landscape and Urban Planning*, Volume 228,2022, 104571,ISSN 0169-2046, <https://doi.org/10.1016/j.landurbplan.2022.104571>. (<https://www.sciencedirect.com/science/article/pii/S0169204622002201>)

Meinhardt, M., Fleischer, M., Fink, M., Kralisch, S., Kenabatho, P., de Clercq, W.P., **Zimba, H.**, Phiri, W. & Helmschrot, J. (2018), Semi-arid catchments under change: Adapted hydrological models to simulate the influence of climate change and human activities on rainfall-runoff processes in southern Africa In: *Climate change and adaptive land management in southern Africa – assessments, changes, challenges, and solutions* (ed. by Revermann, R., Krewenka, K.M., Schmiedel, U., Olwoch, J.M., Helmschrot, J. & Jürgens, N.), pp. 114-130, *Biodiversity & Ecology*, 6, Klaus Hess Publishers, Göttingen & Windhoek. doi:10.7809/b-e.00313.

Nyambe, I., Chabala, A., Banda, K., **Zimba, H.** & Phiri, W. (2018), Determinants of spatio-temporal variability of water quality in the Barotse Floodplain, western Zambia In: *Climate change and adaptive land management in southern Africa- assessments, changes, challenges, and solutions* (ed. Revermann,R., Krewenka, K.M., Schmiedel, U., Olwoch, J.M., Helmschrot, J. &Jurgens, N.) pp.96-105, Biodiversity & Ecology, 6, Klaus Hess Publishers, Gottingen & Windhoek. Doi. 10.7809/b-e.003310.

Measuring data

Zimba, H., Coenders, M., Schilperoort, B., Savenije, Hubert H.G., van de Giesen, N., 2022. *ZAMSECUR Project Field Data Mpika, Zambia*. 4TU.ResearchData. doi: <https://doi.org/10.4121/19372352.v2>

Zimba, Henry; Savenije, Hubert H.G.; van de Giesen, Nick; Coenders, Miriam; Schilperoort, Bart. ZAMSECUR Project miombo woodland, Zambia, Southern Africa. 4TU.ResearchData. Dataset. <https://doi.org/10.4121/20492934.v1>, 2022c.

Book contribution

Mück, M., Helmschrot, J, **Zimba, H.**, Nyambe I.A., Wallner., M, Hipondoka., M, Mufeti., P., Meinhard., M, M., 2015. Remote sensing applications for assessing water-related risks and its interdependencies with land cover change and biodiversity in southern Africa. Global Land Project (GLP) news, November, 2015

